1-1-1995

Stress and mass transport in polymer coatings and films/

Joan Kennetha Vrtis
University of Massachusetts Amherst

STRESS AND MASS TRANSPORT IN POLYMER COATINGS AND FILMS

A Dissertation Presented

by

JOAN KENNETHA VRTIS

Submitted to the Graduate School of the

University of Massachusetts Amherst in partial fulfillment

of the requirements for the degree of

DOCTOR OF PHILOSOPHY

February 1995

Department of Polymer Science and Engineering

STRESS AND MASS TRANSPORT IN POLYMER COATINGS AND FILMS

A Dissertation Presented

by

JOAN KENNETHA VRTIS

Approved as to style and content by:

Richard J. Farris, Chair

William J. MacKnight, Member

Jehuda Greener, Member

William J. MacKnight, Department Head
Polymer Science and Engineering

This dissertation is dedicated to my favorite Hawaiian

ACKNOWLEDGEMENTS

I've been in "school" for a **long** time: thirty-one years with a one year sabbatical. It's not as if I haven't accomplished anything in the last 31 years. I earned my B.S. in Chemistry, a MMetME (Masters in Metallurgical and Materials Engineering), an M.B.A. in Entrepreneurship, a M.S. in Polymer Science and Engineering and now a Ph.D. I think I'm done with school (for awhile, anyway).

I have had the good fortune of honing my people skills and developing a strong work ethic prior to pursuing the Ph.D. My parents set a very good example. They allowed me to experiment with my scientific curiosity at a young age. Fortunately for them, I never endangered the family with my ideas and projects.

Dr. Richard Farris has been a great advisor. I like to pursue my own ideas and work without someone looking over my shoulder. His "hands-off" management style was very much appreciated. He always took a strong interest in my research and had a wealth of ideas on what avenue to pursue next if I hit a roadblock. In retrospect, I've enjoyed the opportunity to work on his "side projects". I cannot thank him enough for his help in my pursuit for employment at Intel Corp in Arizona.

Drs. MacKnight and Greener have been quite helpful and I thank both for participating on my committee. Dr. MacKnight kept an open mind during my proposal defense on a homopolymer exhibiting a three phase structure (crystalline, crystalline-amorphous and amorphous regions). Dr. Greener helped tremendously with my understanding of gelatin. His ideas have helped streamline this dissertation.

Many thanks are extended to Dr. Nalini Easwar and Christine Ofcarcik in the Smith College, Physics Dept. I appreciate the use of their double slit laser interferometry equipment and the hours they spent helping me with the out-of-plane humidity expansion coefficient study. Dr. Lardner, UMASS Mechanical Engineering Dept. has been monumental in the development of the two dimensional bending model. He was very

patient and that did not go unnoticed. Many thanks goes to Dr. Alan Lesser, PSE, for his critique of my two dimensional bending model. Dr. Chinachoti, UMASS Food Science, provided the much appreciated insight on relative humidity generation alternatives.

Joanne Purdy knew my determination to relocate to Arizona. Prior to my job offer from Intel Corp, AZ, my only standing offer was from a company in NJ. Since it was my only offer, I strongly considered accepting the position. Joanne brought me back to reality. If she ever wanted to pursue a social work position, she'd have my recommendation. Many thanks to Eileen Besse and Carol Moro for showing me the ropes around the department.

I'm sure over the past four years my obstinate nature and strong focus have perhaps pushed the limits of some of my colleagues. I thank them for putting up with me. My friends in Dr. Farris' lab (this includes Joanne Curley since she spent about 50% of her time in our lab) have made my research with relative humidity bearable at times. Christian Lietzau, Scott Joslin, Kun Tong, Karla Gagnon, Bob Jennings, Jeff Taylor, Michele Maden, and Chon-Shin Jou exercised quite a bit of patience during my "formative" years in the lab. Bob Fleming , Joanne Curley, Cindy Athanasiou (who never forgot my birthday and always provided the cake), Verna Lo (thanks for the fishing line), Kapil Seth (the cookie monster), Dave Macon (to whom I will my office chair), Meredith White, Shalabh Tandon, Mike Chen and Anthony (is there any place but Greece?) Karandinos added levity to our crowded lab environment.

Fortunately, I had a life outside of the lab. Vicki White and Barb Landini could always make me laugh. Vicki had the knack of putting my mind on a different plane. Barb has been a great deterrent from my research. She and I have similar interests so we were never at odds to find either something athletic to occupy our time or a "no-moo" ice cream and cappacino to get us away from the office. Those times will be sorely missed.

My most favorite person and probably the major mental contributor to this research is my Hawaiian roommate, Colleen R. Kumia. Anyone who could live with me

during the cumalative exam period has got to be a great friend. Half of my Ph.D. hood goes to her. I'd give her half the gown also, but it would probably be too long.

ABSTRACT

STRESS AND MASS TRANSPORT IN POLYMER COATINGS AND FILMS

FEBRUARY 1995

JOAN KENNETHA VRTIS, B.S., UNIVERSITY OF ILLINOIS
M.B.A., DEPAUL UNIVERSITY
M.MET.M.E., ILLINOIS INSTITUTE OF TECHNOLOGY
M.S., UNIVERSITY OF MASSACHUSETTS AMHERST
Ph.D., UNIVERSITY OF MASSACHUSETTS AMHERST

Directed by Professor Richard J. Farris

Water sorption in polymers is a common phenomenon. The sorption process can induce biaxial swelling stresses in polymer coatings causing dimensional instability commonly observed as curling or bending in the system. This dissertation investigates the effect of relative humidity on the stresses, mass transport and the dimensional stability of a bilayer of alkaline processed bone gelatin on a cellulose acetate substrate. Poly(vinyl alcohol), polyimide, epoxy, poly(ethylene terephthalate) and a nickel coating were investigated for comparison.

A two dimensional bending model was developed which was based on a nonlinear mathematical modification to Classical Lamination Theory. The model predicts the dimensional instability, observed as bending or curl, in a gelatin/cellulose acetate bilayer. The stable, equilibrium shape was related to the minimum potential energy in the system. Observed curl behavior showed that the gelatin/cellulose acetate bilayer exhibits a cylindrical geometry at relative humidities less than 54%RH. The bending occurs towards the gelatin coating indicating that the gelatin was in tension. At relative humidities greater

than 54%RH, an inversion occurred in which the bilayer forms a cylindrical shape along an axis 90° to the lower humidity geometry. The cylinder curls towards the cellulose acetate indicating that the gelatin was in compression and cellulose acetate was in tension.

To test the model validity, the moduli, Poisson's ratio and the humidity expansion coefficients for each material in the bilayer was required. The materials were characterized by various methods to determine the required properties. Applying these results to the two dimensional bending model, the predicted bending phenomenon proved to be consistent with the observations.

The biaxial swelling stress as a function of relative humidity was investigated. Gelatin exhibited a stress hysteresis. The stress values determined during desorption were always higher than those obtained during absorption at the same relative humidity. Similar hysteresis behavior was observed in poly(vinyl alcohol) at relative humidities lower than its drying humidity. Hysteresis in the epoxy coating was non-existent.

The mass transport properties for gelatin and cellulose acetate were studied. A holographic interferometry method was developed and compared with a standard gravimetric technique. The holographic method was validated using PMDA-ODA polyimide as a standard.

TABLE OF CONTENTS

LIST OF TABLES

LIST OF FIGURES

CHAPTER 1

INTRODUCTION AND BACKGROUND

Introduction

Polymers exhibit a high propensity to absorb moisture unlike their material counterparts, ceramics and metals. Most polymers display this characteristic to varying degrees. Relative humidity has a direct effect on the dimensional stability of multilayer polymer coating systems. Dimensional instability due to swelling and thermal stresses is commonly observed as curling or bending of the multilayer system and in extreme cases, coating delamination or cracking. This dissertation will focus on those polymers with a high affinity to moisture, specifically, alkaline processed bone gelatin and cellulose acetate. Hygroscopic effects on the dimensional stability are investigated and a theoretical model representing the bending of a two dimensional bilayer polymer system is proposed.

Dissertation Overview

This dissertation will address the stresses and mass transport in polymer films and coatings. Chapter 1 offers a literature review of problems and phenomena that occur in polymer coatings and films with variations in environmental conditions, specifically, relative humidity. Dimensional instability and moisture sorption hysteresis are highlighted.

In chapter 2, the contributing factors to dimensional instability in a coating/substrate bilayer are introduced. Stresses in coatings are discussed, incremental linear elasticity theory is outlined and a two dimensional bending model representing the curling phenomenon in a gelatin/cellulose acetate bilayer is proposed.

The material properties of photographic film components as well as some general polymer and metal coatings are highlighted in chapter 3. A background of the materials and the system designed to control relative humidity is discussed. Tensile and shear moduli, Poisson's ratio, thermal properties, and the degree of crystallinity in each material are featured.

Swelling strains are investigated in chapter 4. The swelling strain due to varying relative humidities is presented. Humidity expansion coefficients for the in-plane and out-of-plane directions for the primary photographic film components are discussed.

Biaxial swelling stresses in coatings and films are detailed in chapter 5. Real time holographic interferometry is employed to quantify the biaxial stresses in coatings as a function of relative humidity. The Holographic Interferometry system adapted to accept relative humidity is outlined. The influence of crosslinking, crystallinity and sorption cycling on the humidity swelling stresses is also investigated.

Chapter 6 features the mass transport properties of a coating/substrate bilayer system. The mass diffusion coefficients determined by Holographic Interferometry are compared with gravimetric results. Biaxial stress as a function of mass uptake is also correlated.

Conclusions made from this investigation and possible future work in understanding the mechanisms of the sorption process and the effect of humidity on other polymer systems is addressed in chapter 7. An analytical solution of the two dimensional bending model for a bilayer system of gelatin coated on cellulose acetate is presented and compared to the observed behavior.

Background

There are two phenomena that have been observed in this work and are difficult to explain: (1) dimensional instability in a polymer-polymer bilayer system with varying

relative humidity and (2) the dependence of the biaxial swelling stress values on the sorption path. The latter phenomenon is known as "moisture sorption hysteresis". It has been these observations that have driven this investigation.

Dimensional Instability

Water sorption in polymers is a common phenomenon. The sorption process can induce swelling stresses in polymer coatings causing dimensional instability commonly observed as bending in the system. Bending or "curl" has been observed in photographic films, medical, electronic, aerospace and food packaging applications [1-11]. In photographic films, the primary system is composed of a gelatin coating on a cellulose acetate, CA, or poly(ethylene terephthalate), PET, substrate. Dimensional instability complicates post coating processing of the film due to the bending of the system. The bending introduces difficulty in (1) perforating the 35mm wide multilayer and (2) high speed processing of the developed product [12].

The gelatin/CA bilayer system exhibits two different bending modes. For this specifice case, below 54%RH, the gelatin is in tension causing a "positive" curl. A cylindrical shape results about the x axis. Above 54%RH, an inversion of the cylindrical shape occurs 90° (about the y axis) to the low humidity curl. The cylindrical geometry bends towards the cellulose acetate. At the high humidities, the gelatin is in compression defined in the photographic industry as a "negative" curl. Figure 1.1 illustrates this phenomenon.

Each bending mode depicts the bilayer as a cylindrical shape. The cylindrical form exists along one of the two principal axes in the plane of the bilayer. Similar characteristics have been observed for thin unsymmetric laminates of graphite - polyimide composites [10]. In each case, it is the stress in the system which causes bending to occur.

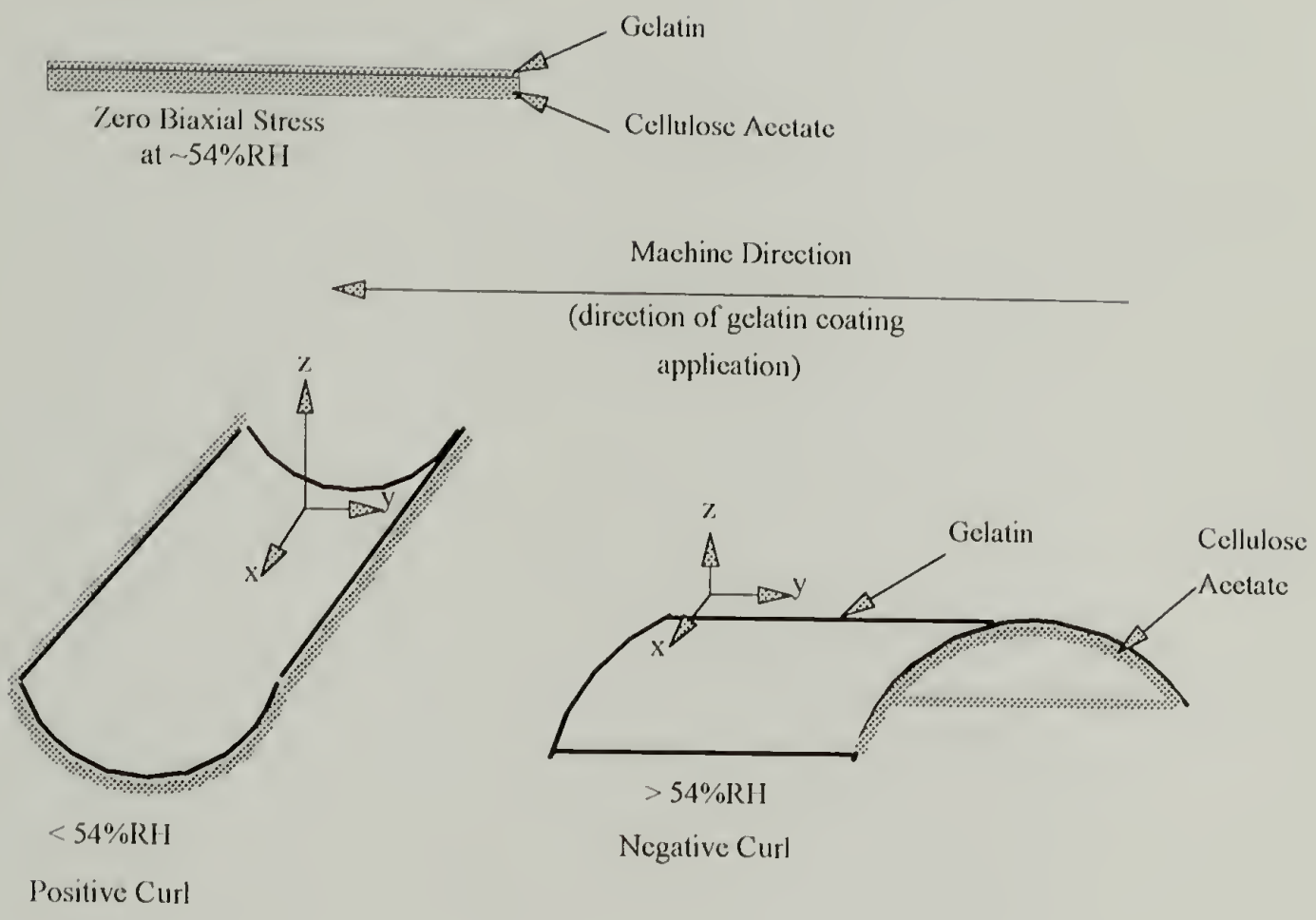

Figure 1.1 Schematic of dimensional instability in a bilayer system of gelatin coated on a cellulose acetate substrate.

The stress is proportional to the product of the modulus and the expansion coefficient as described in equation (1.1) for a constrained isotropic material.

$$E\left[\varepsilon_{ij} - \delta_{ij}\left(\alpha dT - \beta dRH - \xi\, dP\right)\right] = (1+\nu)d\sigma_{ij} - \delta_{ij}\nu d\sigma_{kk} \qquad (1.1)$$

where,

E = tensile modulus

ε_{ij} = strain

δ_{ij} = Kronecker delta

α = thermal expansion coefficient

d = differential operator

T = temperature

β = humidity expansion coefficient

RH = relative humidity

ξ = reaction expansion coefficient

P = extent of the curing reaction

ν = Poisson's ratio

σ_{ij} = stress

The material coefficients, E, ν, β, α, and ξ can depend upon the temperature, relative humidity and extent of reaction and still preserve linearity in terms of stress and strain. For a completely cured system under isothermal conditions and varying relative humidity, the mismatch of humidity expansion coefficients of each material contributes to the bending in the system. In photographic film, the bending primarily results from the difference in humidity expansion coefficients between the photographic emulsion (gelatin with silver halides) and the support (substrates such as cellulose acetate or poly(ethylene terephthalate)) [3]. The zero stress state is the stress at which the photographic film lies flat. For the gelatin/cellulose acetate bilayer investigated, the zero state of stress occurred at 54%RH and ambient temperature. The zero stress state in photographic films is dependent upon drying conditions, gelatin coating thickness and the choice of substrate. It is the decrease or increase in relative humidity from the zero stress state that influences the bending of the system.

In addition to the mismatch of the humidity expansion coefficients, viscoelastic effects that are induced when photographic film is wound into a roll, also contribute to the dimensional instability [3]. In roll form, the film is flat across its width but assumes a lengthwise curvature. The phenomenon of lengthwise "plastic flow" is referred to as "core-set" and has been explained by stress relaxation [3]. Extensive research has been conducted pertaining to the dimensional instability in photographic films [1,2,13-15].

Several techniques are available for measuring swelling stresses in films [7,16-20]. The most common techniques measure the strain or bending and use linear elastic assumptions to determine the stress. These techniques are usually one dimensional techniques requiring knowledge of the Poisson's ratio to apply the results to a two dimensional system (ie., a coating on a substrate). Holographic interferometry techniques directly measure the stress in either a one or two dimensional system. The advantage of this technique is that only the density of the material is required. The techniques mentioned have advantages and disadvantages. Each is best applied to specific sizes and geometries.

Predicting the dimensional instability in the coating system is advantageous to optimizing processing and product design. Modelling is a valuable, economic tool for estimating process and product design requirements. Several models are available for predicting the bending of multilayer system as a result of swelling [6,17,21,22]. The one dimensional models fail to predict the cylindrical shapes observed in a two dimensional photographic films as a function of relative humidity. Hyer proposed a two dimensional model to predict the cylindrical shapes in unsymmetric laminates solely as a function of temperature [23]. A two dimensional model simulating the bending behavior of a coating/substrate system as a function of relative humidity has not been found in the open literature.

Moisture Sorption and Dimensional Hysteresis

Moisture sorption hysteresis is the phenomenon in which different paths exist for adsorption and desorption of moisture from the same material [24]. The mechanical and flow properties of materials exhibiting this hysteresis are often dependent upon the sorption path [2,25]. There are several proposed mechanisms for moisture sorption and moisture sorption hysteresis [24-35]. Early mechanisms postulated that there was a distinction between the two principal classes of sorbed water: (a) water which is bound in some way to the inner and outer surfaces of the absorbant and (b) water which is normally condensed in the material. These mechanisms did not explain the inherent moisture hysteresis. Later mechanisms expanded the earlier proposals by introducing the terms, "bound" and "free" water in the polymer system. "Bound" water represents the water molecules which are hydrogen bonded to the polymer. Specifically in biopolymer such as collagen and gelatin, the water molecule hydrogen bonds with the amine or carbonyl groups in the peptide chain. "Free" water is characterized as the water that fills the interstices in the polymer network. This is most often the amorphous region. The amount of "free" water in the system is dictated by relative humidity (recalling that relative humidity is ratio of the partial pressure of water vapor in air to the equilibrium vapor pressure of water at the same temperature) and therefore the osmotic pressure (known as the Donnan equilibrium) [31]. But this again does not discuss the hysteresis phenomenon. Another mechanism considered is the "Cavity Concept", which addresses the moisture sorption hysteresis. This "concept" suggests that cavities exist in the polymer (in this case, gelatin and casein). A cavity is a pore with a constricted neck. Filling the cavities during absorption is progressive but emptying the cavities during desorption is abrupt [33]. Therefore, there is a difference in moisture content along the desorption and absorption paths.

York [25] experimentally tested the theoretical relationships of moisture sorption hysteresis and concluded that there were three (3) mechanisms in which water can be held: (a) monomolecular layers of water are bound to the surface (referred to as monolayer adsorbed moisture), (b) moisture within the material (known as absorbed moisture) and (c) multimolecular layers of water (termed normally condensed water). The hysteresis mechanism is explained as follows. Assume a dry material is exposed to a certain relative humidity, initially the water molecules adsorb on the surface forming a monomolecular layer. In this phase, the monolayer is subjected to both surface binding forces and diffusional forces. In the next step, the diffusional forces transfer moisture into the material. Therefore, the moisture is absorbed into the bulk. In addition, as more moisture adheres to the surface, it condenses forming a multimolecular layer of water. If the relative humidity (moisture vapor pressure) is reduced, the water molecules at the surface are initially removed before the diffusion forces removed the absorbed moisture out of the material. The rate at which the moisture is removed differs from the rate at which the material takes in moisture.

York's mechanism presents a transport approach. A more recent mechanism which addresses moisture sorption hysteresis in gelatin films on a molecular scale was deduced using circular dichroism studies. Before presenting this mechanism, a brief understanding of the structure of gelatin is required. More extensive details are available in the literature [36]. In general, gelatin is a derivative of collagen. Collagen is a right hand triple α-helix. These rigid rod helices are 300 nm in length. Collagen is a polypeptide. Therefore it consists of a series of amino acids. The three collagen strands are hydrogen bonded to each other thus stabilizing the triple helical structure.

Gelatin is formed by denaturation of the collagen from the rigid rod system to three (3) random coils. Gelatin films can either be amorphous or semicrystalline depending on the drying conditions. A semicrystalline gelatin film is formed by drying the gelatin at 25°C and ~50%RH.

The crystallites in the gelatin are renaturated collagen rigid rods known as "collagen fold crystallites". There are 17 known members in the collagen family of proteins [37]. The common triple helical structure is composed of three polypeptide chains with the repeating sequence Gly-Xxx-Yyy. The Xxx is frequently proline and the Yyy is frequently hydroxyproline. Figure 1.2 represents the most common polypeptide groups.

In addition to displaying moisture sorption hysteresis, gelatin films exhibits a small reduction in stress at low relative humidities. The mechanism that follows accounts for both of these phenomena. First, it is believed that "bound" water stabilizes the triple helix by interchain bridging [34] and that the "bound" water is the primary contributing factor to the hysteresis [33]. In general, the conformations of the single chains of the collagen and gelatin resemble the conformations of poly(L-proline), Form II, which is the trans-conformation [29]. This was determined using circular dichroism (CD). Since the glycyl residue occupies every third residue, the poly(L-proline) trans-conformation of the single collagen or gelatin chains are stabilized only in the triple helical structure. This suggests that CD measurements are directly related to the triple helix content in collagen and gelatin. Experimental results have shown that at relative humidities less that 20%, there is a large decrease in the triple helix content. This suggests that a trans-conformation to cis-conformation transition exists, since the cis-conformation of polyproline is known to hinder hydrogen bonding of the water molecule to the oxygen of the proline's carbonyl groups [29]. The trans- to cis- conformation transition is directly related to the observed stress reduction at low relative humidities. In addition, it is postulated that moisture sorption hysteresis is dependent upon the amounts of the cis- and trans- peptide conformations in the gelatin. In general, as the relative humidity decreases (water content decreases), the triple helix content decreases and an increase in the number of cis- peptide bonds is observed [29]. Therefore, hysteresis is related to the amount of cis- and trans-conformations in the gelatin.

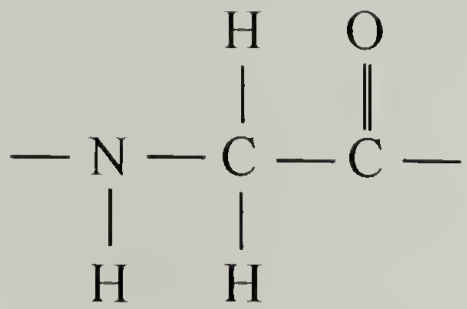

Glycine (Gly)

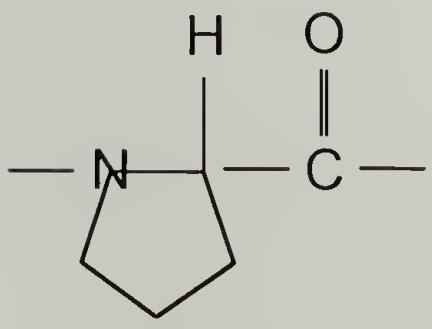

Proline (Pro)

Figure 1.2 Common polypeptide groups in gelatin and collagen

The moisture sorption hysteresis affects the dimensional stability of a material. Dimensional hysteresis is the phenomenon in which different dimensions exist for adsorption and desorption of moisture from the same material. Dimensional hysteresis is observed in gelatin films exposed to various relative humidities [2]. The mechanical properties are affected by the sorption path. In addition, stress reduction is observed at relative humidities less that 20%RH.

References

1. J.Q. Umberger, "The Fundamental Nature of Curl and Shrinkage in Photographic Films," Photographic Science and Engineering, **1**(2), 69 (1957).

2. J.M. Calhoun and D.A. Leister, "Effect of Layers on the Dimensional Instability of Photographic Film," Photographic Science and Engineering, **3**(1), 8 (1959).

3. "Physical Properties of Kodak Aerial Films," Properties of Kodak Materials For Aerial Photographic Systems, Vol. II, (Rochester, NY: Eastman Kodak Co., 1972).

4. I.W. Kellaway, C. Marriott and J.A.J. Robinson, "The Mechanical Properties of Gelatin Films: I. The Influence of Water Content and Preparative Conditions," Canadian Journal of Pharmaceutical Sciences, **13**(4), 83 (1978).

5. H.M. Tong and K.L. Saenger, "Bending-Beam Study of Water Sorption by Thin Poly(methyl Methacrylate) Films," Journal of Applied Polymer Science, **38**, 937 (1989).

6. T.Z. Fu, C.J. Durning and H.M. Tong, "Simple Model for Swelling-Induced Stresses in Supported Polymer Thin Films," Journal of Applied Polymer Science, **43**, 709 (1991).

7. C.S. Jou and R.J. Farris, "Moisture Transport in a Bilayer Cantilever Beam by Holographic Interferometry," (submitted to Acta Polymerica, 1993).

8. G. Shen and G.S. Springer, "Moisture Absorption and Desorption of Composite Materials," Journal of Composite Materials, **10**, 2 (1976).

9. R.B. Pipes, J.R. Vinson and T.W. Chou, "On the Hygrothermal Response of Laminated Composite Systems," Journal of Composite Materials, **10**, 130 (1976).

10. M.W. Hyer, "The Room-Temperature Shapes of Four-Layer Unsymmetric Cross-Ply Laminates," Journal of Composite Materials, **16**, 318 (1982).

11. D.Y. Perera and D. Vanden Eynde, "Moisture and Temperature Induced Stresses (Hygrothermal Stresses) in Organic Coatings," **59**(748), 55 (1987).

12. C.L. Bauer, personal communication, (1991).

13. P.Z. Adelstein, "Physical Properties of Photographic Materials," SPSE Handbook of Photographic Science and Engineering, ed., W. Thomas, (New York: Wiley Interscience, 1973).

14. J.M. Calhoun, "The Physical Properties and Dimensional Instability of Safety Aerographics Film," Photogrammetric Engineering, **13**, 163 (1947).

15. J.M. Calhoun, P.Z. Adelstein and J.T. Parker, "Physical Properties of Estar Polyester Base Aerial Films for Topographic Mapping," Photogrammetric Engineering, **27**, 461 (1961).

16. C.L. Bauer, R.J. Farris and M.S. Vratsanos, "Determination of the Stresses and Properties of Polymer Coatings," Journal of Coatings Technology, **60**(760), 51 (1988).

17. B.S. Berry and W.C. Pritchet, "Bending-Cantilever Method for the Study of Moisture Swelling in Polymers," IBM Journal of Research and Development, **28**(6), 662 (1984).

18. L.T. Nguyen, "Surface Sensors for Moisture and Stress Studies," New Characterization Techniques for Thin Polymer Films, eds., H.M. Tong and L.T. Nguyen, (New York: John Wiley and Sons, 1990).

19. J.K. Vrtis and R.J. Farris, "Experimental Stress Analysis Methods and Some Thin Film Applications," (accepted to Materials Research Society Symposium Proceedings, 1994).

20. J.L. Goldberg, K.M. O'Toole and H. Roper, Journal of Testing and Evaluation, **3**(4), 263 (1975).

21. J.G. Sloan and J.R. Vinson, "Behavior of Rectangular Composite Material Plates Under Lateral and Hygrothermal Loads," Proceedings of the American Society of Engineers Winter Meeting, (New York: American Society of Mechanical Engineers, 1978).

22. P.K. Mallick, Fiber-Reinforced Composites: Materials, Manufacturing and Design, (New York: Marcel Dekker, Inc., 1988).

23. M.W. Hyer, "Calculations of the Room-Temperature Shapes of Unsymmetrical Laminates," Journal of Composite Materials, **15**, 296 (1981).

24. K. Boki and S. Ohno, "Moisture Sorption Hysteresis in Kudzu Starch and Sweet Potato Starch," Journal of Food Science, **56**(1), 125 (1991).

25. P. York, "Analysis of Moisture Sorption Hysteresis in Hard Gelatin Capsules, Maize Starch, and Maize Starch: Drug Powder Mixtures," Journal of Pharmaceutical and Pharmacology, **33**, 269 (1981).

26. H. Liu, L. Zhang, and N.A. Seaton, "Analysis of Sorption Hysteresis in Mesoporous Solids Using a Pore Network Model," Journal of Colloid and Interface Science, **156**, 285 (1993).

27. R.M. Conforti and T.A. Barbari, "A Thermodynamic Analysis of Gas Sorption-Desorption Hysteresis in Glassy Polymers," Macromolecules, **26**, 5209 (1993).

28. H. Hermel, R. Wetzel, E. Buder, C. Roth, H. Herbrich and H. Legutke, "Moisture, Triple Helical Content and Brittlenes of Gelatin Layers," Journal of Photographic Science, **39**, 16 (1991).

29. R. Wetzel, E. Buder, H. Hermel and A. Hüttner, "Conformations of Different Gelatins in Solutions and in Films: An Analysis of Circular Dichroism (CD) Measurements," Colloid and Polymer Science, **265**, 1036 (1987).

30. M.L. Mattli and M. Rüegg, "Thermodynamic Functions of Biopolymer Hydration: I. Their Determination by Vapor Pressure Studies Discussed in an Analysis of the Primary Hydration Process," Biopolymers, **21**, 403 (1982).

31. A.G. Ward and A. Courts, The Science and Technology of Gelatin, (New York: Academic Press, Inc., 1977).

32. C.A.J. Hoeve and P.C. Lue, "The Structure of Water Absorbed in Collagen. I. The Dielectric Properties." Biopolymers, **13**, 1661 (1974).

33. K.S. Rao and B. Das, "Varietal Differences in Gelatin, Egg Albumin and Casein in Relation to Sorption - Desorption Hysteresis with Water," Journal of Physical Chemistry, **72**(4), 1223 (1968).

34. G.N. Ramachandran and R. Chandrasekharan, "Interchain Hydrogen Bonds via Bound Water Molecules in the Collagen Triple Helix," Biopolymers, **6**, 1649 (1968).

35. S.E. Smith, "The Sorption of Water Vapor by High Polymers," Journal of the American Chemical Society, **69**, 646 (1947).

36. B. Alberts, D. Bray, J. Lewis, M. Raff, K. Roberts and J. Watson, Molecular Biology of the Cell, (New York: Garland Publishing, Inc., 1983).

37. J.M. Davis and H.P. Bächinger, "Hysteresis in the Triple Helix-Coil Transition of Type III Collagen," Journal of Biological Chemistry, **268**(34), 25965 (1993).

CHAPTER 2

THEORETICAL STRESS AND BENDING MODEL

Introduction

Stresses in coating systems can present adverse effects such as cracking or delamination of the coating. The stress may also impose a bending moment resulting in dimensional instability of the system. This is commonly observed as bending or curling. In this chapter, the origin of stresses in coatings will be presented. Incremental Linear Elasticity is adopted to theoretically represent the relationship of stress as a function of environmental conditions. A nonlinear modification of Classical Lamination Theory is presented which represents the bending phenomenon observed in a two dimensional bilayer system as a result of humidity gradients.

Stresses in Coatings

Coatings are commercially important. For example, in the electronic industry, coatings are used as passivation layers to insulate the metal circuits between levels. Food science relies on the barrier properties of polymer coatings in packaging to reduce spoilage. And the photographic industry uses coatings as colloid protectors for the silver halide crystals and as a means to filter light in their color films.

There are two types of stress: stress imposed by an external load and an internal or residual stress induced by variations in environmental conditions, curing of the coating, and relaxation due to physical aging, for example. Throughout this text, the internal stress will be implied.

The most common mechanism of internal stress results from the mismatch between the expansion coefficients, eg., the thermal expansion coefficient, TEC, or the humidity expansion coefficient, HEC. For example, in a photographic bilayer system, if the HEC of the coating is greater than the HEC of the substrate, the coating will be in tension and the substrate will be in compression at lower humidities. As observed in the specific case, at relative humidities less that 54%, a gelatin/cellulose acetate bilayer curls towards the gelatin coating into a cylindrical shape along the x axis. This is known as "positive curl". Observations at humidities greater than 54%RH show that the bilayer inverts the cylindrical geometry to the y axis, 90° from the lower humidity curl axis. In addition, the bilayer curls towards the cellulose acetate. Therefore, the coating is in compression and the substrate is in tension. This occurs as a "negative curl" in the system. The bending phenomenon is depicted in figure 2.1.

Since a coating is two dimensionally constrained, moisture removal from the coating by lowering the relative humidity causes in-plane shrinkage of the coating on a rigid substrate. This shrinkage imposes a tensile stress in the coating. Any volumetric change would occur in the out-of-plane direction. As mentioned earlier, another mechanism for stress is physical aging. Physical aging can influence the coating stress by relaxation or rearrangement of the molecules over time.

The sources of stress discussed above are not an exhaustive list. The mechanisms outlined are those believed to apply to this investigation. These mechanisms of stress and others are detailed in the literature [1-8].

The components of stress can be understood further by removing a small volumetric element from the coating. In an orthotropic system, there are 9 components of stress. There are 3 normal stresses which are perpendicular to the volume face and 6 shear stresses which align parallel to the volume face. Figure 2.2 provides a pictorial representation.

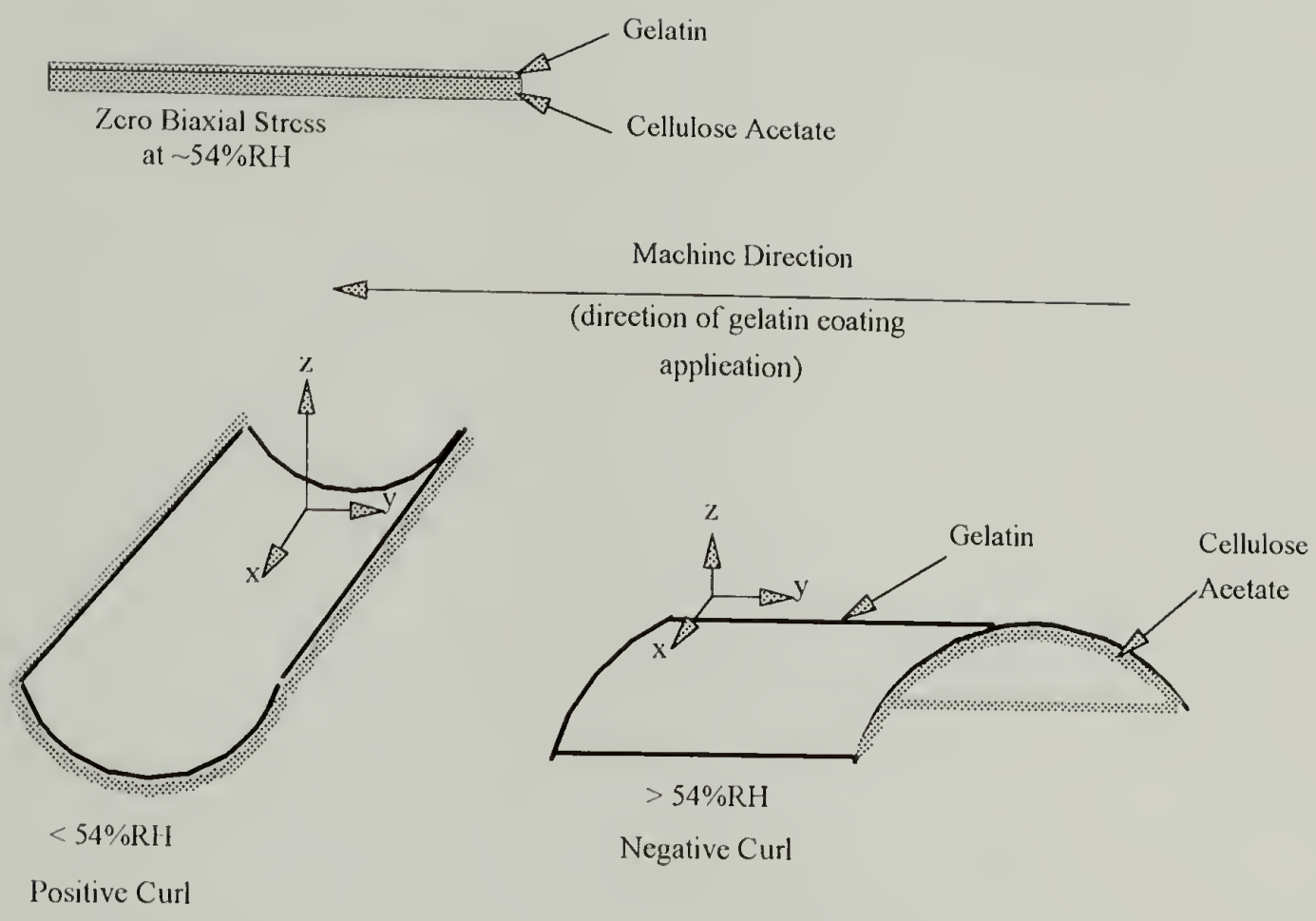

Figure 2.1 Representation of the bending phenomena depicting the result of the mismatch between humidity expansion coefficients of the coating and substrate. This behavior is observed in the gelatin/cellulose acetate bilayer system studied in this work.

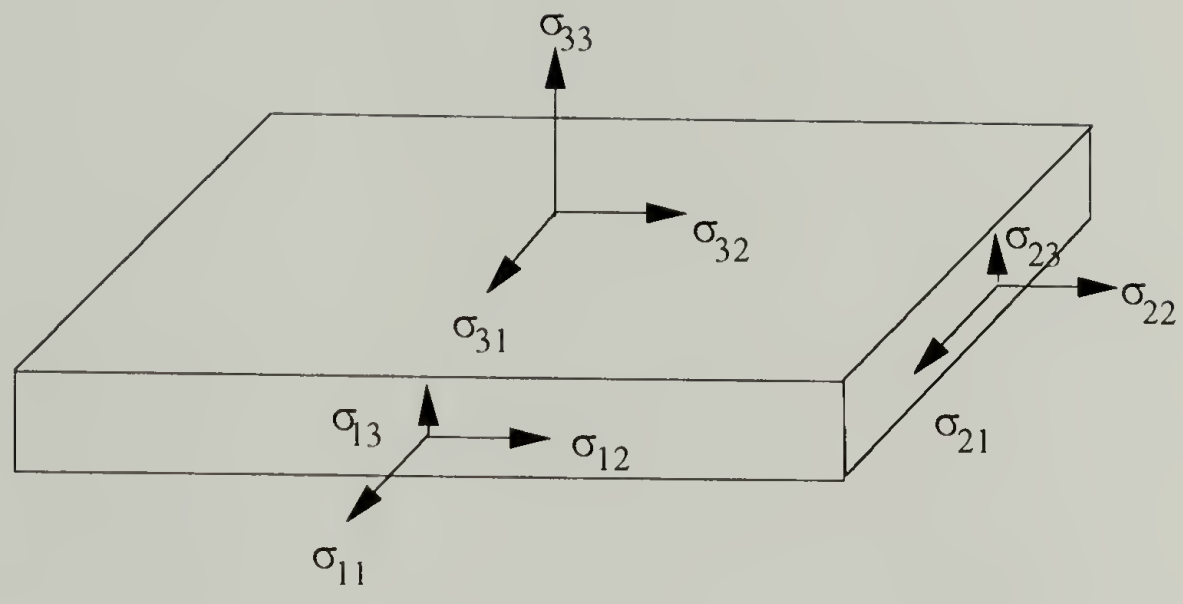

Figure 2.2 Representation of the possible stresses in a volumetric element of an orthotropic coating

By symmetry arguments, the 6 shear stress components are reduced to 3 shear components where $\sigma_{ij} = \sigma_{ji}$ (for $i \neq j$). Since a coating is a two dimensionally constrained system, the out-of-plane normal stress, σ_{33} is zero. Aleck [9] illustrated that away from the edge of the coating, the shear stresses, σ_{13} and σ_{23} are zero. Therefore, the stresses required to understand a coating system have been reduced from 9 components to 3 components: 2 normal stresses, σ_{11} and σ_{22} and a single shear stress, σ_{12}.

Since the stresses required are in the plane of the coating, a plane stress analysis can be used to resolve the stress in the coating. This is applied theoretically using linear elastic assumptions.

Incremental Linear Elasticity Theory

Incremental linear elasticity describes the relationship of stress to strain at incremental intervals. The strain can be externally applied or induced by environmental or processing conditions. Incremental linear elasticity assumes the material is homogeneous, isotropic, elastic and in the small strain regime.

The bending curvature in the coating/substrate system is related to the stress in the coating. Therefore, it is important to quantify the induced stresses in the system. In an isotropic material, swelling stresses are purely dilatational and therefore shear stresses are non-existent. In this case, the swelling stress in an isotropic system is directly proportional to the humidity expansion coefficients and tensile moduli. Incremental Linear Elasticity Theory describes this relationship:

$$E[d\varepsilon_{ij} - \delta_{ij}(\alpha dT + \beta dRH)] = (1+\nu)d\sigma_{ij} - \nu\delta_{ij}d\sigma_{kk} \qquad (2.1)$$

where,

E = tensile modulus	ε_{ij} = strain
δ_{ij} = Kronecker delta	α = thermal expansion coefficient
d = differential operator	T = temperature
β = humidity expansion coefficient	RH = relative humidity
ν = Poisson's ratio	σ_{ij} = stress

In a coating, the material is constrained in two dimensions. Therefore, under isothermal conditions, $dT = 0$, and by definition of a two dimensionally constrained, linear elastic, isotropic, homogeneous material, $d\varepsilon_{11} = d\varepsilon_{22} = 0$ and $d\sigma_{11} = d\sigma_{22} = d\sigma$. This reduces Equation (2.1) to:

$$-[E\beta/(1 - \nu)] = d\sigma/dRH \qquad (2.2)$$

This describes the dependence of the stress in the coating with relative humidity. It is often assumed that the material constants are independent of humidity changes. Therefore, as the humidity is increased, the stress in the coating would decrease.

Analogously for constant humidity conditions, $dRH = 0$, Equation (2.1) becomes:

$$-[E\alpha/(1 - \nu)] = d\sigma/dT \qquad (2.3)$$

In this case, the ratio of the two dimensional stress to the temperature is proportional to the product of the stiffness and thermal expansion coefficient.

For a one dimensionally constrained strip under isothermal conditions, $dT = 0$, $d\sigma_{22} = d\sigma_{33} = 0$, $d\varepsilon_{11} = 0$ and $d\sigma_{11} = d\sigma$, equation (2.1) is now written as:

$$-[E\beta] = d\sigma/dRH \qquad (2.4)$$

By combining equations (2.2) and (2.4), Poisson's ratio can be determined using equation (2.5):

$$\upsilon = (1 - \frac{\sigma_{1D}}{\sigma_{2D}}) \qquad (2.5)$$

Stress as a function of environmental conditions, ie., temperature and humidity, can be resolved by determining the expansion coefficients and tensile modulus of the isotropic coating. There are several techniques which quantify the stress as a function of temperature and humidity [10-15]. Chapter 5 provides an outline of some of these techniques and highlights their advantages and disadvantages.

Incremental linear elasticity is used to quantify the stress in an isotropic coating, but the dimensional instability in the coating/substrate system is best described by modelling this two dimensional system using a modification to Classical Lamination Theory.

Two Dimensional Bending Model

Historically, the dependence of relative humidity on the stress and therefore the dimensional instability in a multilayered system has been a great concern in the photographic industry and more recently in the aerospace and electronics industries [16-27]. Mathematical models depicting the dimensional instability observed as bending have been proposed. Although, these models provide close correlation to the actual observation, they have been primarily limited to one dimensional systems [18,21,26,27].

The bending curvature dependence on relative humidity observed in this investigation was described earlier and depicted in Figure 2.1. It is apparent that the one

dimensional models presented above would not adequately describe the bending inversion observed in the gelatin/cellulose acetate bilayer.

Therefore, a two dimensional model is proposed to predict the bending curvature of a coating/substrate bilayer subjected to various relative humidities. This mathematical model is based on a non-linear modification of classical lamination theory.

A derivation of classical lamination theory has been presented by Jones [28]. Lamination theory is extensively applied in understanding the stresses and strains in laminated composite systems. It is commonly used to predict the response of laminates under external and thermal loads. The basic assumptions of this theory are [29]:

(a.) The width and the length of the laminate must be much larger than the thickness, (width, length >> thickness).

(b.) A perfect interlaminar bond must exist between the laminas. Therefore the strains in each lamina at the interface are equivalent.

(c.) The strain distribution in the thickness direction is linear.

(d.) Continuum mechanics applies. Therefore, the laminas are macroscopically homogeneous.

(e.) The laminas are linear elastic.

(f.) A line perpendicular to the neutral axis before deformation remains perpendicular after deformation (Kirchoff's Hypothesis).

The general equations have been widely published [28-33]. These equations will not be reiterated in this text but will be communicated as required in the development of the two dimensional model.

Classical lamination theory predicts the shapes of unsymmetrical laminates as saddle structures. Figure 2.3 illustrates this predicted shape. Observations documenting cylindrical shapes in cured unsymmetrical laminates have been published [34]. These shapes do not conform to the classical lamination theory.

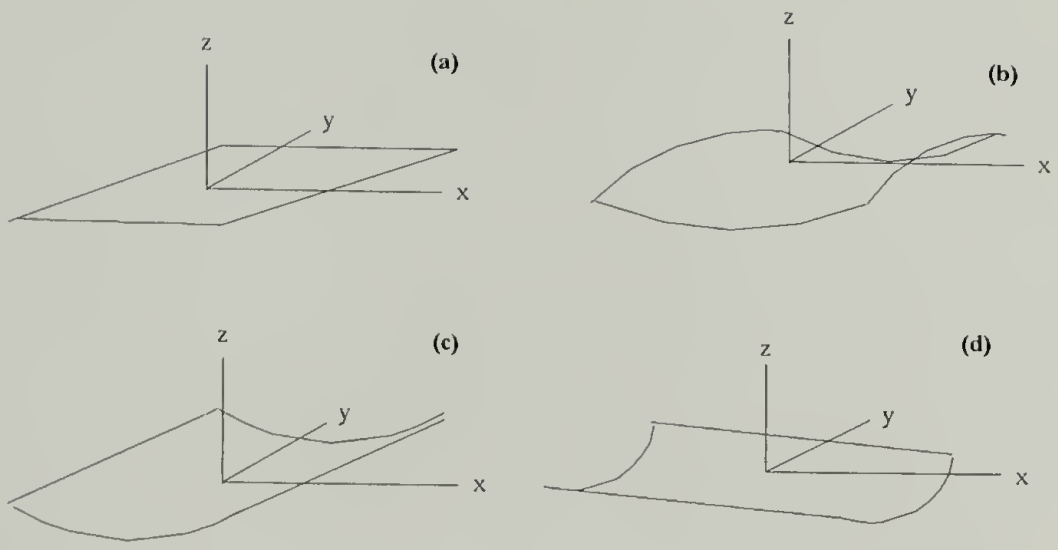

Figure 2.3 Possible shapes in an unsymmetrical laminate: (a) flat, room temperature shape, (b) saddle shape predicted by classical lamination theory, (c) & (d) observed cylindrical shapes. Note: cylindrical shapes illustrated in (c) & (d) depict the same bending phenomenon observed in the coating/substrate system represented in Figure 2.1.

In 1981, Hyer [35] proposed a non-linear mathematical modification to the classical lamination theory that represents the cylindrical structures. His model predicts the response of unsymmetrical laminates subjected solely to thermal loads.

The two dimensional bending model derived in the remainder of this chapter is based on Hyer's work and is designed to predict the response of a coating/substrate bilayer as a result of swelling due to relative humidity changes.

The Theorem of Minimum Potential Energy [30] is applied to the case of pure bending. The observed shapes are associated with the minimum energy in the system. Swelling is purely dilatational and in the observed bending case, the shear stresses are non-existent [31]. For a generalized elastic body, the potential energy is the summation of the strain energy of the elastic body, the work done by the surface tractions and the work done by the body forces. Mathematically, this is represented in equation (2.6) [30]:

$$W = \int_{volume} \omega dV - \int_{surface} T_i U_i dS - \int_{volume} F_i U_i dV \qquad (2.6)$$

where,

W = potential energy

V = volume of the system

U_i = i^{th} component of the deformation

F_i = i^{th} component of body force

ω = strain energy density function

T_i = i^{th} component of the surface traction

S = surface over which tractions apply

In the absence of external loads and body forces, the Minimum Potential Energy equation is reduced to:

$$W = \int_{vol} \omega dV \qquad (2.7)$$

with the strain energy density function described by equation (2.8):

$$\omega = \frac{1}{2} C_{ijkl} e_{ij} e_{kl} - \gamma_{ij} e_{ij} \Delta RH \qquad (2.8)$$

where,

C_{ijkl} = elastic constants of the material

e_{ij} = strains in the material

γ_{ij} = coefficients are related to the elastic coefficients, C_{ijkl}, and the humidity expansion coefficient, β.

ΔRH = relative humidity gradient

Assuming that the system undergoes a translation, e^{o}_{ij}, and rotation, z, about the midplane as a result of loading, the bending curvature is related to the strains through equations (2.9 - 2.11) for the two dimensional case, i, j = 1, 2:

$$e_{11} = e^{o}_{11} - z\frac{\partial^2 w}{\partial x^2} \qquad (2.9)$$

$$e_{22} = e^{o}_{22} - z\frac{\partial^2 w}{\partial y^2} \qquad (2.10)$$

$$e_{12} = e^{o}_{12} - z\frac{\partial^2 w}{\partial x \partial y} \qquad (2.11)$$

In general, the kinematic relations are linear in the small strain regime. In the proposed model, the strain - displacement equations are given non-linear solutions in order to approximate the bending phenomenon. This approximation assumes the elongation and shearing strains and the squares of the rotations are the same order of magnitude and are small compared with unity [34].

$$e_{11}^{o} = \frac{\partial u}{\partial x} + \frac{1}{2}\left(\frac{\partial w}{\partial x}\right)^2 \tag{2.12}$$

$$e_{22}^{o} = \frac{\partial v}{\partial y} + \frac{1}{2}\left(\frac{\partial w}{\partial y}\right)^2 \tag{2.13}$$

$$e_{12}^{o} = \frac{1}{2}\left(\frac{\partial u}{\partial y} + \frac{\partial v}{\partial x} + \left(\frac{\partial w}{\partial x}\right)\left(\frac{\partial w}{\partial y}\right)\right) \tag{2.14}$$

where,

z = 0 at the midplane of the bilayer system

u = laminate midplane displacement in the x-direction

v = laminate midplane displacement in the y-direction

w = out of plane displacement of the midplane

Using large (Lagrangian) strain, the strain - displacement equations allow for the departure from classical lamination theory. The elastic constants, C_{ijkl}, are related to the reduced stiffness constants, $\overline{Q}_{ij}$, and the coefficient, γ_{ij}, relates the reduced stiffness, $\overline{Q}_{ij}$, to the humidity expansion coefficient, β_k. The reduced stiffnesses are detailed in equations (2.15 and 2.16).

$$
\begin{aligned}
Q_{11} &= E_{11}(1-\nu_{23}\nu_{32})/\Delta \\
Q_{22} &= E_{22}(1-\nu_{31}\nu_{13})/\Delta \\
Q_{33} &= E_{33}(1-\nu_{12}\nu_{21})/\Delta \\
Q_{12} &= E_{11}(\nu_{21}+\nu_{31}\nu_{23})/\Delta = E_{22}(\nu_{12}+\nu_{13}\nu_{32})/\Delta \\
Q_{13} &= E_{11}(\nu_{31}+\nu_{21}\nu_{32})/\Delta = E_{22}(\nu_{13}+\nu_{12}\nu_{23})/\Delta \\
Q_{23} &= E_{22}(\nu_{32}+\nu_{21}\nu_{31})/\Delta = E_{22}(\nu_{23}+\nu_{21}\nu_{13})/\Delta \\
Q_{44} &= G_{23} \\
Q_{55} &= G_{13} \\
Q_{66} &= G_{12} \\
\Delta &= 1-\nu_{12}\nu_{21}-\nu_{23}\nu_{32}-\nu_{31}\nu_{13}-2\nu_{12}\nu_{32}\nu_{13}
\end{aligned}
\qquad (2.15)
$$

where, ν_{ij} is Poisson's ratio and E_{ij} and G_{ij} are the tensile and shear moduli, respectively.

For the observed bending phenomenon, the transverse shear deformation and transverse normal stresses can be neglected, reducing equation (2.15) to equation (2.16).

$$
\begin{aligned}
\overline{Q}_{11} &= Q_{11}m^4+2(Q_{12}+2Q_{66})m^2n^2+Q_{22}n^4 \\
\overline{Q}_{12} &= (Q_{11}+Q_{22}-Q_{66})m^2n^2+Q_{12}\left(m^4+n^4\right) \\
\overline{Q}_{22} &= Q_{11}n^4+2(Q_{12}+2Q_{66})m^2n^2+Q_{22}m^4 \\
\overline{Q}_{66} &= (Q_{11}+Q_{22}-2Q_{12})m^2n^2+Q_{66}\left(m^2-n^2\right)^2
\end{aligned}
\qquad (2.16)
$$

where, $m = \cos\theta$ and $n = \sin\theta$ which relates the Q_{ij}'s to the x, y, z axis. θ equals zero for a coating/substrate bilayer in which the principal axis align with the x, y, z axes. The stiffness matrix, Q_{ij}, for the two dimensional case is reduced to equation (2.17):

$$Q_{ij} = \begin{bmatrix} \dfrac{E_{11}}{1 - \nu_{12}\nu_{21}} & \dfrac{\nu_{12}E_{22}}{1 - \nu_{12}\nu_{21}} & 0 \\ \dfrac{\nu_{21}E_{11}}{1 - \nu_{12}\nu_{21}} & \dfrac{E_{22}}{1 - \nu_{12}\nu_{21}} & 0 \\ 0 & 0 & G_{12} \end{bmatrix} \tag{2.17}$$

Equation (2.8) can be expanded by substitution of these relationships to yield:

$$\begin{aligned} \omega = {} & \frac{1}{2}\overline{Q}_{11}e_{11}^2 + \overline{Q}_{12}e_{11}e_{22} + 2\overline{Q}_{66}e_{12}^2 + \frac{1}{2}\overline{Q}_{22}e_{22}^2 \\ & -\left(\overline{Q}_{11}\beta_x^b + \overline{Q}_{12}\beta_y^b\right)e_{11}\Delta RH - \left(\overline{Q}_{12}\beta_x^b + \overline{Q}_{22}\beta_y^b\right)e_{22}\Delta RH \end{aligned} \tag{2.18}$$

Now that the strain energy density function has been determined, the deformations, u, v, and w as a function of x and y must be selected to minimize the potential energy, W. Since only an approximate solution is sought, the following assumptions are made:

(a.) In attaining the cylindrical shapes, the midplane elongation strains, e_{11}^o and e_{22}^o are independent of x and y and therefore do not vary much from linearity.

(b.) The midplane shear strains are negligible ($e_{12}^o = 0$) since the swelling is purely dilatational.

Mathematical non-linearity (as opposed to material non-linearity) is introduced by adopting the form of deformation, w(x,y) as:

$$w(x,y) = \frac{1}{2}\left(ax^2 + by^2\right) \tag{2.19}$$

As a result, the cylindrical shapes can be resolved. The axes of bending curvature are related to constants a and b. In classical lamination theory, a = -b represents the saddle geometry. Using equation (2.18), the two cylindrical geometries are defined when a = 0, b ≠ 0and a ≠ 0, b = 0. The choice of the approximate solutions for the deformations, u° and v°, is influenced by the nature of the observed geometries and must force the shear strain, e_{12}^o, to equal zero. Equations (2.20) and (2.21) represent these solutions:

$$u(x,y) = cx - \frac{a^2x^3}{6} - \frac{abxy^2}{4} \tag{2.20}$$

$$v(x,y) = dy - \frac{b^2y^3}{6} - \frac{abx^2y}{4} \tag{2.21}$$

where, c and d are constants. Incorporating equations (2.20 and 2.21) into equations (2.12 - 2.14) yields:

$$e^o_{11} = c - \frac{aby^2}{4} \tag{2.22}$$

$$e^o_{22} = d - \frac{abx^2}{4} \tag{2.23}$$

$$e^o_{12} = 0 \tag{2.24}$$

Equations (2.22 - 2.24) are inserted into equations (2.9 - 2.11):

$$e_{11} = c - \frac{aby^2}{4} - z\frac{\partial^2 w}{\partial x^2} \tag{2.25}$$

$$e_{22} = d - \frac{abx^2}{4} - z\frac{\partial^2 w}{\partial y^2} \tag{2.26}$$

$$e_{12} = 0 - \frac{\partial^2 w}{\partial x \partial y} \tag{2.27}$$

Recalling the deformation relationship introduced in equation (2.19), the strains are reduced to:

$$e_{11} = c - \frac{aby^2}{4} - za \tag{2.28}$$

$$e_{22} = d - \frac{abx^2}{4} - zb \tag{2.29}$$

$$e_{12} = 0 \tag{2.30}$$

a, b, c, and d are generalized coordinates and must be determined. The minimum of the potential energy, W, is now calculated by finding solutions to a, b, c, and d so that the first variation of W is zero. This is accomplished by applying equation (2.31):

$$\delta W = \left(\frac{\partial W}{\partial a}\right)\delta a + \left(\frac{\partial W}{\partial b}\right)\delta b + \left(\frac{\partial W}{\partial c}\right)\delta c + \left(\frac{\partial W}{\partial d}\right)\delta d = 0 \tag{2.31}$$

The application of this derivation is now applied to a bilayer system consisting of a coating on a substrate. This system is depicted in Figure 2.4.

For the x, y and z coordinate system, the following integration limits are applied:

$$-\frac{L_x}{2} \le x \le \frac{L_x}{2} \tag{2.32}$$

$$-\frac{L_y}{2} \le y \le \frac{L_y}{2} \tag{2.33}$$

$$h_{k-1} \le z \le h_k \tag{2.34}$$

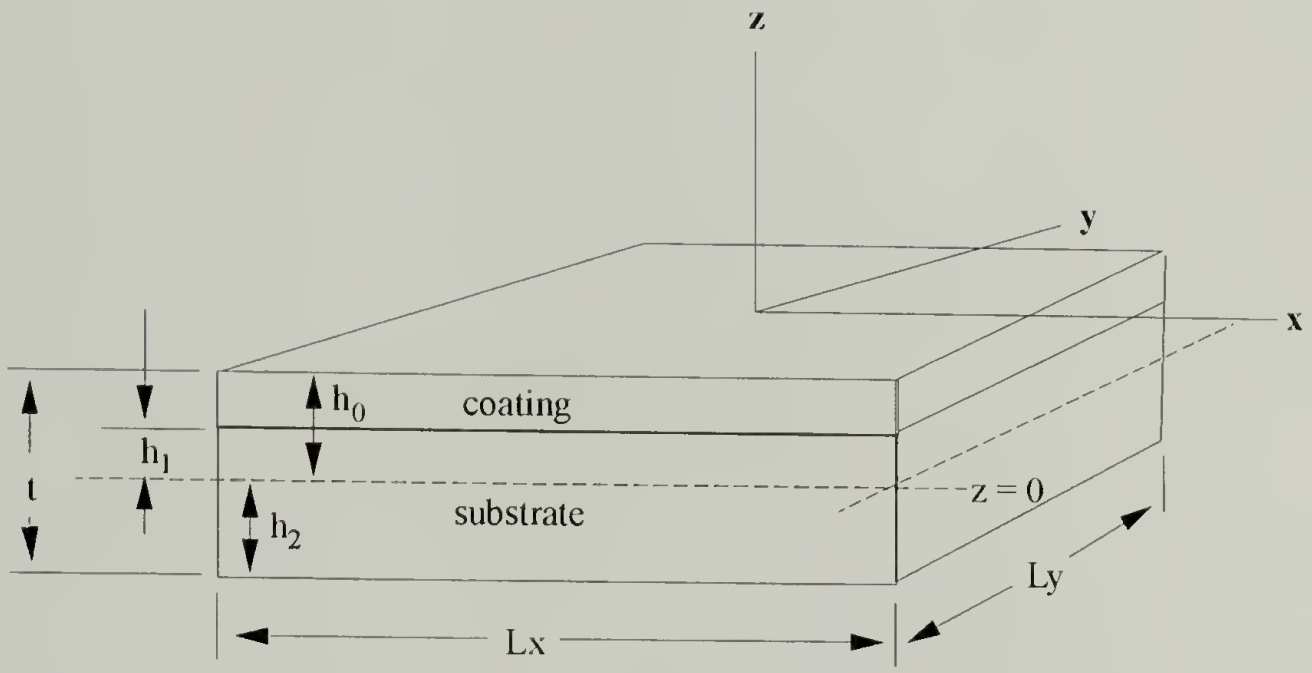

Figure 2.4 Bilayer system of a coating on a substrate. This system represents the bilayer studied in this investigation. The midplane is positioned at z = 0.

where,

Lx, Ly = the lengths of the sides of the bilayer system along the x and y axis, respectively

h = thickness

k = 1, 2

Equation (2.7) is now written as:

$$W=\sum_{k=1}^{2}\int_{h_{k-1}}^{h_k}\int_{-L_y/2}^{L_y/2}\int_{-L_x/2}^{L_x/2}\omega\left(a,b,c,d,\overline{Q}_{ij},\beta_x^b,\beta_y^b,\Delta RH,x,y,z\right)dxdydz \qquad (2.35)$$

Substituting equations (2.22 - 2.24) into the strain energy density equation (2.18):

$$\begin{aligned}\omega=&\frac{1}{2}\overline{Q}_{11}\left(c^2-\frac{abcy^2}{2}-2acz+\frac{a^2b^2y^4}{16}+\frac{a^2by^2z}{2}+a^2z^2\right)\\&+\overline{Q}_{12}\left(cd-\frac{abcx^2}{4}-bcz+\frac{a^2b^2x^2y^2}{16}-\frac{abdy^2}{4}+\frac{ab^2y^2z}{4}-adz+\frac{a^2bx^2z}{4}+abz^2\right)\\&+\frac{1}{2}\overline{Q}_{22}\left(d^2-\frac{abdx^2}{2}-2bdz+\frac{a^2b^2x^4}{16}+\frac{ab^2x^2z}{2}+b^2z^2\right)\\&-\left(\overline{Q}_{11}\beta_x^b+\overline{Q}_{12}\beta_y^b\right)\left(c-\frac{aby^2}{4}-az\right)\Delta RH\\&-\left(\overline{Q}_{12}\beta_x^b+\overline{Q}_{22}\beta_y^b\right)\left(d-\frac{cdx^2}{4}-bz\right)\Delta RH\end{aligned} \qquad (2.36)$$

In lamination theory, the stiffness matrices, Aij, Bij, and Dij are related to the reduced stiffness, $\overline{Q}_{ij}$ [29]. For the coating/substrate system, the system stiffness matrices can be similarly calculated. The stiffness elements are calculated from:

$$A_{ij} = \sum_{k=1}^{2} \int_{h_{k-1}}^{h_k} \overline{Q}_{ij} dz \tag{2.37}$$

$$B_{ij} = \sum_{k=1}^{2} \int_{h_{k-1}}^{h_k} \overline{Q}_{ij} z dz \tag{2.38}$$

$$D_{ij} = \sum_{k=1}^{2} \int_{h_{k-1}}^{h_k} \overline{Q}_{ij} z^2 dz \tag{2.39}$$

A_{ij} is the extensional stiffness matrix for the bilayer. B_{ij} is the coupling stiffness matrix for the bilayer and D_{ij} is the bending stiffness matrix for the bilayer.

In addition, the in-plane swelling loads, N_x^H and N_y^H, and the swelling moments, M_x^H and M_y^H, are defined in equations (2.40 - 2.43):

$$N_x^H = \Delta RH \sum_{k=1}^{2} \int_{h_{k-1}}^{h_k} \left(\overline{Q}_{11} \beta_x^b + \overline{Q}_{12} \beta_y^b \right) dz \tag{2.40}$$

$$N_y^H = \Delta RH \sum_{k=1}^{2} \int_{h_{k-1}}^{h_k} \left(\overline{Q}_{12} \beta_x^b + \overline{Q}_{22} \beta_y^b \right) dz \tag{2.41}$$

$$M_x^H = \Delta RH \sum_{k=1}^{2} \int_{h_{k-1}}^{h_k} \left(\overline{Q}_{11} \beta_x^b + \overline{Q}_{12} \beta_y^b \right) z dz \tag{2.42}$$

$$M_y^H = \Delta RH \sum_{k=1}^{2} \int_{h_{k-1}}^{h_k} \left(\overline{Q}_{12} \beta_x^b + \overline{Q}_{22} \beta_y^b \right) z dz \tag{2.43}$$

Using equation (2.31), take the first variation of equation (2.36) to yield a function [35]:

$$\delta W = f_1(a,b,c,d)\delta a + f_2(a,b,c,d)\delta b + f_3(a,b,c,d)\delta c + f_4(a,b,c,d)\delta d \tag{2.44}$$

From equation (2.44), f_1, f_2, f_3 and f_4 were determined as:

$$f_1 = 0 = \frac{N_x^{II} L_y^2 b}{48} + M_x^{II} + \frac{N_y^{II} L_x^2 b}{48} - J_1 bc + J_2 ab^2 + J_3 bc + J_4 ab^2 + J_5 bd + J_6 bd + J_7 ab^2 - B_{11} c + 2J_8 ab + J_9 b^2 - B_{12} d + 2J_{10} ab + D_{12} b + J_{11} b^2 + D_{11} a \quad (2.45)$$

$$f_2 = 0 = \frac{N_x^{II} L_y^2 a}{48} + M_y^{II} + \frac{N_y^{II} L_x^2 a}{48} - J_1 ac + J_2 a^2 b + J_3 ac + J_4 a^2 b + J_5 ad + J_6 ad + J_7 ab^2 + J_8 a^2 + B_{12} c + 2J_9 ab + J_{10} a^2 + D_{12} a - B_{22} d + 2J_{11} ab + D_{22} b \quad (2.46)$$

$$f_3 = 0 = -N_x^{II} + A_{11} c - J_1 ab + A_{12} d + J_3 ab - B_{11} a + B_{12} b \quad (2.47)$$

$$f_4 = 0 = -N_y^{II} + A_{12} c - J_5 ab + A_{22} d + J_6 ab - B_{12} a + B_{22} b \quad (2.48)$$

where,

$$J_1 = \frac{A_{11} L_y^2}{48} \qquad J_2 = \frac{A_{11} L_y^4}{1280}$$

$$J_3 = \frac{A_{12} L_x^2}{48} \qquad J_4 = \frac{A_{12} L_x^2 L_y^2}{1152}$$

$$J_5 = \frac{A_{12} L_y^2}{48} \qquad J_6 = \frac{A_{22} L_x^2}{48}$$

$$J_7 = \frac{A_{22} L_x^4}{1280} \qquad J_8 = \frac{B_{11} L_y^2}{48}$$

$$J_9 = \frac{B_{12} L_y^2}{48} \qquad J_{10} = \frac{B_{12} L_x^2}{48}$$

$$J_{11} = \frac{B_{22} L_x^2}{48}$$

By arranging equations (2.47) and (2.48) in terms of c and d and incorporating these equations into equations (2.45) and (2.46), they can be written in terms of a and b. The solutions to these equations are determined numerically.

The numerical solution is dependent upon the moduli and the humidity expansion coefficients for each layer. In chapters 3 and 4, these properties are characterized for a bilayer system consisting of a gelatin coating on a cellulose acetate substrate. Application of this model to a bilayer system subjected to various humidities is presented in chapter 7.

In order for the model to be valid, the mid-plane of the bilayer system must be a developable surface [32] and the second variation of the total potential energy, $\delta^2 W$, must be positive definite [36].

In pure bending, it is assumed that the mid-plane is the neutral surface of the system. This condition is satisfied only if the thickness of the bilayer system is small in comparison to the radius of bending curvature. If the bilayer is bent to an undevelopable surface, then the mid-plane would have to compensate by stretching during the bending.

For a stable geometric shape, the total potential energy must be minimized. This requires the coefficients of the matrix of the second variation, $\delta^2 W$, be positive definite. Stability theory is discussed in detail elsewhere [36].

The following chapters will present the techniques employed to characterize the bilayer materials. Results of these experiments will incorporated into the numerical analysis of the two dimensional bending model.

References

1. D.Y. Perera, and D.V. Eynde, "Moisture and Temperature Induced Stresses (Hygrothermal Stresses) in Organic Coating," J. of Coatings Technology, **59**(748), 55 (1987).

2. S.G. Croll, "The Origin of Residual Internal Stress in Solvent-Cast Thermoplastic Coatings," Journal of Applied Polymer Science, **23**(3), 847 (1979).

3. C.L. Bauer, R.J. Farris and M.S. Vratsanos, "Determination of the Stresses and Properties of Polymer Coatings," Journal of Coatings Technology, **60**(760), 51 (1988).

4. S. Sackinger, The Determination of Swelling Stresses in Polyimide Films, Ph.D. diss., University of Massachusetts, Amherst, MA, (1990).

5. I.C. Noyan and J.B. Cohen, Residual Stress: Measurement by Diffraction and Interpretation, (New York: Springer-Verlag, 1987).

6. J.F. Taylor, An Experimental Evaluation of the State of Stress and Mechanical Performance of a Polyacrylate Photoresist Coating, Ph.D. diss., University of Massachusetts, Amherst, MA, (1993).

7. E.M. Corcoran, "Determining Stresses in Organic Coatings Using Plate Beam Deflection," Journal of Paint Technology, **41**(538), 635 (1969).

8. K. Sato, "The Internal Stress in Coating Films," Progress in Organic Coatings, **8**, 143 (1980).

9. B.J. Aleck, "Thermal Stresses in a Rectangular Plate Clamped Along an Edge," Journal of Applied Mechanics, **16**, 118 (1949).

10. C.S. Jou, Stresses Associated with Transport in Polymeric Films, Ph.D. diss., University of Massachusetts, Amherst, MA, (1993).

11. M.H. Chipalkatti, Stresses and Deformation Coupled Moisture Transport in Polymers, Ph.D. diss., University of Massachusetts, Amherst, MA, (1988).

12. T.P. Weibs, S. Hong, J.C. Bravman and W.D. Nix, "Mechanical Defection of Cantilever Microbeams: A New Technique for Testing the Mechanical Properties of Thin Films," Journal of Materials Reseach, **3**(5), 931 (1988).

13. D.S. Campbell, "Mechanical Properties of Thin Films," Handbook of Thin Film Technology, eds. L.I. Maissel and R. Glang, (New York: McGraw Hill Book Co., 1988).

14. P. Singer, "Film Stress and How to Measure It," Semiconductor International, (October 1992).

15. M.A. Maden, The Determination of Stresses and Material Properties of Polyimide Coatings and Films Using Real Time Holographic Interferometry, Ph.D. diss., University of Massachusetts, Amherst, MA, (1992).

16. J.M. Calhoun, "The Physical Properties and Dimensional Behavior of Motion Picture Film," Journal of the Society of Motion Picture Engineering, **43**, 227 (1944).

17. J.M. Calhoun, "The Physical Properties and Dimensional Stability of Safety Aerographic Film," Photogrammetric Engineering, **13**, 163 (1947).

18. J.Q. Umberger, "The Fundamental Nature of Curl and Shrinkage in Photographic Films," Photographic Science and Engineering, **1**(2), 69 (1957).

19. "Physical Properties of Kodak Aerial Films," Properties of Kodak Materials for Aerial Photographic Systems, Vol. II, (Rochester, NY: Eastman Kodak Co., 1972).

20. J.M. Calhoun and D.A. Leister, "Effect of Gelatin Layers on the Dimensional Stability of Photographic Film," Photographic Science and Engineering, **3**(1), 8 (1959).

21. J.M. Centa, "Effect of Base and Emulsion Thickness on Dimensional Stability of Graphic Arts Films," Proceeding of the Annual Technical Meeting: Technical Associates of Graphic Arts, **8**, 75 (1956).

22. R.B. Pipes, J.R. Vinson and T.W. Chou, "On the Hygrothermal Response of Laminated Composite Systems," Journal of Composite Materials, **10**, 129 (1976).

23. J.M. Whitney and J.E. Ashton, "Effect of Environment on the Elastic Response of Layered Composite Plastics," AIAA Journal, **9**, 9 (1971).

24. "Effects of Relative Humidity and Elevated Temperatures on Composite Structures," Proceedings of the AFOSR Workshop, Newark, DE, March (1976).

25. D.L. Flaggs, Elastic Stability of Generally Laminated Composite Plates Including Hygrothermal Effects, M.MMAE. thesis, University of Delaware, Newark, DE, (1977).

26. B.S. Berry and W.C. Pritchet, "Bending-Cantilever Method for the Study of Moisture Swelling in Polymers," IBM Journal of Research and Development, **28**(6), 662 (1984).

27. T.Z. Fu, C.J. Durning and H.M. Tong, "Simple Model for Swelling-Induced Stresses in a Supported Polymer Thin Film," Journal of Applied Polymer Science, **43**, 709 (1991).

28. R.M. Jones, Mechanics of Composite Materials, (New York: McGraw-Hill Book Co. 1975).

29. P.K. Mallick, Fiber-Reinforced Composites, (New York: Marcel Dekker, Inc., 1988).

30. J.R. Vinson, Structural Mechanics: The Behavior of Plates and Shells, (New York: John Wiley & Sons, Inc., 1974).

31. J.R. Vinson and R.L. Sierakowski, The Behavior of Structures Composed of Composite Materials, (Boston, MA: Kluwer Academic Publishers, 1993).

32. S. Timoshenko and S. Woinowsky-Krieger, Theory of Plates and Shells, 2nd ed., (New York: McGraw-Hill Book Co., 1959).

33. S.W. Tsai and H.T. Hahn, Introduction to Composite Materials, (Westport, CT: Technomic Publishing Co., 1980).

34. H.W. Hyer, "Some Observations on the Cured Shape of Thin Unsymmetric Laminates," Journal of Composite Materials, **15**, 175 (1981).

35. H.W. Hyer, "Calculations of Room-Temperature Shapes of Unsymmetric Laminates," Journal of Composite Materials, **15**, 296 (1981).

36. G.J. Simitses, An Introduction to the Elastic Stability of Structure, (Englewood, NJ: Prentice-Hall, Inc., 1976).

CHAPTER 3

MATERIAL PROPERTIES

Introduction

The preceding chapter outlined incremental linear elasticity theory and applied a modified version of classical lamination theory in the development of a two dimensional bending model for a bilayer system. Both of these theories require knowledge of the tensile and shear moduli, Poisson's ratio, and thermal and humidity expansion coefficients of the coating and substrate materials. This chapter will discuss the methods employed for determining these material properties (humidity expansion will be addressed in chapter 4) as well as the results of the experiments. Background pertaining to the materials and details regarding the use of saturated binary aqueous salt solutions to generate relative humidity are also highlighted.

Experimental

Materials

The materials used throughout this investigation are tabulated in Table 3.1. An alkaline processed bone gelatin coating on either cellulose acetate, CA, or poly(ethylene terephthalate), PET are the primary bilayer systems investigated.

Table 3.1. List of coating materials investigated on corresponding substrates.

Coating Materials	Density (g/cc)	Coating Substrate	Density (g/cc)
[a,b]Alkaline Processed Bone Gelatin	1.428	[b,c]Cellulose Acetate, CA	1.291
[a,b,d]Poly(vinyl alcohol), PVOH	1.27	[b]Poly(ethylene terephthalate), PET	1.40
[c]Bisphenol A Epoxy	1.10	Tin Plated Steel	n/a
[f]Polyimide	1.425	Glass	n/a
[b,g]Nickel	8.90	Tin Plated Steel	n/a
[b,g]Copper	8.92	Acrylate Base Photoresist on a Silicon Wafer	n/a

[a] density determined via comparison with known solvent densities
[b] weight per volume method used to measure density
[c] [1], [d] [2] ,[e] [3], [f] [4], [g] [5]

Gelatin Coating on Cellulose Acetate or Poly(ethylene terephthalate) Substrate. The alkaline processed bone gelatin coated on cellulose acetate and PET was provided by the Eastman Kodak Co., Rochester, NY. The physical properties of photographic materials are outlined in several sources [6-9].

Chapter 1 provides a detailed summary about gelatin. In general, gelatin is very sensitive to moisture. It is manufactured from the protein of collagen and used as a colloid protector in photographic applications [10,11]. Gelatin is a random coil system comprised of a series of amino acids. It has a high propensity to absorb moisture due to the hydrogen bonding of the water molecules to the hydrophilic amino acid groups. The properties of gelatin are controlled by crosslinking and varying the degree of crystallinity [11-16]. Gelatin absorbs 9 - 15% of moisture at 50%RH [17]. Moisture sorption

hysteresis, that is the separation of moisture sorption and desorption isotherms, is a common phenomenon in gelatins [18]. Therefore the material characteristics are dependent upon the sorption path (ie. whether measured along the moisture desorption or absorption path).

Cellulose acetate is commonly prepared by a solution process employing sulfuric acid as the catalyst with acetic anhydride in an acetic acid solvent [1]. Cellulose acetate is hydrophilic , absorbing 2 - 6.5% water in 24 hours [1].

The poly(ethylene terephthalate), PET, studied is manufactured by the Eastman Kodak Co. under the trade name, ESTAR®. It is biaxially oriented and has a crystallinity of 34.2% as determined by wide angle x-ray and differential scanning calorimetry methods. PET absorbs 0.45% moisture at 54% RH [7].

Poly(vinyl alcohol) Coating on Poly(ethylene terephthalate) Substrate. The poly(vinyl alcohol) used in this investigation is a fully hydrolyzed grade polymer, designated as Airvol® 325, and was supplied by Air Products and Chemicals, Inc. A 10% w/w PVOH (containing no additives) was blade coated on a PET substrate and dried at 54%RH, 21°C for 24 hours. This grade of PVOH is used commercially in spin sizing of textiles, adhesives for envelopes, bookbinding, carton sealing and cigarette filters, surface sizing and pigment coating in paper production and as films and molded products [2].

PVOH is produced by the hydrolysis of poly(vinyl acetate). The amount of moisture absorbed is dependent upon the percent hydrolysis. The resistance to humidity decreases with increased hydrolysis. A fully hydrolyzed PVOH is 98.0 - 98.8 mol. % hydrolyzed [2,19].

Epoxy Coating on Tin Plated Steel Substrate. A diglycidyl ether of bisphenol A epoxy, Shell's Epon® 828 resin, was combined with their V40 crosslinking agent, a

polyamide, and spin coated onto tin-plated steel. It was cured on a hot plate at 54%RH, 70°C for 2 hours.

Epoxies have tendency to absorb water with the amount absorbed dependent upon functionality and choice of crosslinking agent. The Epon 828® crosslinked with the V40 curing agent absorbs 3.9% moisture at elevated temperatures [3,20].

Polyimide Coating on Glass Substrate and as Free Film. Pyromellitic dianhydride - oxydianiline, PMDA-ODA, polyimide precursor was supplied by the DuPont Corporation, Wilmington, DE. A solution of 20% polyamic acid in NMP was spin coated on glass and sequentially cured under vacuum at 85°C for ½ hour, 150°C for ½ hour followed by a 1 hour cure at 400°C to form a planar isotropic polyimide coating. A free film known as Kapton® was also provided. This polyimide sheet is anisotropic.

PMDA-ODA polyimide cured at 400°C absorbs 3.6% moisture at 85%RH and 21°C [4].

Metal Coatings. Nickel was electroplated onto tin-plated steel by a local plating house. IBM provided the copper coated on photoresist/silicon wafer samples.

Relative Humidity Generation

The mechanical and physical properties of polymers are often affected by temperature and humidity gradients. Relative humidity was controlled using saturated binary aqueous salt solutions. A list of the inorganic salts is provided in Table 3.2.

Table 3.2. Relative humidity generated by binary saturated aqueous solutions [21,22]

Salt	Relative Humidity (%)	Valid Temperature Range (°C)
Lithium Chloride (LiCl)	11 ± 1	0 - 55
Potassium Acetate (CH_3COOK)	22 ± 1	15 - 30
Magnesium Chloride ($MgCl_2$)	32 ± 1	5 - 45
Potassium Carbonate (K_2CO_3)	43 ± 0	0 - 30
Magnesium Nitrate (Mg_2NO_3)	54 ± 3	10 - 30
Sodium Bromide (NaBr)	59 ± 2	15 - 25
Sodium Chloride (NaCl)	75 ± 1	0 - 75
Potassium Chloride (KCl)	81 ± 1	10 - 35
Water	100	5 - 95

The relative humidity is transported to the sample by bubbling a compressed gas through the saturated salt solutions. The compressed gas is either nitrogen or helium depending on the experimental technique used. A schematic of the relative humidity transport system is illustrated in Figure 3.1. A Taylor Humidiguide® hygrometer/thermometer was employed to monitor the humidity and temperature. This hygrometer has a sensitivity of ± 3% RH. Its sole purpose throughout this investigation was to ensure the relative humidity and temperature had reached equilibrium. Compressed gas was passed through Drierite®, $CaSO_4$, to achieve 0%RH. The reported literature values listed in Table 3.2 are used in all calculations.

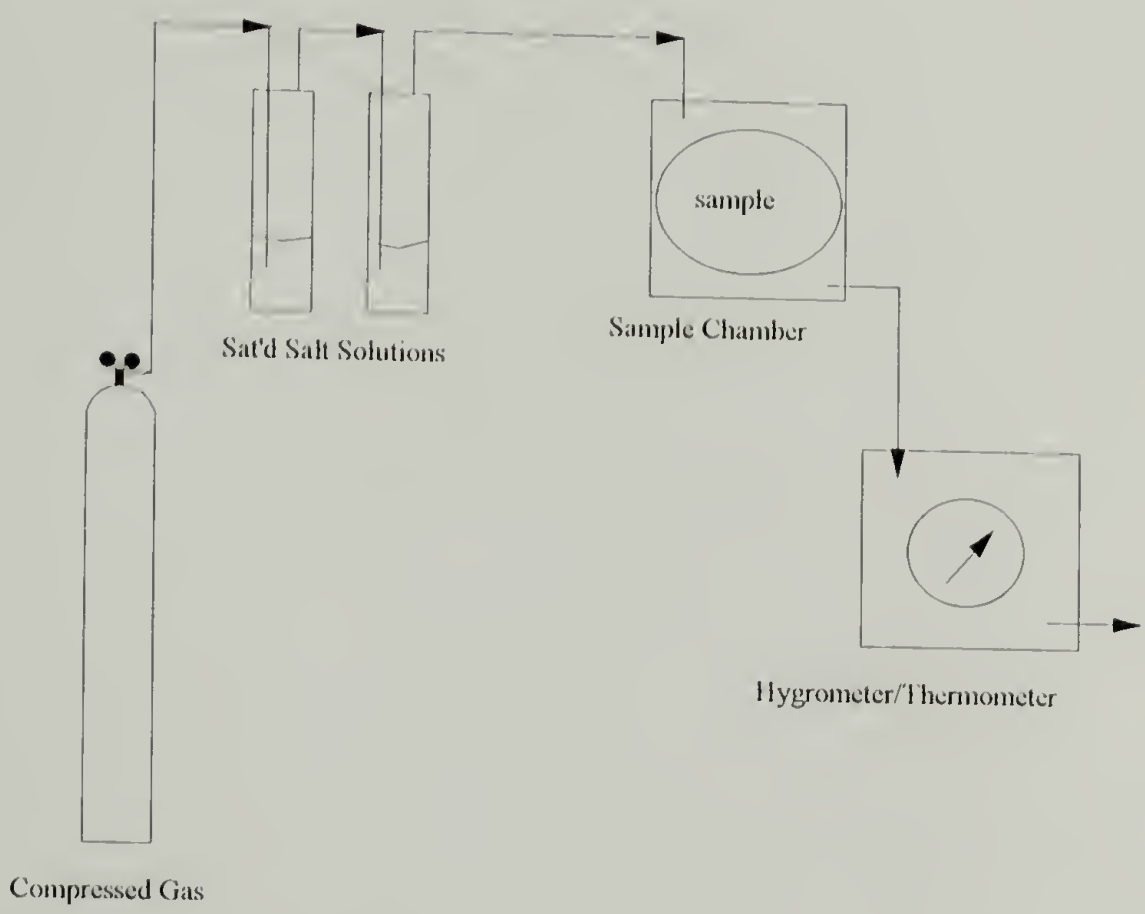

Figure 3.1 Schematic of relative humidity generation system.

Mechanical Properties

Tensile Properties and Machine Compliance. The tensile properties of gelatin and cellulose acetate were investigated as a function of relative humidity using a Toyo Baldwin Tensile Test machine and screw-driven Instron Universal Tensile Test equipment. Machine compliance for each instrument was determined. Young's elastic moduli, yield strength and elongation at break were measured as a function of relative humidity.

For each test, uniaxial samples of gelatin and cellulose acetate were fabricated. The gelatin investigated is an alkaline processed cattle bone gelatin (Kodak designation: SC5-5S-5020-01, Type IV, Class 84 gelatin with 2% Olin 10G surfactant). The 18.6 μm gelatin coating was removed from the 127 μm cellulose acetate substrate (Kodak designation: 20T1-88) for mechanical testing. The length to width ratio of each sample was at least 7:1 (100 mm long by 15 mm wide, on average) to eliminate two dimensional considerations. A 10 pound (Interface Corp. SM-10) load cell was used to measure the force and an LVDT (Linear Variable Differential Transformer) was used to measure the displacement. The strain rate was 1% strain/min. Data was acquired using a PC with an A/D board interface and later analyzed. Figure 3.2 depicts the tensile test set-up modified to introduce varying humidities.

The compliance of the tensile test equipment is an artifact of the equipment design and therefore the results must be corrected. The machine compliance for both tensile testers was determined using uniaxial samples of cellulose acetate and PET. The machine compliance test procedure is outlined in the literature [23,24]. Cellulose acetate samples were used to test the Instron equipment. The width of the cellulose acetate averaged 15 mm and the mean thickness was 127 μm. The gage lengths varied from 102 to 175 mm. Twelve uniaxial samples of each gage length were tested. Similarly, PET was used to study the compliance of the Toyo Baldwin equipment.

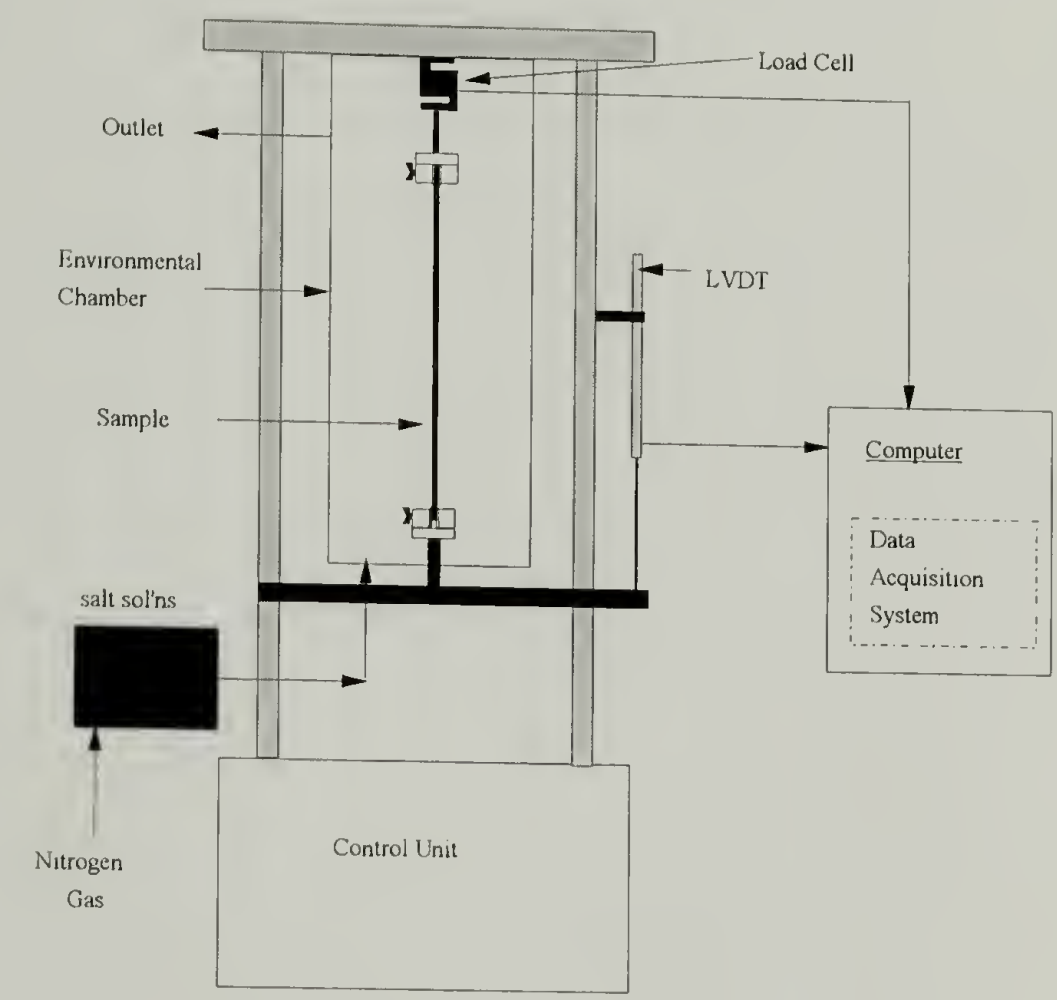

Figure 3.2 Tensile test equipment modified with a relative humidity environmental chamber.

Uniaxial samples of Estar®, PET, were used. The width of these samples averaged 4.5 mm and the mean thickness was 97.4 μm. The gage lengths varied from 50 to 102 mm. A 10 pound (SM-10) load cell was used to measure the force. The crosshead speed was 50 mm/min.

The following equation was used to calculate the machine compliance:

$$C_a = \frac{\delta_T}{F} = C_m + \frac{L_0}{AE} \qquad (3.1)$$

where, C_a = apparent compliance, mm/N

C_m = machine compliance, mm/N

δ_T = total displacement of the machine and sample, mm

F = force, N

L_0 = gage length, mm

A= initial cross sectional area, mm^2

E = tensile modulus, N/mm^2

The y-intercept on a plot of apparent compliance vs. the gage length is the machine compliance. The tensile modulus can then be corrected for the machine compliance which yields equation (3.2):

$$E = \frac{L_0}{A(C_a - C_m)} \qquad (3.2)$$

Other tensile properties (tensile strength, elongation, etc) were determined by standard analysis [25].

Shear Modulus. For a linear elastic, isotropic material, the shear modulus was obtained by the simple relationship between to the tensile modulus and the Poisson's ratio through equation 3.3 [26]:

$$G_{12} = \frac{E}{2(1+\nu_{12})} \tag{3.3}$$

where,

G_{12} = shear modulus in the plane of the coating (GPa)

E = tensile modulus (GPa) (Note: $E = E_{11} = E_{22}$)

ν_{12} = Poisson's ratio in the plane of the coating

For an anisotropic material, the shear modulus in the plane of the film was obtained by measuring the Young's modulus at some angle, θ, to the principal axes. A tensor transformation equation for an orthotropic material is applied which relates the shear modulus to the Young's modulus at angle, θ. The mathematical details are elaborated elsewhere [27].

$$\frac{1}{E_{xx}} = \frac{\cos^4\theta}{E_{11}} + \frac{\sin^4\theta}{E_{22}} + \frac{1}{4}\left(\frac{1}{G_{12}} - \frac{2\nu_{12}}{E_{11}}\right)\sin^2 2\theta \tag{3.4}$$

Uniaxial samples are cut at a 45° angle from the principal axis and the tensile modulus determined as described earlier in the text.

Effect of Moisture Sorption Hysteresis on the Tensile Properties. In general, moisture has a large effect on the mechanical properties of these hydrophilic materials [7,9]. Moisture acts as a plasticizer resulting in reduced strength and increased elongation at break. Several mechanisms regarding moisture sorption have been postulated [28-30]. Moisture sorption hysteresis, that is the separation of moisture sorption and desorption isotherms, is a common phenomenon in moisture sensitive materials [8]. Due to this moisture sorption hysteresis in gelatin, further tensile testing was performed to investigate the elastic moduli's dependence on the sorption path.

The alkaline processed bone gelatin coating investigated (Kodak sample designation: 8244-15) was fully amorphous (0% crystallinity) and free of any crosslinking agent. It was removed from the PET substrate prior to testing. The test sample geometry was 16.0 μm thick and 50 mm long with an average width of 2.75 mm. Four sets of 10 samples were fabricated. Two sets were used for the desorption run and the remaining two for the absorption run.

The tensile test was performed on the samples using the Toyo Baldwin tensile test equipment. The crosshead speed was 20 mm/min. For the desorption run, the gelatin was initially subjected to 54%RH for 1.5 hours, then to 33%RH. After 1.5 hours at 33%RH, the stress as a function of strain was monitored.

Similarly for the absorption run, the gelatin was initially subjected to 0%RH for 1.5 hours, then 33%RH. After 1.5 hours at 33%RH, the stress - strain relationship was determined.

Poisson's Ratio

Poisson's ratio is the ratio of the lateral to axial strains in simple tension. As derived in chapter 2, if a material is isotropic, linear elastic and homogeneous, Poisson's ratio can be determined (for small strains) by applying Incremental Linear Elasticity Theory. Under isothermal conditions, Poisson's ratio is related to the ratio of one dimensional stress to two dimensional stress through equation (3.5):

$$\upsilon = (1 - \frac{\sigma_{1D}}{\sigma_{2D}}) \qquad (3.5)$$

Holographic Interferometry was used to measure the one- and two-dimensional stresses in the material as a function of relative humidity. Chapter 5 offers a more detailed

explanation of the Holographic Interferometry technique. In general, the technique is based on Vibrating Membrane Theory [31]. For a circular geometry, the vibrating membrane equation reduces to:

$$\sigma_{2D} = 4\pi^2 \rho R^2 \frac{\upsilon_{ni}^2}{Z_{ni}^2} \tag{3.4}$$

where,

σ_{2D} = biaxial stress, (MPa)

π = 3.141.....

ρ = material density, (g/cc)

R = membrane radius, (cm)

υ_{ni} = resonant frequency, (Hz)

Z_{ni} = ith zero of the nth order Bessel's Function

Similarly for a vibrating string, the equation yields [32]:

$$\sigma_{1D} = 4\rho L^2 \frac{\upsilon_i^2}{n_i^2} \tag{3.5}$$

where,

σ_{1D} = uniaxial stress, (MPa)

L = length of the string, (cm)

n_i = node of inflection

Since the density of the material is known, only the resonant frequencies need to be determined.

The sample preparation technique is detailed in chapter 5. The one- and two-dimensional samples were mounted in the holographic chamber so that the resonant frequency patterns could be superimposed over one another. Therefore, both samples were exposed to the same environmental conditions for the same time interval. This eliminated any environmental variation between the samples during testing. Figure 3.3 demonstrates the sample set-up.

Thermal Properties

The degradation temperature, glass transition and melt temperatures and the thermal expansion coefficients of gelatin, cellulose acetate and PET were determined. TA Instruments Thermogravimetric Analyzer, TGA, was employed to measure the degradation temperature and weight loss as a function of temperature. A TA Instruments Differential Scanning Calorimeter, DSC, was used to determine the Tg and Tm of each material. In addition, the thermal expansion coefficients of gelatin, cellulose acetate and PET were investigated using TA Instruments Thermomechanical Analyzer, TMA. Details of these techniques and the corresponding analysis are available through several sources [32-34].

Generally in photographic applications, the thermal expansion is less important than humidity expansion [6]. The thermal dimensional changes in the gelatin/CA and gelatin/PET bilayer systems are primarily due to the substrate [8]. The glass transistion temperature, Tg, and melt transition, Tm, for gelatin is highly dependent upon its moisture content. The Tg and Tm decrease with increasing relative humidity. An extensive study regarding the effect of humidity on the transition temperatures was documented by Marshall and Petrie [35,36].

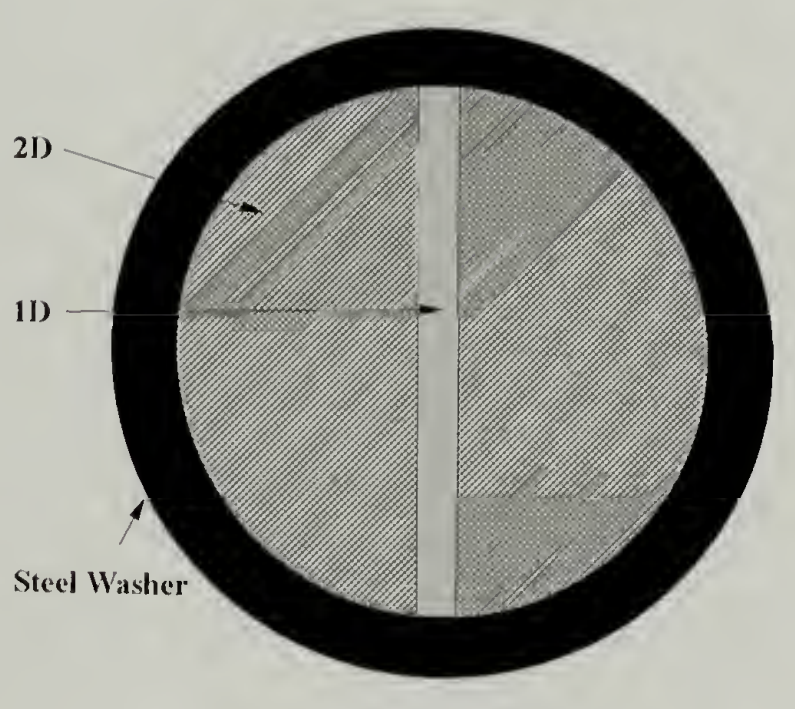

Figure 3.3 Holographic interferometry sample set-up for Poisson's ratio determination.

In their work, it was shown that at higher water contents, the transition temperatures are lower and the temperature interval between the Tg and Tm becomes increasingly larger resulting in a greater separation between the Tg and Tm. At lower water contents, the opposite holds true. The transition temperatures are higher and the separation between the Tg and Tm narrows with reduced water content.

Thermogravimetric Analysis. The TGA was performed in the temperature range of 25 to 400°C in nitrogen. The weight loss as a function of temperature and the degradation temperature were then recorded. The average sample weight was 20 mg.

Differential Scanning Calorimetry. The DSC's were run in nitrogen at a ramp rate of 10°C/min from 25°C to a temperature below the degradation temperature. Sample sizes averaged 10 mg.

Thermomechanical Analysis. The TMA was set up for thin films. A small force of 0.001N was applied to the thin, 3 mm wide by 25 mm long sample strip. A temperature ramp of 5°C/min was then employed and the dimensional change monitored.

Crystallinity Determination

The percent crystallinity, χc, of gelatin was calculated using the melt enthalpy method outlined by Kämpf [37]. In general, χc is determined using equation (3.8):

$$\chi_c = \frac{\Delta H_{sc}}{\Delta H_c} \times 100 \qquad (3.8)$$

where,

ΔH_{sc} = melt enthalpy for the semi-crystalline polymer (cal/g)

ΔH_c = enthalpy of fusion for fully crystalline polymer (cal/g)

The fully crystalline melt enthalpy of collagen was adopted to determine the degree of crystallinity in gelatin. This is valid since gelatin is the random coil derivative of collagen which is a rigid rod, triple alpha helix. The ΔH_c for collagen was extracted published results [38,39]. It is based on the melting point depression of a crystalline polymer by a diluent. This relationship is explained in detail elsewhere [40]. The ΔH_c for collagen used to calculate the degree of crystallinity is 24 cal/g [41].

Results and Discussion

Mechanical Properties

Tensile Properties and Machine Compliance. The machine compliance was determined by extrapolating a plot of the apparent compliance vs. the gage length to the y-axis [23,24]. The intercept is the machine compliance. Figure 3.4 represents the compliance data for the screw driven Instron Universal Tensile Test equipment with a 10 pound (Interface Corp. SM-10) load cell.

The machine compliance, Cm, for the Instron equipment was 0.00463 mm/N and Cm = 0.00805 mm/N for the Toyo Baldwin equipment. This data was used to correct the tensile moduli of the gelatin and cellulose acetate. The apparent moduli and the corrected moduli are tabulated in Table 3.3.

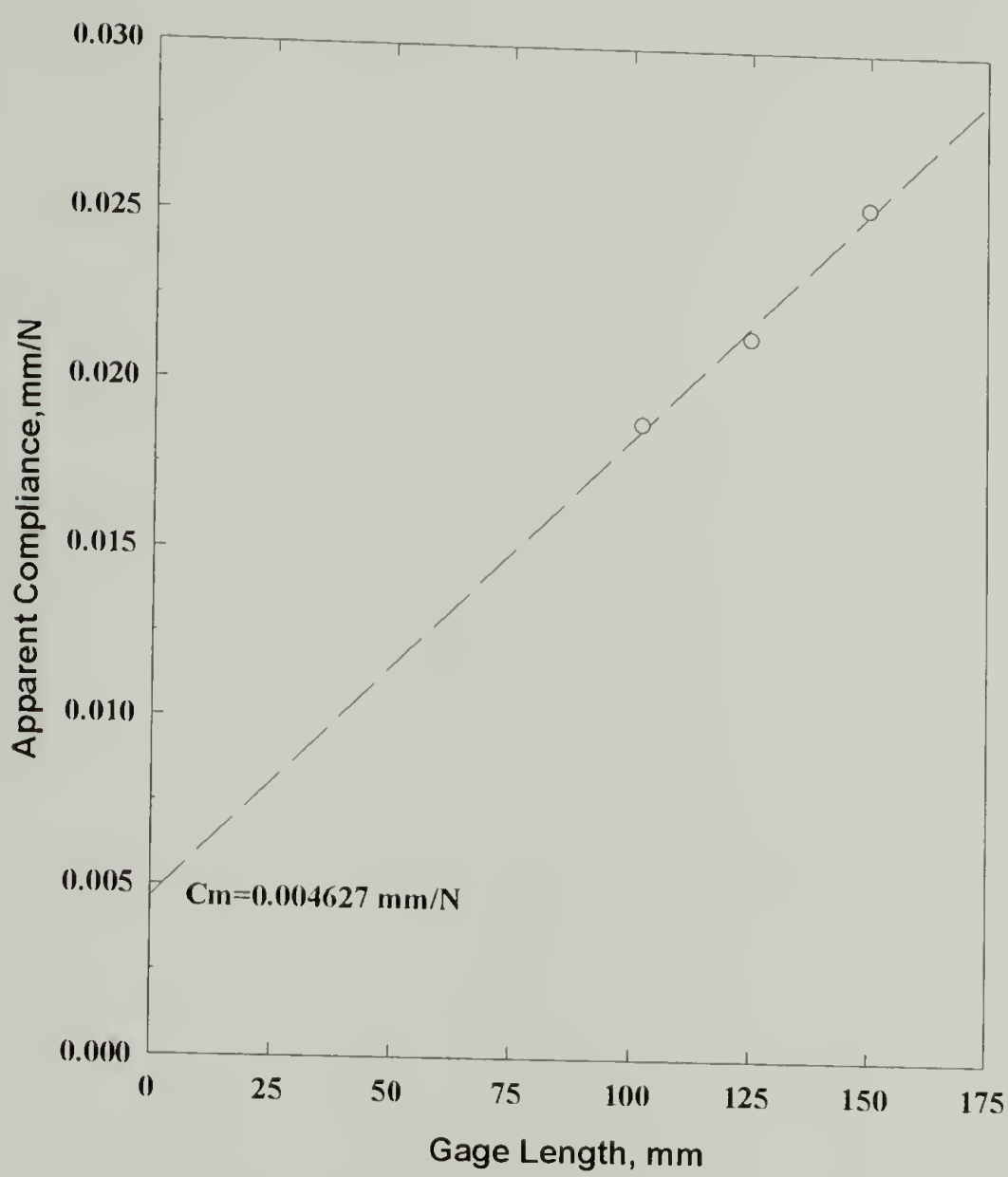

Figure 3.4 Machine compliance determination using ASTM D3379. The y-intercept represents the compliance for the screw driven Instron tensile test equipment. Similar results were obtained for the Toyo Baldwin tensile test equipment.

Table 3.3. Apparent and corrected tensile moduli for gelatin and cellulose acetate.

Sample Description	**Apparent Tensile Modulus, (w/o Machine Compliance Correction) GPa**	**Tensile Modulus, (Corrected for Machine Compliance) GPa (10^5 psi)**
Cellulose Acetate (gelatin coating direction)	2.85 ± 0.41	3.72 (5.39)
Cellulose Acetate (⊥ to coating direction)	3.07 ± 0.64	4.05 (5.87)
Gelatin (33%RH)	3.04 ± 0.44	3.51 (5.08)
Gelatin (43%RH)	2.86 ± 0.38	3.09 (4.48)
Gelatin (54%RH)	2.58 ± 0.27	2.75 (3.99)
Gelatin (59%RH)	2.44 ± 0.28	2.48 (3.60)
Gelatin (75%RH)	1.69 ± 0.13	1.75 (2.54)

The stiffer the material, the more apparent the affect of the machine compliance. The machine compliance of the Instron accounts for a 23% difference in the apparent moduli values from the calculated corrected values. Similarly, the Toyo Baldwin machine compliance accounts for a 26% variation from the apparent modulus of these materials.

A comparison of the stress vs. strain curves for gelatin are depicted in Figure 3.5. It is apparent that the tensile properties are highly dependent on relative humidity. Similar results are noted in the literature [6,39]. In the plane of the gelatin coating, the material is isotropic since the mechanical properties were the same in all directions.

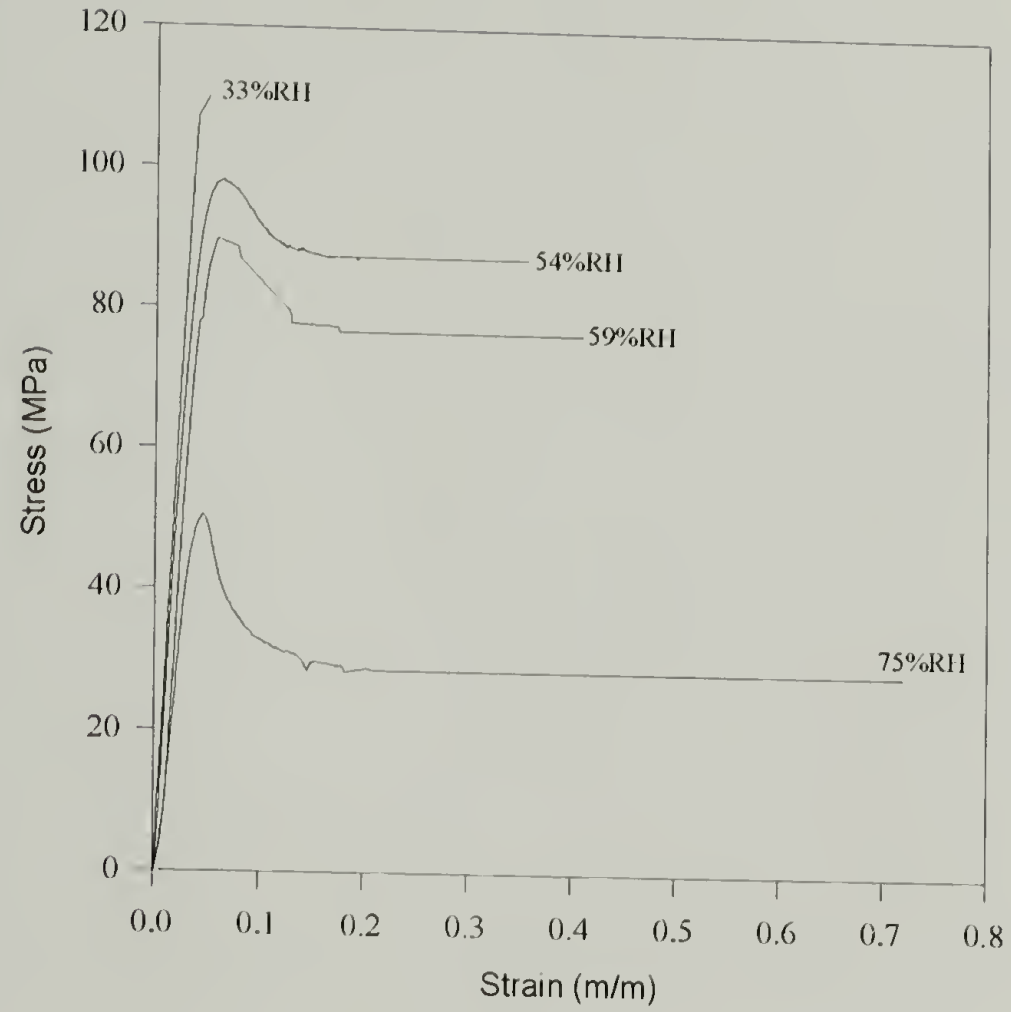

Figure 3.5 Comparison of stress vs. strain curves for gelatin at various relative humidities measured using the Toyo Baldwin tensile test equipment with relative humidity chamber.

It was experimentally determined that the tensile moduli of cellulose acetate are independent of relative humidity. This is not the case for gelatin. Figure 3.6 depicts the effect of relative humidity on the moduli of gelatin and cellulose acetate. Note that cellulose acetate exhibits two moduli. The anisotropy of the material is a result of the film manufacturing process. For the gelatin/CA bilayer system, the principal directions of the cellulose acetate are oriented with respect to the gelatin coating direction.

The yield and ultimate strength and the elongation at break of gelatin and cellulose acetate are highly dependent upon relative humidity. The yield strength of the gelatin is much greater than its ulimate strength as seen in Figure 3.5. For cellulose acetate the opposite is true. Figure 3.7 illustrates the typical stress-strain characteristics of cellulose acetate. Figures 3.8 and 3.9 depict the effect of relative humidity on these mechanical properties. These results correlate well with published values [6,38].

Shear Modulus. The alkaline processed bone gelatin is planar isotropic and therefore using linear elastic assumptions, the shear modulus was determined using equation (3.3).

The shear moduli for gelatin using linear elastic assumptions and a Poisson's ratio of 0.37 were calculated as 2.79 GPa at 33%RH and 1.39 GPa at 75%RH. The shear modulus of gelatin is also highly dependent upon relative humidity.

It was apparent from the tensile test results that the cellulose acetate is an anisotropic material. Therefore the relationship described earlier in equation (3.4) relates the shear modulus to the tensile moduli. Uniaxial samples cut 44° from principal axis (along the gelatin coating direction) were tested as outlined earlier. The compliance correction was made and the results are tabulated in Table 3.4.

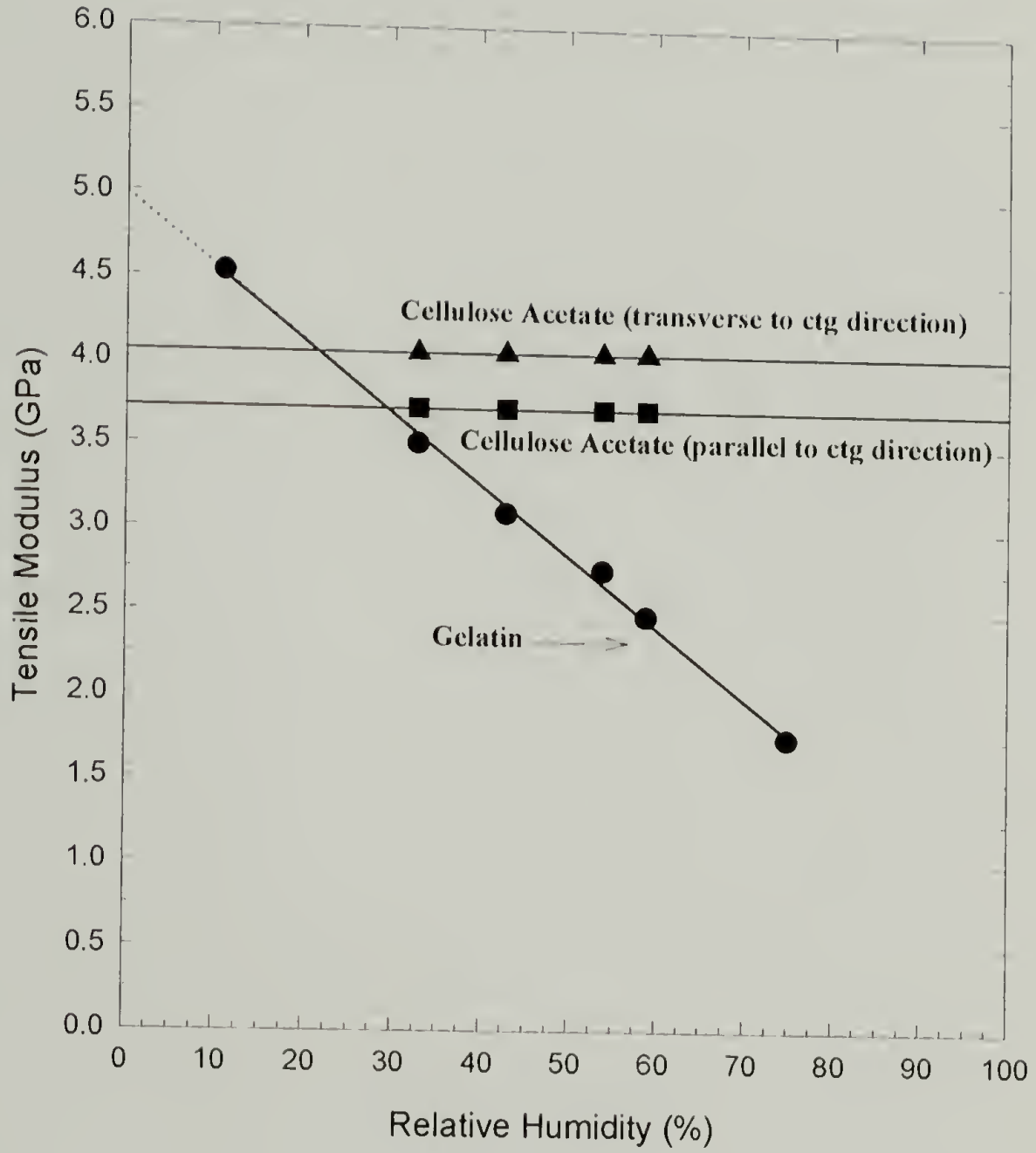

Figure 3.6 Comparison of the effect of relative humidity on the tensile (Young's) moduli of gelatin and cellulose acetate.

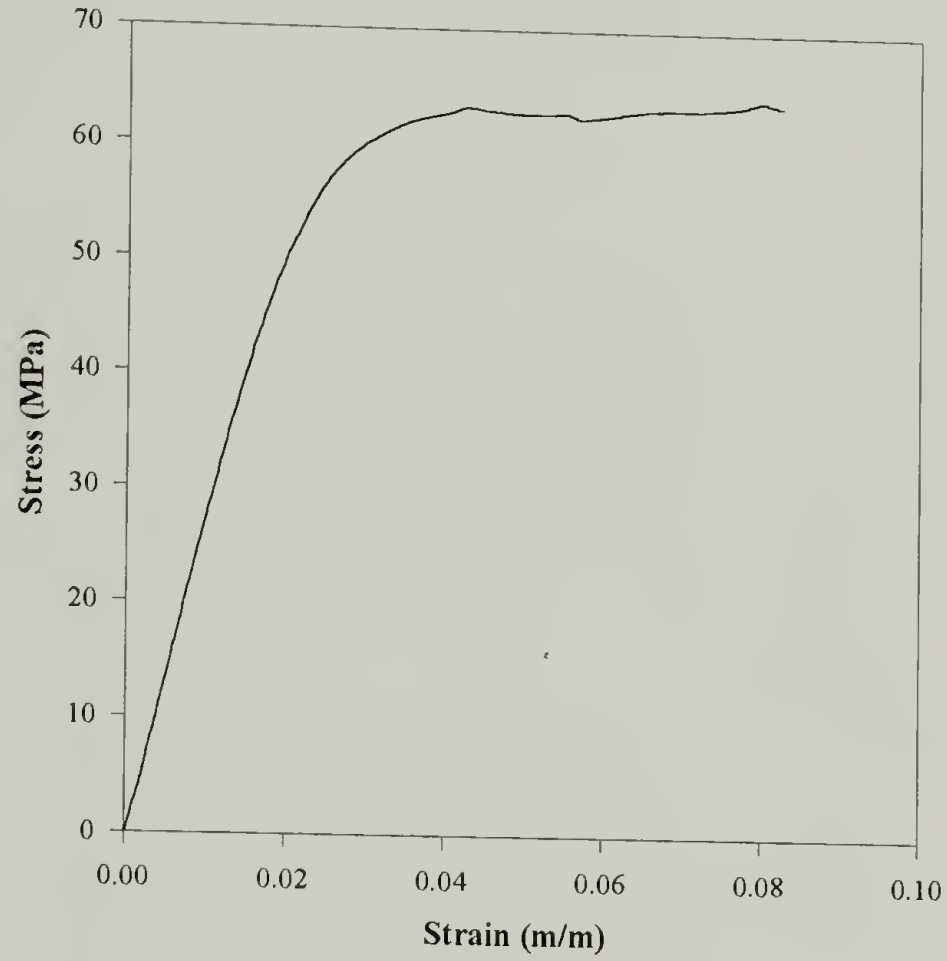

Figure 3.7 Typical stress vs. strain curve for cellulose acetate. This test was performed at 54%RH, 21°C.

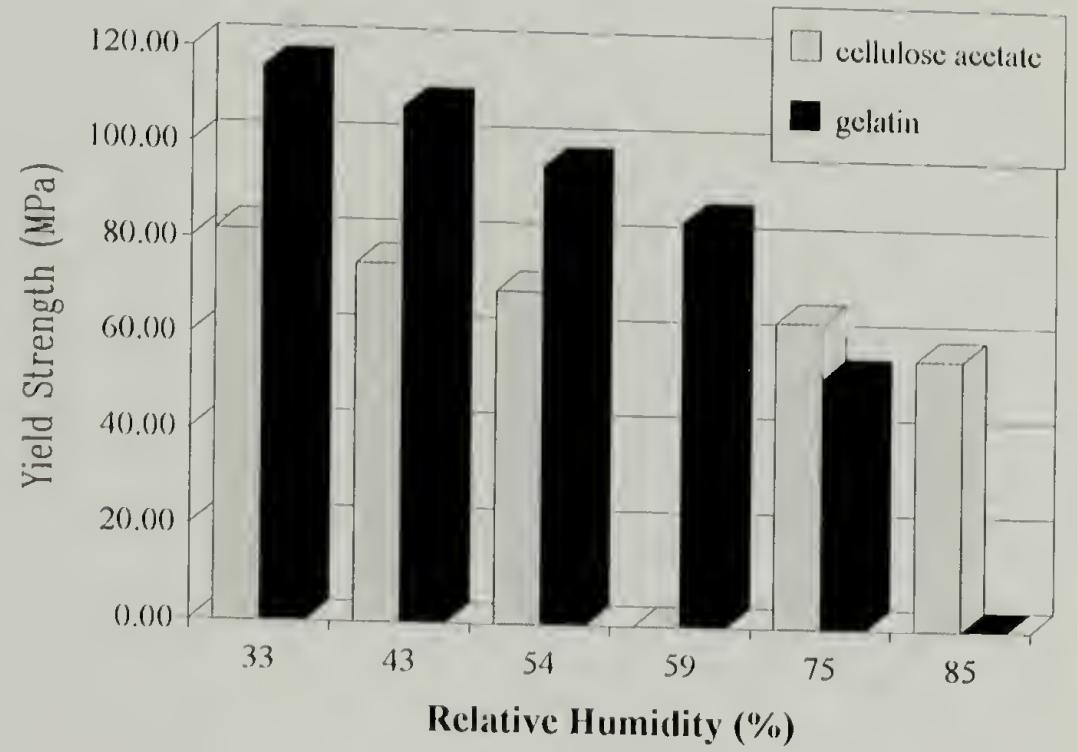

Figure 3.8 Comparison of yield strength for cellulose acetate and alkaline processed bone gelatin. Note: strength values for cellulose acetate were not obtained at 59%RH nor for gelatin at 85%RH.

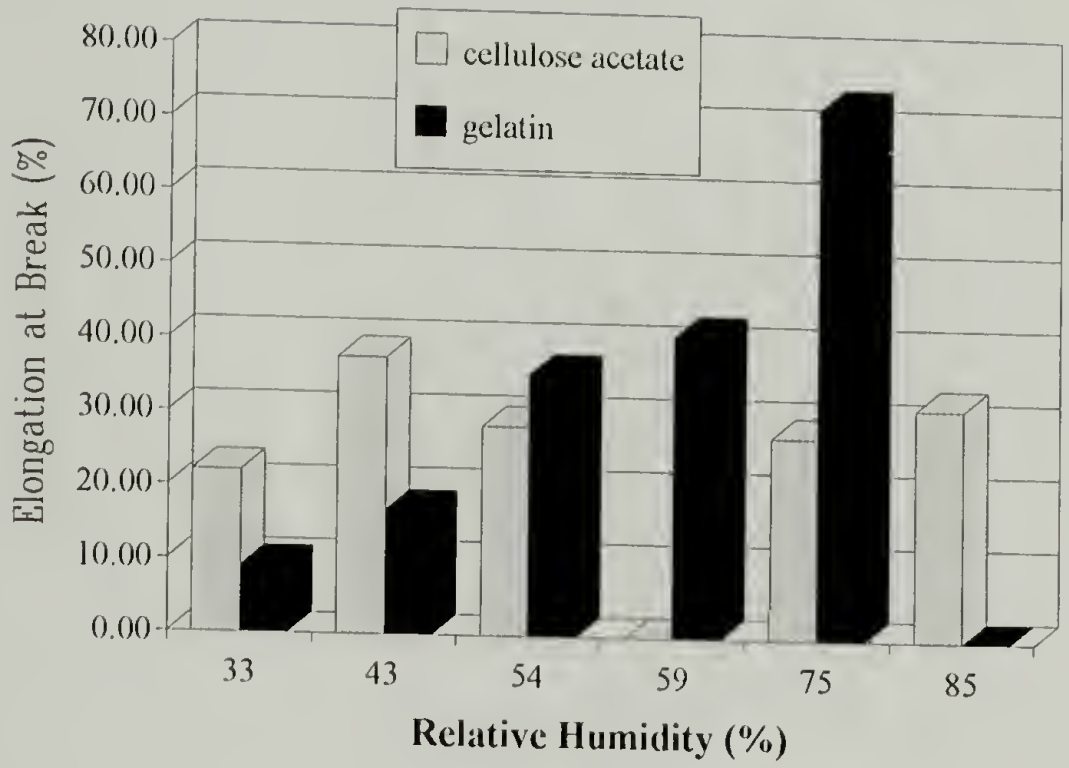

Figure 3.9 Comparison of percent elongation at break for cellulose acetate and alkaline processed bone gelatin. Note: elongation values for cellulose acetate were not obtained at 59%RH nor for gelatin at 85%RH.

Table 3.4. Results of the shear modulus determination on cellulose acetate film.

Angle, Θ (deg.)	Tensile Modulus $E_{@44°}$, (GPa)	Tensile Modulus E_{11}, (GPa)	Tensile Modulus E_{22}, (GPa)	Shear Modulus G_{12}, (GPa)
44	3.472	3.72	4.05	0.94

Effect of Moisture Sorption Hysteresis on the Tensile Properties The effect of moisture sorption hysteresis on the tensile properties of alkaline processed bone gelatin (Kodak designation: 8244-15) was investigated. The test design was described earlier. The results are summarized in Table 3.5.

Table 3.5 The effect of moisture sorption hysteresis on the elastic (Young's) modulus of alkaline processed bone gelatin. Each sample was equilibrated for 1.5 hours at the indicated relative humidity.

Relative Humidity (%)	Sorption Path	Modulus, E (GPa)	Yield Strength, σ, (MPa)	Elongation at Break (%)
$0 \rightarrow 33$	Absorption	5.55	110.1	5.1
$54 \rightarrow 33$	Desorption	5.24	122.6	4.0

There is no apparent effect on the modulus resulting from moisture sorption hysteresis. It is evident that the tensile modulus results in Table 3.5 is larger than that conveyed in earlier tensile test experiments (reference Table 3.3). There are two plausible

reasons. The first is that two different gelatin samples from different gelatin batches were used. The gelatin used in this test was stored in a freezer to inhibit aging affects. The gelatin used in the initial tensile properties testing was not stored in a controlled environment and therefore physical aging may have occurred, skewing the results. Secondly, the gelatin used in the moisture sorption hysteresis test was removed from a PET substrate. This gelatin was coated using commercial production equipment. The gelatin used in the initial tensile testing was removed from a cellulose acetate substrate and was fabricated on laboratory coating equipment.

Poisson's Ratio

Poisson's ratio for gelatin was investigated as a function of relative humidity. Poisson's ratio was evaluated during the desorption and absorption to determine if there was sorption path dependence. Table 3.6 summarizes the results.

Table 3.6 Poisson's ratio for gelatin using holographic interferometry and incremental linear elastic assumptions.

Relative Humidity %	**Sorption Path**	**1-D Stress, σ_{1D}, MPa**	**2-D Stress, σ_{2D} MPa**	**Poisson's Ratio, ν** (±0.01)
43 → 33	Desorption	15.58	25.21	0.38
33 → 43	Absorption	8.88	13.87	0.36
43 → 54	Absorption	3.97	6.32	0.37

The Poisson's ratio for gelatin is 0.37 ± 0.01. From these results, it is apparent that Poisson's ratio is independent of relative humidity and sorption path. Table 3.7 summarizes Poisson's ratios for gelatin, cellulose acetate, epoxy, and polyimide.

Table 3.7 Poisson's ratio for alkaline processed bone gelatin (removed from CA substrate), cellulose acetate, epoxy and PMDA-ODA polyimide.

Poisson's Ratio	**Gelatin**	**Cellulose Acetate[a]**	**Epoxy[b]**	**PMDA-ODA Polyimide[c]**
ν	0.37	0.34	0.33	0.34

[a] general Poisson's ratio for polymers [39], [b] [40], [c] cured at 400°C, 1% strain applied [41]

Thermal Properties

The thermal properties for alkaline processed bone gelatin, cellulose acetate and poly(ethylene terephthalate), PET, are tabulated in Table 3.8. These results correlate well with literature values.

Gelatin exhibits an initial weight loss at 100°C resulting from water loss. The amount of water lost is dependent upon the sample's initial moisture content. Thermal degradation of the gelatin begins at 275°C with weight decreasing rapidly to 400°C, where it completely degraded. Cellulose acetate exhibits a 10.6% weight loss between 195° and 275° and then rapidly loses weight beginning at 283°C.

Cellulose acetate is manufactured by casting a film from a solvent based polymer system. Therefore, the initial weight loss is a result of solvent loss.

The onset of weight loss for PET begins at 375°C with no significant prior loss since the film is manufactured from a melt.

Table 3.8 Thermal properties of alkaline processed bone gelatin, cellulose acetate and poly(ethylene terephthalate) measured by the various thermal techniques described earlier in the text.

Property	Gelatin (SC5-5S-5020-01)	Cellulose Acetate	PET
Degradation Temperature, Td, (°C)	275	283	375
Glass Transition, Tg, (°C)	217[a]	124.8	282.8
Melt Transition, Tm, (°C)	230[a]	279.1	256.0
[b]Thermal Expansion Coefficient, μm/m°C (Parallel to Coating Direction (md))	39.6	108	17.0
[b]Thermal Expansion Coefficient, μm/m°C (Perpendicular to Coating Direction (td))	39.5	113	16.6

[a] reported values for dried gelatin [35,36]
[b] determined during second heating

Degree of Crystallinity

The Eastman Kodak Co. provided samples of various melt enthalpies, ΔHm, and with varying amounts of crosslinking agent. A list of the samples and the corresponding melt enthalpies and percent crosslinking agent are listed in Table 3.9.

Table 3.9. Description of the different samples of alkaline processed bone gelatin coated on either cellulose acetate or PET substrates.

Kodak Designation for Gelatin	Substrate	Gelatin Thickness (μm) ±0.5	Melt Enthalpy ΔHm, (cal/g)	Crosslinking Agent (%)	χ_c (%)
SC5-5S-5020-01	CA	18.6	[a]4.0	[a]0.00	16.7
8244-15	PET	16.0	0.0	0.00	0.0
8244-9	PET	24.6	2.0	3.16	8.3
8244-18	PET	24.5	0.0	0.00	0.0
8244-27	PET	24.5	0.0	1.58	0.0
8244-36	PET	25.8	4.0	3.16	16.7
8247-1-3	PET	24.5	4.0	1.58	16.7
8247-2-3	PET	25.8	4.0	0.00	16.7
8247-3-3	PET	24.7	0.0	3.16	0.0
8247-4-3	PET	24.8	2.0	0.00	8.3

[a] values communicated per Beta Ni, Eastman Kodak Co. [43]

The literature value of 24 cal/g for the crystalline melt enthalpy, ΔHc, of collagen was used to calculate percent crystallinity, χ_c, in the gelatin [42].

Conclusions

An overall characterization of the mechanical and physical properties of the materials under investigation was performed. The measured values correlated well with published results. This study focused specifically on the material properties of alkaline processed bone gelatin, cellulose acetate and poly(ethylene terephthalate). Other materials

investigated include a bisphenol A epoxy, polyimide, poly(vinyl alcohol), nickel and copper coatings.

It was observed that the mechanical properties of gelatin and cellulose acetate are greatly affected by relative humidity. The modulus of gelatin decreases linearly with increasing relative humdity. The moduli of cellulose acetate are independent of relative humidity although the yield strength and elongation at break are dependent upon humidity as is the case for gelatin. It was determined that the gelatin is isotropic in the plane of the coating. The cellulose acetate exhibited two moduli in the plane of the film which is characteristic of an anisotropic material. The shear and tensile moduli of gelatin are not affected by moisture sorption hysteresis although the trend indicates other mechanical properties are dependent upon the sorption path.

Poisson's ratio for gelatin (Kodak designation: SC5-5S-5020-01) is 0.37 ± 0.01. This value was determined using Holographic Interferometry. It was experimentally determined that the Poisson's ratio for gelatin is unaffected by the moisture sorption hysteresis.

The thermal expansion coefficients, TEC, for gelatin, cellulose acetate and PET are not similar. The mismatch between the coating and substrate TEC's contributes to the dimensional instability in the bilayer systems studied. As stated earlier, the effect of relative humidity on the gelatin/CA or gelatin/PET bilayer systems is greater than the effect of temperature.

References

1. R.J. Brewer, "Cellulose Esters, Organic," Encyclopedia of Polymer Science and Engineering, eds. H. Marks and N. Bikales, Vol. 3, (New York: Wiley Interscience, 1986).

2. "Airvol® Polyvinyl Alcohol," (Pittsburgh, PA: Air Products and Chemicals, Inc., 1990).

3. Technical Bulletin No.: SC: 235-91.828, (Houston, TX: Shell Chemical Co., 1991).

4. R. Subramanian, M.T. Pottiger, J.H. Morris and J.P. Curilla, "Effect of Moisture on the Physical Properties of Polyimide Films," Materials Research Society Symposium Proceedings, Vol. 227, (1991).

5. R.C. Weast, Handbook of Chemistry and Physics, 60th ed., (Boca Raton, FL: CRC Press, Inc., 1979).

6. P.Z. Adelstein, "Physical Properties of Photographic Materials," SPSE Handbook of Photographic Science and Engineering, ed. W. Thomas, (New York: Wiley Interscience, 1973).

7. "Physical Properties of Kodak Aerial Films," Properties of Kodak Materials for Aerial Photographic Systems, Vol II, (Rochester, NY: Eastman Kodak Co., 1972).

8. "Physical and Chemical Behavior of Kodak Aerial Films," Properties of Kodak Materials for Aerial Photographic Systems, Vol III, (New York: Eastman Kodak Co., 1972).

9. J.M. Calhoun, "Properties and Dimensional Stability of Safety Aerographic Film," Photogrammetric Engineering, **13**, 163 (1947).

10. Rose, P.I., "Gelatin: I. General Properties," The Theory of the Photographic Process, 4th ed., eds., J.F. Hamilton, G.C. Higgins and J.E. Starr, (Rochester, NY: Eastman Kodak Co., 1977).

11. A.G. Ward and A. Courts, The Science & Technology of Gelatin, (London: Academic Press, 1977).

12. J. Pouradier, "II: Properties of Gelatin in Relation to Its Use in the Preparation of Photographic Emulsions," The Theory of the Photographic Process, 4th ed., eds., J.F. Hamilton, G.C. Higgins and J.E. Starr, (Rochester, NY: Eastman Kodak Co., 1977).

13. T.H. James and G.C. Higgins, Fundamentals of Photographic Theory, (New York: Morgan and Morgan, 1960).

14. G. Xu and E. Ruckenstein, "Emulsion Pathway for Gelatin Crosslinking," Journal of Applied Polymer Science, **47**, 1343 (1993).

15. N. Yamamoto and Y. Oishi, "Photographic Gelatin Hardening Composition," U.S. Patent No.: 3,325,287, June 13, 1967.

16. B.M. Burness and B.D. Wilson, "Bis(Beta-Acyloxyethyl) Ketones as Gelatin Hardeners," U.S. Patent No.: 3,360,372, December 26, 1967.

17. P.I. Rose, "Gelatin," Encyclopedia of Polymer Science and Engineering, eds. H. Marks and N. Bikales, Vol. 3, (New York: Wiley Interscience, 1986).

18. P. York, "Analysis of Moisture Sorption Hysteresis in Hard Gelatin Capsules, Maize Starch, and Maize Starch: Drug Powder Mixture," Journal of Pharmacy and Pharmacology, **33**, 269 (1980).

19. F.L. Marten,"Vinyl Alcohol Polymers," Encyclopedia of Polymer Science and Engineering, eds. H. Marks and N. Bikales, Vol. 17, (New York: Wiley Interscience, 1986)

20. W.C. Wake, Developments in Adhesives, (London: Applied Science Publishers, Ltd., 1977).

21. L. Greenspan, "Humidity Fixed Points of Binary Saturated Aqueous Solutions," Journal of Research of the National Bureau of Standards: *A. Physics and Chemistry*, **81A**(1), 89 (1977).

22. F.E.M. O'Brien, "Control of Humidity by Saturated Salt Solutions," Journal of Scientific Instrumentation, **25**, 73 (1948).

23. "Standard Test Methods for Tensile Stength and Young's Modulus for High Modulus Single Filament Materials," ASTM Designation: D3379, American Society for Testing and Materials, Philadelphia, PA (1988).

24. D.E. Turek, "On the Tensile Testing of High Modulus Polymers and the Compliance Correction," Polymer Engineering and Science, **33**(6), 328 (1993).

25. "Standard Test Methods for Tensile Properties of Thin Plastic Sheeting," ASTM Designation: D882, American Society for Testing and Materials, Philadelphia, PA (1988).

26. J.R. Vinson and R.L. Sierakowski, The Behavior of Stuctures Composed of Composite Materials, (Boston, MA: Kluwer Academic Publishers, 1993).

27. S.W. Tsai and H.T. Hahn, Introduction to Composite Materials, (Westport, CT: Technomic Publishing Co.,1980).

28. S.J. Gregg, The Surface Chemistry of Solids, 2nd ed., (London: Chapman and Hall, Ltd., 1961).

29. G.N. Ramachandran and R. Chandrasekharan, "Interchain Hydrogen Bonds via Bound Water Molecules in the Collagen Triple Helix," Biopolymers, **6**, 1649 (1968).

30. M. Lüscher-Mattli and M. Rüegg, "Thermodynamic Functions of Biopolymer Hydration. I. Their Determination by Vapor Pressure Studies, Discussed in an Analysis of the Primary Hydration Process," Biopolymers, **21**, 403 (1982).

31. M.A, Maden, The Determination of Stresses and Material Properties of Polyimide Coatings and Films Using Real Time Holographic Interferometry, Ph.D. diss., University of Massachusetts, Amherst, MA, (1992).

32. D. Campbell and J.R. White, Polymer Characterization: Physical Techniques, (New York: Chapman and Hall Publishing Co., 1989).

33. J.I. Kroschwitz, ed., Polymers: Polymer Characterization and Analysis, (New York: John Wiley and Sons, 1990).

34. J.F. Rabek, Experimental Methods in Polymer Chemistry, (New York: John Wiley and Sons, 1980).

35. A.S. Marshall and S.E.B. Petrie, "Thermal Transitions in Gelatin and Aqueous Gelatin Solutions," Journal of Photgraphic Science, **28**, 128 (1980).

36. A.S. Marshall and S.E.B. Petrie, "Thermal Transitions and Physical Aging in Gelatin," Proceedings of the Eleventh North American Thermal Analysis Society Conference, Vol. II (1981).

37. G. Kämpf, Characterization of Plastics by Physical Methods, (New York: Hanser Publishers, 1986).

38. E. Bradbury and C. Martin, "Mechanical Properties and Structure of Sol-Type and Gel-Type Gelatine Films," Nature, **168**, 837 (1951).

39. L.T. Manzione, Plastic Packaging of Microelectronic Devices, (New York: Van Nostrand Publishing Co., 1990).

40. A.R. Plepys, A Study of Residual Stress Formation in Three Dimensionally Constrained Epoxy Resins, Ph.D. diss., University of Massachusetts, Amherst, MA, (1992).

41. C.L. Bauer and R.J. Farris, "Determination of Poisson's Ratio for Polyimide Films," Polymer Engineering and Science, **29**(16), 1107 (1989).

42. P.J. Flory and R.R. Garrett, "Phase Transitions in Collagen and Gelatin Systems," Journal of American Chemical Society, **80**, 4836 (1958).

43. B. Ni, personal communication, 1992.

44. L.P. Witnauer and J.G. Fee, "Effects of Diluents on Fusion Temperature of the Crystalline Regions in Plain and Tanned Cowhide," Journal of Polymer Science, **26**, 141 (1957).

CHAPTER 4

SWELLING STRAINS

Introduction

The mismatch between the in-plane humidity expansion coefficient, β, of the coating with that of the substrate can result in dimensional instability in the bilayer system. The humidity expansion coefficients were determined by plotting the humidity swelling strain as a function of relative humidity for each material. The slope of this curve is the humidity expansion coefficient. In this chapter, the in-plane and out-of-plane humidity swelling strains have been investigated. The in-plane humidity swelling strain was measured using a mechanical technique. The out-of-plane humidity swelling strain was studied in conjunction with the Smith College Physics Department using a optical technique known as Double Slit Laser Interferometry. The out-of-plane humidity expansion coefficient is important for materials that are stored or used in roll from. The results of the in-plane humidity swelling experiment will be incorporated into the two dimensional bending model in chapter 7. The swelling strains discussed throughout this chapter are humidity induced.

Experimental

Prior to discussing the humidity swelling strains in the bilayer system, familiarization of the terms applied throughout this chapter is prudent. The terms are represented in figure 4.1 and the orientation of the in-plane strain and the out-of-plane strain are illustrated.

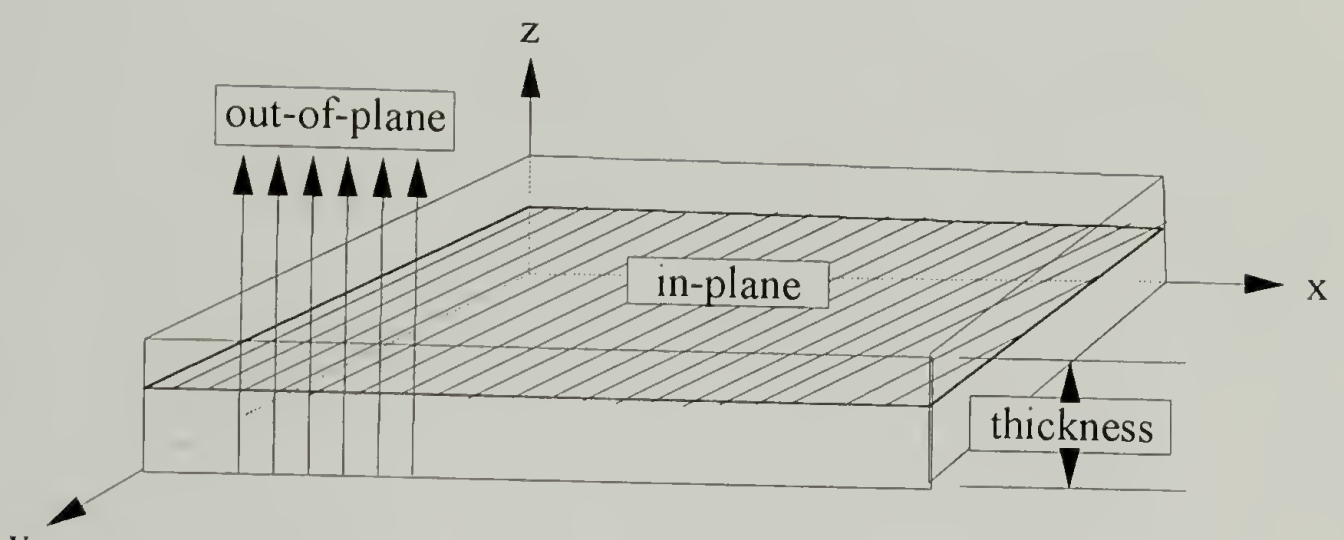

Figure 4.1 Orientation of plane humidity swelling strains. In-plane strain lies in the x-y plane and out-of-plane strain is in the z-direction. Thickness is also characterized in the z-direction.

In-Plane Humidity Swelling Strain

The in-plane humidity swelling strain was determined using an apparatus designed to measure uniaxial humidity swelling strains in the planar direction [1]. A schematic of the apparatus is shown in figure 4.2.

The experiment was performed by securing a 5 x 100 mm uniaxial sample of a known thickness between the clamps. After the counterweight was hung in place, relative humidity was introduced into the sample chamber. Relative humidity was generated using binary aqueous saturated salt solutions which was described in chapter 3. The length change due to moisture was monitored using a Linear Variable Differential Transformer, LVDT. The swelling strain was then calculated as the length change due to humidity exposure divided by the initial length of the sample.

A plot of humidity swelling strain at equilibrium vs. relative humidity was generated. The first derivative of the curve (or the slope) is considered the humidity expansion coefficient, HEC. In the literature, HEC is synonymous with the symbol, β, and is used interchangeably throughout this text.

The effect of the load from the counterweight on the actual humidity expansion coefficient has also been investigated. Three separate humidity swelling experiments were performed; each with a different weight. The apparent humidity expansion coefficient was determined for each experiment as described earlier. The apparent humidity expansion coefficients were then plotted against the displacement weight which is related to the counterweight by equation (4.1). The displacement weight is defined as:

$$\text{Displacement Weight} = \text{Counterweight} - \text{Clamp Weight} - \text{LVDT Core Weight} - \text{Friction Weight} \quad (4.1)$$

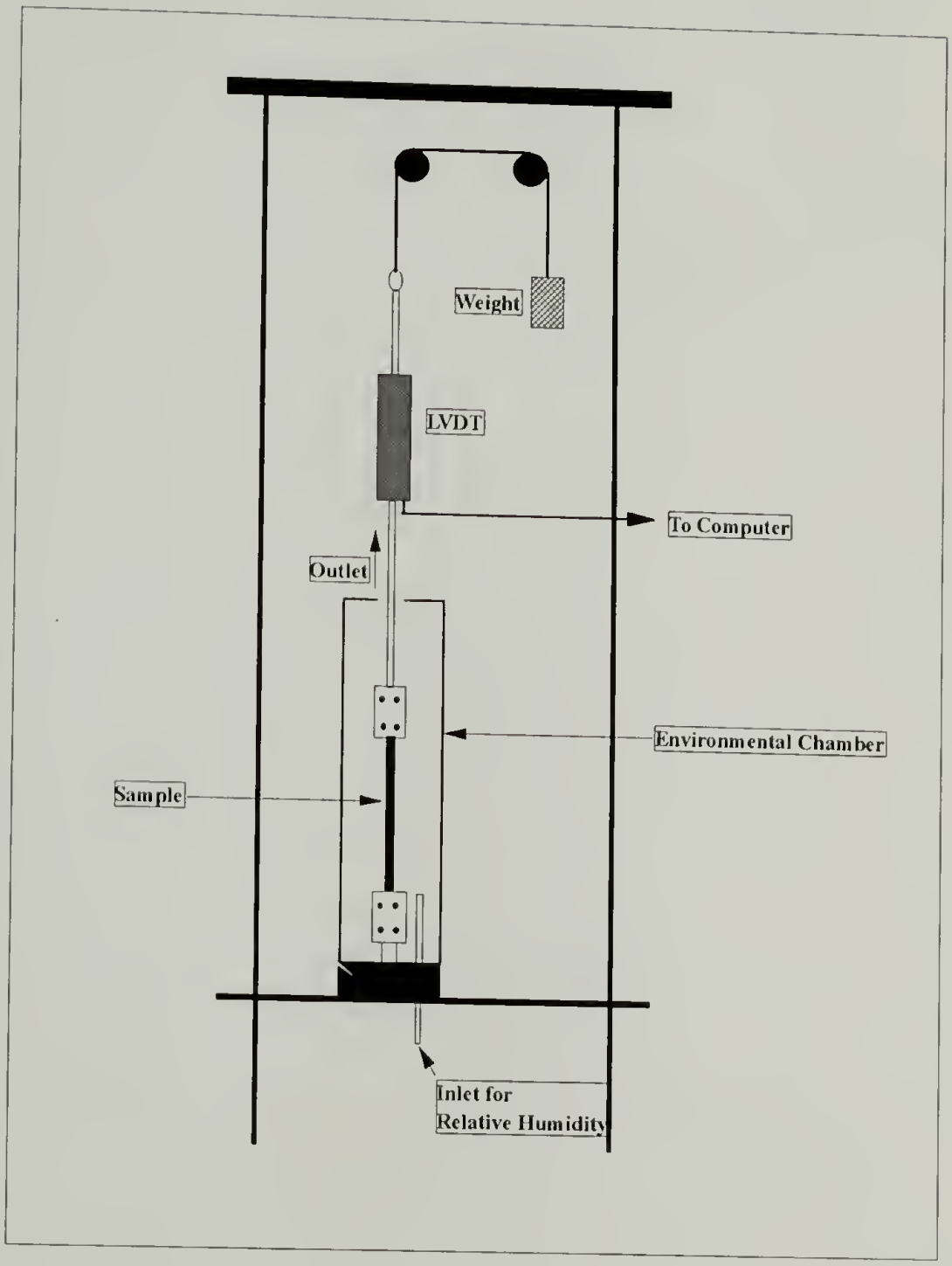

Figure 4.2 Apparatus for measuring in-plane humidity swelling strains in the x-y plane.

The friction weight compensates for the friction of the pulleys. It is defined as the minimum weight required to move the clamp and core. The zero-intercept of the apparent humidity expansion coefficient vs. displacement weight curve is considered the actual humidity expansion coefficient for the material.

Out-of-Plane Humidity Swelling Strain

Optical methods are commonly employed to measure the thickness of films and fibers [2,3,4,5,6]. An optical technique known as Double Slit Laser Interferometry was employed to determine the out-of plane humidity swelling strain of the gelatin coating. Figure 4.3 illustrates the schematic of the optical set-up.

This technique was used to investigate the out-of-plane humidity swelling characteristics of alkaline processed bone gelatin (# SC5-5S-5020-01: 16.7% crystalline, 0% crosslinking agent). The initial thickness of the gelatin at 0%RH was measured using an Olympus CK2 Inverted Microscope. The gelatin was stacked to a (dry) thickness of 197.4 μm. The stacked sample was then secured over one of the 139 μm slits in the laser interferometry unit. The double slit system was placed inside an optical glass chamber and humidity was introduced. The fringe shift was monitored. The fringe shift is directly related to the displacement or thickness change in the film.

Initially the sample was subjected to dry nitrogen gas for 24 hours. The absorption process began with 23%RH, then 54%RH followed by 75%RH and desorbed to 0%RH. A second run was performed on the same sample with the same sorption cycle. Two separate samples were run to ensure repeatability.

The refractive index, n, of the gelatin as a function of relative humidity, RH, was assumed. The refractive index of dry gelatin is 1.54 and 1.51 for wet gelatin (100%RH) [7].

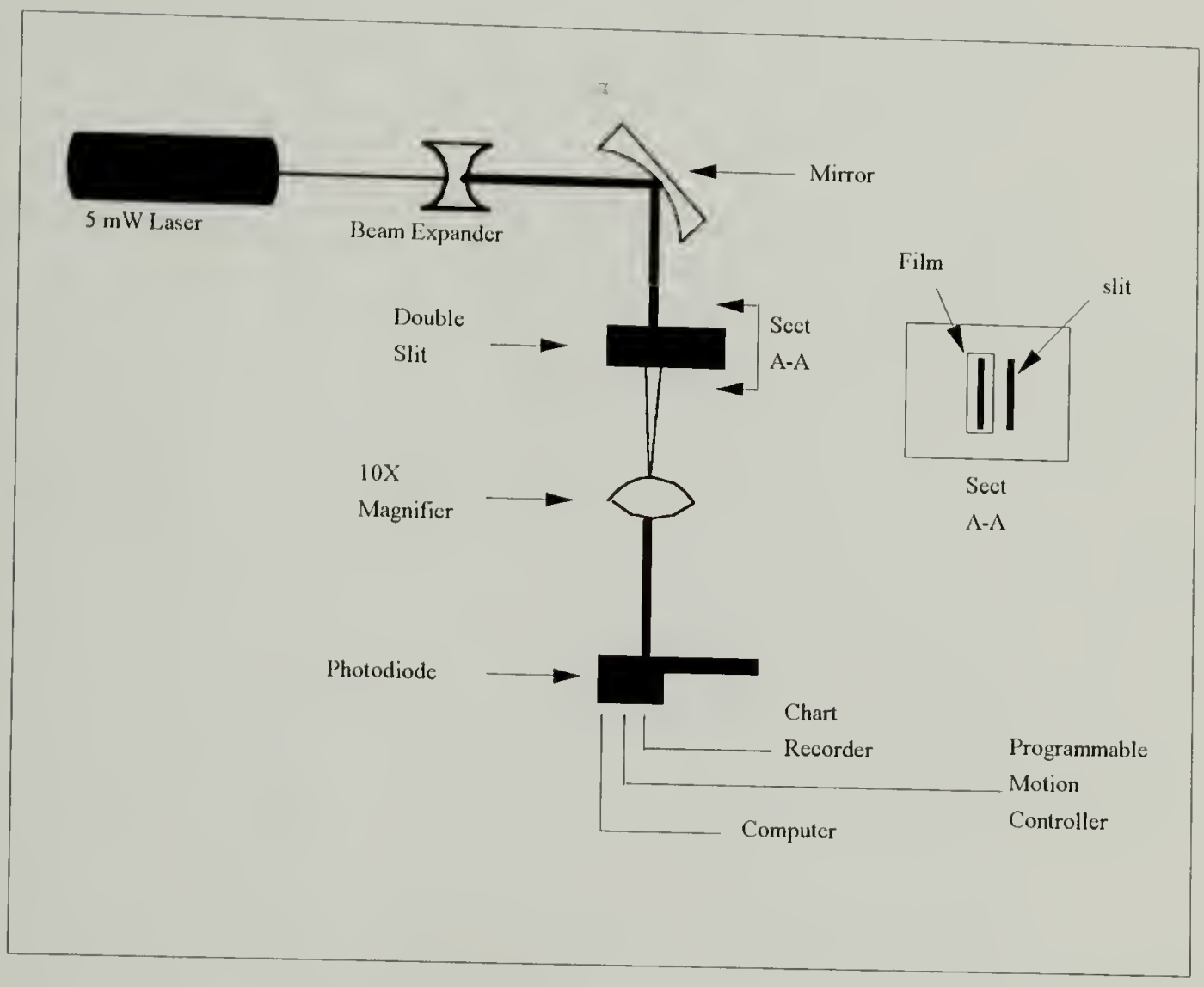

Figure 4.3 Schematic of out-of-plane humidity swelling strain set-up.

It was postulated that the refractive index is a linear function between 0 and 100%RH. Using standard linear regression, the resulting equation is:

$$n = 1.54 - 3x10^{-4}(\%RH)^{-1} \tag{4.2}$$

Mathematically, the thickness change, Δt, is derived from the refractive index, n, and the optical path length, o.p.d. by equation (4.3):

$$o.p.d. = (n-1)\Delta t \tag{4.3}$$

The o.p.d. is defined as the product of the refractive index of the material and the physical path length from the light source to the material. The o.p.d. is related to the ratio of the fringe shift, ΔN as a function of relative humidity to the average width, N; and the wavelength, λ, of the light source via equation (4.4). In this specific technique, the light source is a 5 mW helium neon laser.

$$o.p.d. = \frac{\Delta N}{N}\lambda \tag{4.4}$$

Combining equations (4.3) and (4.4) yields an expression for the swelling displacement, Δt.

$$\Delta t = \frac{\Delta N}{N}\lambda(n-1)^{-1} \tag{4.5}$$

The humidity swelling strain is calculated as the thickness change due to humidity exposure divided by the initial thickness of the sample. The slope of the swelling strain vs. relative humidity yields the out-of-plane humidity expansion coefficient.

The optical technique described is detailed elsewhere [8]. The disadvantage of this technique results from the coupled nature of the thickness and refractive index. Therefore either the thickness or the refractive index of the material must be known in order to solve for the other.

Results and Discussion

The tendency for moisture (resulting from relative humidity) to enter and swell materials is dependent upon several factors: (a.) the thermodynamically favored dilution effect on the polymer network, (b.) osmotic pressure effects and (c.) the dependence on the degree of crosslinking and the network chain conformations (in the case of gelatin) [14].

In-Plane Humidity Expansion Coefficient

The in-plane humidity swelling coefficients were determined for gelatin and cellulose acetate by monitoring the swelling strain as a function of time at various relative humidities. Figures 4.4 and 4.5 represent the characteristic absorption curves alkaline processed bone gelatin and cellulose acetate at various relative humidities, respectively.

The 25.8 μm thick gelatin film (# 8247-2-3) reached equilibrium in 5 hours. The 127 μm thick cellulose acetate equilibrated at each humidity in 4 hours.

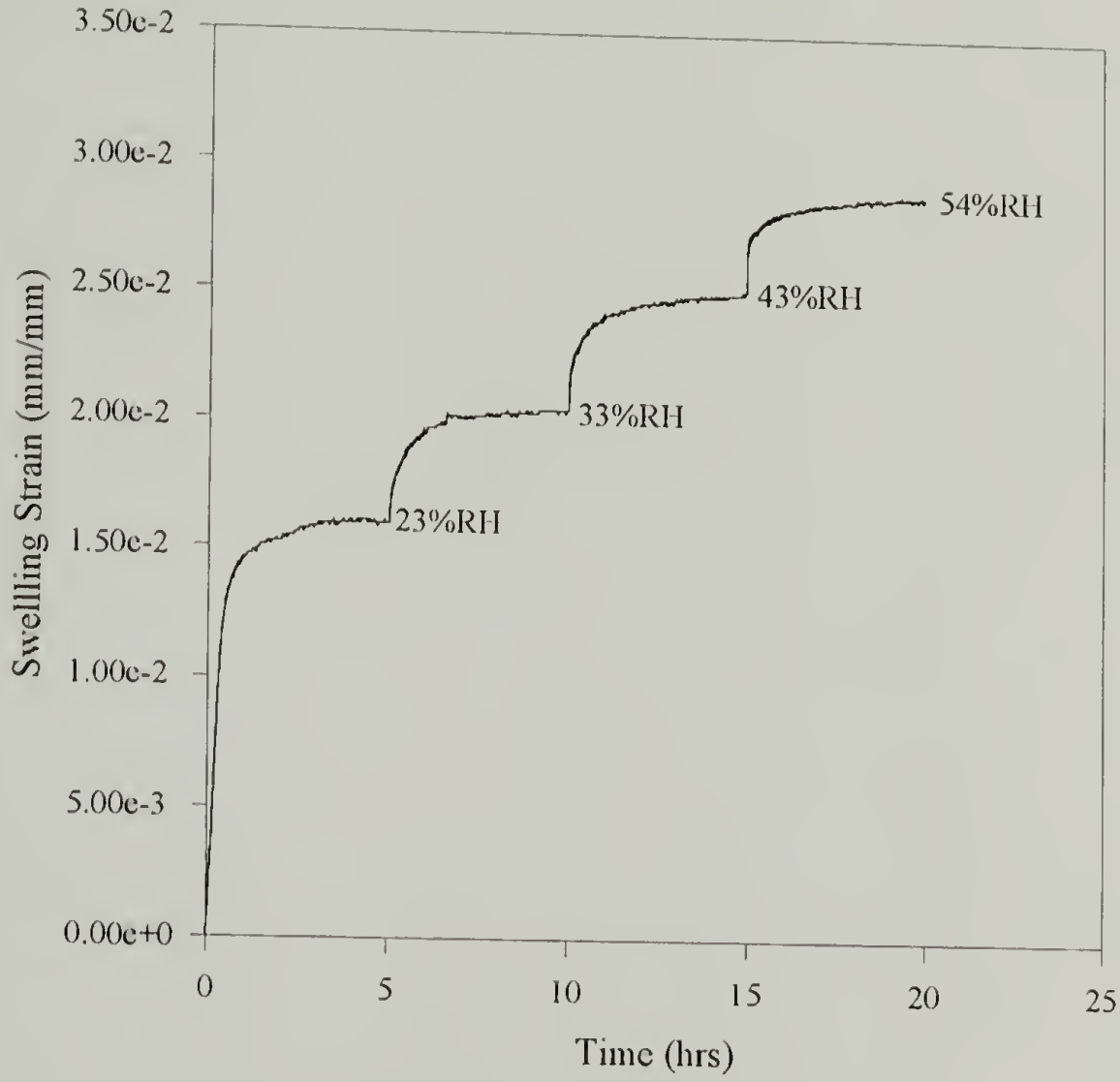

Figure 4.4 Characteristic humidity swelling strain vs. time curves for alkaline processed bone gelation. This particular gelatin sample (#8247-2-3) was 16.7% crystalline and had no crosslinking agent added.

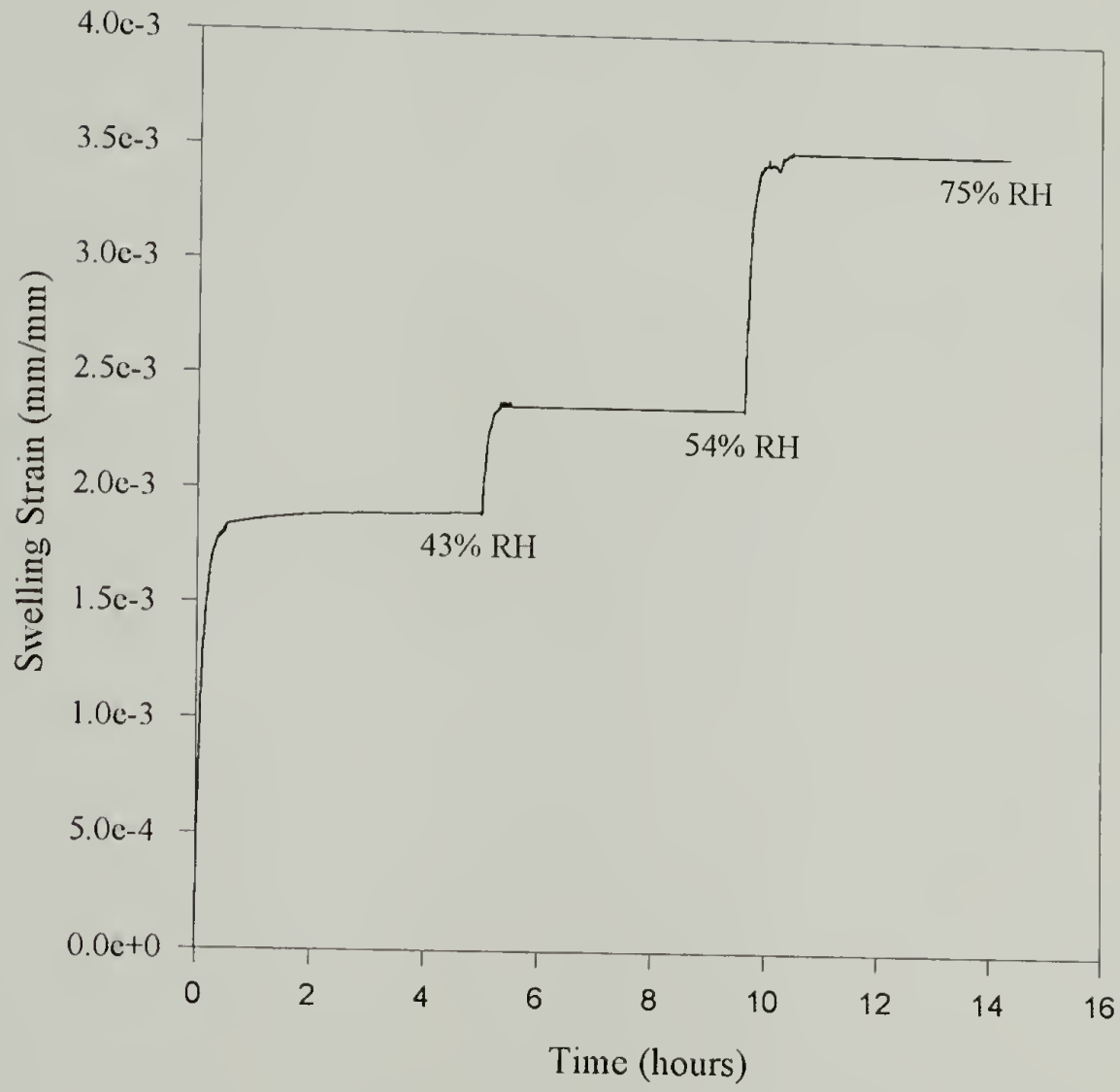

Figure 4.5 Typical humidity swelling strain vs. time curves for cellulose acetate. At equilibrium, this information is used to plot the swelling strain against the relative humidity.

This would imply that the mass diffusion coefficient for the cellulose acetate is greater than that for the gelatin.

Figure 4.6 represents the dimensional hysteresis observed between the desorption and absorption paths. In the case of unsupported gelatin (ie., gelatin removed from the substrate), the desorption swelling strain was greater that the absorption swelling strain. This is not uncommon and has been observed by others [12].

Figures 4.7 and 4.8 represent typical swelling strain vs. relative humidity curves during moisture absorption for gelatin (# SC5-5S-5020-01) and cellulose acetate. These curves were generated from the equilibrium swelling strain vs. time. It was determined that the gelatin is isotropic in the plane of the coating due to the independence of the humidity swelling coefficient and tensile modulus on direction in the plane. This was not the case for cellulose acetate. The humidity swelling coefficient for a uniaxial sample of cellulose acetate with its principal axis aligned perpendicular to the gelatin coating direction was greater than a sample aligned parallel to the gelatin coating direction.

As seen in figure 4.7, the humidity swelling strain characteristics for gelatin film do not behave linearly with relative humidity. This non-linearity has been observed by others [11]. It was noted later in this investigation , that the useable relative humidity range for gelatin films fell between 23% and 75% RH [9]. Therefore, the humidity expansion coefficient was calculated within this limit.

As figure 4.7 indicates, the gelatin begins to creep around 75%RH. The creep behavior of gelatin has been published [10]. This creep was due impart to the design of the experiment in which a small counterweight was hung from the sample to maintain a constant load. Near 75%RH, the Tg of gelatin is near room temperature which accentuates this phenomenon. This weight may be imposing a false value for the actual swelling strain.

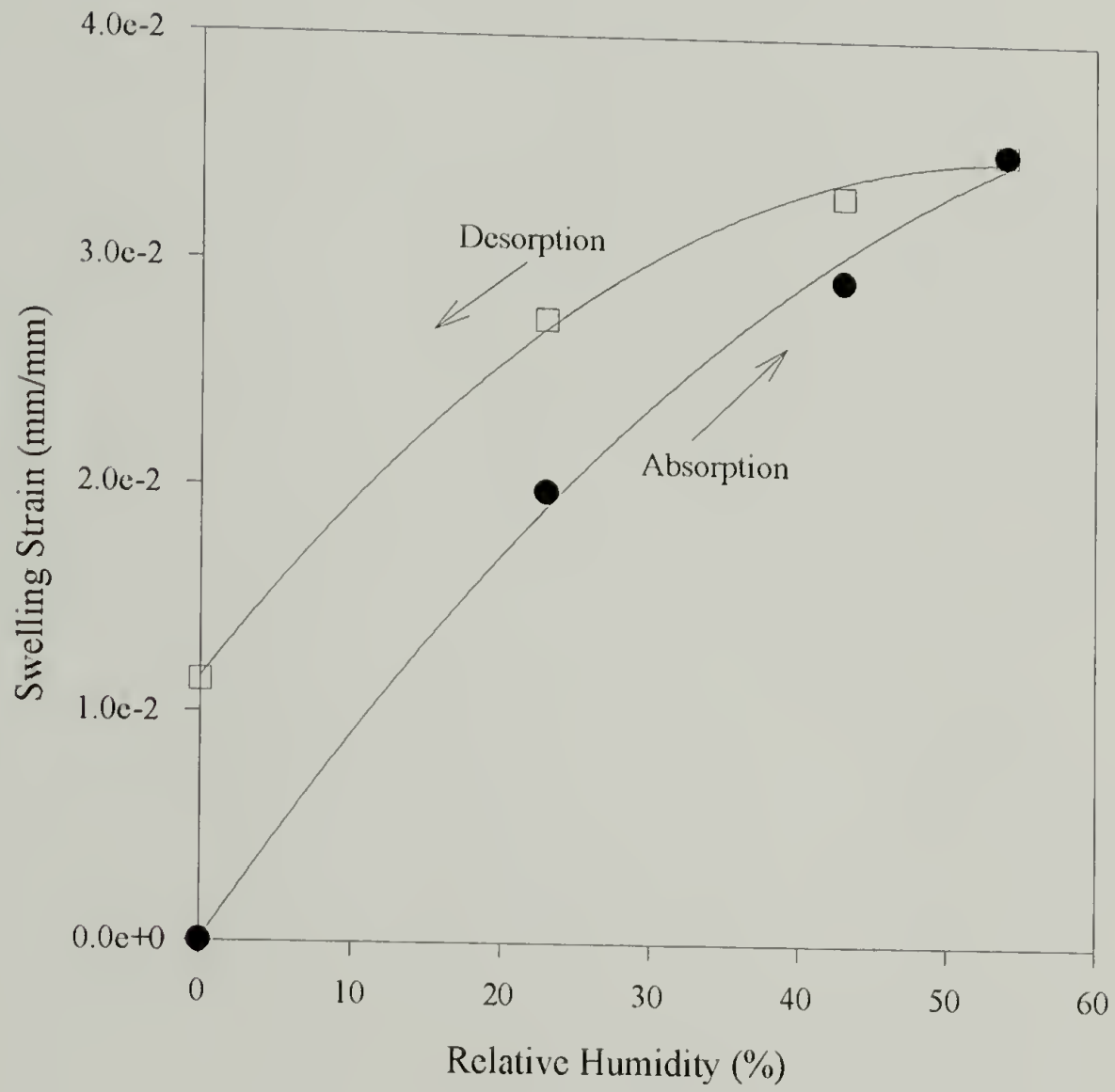

Figure 4.6 Dimensional hysteresis of gelatin (#8247-2-3). This data was generated using a counterweight of 230 g and has not been corrected for zero counterweight load.

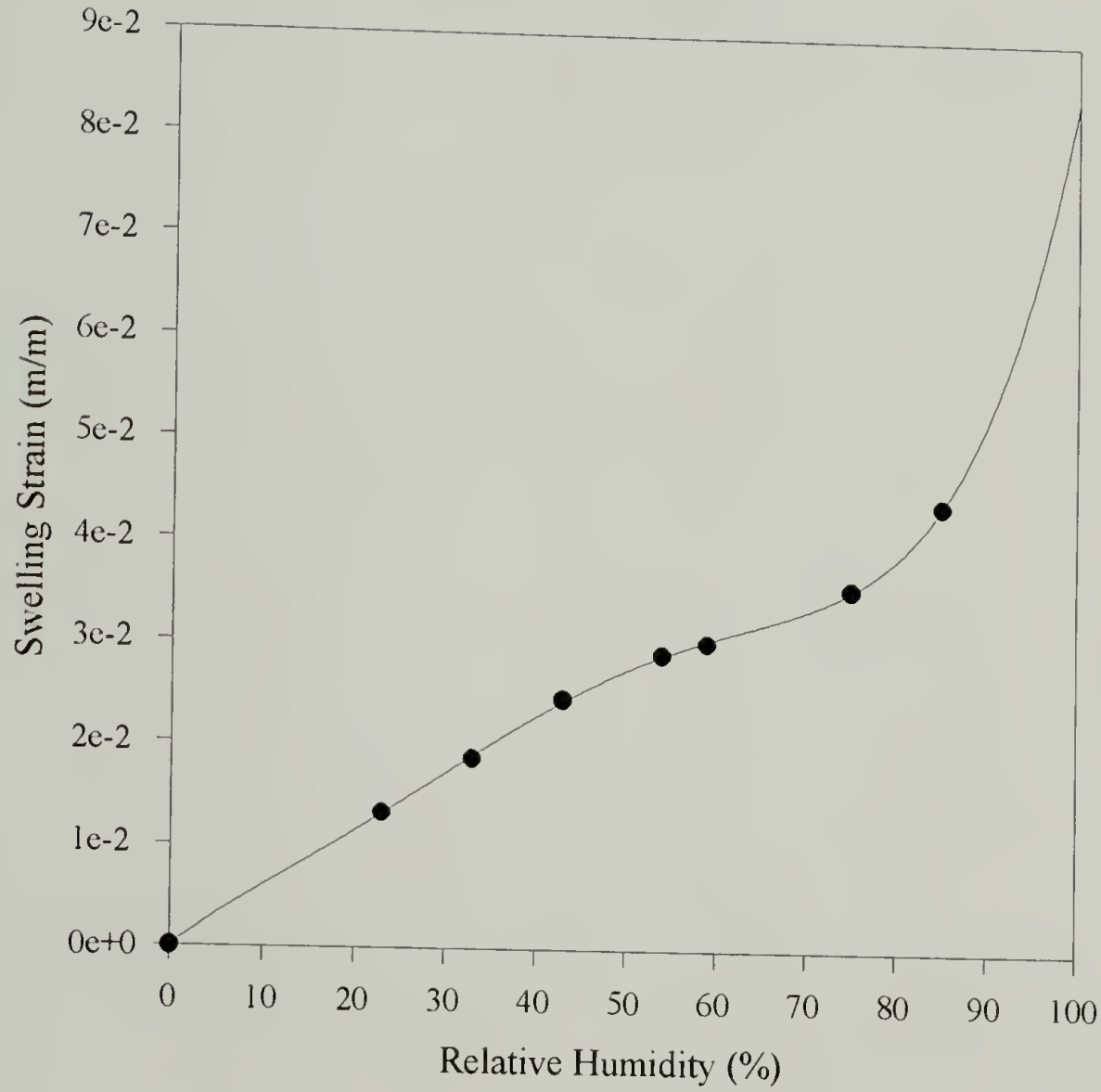

Figure 4.7 Typical swelling strain vs. relative humidity for gelatin (# SC5-5S-5020-01). This represents the absorption path of a gelatin sample fabricated perpendicular to the coating direction.

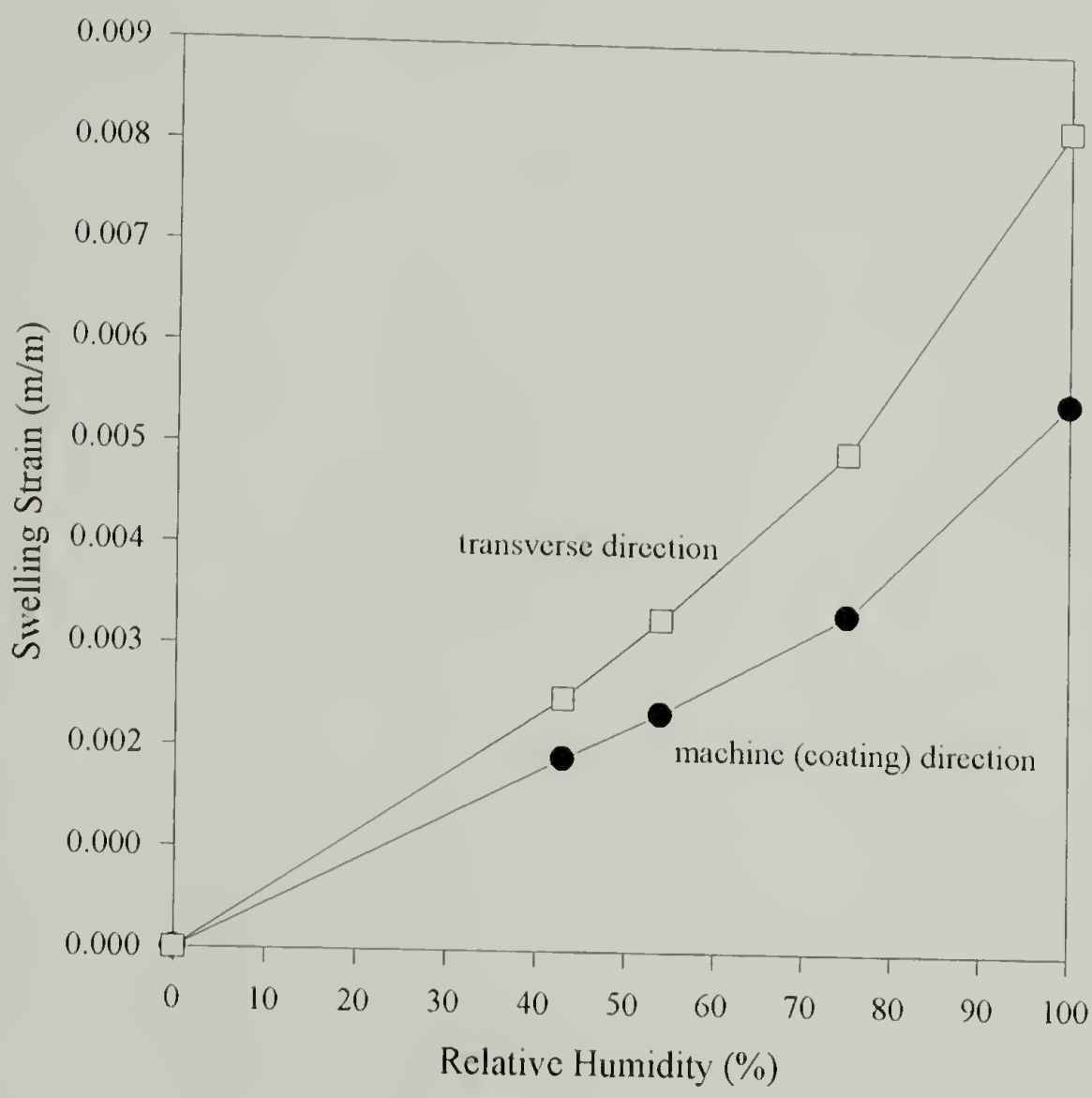

Figure 4.8 Typical swelling strain vs. relative humidity for cellulose acetate substrate.

Therefore, experiments were conducted to investigate the effect of the counterweight on the humidity expansion coefficient on gelatin film.

In these experiments, three counterweights were used: 130 g, 180 g, and 230 g. The counterweights relate to equivalent displacement weights of 35 g, 85 g, and 135 g, respectively as described in equation (4.1). The tests were performed as described in the Experimental section. Figure 4.9 illustrates the results of the absorption experiment.

From the information in figure 4.9, the slope of each curve represents the apparent humidity expansion coefficient. The actual humidity expansion coefficient was determined by plotting the apparent humidity expansion with respect to the displacement weight. This relationship is presented in figure 4.10.

Table 4.1 summarizes the results of figures 4.8 and 4.10. The humidity expansion coefficients for cellulose acetate and gelatin differ by a order of magnitude. It is this mismatch that imposes the bending moment in a bilayer system of gelatin and cellulose acetate. The anisotropy of the cellulose acetate is apparent by the dependence on the humidity expansion coefficient on the direction. The samples were prepared along the principal axes of the cellulose acetate which are oriented parallel and perpendicular to the machine coating direction of the gelatin. As indicated in figure 4.5, at 100%RH, the cellulose acetate sample showed signs of creep. This is due to the load on the sample as required in the test set-up.

Since both gelatins had 16.7% crystallinity and 0% crosslinking agent, there should be no difference between the HEC's. This is, in fact, the result for the absorption path. A comparison study of the desorption path was not performed.

The desorption HEC is less that the absorption HEC for gelatin (# 8247-2-3). The difference between the desorption and absorption swelling characteristics for gelatin has been published although the dependence of the HEC on the sorption path was not noted [11,12,13].

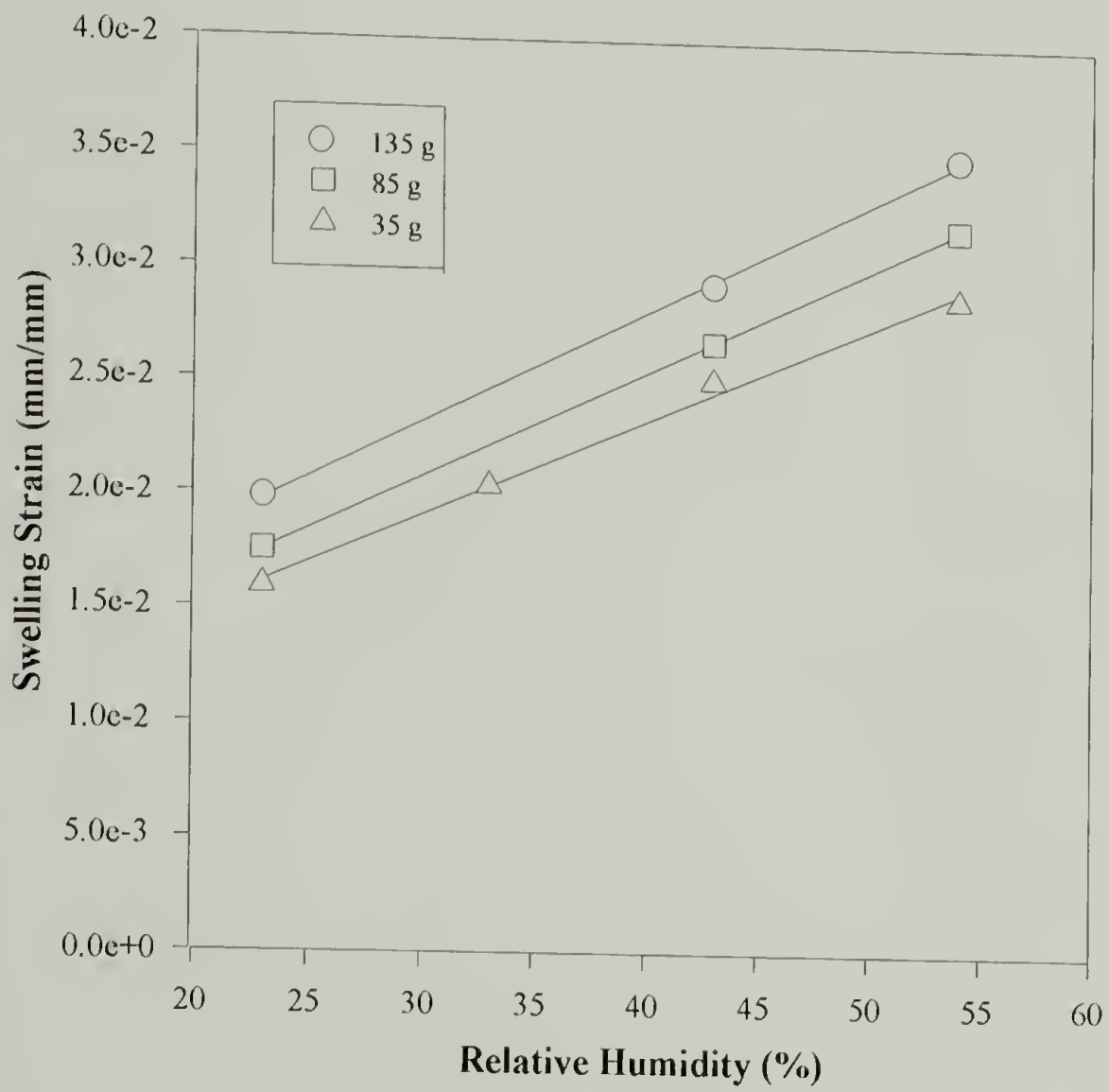

Figure 4.9 The effect of the counterweight size on the absorption swelling strain in alkaline processed bone gelatin (# 8247-2-3: 16.7% crystalline, 0% crosslinking agent). The weights indicated are the displacement weights which are related to the counterweight by equation (4.1).

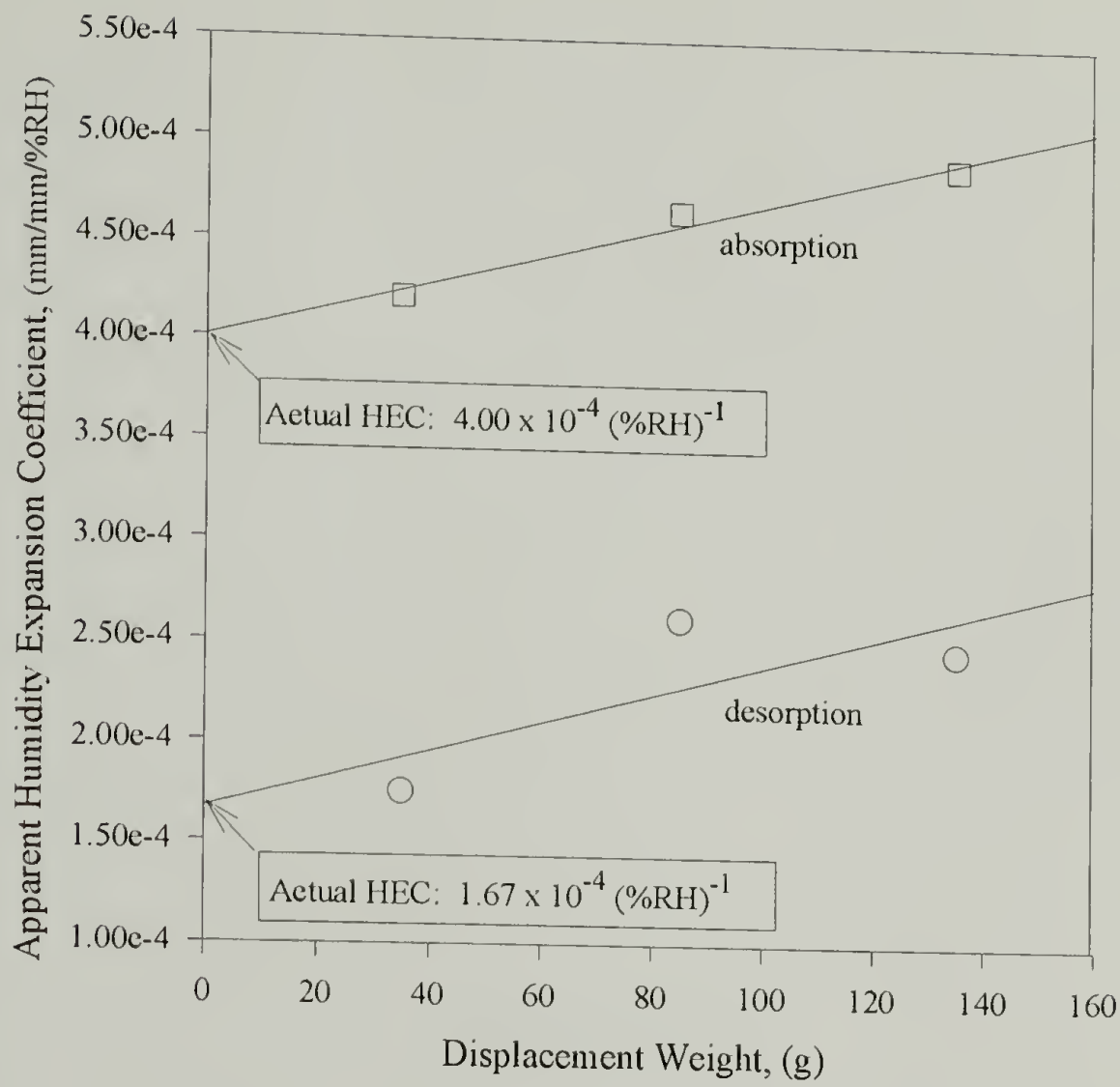

Figure 4.10 Plot of the apparent humidity expansion coefficients vs. displacement weight for absorption and desorption of humidity in gelatin (#8247-2-3). The actual humidity expansion coefficients are the ordinate intercepts of the curves.

The photographic industry customarily determines the humidity expansion coefficient from the absorption part of the sorption cycle [12].

Table 4.1 Summary of the actual humidity expansion coefficients for cellulose acetate and alkaline processed bone gelatins (# 8247-2-3 and SC5-5S-5020-01).

Material	**Sorption Path**	**Humidity Expansion Coefficient, β, (mm/mm/%RH)**
Cellulose Acetate (perpendicular to the gelatin coating direction)	Absorption	6.53 E-05
Cellulose Acetate (parallel to the gelatin coating direction)	Absorption	4.45 E-05
Gelatin (# SC5-5S-5020-01)	Absorption (23%RH to 75%RH)	4.32 E-04
Gelatin (# 8247-2-3)	Absorption	4.00 E-04
Gelatin (# 8247-2-3)	Desorption	1.67 E-04

The difference between the desorption and absorption characteristics is known as hysteresis. The hysteresis mechanisms were discussed in chapter 1 and therefore are not reiterated in detail here. In general, there are two categories of water in the gelatin network: "bound" water which is hydrogen bonded to the backbone and hydrophilic side chains of the gelatin and "free" water which is not bound but instead occupies free space in the amorphous regions of the network. The amount of "bound" water is dependent upon the energy to form or break hydrogen bonds. The quantity of "free" water is dependent upon the osmotic pressure in the system (imposed by the relative humidity). Since the

osmotic pressure in the network is related to the relative humidity, this pressure would not be dependent upon the sorption path. Therefore, the amount of "free" water in the system should be the same, independent of sorption path. This concludes that the "bound" water is the primary contributor of the hysteresis characteristics of gelatin.

Out-of-Plane Humidity Expansion Coefficient

The out-of-plane humidity swelling coefficient was determined for bone alkaline processed gelatin coating (# SC5-5S-5020-01) removed from a cellulose acetate substrate. Table 4.2 tabulates the thickness change as a function of relative humidity.

The change in thickness from 0%RH for the first absorption run greatly differs from the second absorption run. There are several possible reasons. First, the gelatin network collapses forming additional collagen fold crystallites which is a triple α-helix structure. Since moisture swells in the amorphous region of the polymer, the additional formation of crystallites after the first sorption run would reduce the propensity for moisture. This coincides with arguments published by Calhoun and Leister regarding the relaxation of the gelatin [12].

It is feasible that the constrained drying conditions during film fabrication creates a film with excess energy. After a first pass through the sorption cycle, the energy is released. Thus, subsequent runs differ from the first. This is analogous to the thermal investigations performed by Jennings [15] on polyimide films.

Another reason may be that the sample was not completely dried at 0%RH. Also recall that the first desorption path indicated that only 1.792 μm of the 6.773 μm thickness change due to swelling was recovered. Therefore the initial thickness is no longer 197.4 μm but is instead, 202.4 μm. The "excess" thickness may be due to the remaining water in the network that is hydrogen bonded to the gelatin.

The out-of-plane humidity swelling strain as a function of relative humidity is depicted in Figure 4.11. There is a difference in the humidity expansion coefficient between the two sorption runs.

Table 4.2 Thickness change of gelatin sample measured by double slit laser interferometry. Initial thickness at 0%RH is 197.4 μm (8 sheets, 24.68 μm thick of gelatin stacked).

Sorption Path	**Relative Humidity (%)**	**Fringe Shift, ΔN/N**	**Thickness difference μm**	**Strain x 10^2 (m/m)**
Absorption Cycle 1	0		0	0
	23	1.0648	1.264	0.640
	54	2.5345	4.325	2.191
	75	2.0041	6.773	3.430
Desorption Cycle 1	75		0	0
	0	1.5289	1.792	0.907
Absorption Cycle 2	0		0	0
	23	0.4295	0.510	0.258 (0.252)
	54	1.0177	1.739	0.881 (0.859)
	75	1.7328	2.996	1.520 (1.480)

Values in (parentheses) indicate swelling strain adjusted for the change in initial thickness from 197.4 to 202.4 μm based on desorption run values.

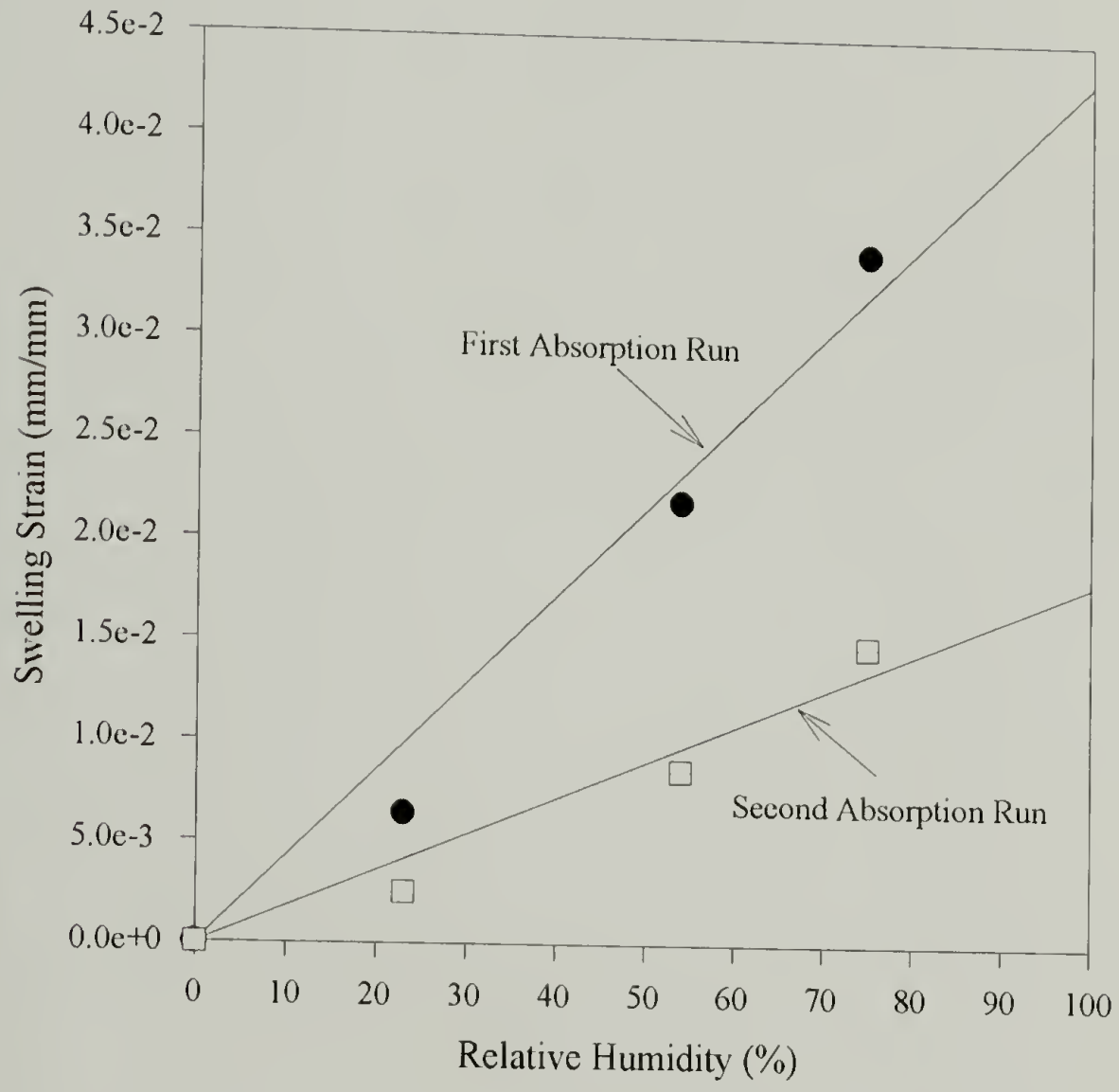

Figure 4.11 Out-of-plane swelling strain as a function of relative humidity for alkaline processed bone gelatin coating removed from cellulose acetate substrate. Second absorption run values adjusted for initial length of 202.4 μm.

Figure 4.11 indicates that the out-of-plane humidity expansion coefficient is either dependent on the sorption cycle or perhaps the gelatin structure changed resulting in less moisture absorption. Table 4.3 summarizes the out-of-plane humidity expansion coefficients for each cycle.

Table 4.3 Humidity expansion coefficients for gelatin (# SC5-5S-5020-01). The HEC's differ depending on the sorption cycle. Values are indicated for the HEC's from 0%RH to 75%RH and the HEC's from 23%RH to 75%RH [9].

Absorption Run No.	**Humidity Expansion Coefficient (0%RH to 75%RH) (mm/mm/%RH)**	**Humidity Expansion Coefficient (23%RH to 75%RH) (mm/mm/%RH)**
1	4.31 E-04	5.33 E-04
2	1.80 E-04	2.33 E-04

The in-plane HEC for gelatin (# SC5-5S-5020-01) during the first absorption run from 23%RH to 75%RH was 4.32 E-04 mm/mm/%RH. This is essentially the same relationship for the out-of-plane humidity expansion coefficient for absorption run no. 1 if the HEC is determined using the 0%RH to 75%RH data. From this data, the material is volumetrically isotropic as opposed only planar isotropic as discussed earlier.

If the 23%RH to 75%RH out-of-plane humidity swelling strain data is applied, then the gelatin is only isotropic in the plane of coating and is anisotropic out of the plane. This result coincides with the literature [14]. It has been determined by optical rotation measurements that gelatin exhibits swelling anisotropy. Swelling anisotropy is the ratio of the out-of-plane swelling to the in-plane swelling of the gelatin. This ratio should be

greater than one for alkaline processed bone gelatin dried at 25°C and ~50%RH. Comparing the out-of-plane to the in-plane HEC, the swelling anisotropy is 1.23 for gelatin (#SC5-5S-5020-01) between the humidity range of 23% to 75%RH.

Conclusions

The in-plane humidity expansion coefficients for gelatin and cellulose acetate were determined. The gelatin HEC (4.00 E-04 mm/mm/%RH) is an order of magnitude greater that the cellulose acetate HEC (4.45 E-05 mm/mm/%RH) along the gelatin coating direction. It is this mismatch of the HEC's which contributes to the dimensional instability in a bilayer system of gelatin and cellulose acetate. In addition, the in-plane HEC of cellulose acetate perpendicular to the gelatin coating direction is 6.53 E-05 mm/mm/%RH. This anisotropy of the cellulose acetate is a primary contributor to the inversion of the cylindrical shapes observed at various humidities (reference chapter 2)

The gelatin shows planar isotropy whereas the cellulose acetate results indicate anisotropy. The reason for the anisotropy results from the casting process used to fabricate the cellulose acetate film.

There is a hysteresis in the humidity swelling strain of gelatin. This hysteresis is apparent by the dependence of the HEC on the sorption path. The absorption HEC is greater than the desorption HEC as a result of the proposed hysteresis mechanism.

The out-of-plane humidity expansion coefficient of gelatin showed a dependence on the sorption cycle. Assumptions were made regarding the refractive index change of the gelatin with relative humdity. The out-of-plane HEC, (4.32 E-04 mm/mm/%RH) determined from 0%RH to 75%RH, indicates that the overall volume of gelatin was isotropic. If the calculation of the HEC is limited to the 23%RH to 75%RH range, the gelatin is planar isotropic but anisotropic through the thickness or out of the plane. This observation agrees with that reported in the literature.

References

1. S.T. Sackinger, The Determination of Swelling Stresses in Polyimide Films, Ph.D. diss., University of Massachusetts, Amherst, MA, (1990).

2. T. Ohyama and Y.H. Mori, "Optical Method for Measuring Uniform Thickness of the order of 10 μm - 1 mm of Transparent Solid and Liquid Films," Review of Scientific Instrumentation, **58**(10), 1860 (1987).

3. M. Koedam, "Determination of Small Dimensions by Diffraction of a Laser Beam," Philips Technical Review, **27**(7), 208 (1966).

4. A.J. Perry, B. Ineichen and B. Eliasson,"Fiber Diameter Measurement by Laser Diffraction," Journal of Materials Science, **9**, 1376 (1974).

5. T. Ohyama, K. Endoh, A. Mikami and Y.H. Mori, "Optical Interferometry for Measuring Instantaneous Thickness of Transparent Solid and Liquid Films," Review Scientific.Instrumentation, **59**(9), 2018 (1988).

6. K.L. Saenger and H.M. Tong, "Laser Interferometry: A Measurement Tool for Thin Film Polymer Properties and Processing Characteristics," New Characterization Techniques in Thin Polymer Films, eds., H.M. Tong and L.T. Nguyen, (New York: John Wiley and Sons, Inc., 1990).

7. B. Ni, personal communication, January, 1993.

8. N. Easwar, C. Ofcarcik, J.K. Vrtis and R.J. Farris, "Optical Interferometric Method for the Measurement of the Out of Plane Thickness Changes of Weakly Absorbing Thin Solid Films," (in process).

9. J. Greener, personal communication, June, 1994.

10. J. Eliassaf and F.R. Eirich, "Creep Studies on Gelatin at 100% Relative Humidity," Journal of Applied Polymer Science, **IV**(11), 200 (1960).

11. "Physical and Chemical Behaviour of *Kodak* Aerial Films," Properties of *Kodak* Materials for Aerial Photographic Systems, Vol. III, (Rochester, NY: Eastman Kodak Co., 1974).

12. J.M. Calhoun and D.A. Leister, "Effect of Gelatin Layers on the Dimensional Stability of Photographic Film," Photographic Science and Engineering, **3**, 8 (1959).

13. J.M. Calhoun, P.Z. Adelstein and J.T. Parker, "Physical Properties of *Estar* Polyester Base Aerial Films for Topographic Mapping," Photogrammetric Engineering, **27**, 461 (1961).

14. P.I. Rose, "Gelatin: I. General Properties," The Theory of the Photographic Process, 4th ed., eds., J.F. Hamilton, G.C. Higgins and J.E. Starr, (Rochester, NY: Eastman Kodak Co., 1977).

15. R.M. Jennings, An Investigation of the Effects of Curing Conditions on the Residual Stress and Dimensional Instability of Polyimide Films, Ph.D. diss., University of Massachusetts, Amherst, MA, (1993).

CHAPTER 5

STRESSES IN COATINGS AND FILMS

Introduction

Stresses in coatings often result in dimensional instability of the system [1,2]. This phenomenon is often observed by the curling or bending of the coating/substrate bilayer. This has been a great concern in the photographic industry and more recently in the aerospace and electronics industries [3-9]. The bending of the bilayer is induced by (a.) the mismatch between the expansion coefficients (both thermal and hygroscopic) [1,10-14], (b.) physical aging (often termed "degradation") in which the molecular rearrangement over time changes the material properties [15] and (c.) solvent removal or chemical reaction resulting in the shrinkage of the material [16]. Understanding the source of coating stresses is advantageous to optimizing the product design.

There are several techniques available to study stresses in coating and films. Several of these techniques have been outlined by Maden [17]. Stress measurement methods are divided into three categories: (a.) techniques which measure the strain (or radius of curvature) in the system and relate this to stress via linear elastic assumptions, (b.) techniques which apply a force to the material to measure the resulting displacement and (c.) techniques that measure the response of the material due to vibration.

In general, the most common method of measuring stress is a beam bending technique [2]. This is an indirect stress measurement technique based on Beam Bending Theory. In beam bending , the strain (in the form of bending curvature) in the system is measured. Linear elastic assumptions are made to relate the strain to the stress. Thus if a material is not linear elastic, the technique only provides an approximation. The disadvantage of using beam bending is that it is a one dimensional technique. To analyze a

two dimensional system, Poisson's ratio is required. This imposes additional error into the calculated stress values. Therefore, a direct method for determining the stress dependence on environmental conditions is desired. The technique adopted for this investigation is Holographic Interferometry.

This chapter will focus on the effect of relative humidity on the stresses in coatings and films. Several materials were investigated: alkaline processed bone gelatin which was machine-coated by Eastman Kodak on substrates of cellulose acetate and PET, poly(vinyl alcohol), PVOH, blade-coated on PET, diglycidyl ether of bisphenol A, (DGEBA), epoxy spin-coated on tin plated steel and nickel electroplated to steel. In this chapter, real time holographic interferometry was used to determine the biaxial stresses in coatings and films as a function of relative humidity.

Holographic interferometry normally requires the sample to be under vacuum to eliminate lateral pressure effects imposed by air. Pressure effects depress the apparent stress values [17]. Since the effect of relative humidity on the stresses in the materials is proposed, the effect of moisture introduction to the sample and its effect on holographic interferometric results are discussed.

Experimental

Holographic interferometry was used to directly determine the stress in the coatings and films. Chapter 3 briefly outlined the governing equations for this technique and further details regarding the mathematical derivation and the effect of air dampening is discussed elsewhere [17]. In general, holographic interferometry is based on the vibrating membrane equation:

$$\sigma \nabla^2 \omega = \rho \frac{\partial^2 \omega}{\partial t^2} \qquad (5.1)$$

where,

σ = biaxial stress in the membrane

∇^2 = LaPlacian operator, $\frac{\partial^2}{\partial r^2}+\frac{1}{r}\frac{\partial}{\partial r}+\frac{1}{r^2}\frac{\partial^2}{\partial \theta^2}+\frac{\partial^2}{\partial z^2}$

ω = out of plane displacement (or deflection)

ρ = density of the membrane

$\frac{\partial^2 \omega}{\partial t^2}$ = out of plane acceleration as a function of time

The membrane equation can be solved for a circular geometry by assuming the deflection at the outer radius is zero, $\omega(r = R) = 0$. This reduces equation (5.1) to:

$$\sigma_{2D} = 4\pi^2 \rho R^2 \frac{\nu_{ni}^2}{Z_{ni}^2} \qquad (5.2)$$

where,

σ_{2D} = biaxial stress, (MPa)

π = 3.14.....

ρ = material density, (g/cm^3)

R = membrane radius, (cm)

ν_{ni} = resonant frequency, (Hz)

Z_{ni} = i^{th} zero of the n^{th} order Bessel's Function

It is apparent from equation (5.2) that only the density of the material is required to determine the stress in the membrane. Using special sample preparation techniques to preserve the state of stress in the coating and by performing the test under specific environmental conditions which reduces air pressure loading effects, the stress in a coating can be directly measured.

Sample Preparation

Preparation of the holographic interferometric membrane sample is critical in order to satisfy the boundary conditions for the solution to the general equation. The state of stress in the coating must be maintained in order to truly characterize its stress. Therefore, special sample preparation techniques are adopted to satisfy this requirement. For a coating/substrate system in which the substrate is sufficiently thicker and stiffer than the coating, there is no shear or normal traction between the coating and the substrate beyond a few film thicknesses from the system's edge. Therefore, if a rigid washer is adhered to the coating >3 film thicknesses from the edge, the original state of stress is preserved. Chapter 2 provides a detailed analysis of the state of stress in coating systems. Several methods can be applied to prepare a uniform free film sample [18,19,20]. The method chosen is dependent upon the material. Therefore the methods described below are specific to each material system.

Membranes of gelatin were made by subjecting the bilayer system (gelatin/CA or gelatin/PET) to a relative humidity which caused the system to be free from stress. In the stress free state, the bilayer is flat. For gelatin/CA, that relative humidity was ~54%RH. For the gelatin/PET samples, the bilayer was flat at ~75%RH. A rigid steel washer was then adhered to the gelatin coating using Super Glue® and pressure was applied to ensure uniform adherence. After the glue was dried, the substrate was removed at a take-off angle of ~5°. It should be noted that a release agent between the gelatin and the cellulose acetate substrate was used in order to aid the substrate removal process. No coating release layer was required for the gelatin on a PET substrate due to the PET's relatively low surface energy.

Air Products Airvol® 325 PVOH was blade coated on a PET substrate which was secured to a 1/4" sheet of PMMA and dried at 21°C, 54%RH. Membranes were made

from the bilayer system. Analogous to the gelatin membrane preparation, a steel washer was adhered to PVOH with a 5 minute room temperature cure epoxy from 3M Corp. The PET was easily removed at a small take-off angle.

An epoxy coating of Shell's EPON 828 (diglycidyl ether of bisphenol A type epoxy resin) with a V-40 (a polyamino amide) curing agent was spin-coated to tin plated steel and cured at 70°C for 4 hours. A steel washer was adhered to the epoxy coating using a 5 minute curing epoxy. The complete assembly was submerged in mercury. The mercury forms an amalgam with the tin thus removing the substrate which results in a free standing membrane of epoxy [20].

Nickel was electroplated on tin plated steel by Berkshire Manufacturing. The sample preparation was the same as the epoxy membrane except Super Glue was used to adhere the steel washer to the nickel. An amalgam of mercury with tin was utilized to free the membrane from the substrate.

Holographic Interferometry and Relative Humidity

In holographic interferometry, the sample is normally tested under vacuum. This eliminates pressure effects that result in deflated stress values. The deflated stress values would require a data correction simular to that proposed by Lax [21]. To avoid this phenomenon when introducing relative humidity to the membrane sample, helium gas was used due to its low molecular weight. A nickel membrane was used to investigate the possible effects of relative humidity on the actual stress values.

Figure 5.1 depicts the holographic interferometry set-up with relative humidity adaptation. The source of the relative humidity was described in chapter 3.

Swelling Stress Dependence on Relative Humidity

In polymers, relative humidity can induce stress by swelling the material [1,3,10,15,22,23]. Dimensional instability is often observed as a result of this stress. The humidity induced swelling stress in a coating/substrate bilayer can impose a bending moment which may cause difficulty in processing [4,9]. The equilibrium moisture content in these materials is a function of relative humidity in the atmosphere [24]. Moisture hysteresis between the absorption and desorption paths of the sorption cycle is a common phenomenon [25-28]. Since the relative humidity is related to the moisture content in a material, the swelling stress is dependent on moisture content. Therefore, the sorption path also affects the radius of curvature resulting from the stress in the materials [3].

An investigation of the swelling stresses was performed using Real-Time Holographic Interferometry. The membrane samples were exposed to various relative humidities. At each humidity, the equilibrium swelling stress in the membrane was determined.

Swelling Stress Dependence on Crystallinity and Crosslinking

The drying conditions of the gelatin coating dominate its degree of crystallinity [29]. Moisture swelling occurs in the amorphous region of the polymer. Therefore, the degree of crystallinity can influence the moisture sorption hysteresis loop. Gelatin is commonly catagorized as cold-dried (or gel type) and hot-dried (or sol type) [30,31]. Cold-dried gelatin is dried at room temperature (25°C) and ~50%RH.

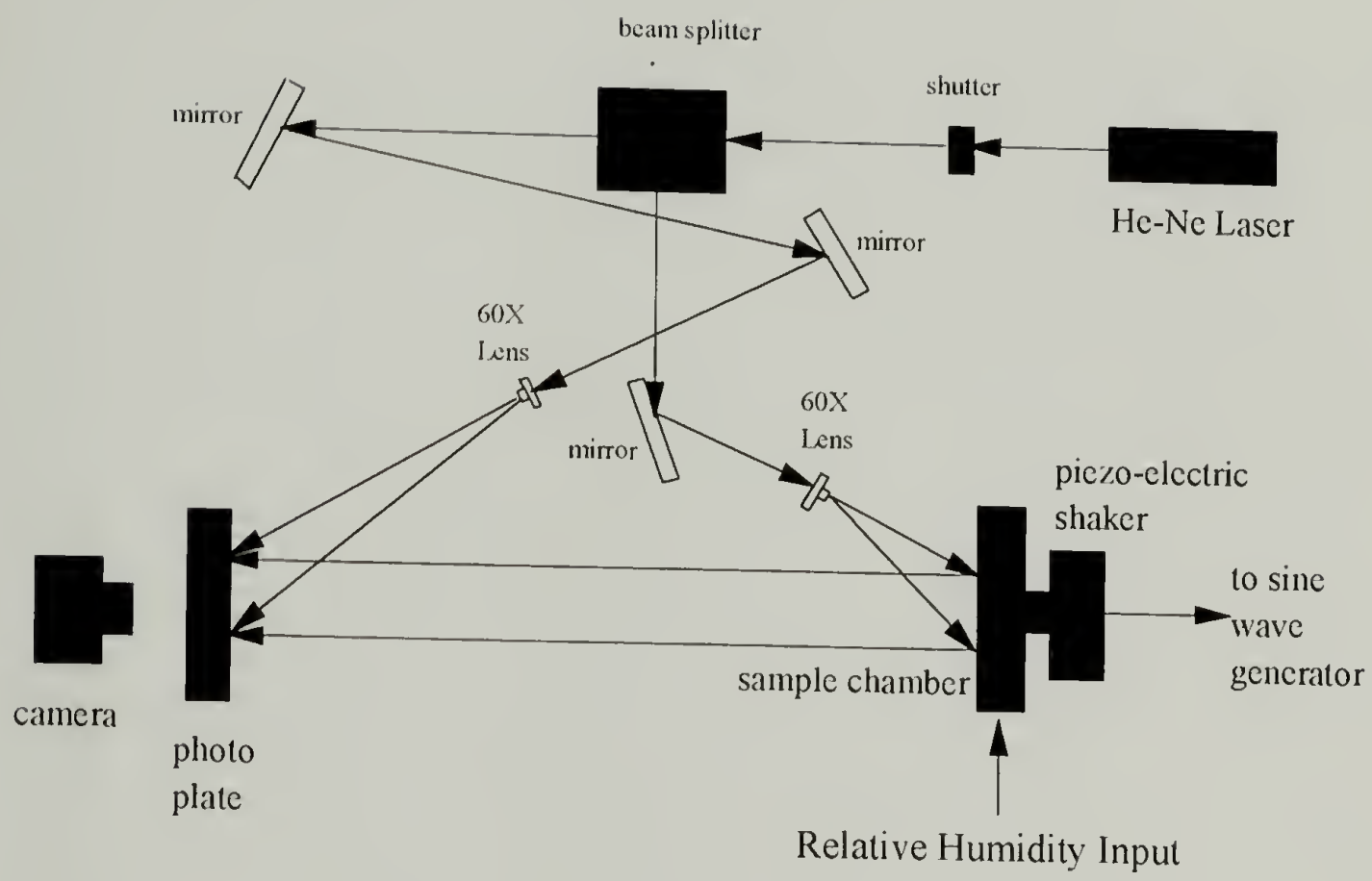

Figure 5.1 Holographic interferometry set-up for relative humidity introduction.

Hot-dried gelatin is dried at elevated temperatures (~60°C) between 50% to 70%RH. The cold-dried gelatin has the propensity to form collagen fold crystallites which comprises the crystalline portion of the film. The degree of crystallinity is dependent upon the rate at which the gelatin is dried [32]. Hot-dried gelatin is a completely amorphous network. Studies have shown that the mechanical and swelling properties of gelatin are dependent upon the drying conditions [30-34].

Crosslinking agents, often referred to as "hardeners" in the photographic industry, are added to the gelatin to improve its mechanical properties [35]. Several crosslinking agents are available for gelatin [36-38]. Although the mechanical properties are improved by crosslinking, the swelling properties diminish. A balance between the degree of crystallinity and the amount of crosslinking is required to balance the mechanical and swelling properties of gelatin.

Gelatin membranes were made from gelatin/PET samples supplied by the Eastman Kodak Co. Eastman Kodak characterized the melt enthalpies of each sample. The melt enthalpy is related to the crystallinity in polymers, Membranes of various crystalline content were tested. Holographic Interferometry was used to measure the swelling stress at various relative humidities as a function of crystallinity.

Different percentages of a crosslinking agent were added to the gelatin during manufacturing. Holographic Interferometry was employed to determine the swelling stress as a function of percentage crosslinking agent.

Results and Discussion

Holographic Interferometry and Relative Humidity

A nickel membrane was used to investigate the possible dampening effects of relative humidity on the actual stress values. The membrane was subjected to three

different environments: vacuum, dry helium and various relative humidity transported via helium gas. The generation of relative humidity was described in chapter 3. The resonant frequencies were monitored in each case. At least 10 modes of vibration were recorded for each test run. The effect of the environment on the actual stress values was analyzed by comparing the stress vs. vibration mode for each environment. Figure 5.2 provides a comparison of the stress values in vacuum, helium at 0%RH and helium at 75%RH.

The experimental error for the holographic interferometry is 5%. Therefore, no corrections of the apparent stress values are required if helium is used as the transport gas.

Figure 5.3 depicts the biaxial stress of the nickel membrane subjected to various relative humidities. Again, it is apparent that the stress values fall within the experimental error. Therefore no correction is required as would be the case if air was used as the transport medium.

Swelling Stress Dependence on Relative Humidity

The gelatin showed very interesting results regarding its swelling stress dependence on relative humidity. A stress hysteresis was evident and was similarly observed by others who performed uniaxial stress tests [7]. Each value on the biaxial swelling stress vs. relative humidity curve represents equilibrium values. In other words, the stress was allowed to equilibrate at each relative humidity. Figure 5.4 illustrates the equilibrium stress behavior of gelatin as a function of relative humidity.

Figure 5.5 isolates the desorption behavior of the gelatin (#SC5-5S-5020-01) and the regression values are summarized in Table 5.1.

The drop of 4 MPa in the biaxial stress at 0%RH between the first desorption run and subsequent runs was a result of stress relaxation [7]. It has been noted in the literature that below 20%RH, the gelatin has a tendency to stress relax.

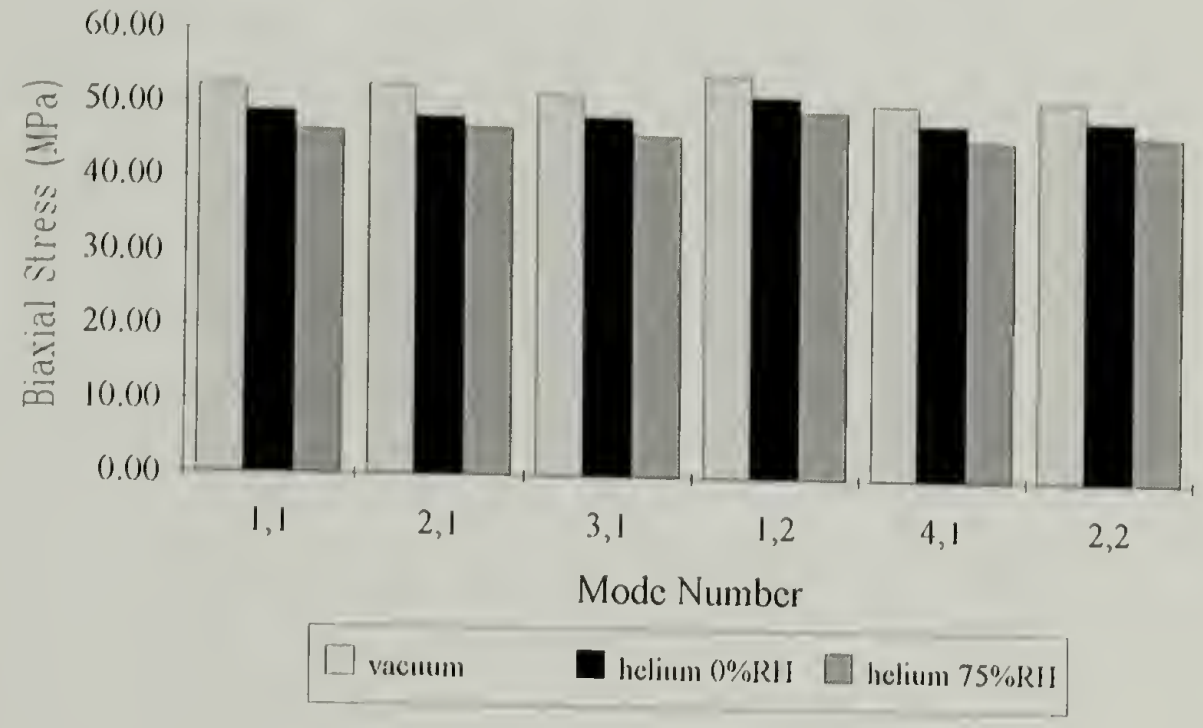

Figure 5.2 Comparison of apparent biaxial stress values for a nickel membrane subjected to three different environments.

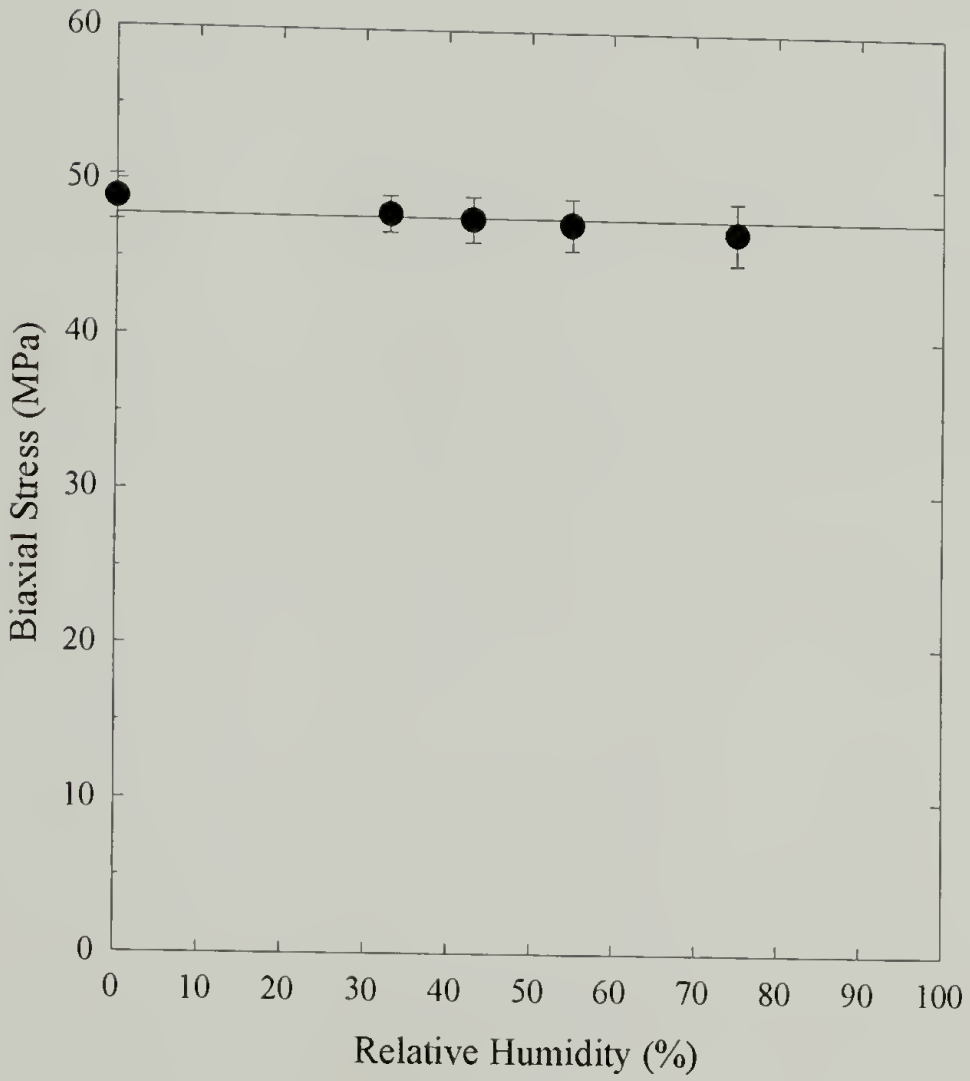

Figure 5.3 Effect of relative humidity on the actual stress values measured on a nickel membrane using holographic interferometry.

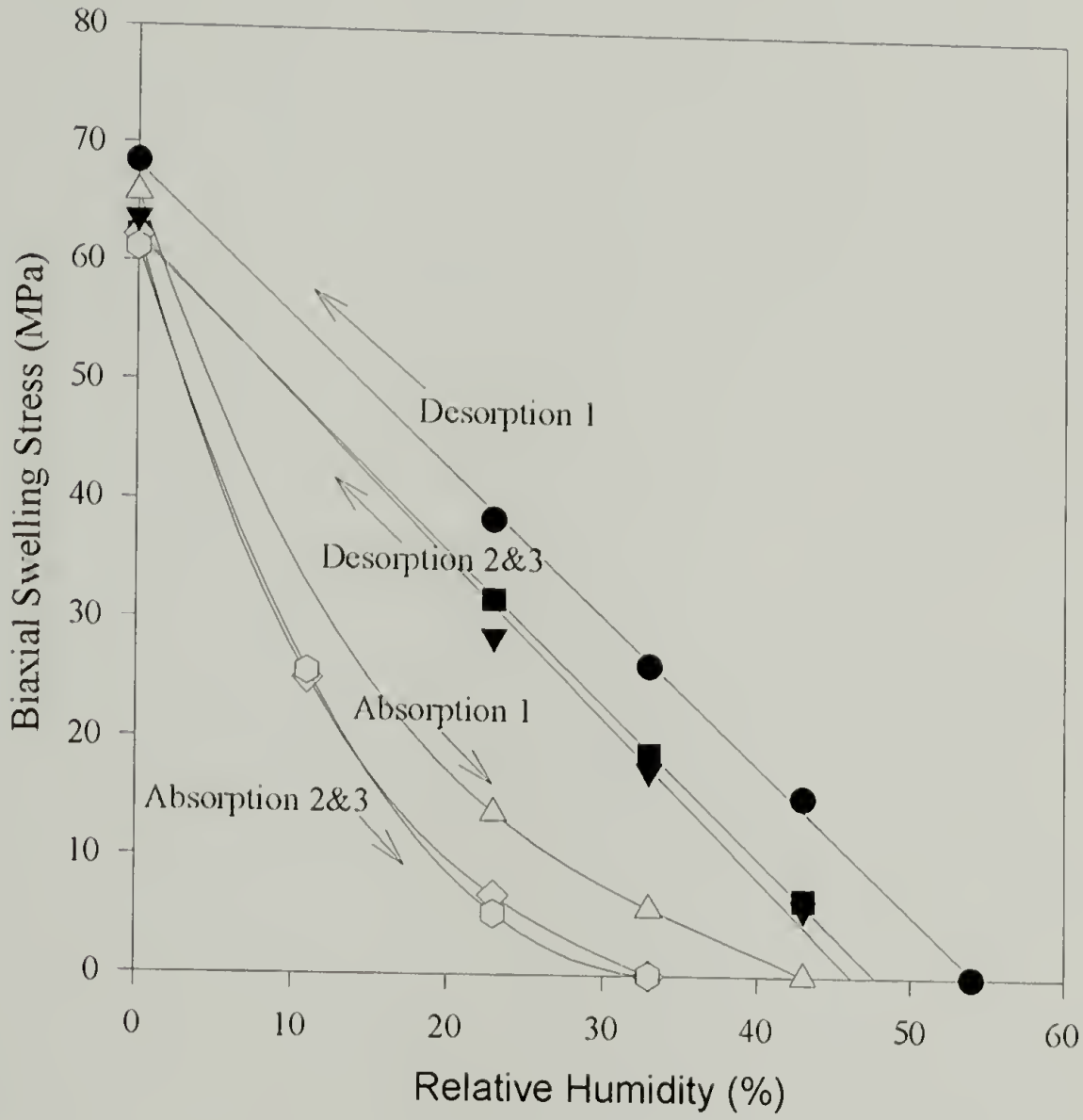

Figure 5.4 Dependence of relative humidity on the equilibrium biaxial swelling stress of alkaline processed bone gelatin coating. Hysteresis between desorption and absorption paths is evident.

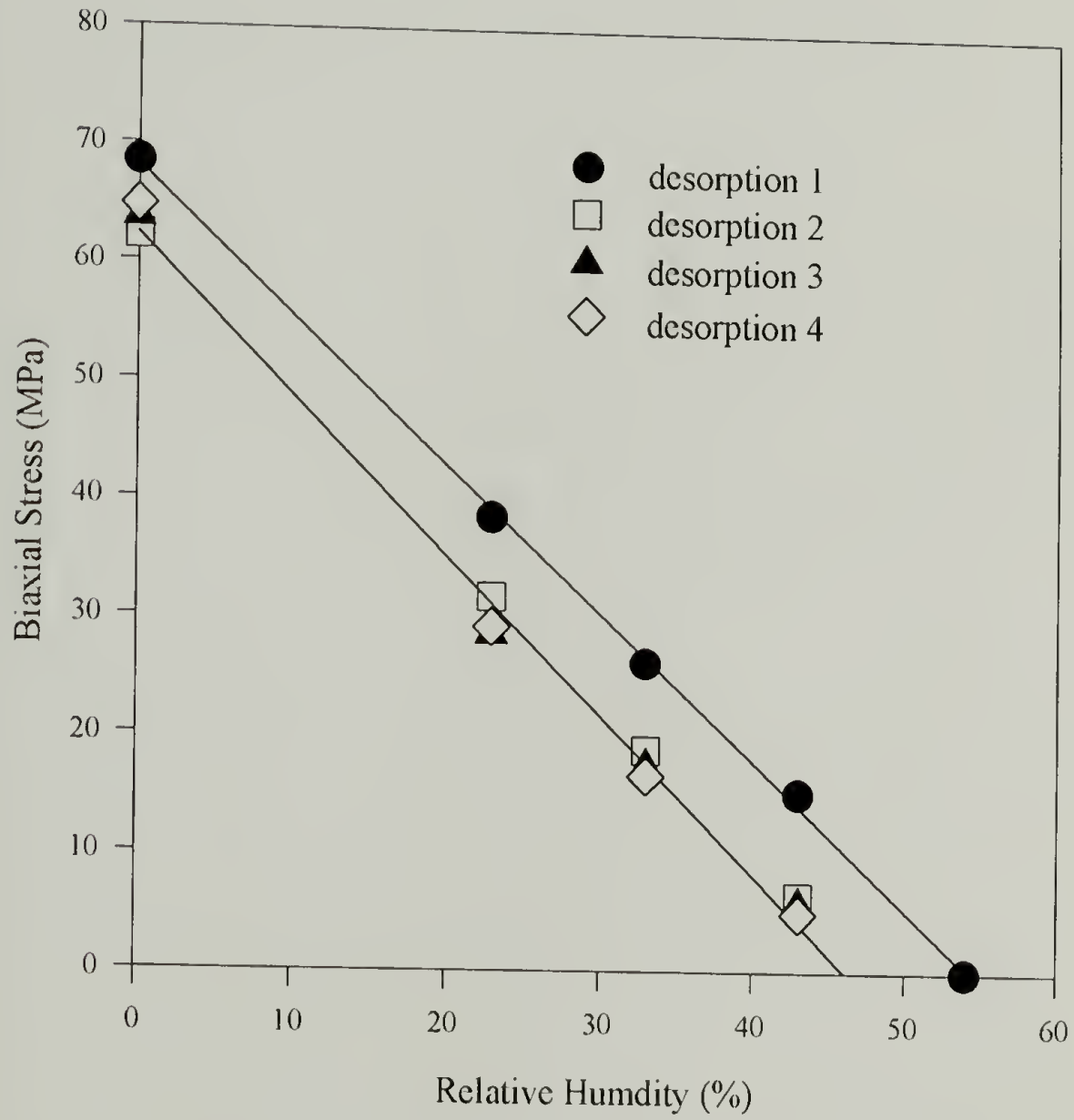

Figure 5.5 Comparison of desorption paths for gelatin subjected to various relative humidities from 54% to 0%RH.

Recall that the membrane is under constant strain since a rigid washer was secured to the coating at zero stress prior to the substrate removal. It was apparent at lower humidities that the membrane exhibited very high stress of 68 MPa. With time (48 hours), the biaxial stress relaxed to 62 MPa.

Table 5.1 Comparison of linear regression values for desorption runs of gelatin subjected to various relative humidities.

Desorption Run No.	Slope (MPa/%RH)	Intercept (MPa)
1	-1.25	68.0 ± 0.4
2, 3, 4	-1.30	62.0 ± 0.8

The absorption mechanism in gelatin differs from the desorption as indicated by the non-linearity of the absorption curves in Figure 5.4. The curves are fitted by a 3rd order polynomial equation. Table 5.2 provides a comparison of each absorption run.

Table 5.2 Comparison of curve fit values for gelatin during absorption. A 3rd order polynomial regression is used where $f(RH) = a + b(RH) + c(RH)^2 + d(RH)^3$.

Absorption Run No.	a (MPa)	b (MPa/%RH)	c (MPa/%RH^2)	d (MPa/%RH^3)	Correlation(%)
1	65.73	-3.85	0.086	-7.52×10^{-4}	100
2, 3	61.63	-4.31	0.101	-8.16×10^{-4}	99.96

The first sorption cycle is represented in Figure 5.6. The stress drops rapidly with the introduction of relative humidity. The stress reaches zero at 43%RH. Above 43%RH the membrane is in tension; below 43%RH, it is in compression which is observed as buckling of the membrane. A large hysteresis is also apparent between the sorption paths. In addition, after 48 hours at 0%RH, the swelling stress dropped 4 MPa. Figures 5.7 illustrates the comparison of each absorption path on the biaxial swelling stress.

Moisture sorption hysteresis was an evident characteristic of this material. Details regarding moisture sorption hysteresis were introduced in chapter 1. In general, it is believe to be a result of the network chain conformations. Details regarding the molecular structure of gelatin are available elsewhere [35,39-42]. The conformation of the single chains in the triple helix structure of collagen and gelatin resembles the conformation of a poly(L-proline), Form II, helix which is the trans form of poly(L-proline). Circular dichroism, CD, studies indicate a decrease in the triple helix content of gelatin at humidities < 20% [29,43]. The decrease in the triple helix content is due to the increasing number of cis-conformations with decreasing relative humdity. This is believed to be a contributing factor to the stress relaxation and therefore the 4 MPa drop in stress in the gelatin membrane. Since gelatin has a glycyl residue at every third position along the backbone chain, the poly(L-proline), Form II. It is postulated that the trans-conformations of the single chains of collagen and gelatin are stabilized only in the triple strand structure [43]. For clarity, figure 5.8 is provided to depict the cis- and trans-conformations, (Form I and Form II, respectively) [44]. Circular dichroism is used to determine the triple helix content and monitor the helix to random coil transitions. Circular dichroism is a common technique used to investigate biopolymers. Details regarding CD are described elsewhere [45].

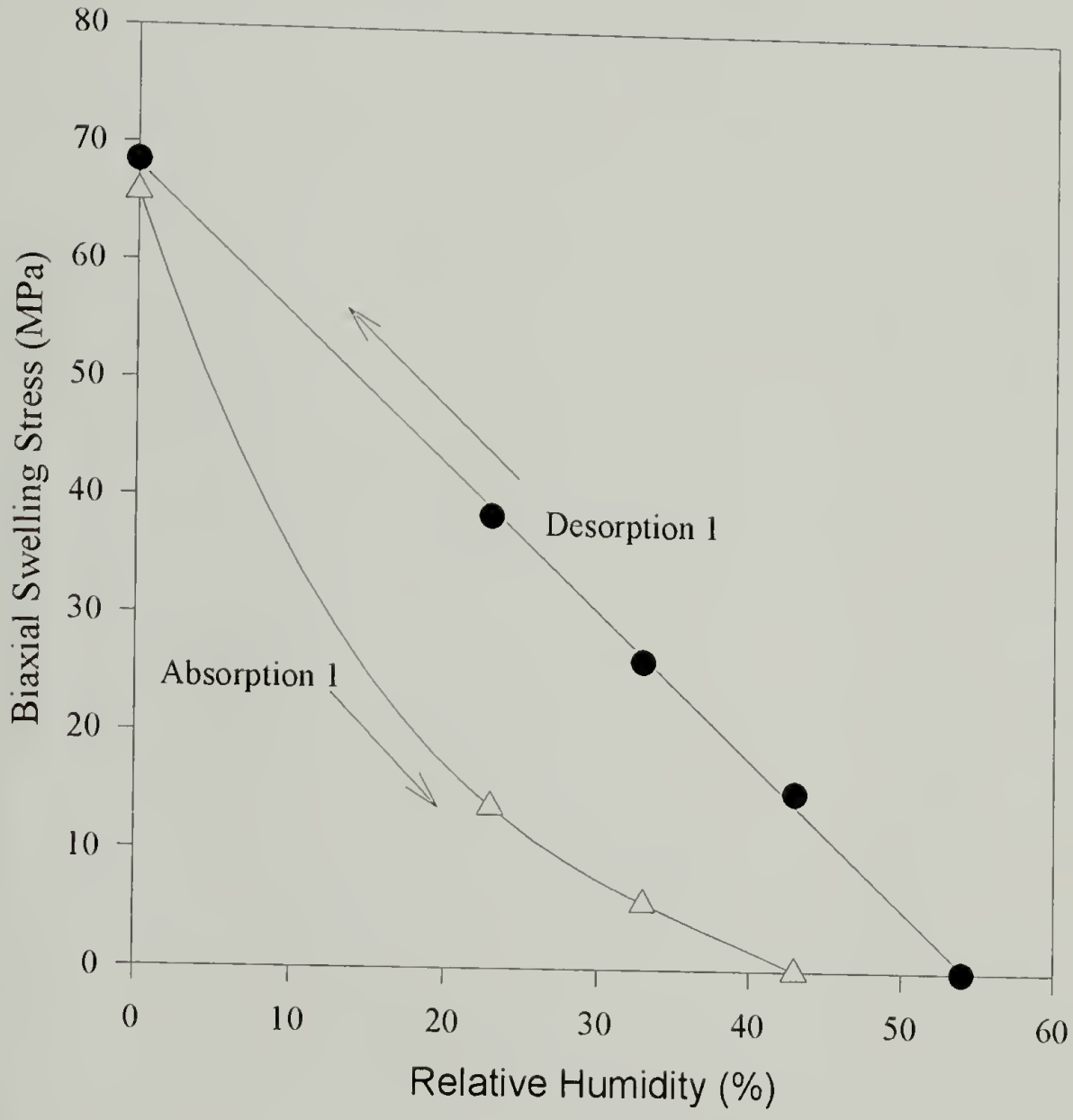

Figure 5.6 First sorption cycle for gelatin initially subjected to desorption from 54%RH.

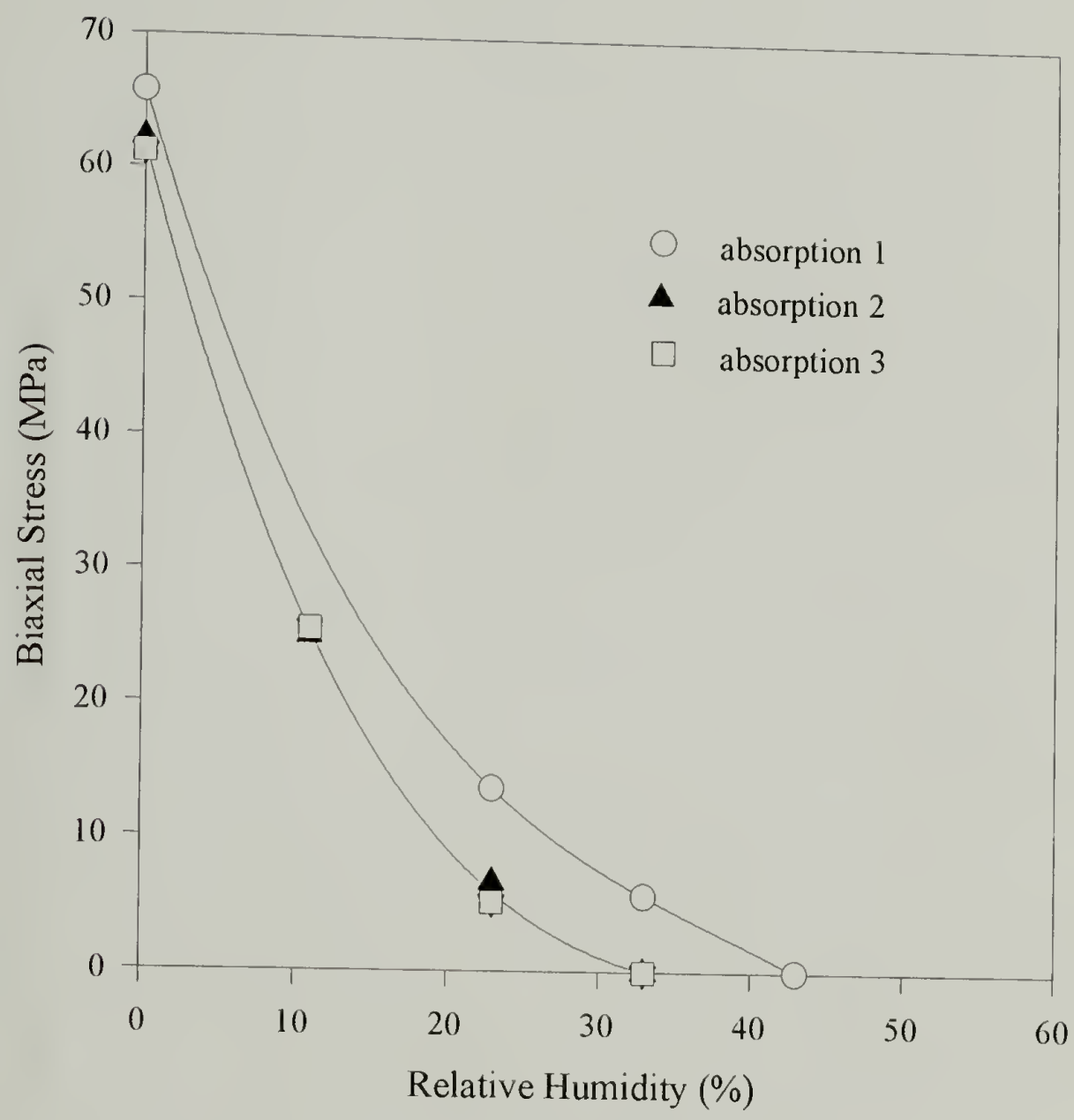

Figure 5.7 Absorption characteristics of biaxial swelling stress as a function of relative humidity for gelatin.

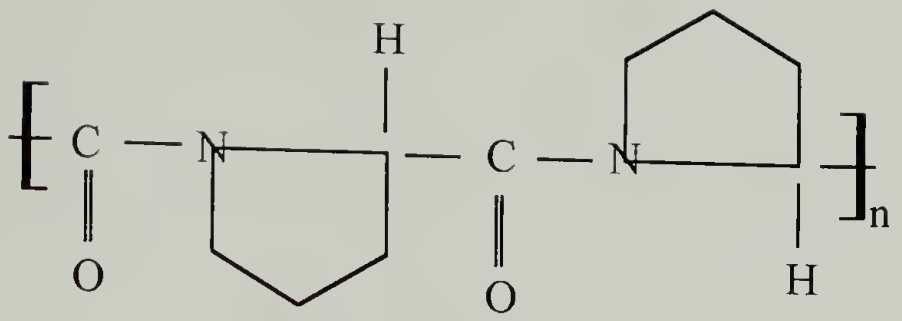

Poly(L-proline), Form II

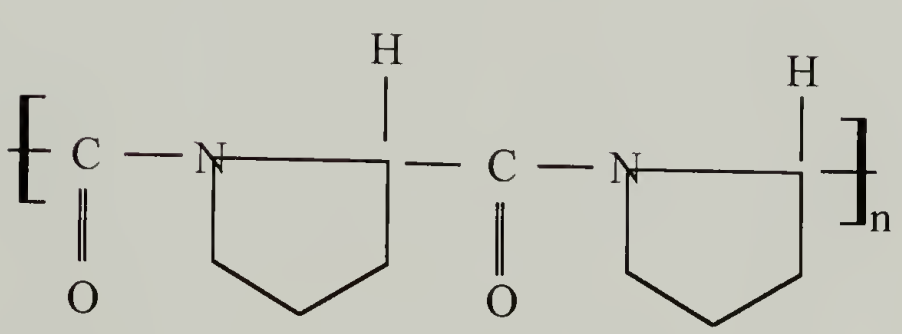

Poly(L-proline), Form I

Figure 5.8 Conformations of Poly(L-proline). Form II is the trans-conformation, Form I depicts the cis-conformation. Form I exists at low relative humidities thus hindering the hydrogen bonding between water molecules and the oxygen of the carbonyl group.

The binding of the water molecules to the C-O groups in the gelatin are essential to form the hydrogen bonding which stabilizes the triple helix structure. It was found that the water molecules are less accessible to bind with the C-O groups in the cis-conformation than the trans-conformation. Rao and Das [25] attribute the hysteresis behavior to different amount of cis- and trans-conformations during the desorption and absorption paths. Therefore, as the water content in gelatin films decrease, the triple helix content decreases and an increase in the cis-conformation is observed [43].

The PVOH coating exhibited hysteresis below 54%RH. Recall that the sample during fabrication was dried at 54%RH, 21°C. Above 54%RH there is no evidence of hysteresis. It seems apparent that the fabrication conditions dictate the hysteresis in this material. If that is true, it seems plausible that tailoring the fabrication conditions could minimize the moisture hysteresis. This is outside the scope of this research and will be addressed in chapter 7. PVOH is known to form hydrogen bonds with water [46]. Moisture sorption hysteresis arguments regarding the amounts of cis- and trans-conformations made by Rao and Das [25] are valid for PVOH. Figure 5.9 shows the sorption characteristics of the PVOH coating.

The sorption paths for each of the two runs were identical and therefore no stress relaxation was observed. Additionally, the biaxial stress as a function of time was monitored to ensure equilibrium was achieved at each relative humidity. Figure 5.10 illustrates a typical biaxial stress vs. time curve for PVOH for the absorption cycle of each run from 0% to 23%RH.

Figure 5.10 is similar to characteristic mass transport curves. A correlation between the swelling stress and the mass uptake is discussed in chapter 6.

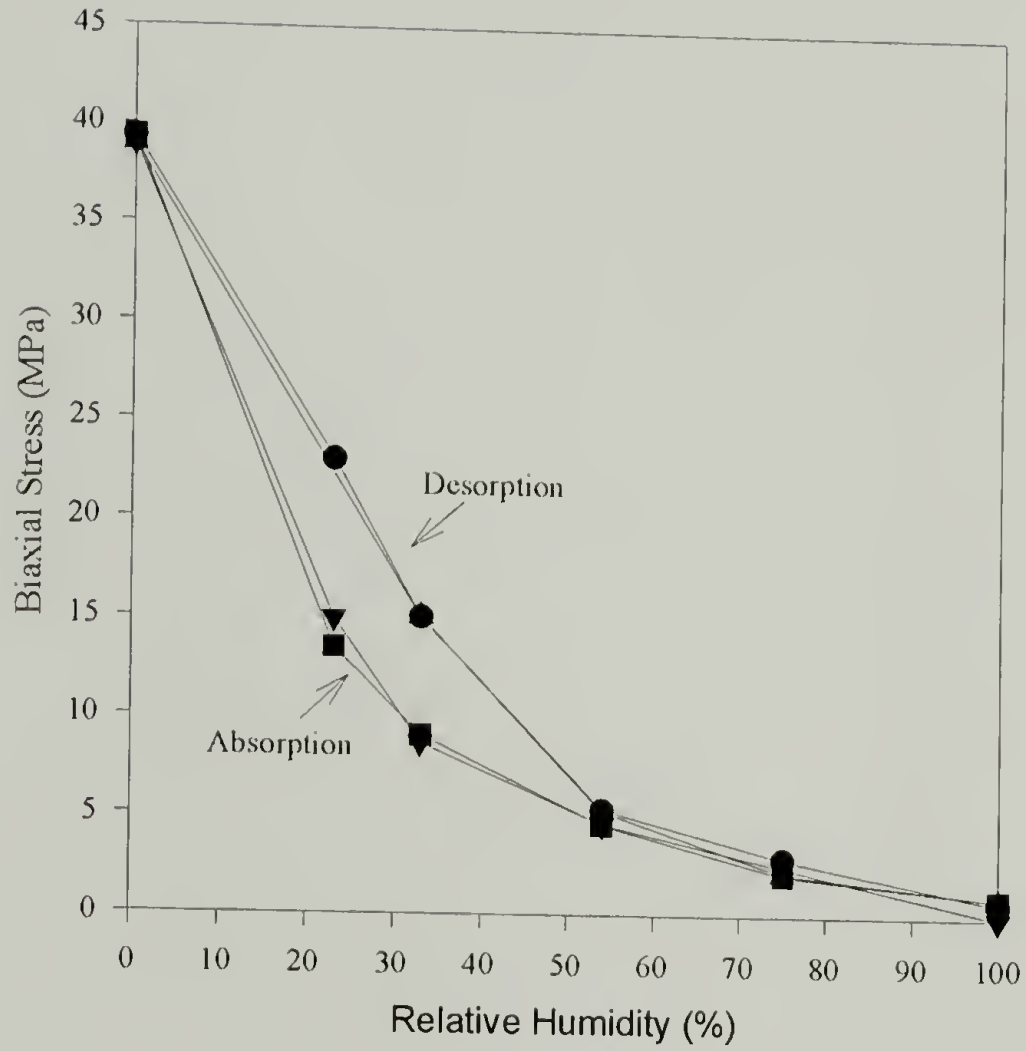

Figure 5.9 Sorption characteristics of PVOH. Hysteresis is evident at relative humidities less than 54%.

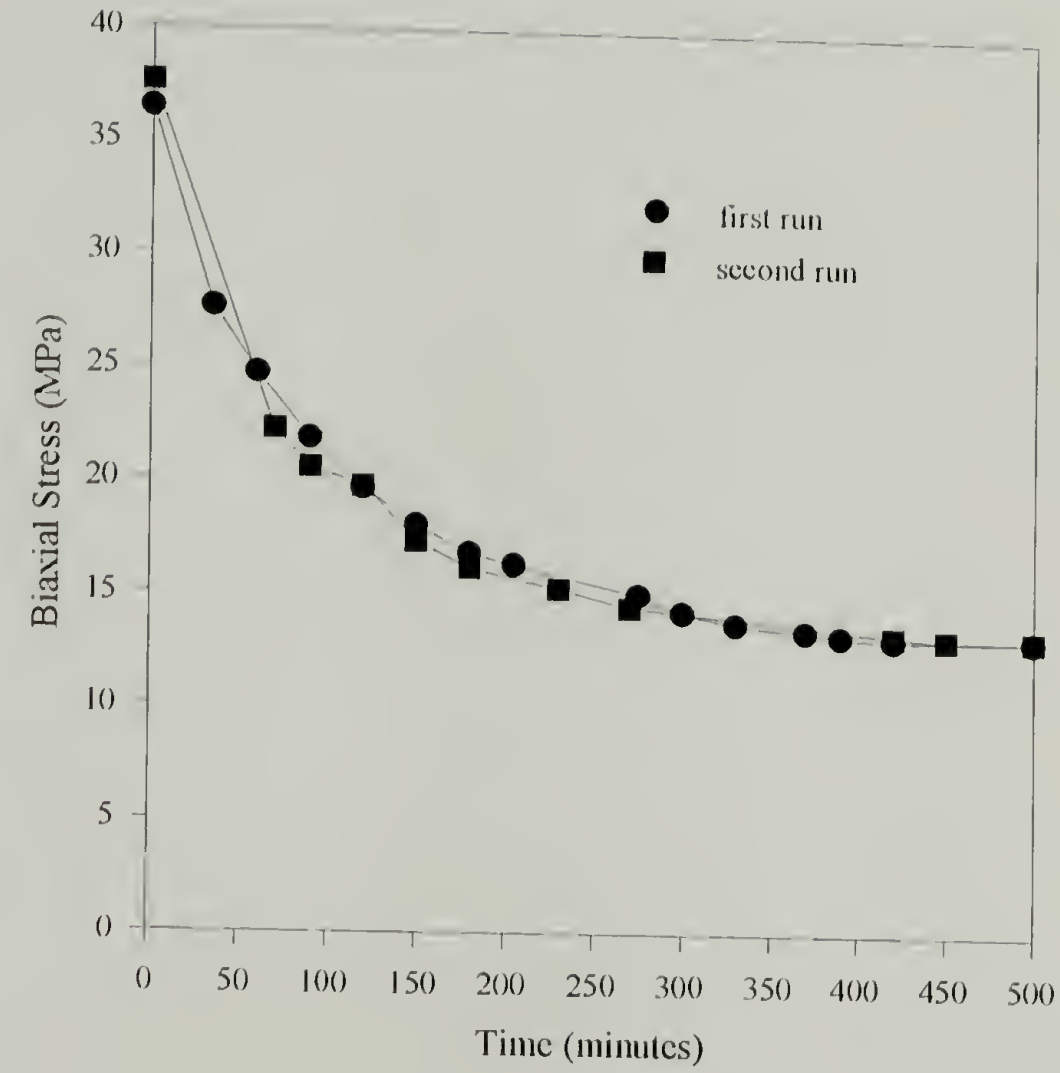

Figure 5.10 Biaxial swelling stress as a function of time for PVOH equilibrated at 0%RH and subjected to 23%RH.

Similar tests were performed on the bisphenol A epoxy coating. In this case, no hysteresis existed. The desorption and absorption paths were the same. Bisphenol A type epoxy does not undergo conformation changes. Moisture penetrates into the crosslinked network and acts as a "free" water, ie., not bound by hydrogen bonding. The amount of "free" water in a polymer network is dictated by osmotic pressure (via relative humidity). Recall that hysteresis is dependent upon the amount of "bound" water in the network. If little or no hydrogen bonding with the water molecules takes place, then hysteresis is non-existent. Figure 5.11 depicts the effect of relative humidity on the stress in the epoxy.

Swelling Stress Dependence on Crystallinity and Crosslinking

Alkaline processed bone gelatin/PET bilayer samples were provided by the Eastman Kodak Co. The bilayer samples were stored in a freezer to minimize the physical aging process prior to testing. Table 5.3 outlines the specific characteristics of each sample.

It was observed that the gelatin/PET bilayer lies flat at 75%RH. Therefore the gelatin membrane samples were made by equilibrating the bilayer in a 75%RH atmosphere at 20°C. An aluminum washer was adhered to the gelatin with an acrylate adhesive. After one (1) hour, the PET substrate was removed from the gelatin coating by peeling at an angle $< 5°$. The membrane sample was placed in the holographic interferometry chamber and equilibrated for two (2) hours at 75%RH, 20°C. The stress as a function of relative humidity was monitored. Desorption began at two (2) hour intervals allowing for equilibration at each relative humidity. The sorption cycle was run as follows: 75%RH to 54%RH to 43%RH to 33%RH to 23%RH to 0%RH to 23%RH to 33%RH to 43%RH to 54%RH to 75%RH. This cycle was repeated to investigate the biaxial swelling stress dependence on the sorption cycle.

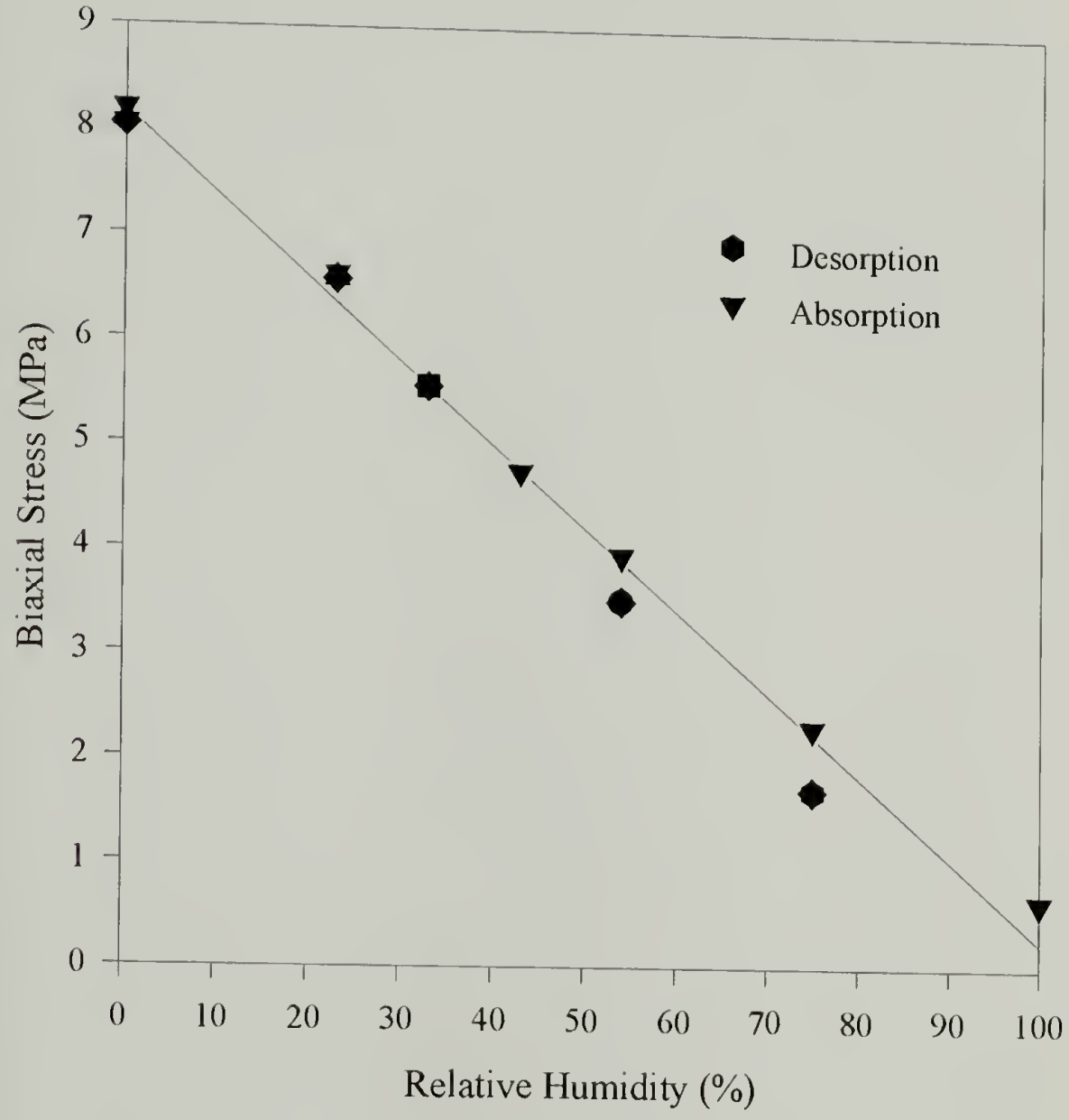

Figure 5.11 Sorption characteristics of Epon 828/V40 epoxy cured at 70°C. Hysteresis is essentially non-existent.

Table 5.3 Percent crystallinity and amount of crosslinking agent in each alkaline processed bone gelatin coating. Bilayer samples were provided by the Eastman Kodak Co.

Gelatin: Kodak I.D. No.	Crystallinity (%)	Crosslinking Agent (%)
8244-9	8.3	3.16
8244-18	0.0	0.00
8244-27	0.0	1.58
8244-36	16.7	3.16
8247-2-3	16.7	0.00
8247-3-3	0.0	3.16
8247-4-3	8.3	0.00

Each gelatin membrane in Table 5.3 was subjected to these sorption cycles. Figure 5.12 represents the characteristic stress vs. relative humidity curves for the gelatin sample.

Prior to presenting the results of this investigation, it is prudent to understand the terms adopted to explain the experimental findings are understood. Figure 5.13 illustrates the terms used to describe the results.

As discussed earlier, gelatin exhibits a moisture sorption hysteresis. Review of figure 5.12 indicates that the biaxial stress as a function of relative humidity was sorption path dependent. The ratio of biaxial stress to relative humidity (the slope of the desorption curve) varies considerably from run #1 to run #2. This is uncharacteristic of the behavior observed in a gelatin coating extracted from a cellulose acetate substrate (reference figure 5.4).

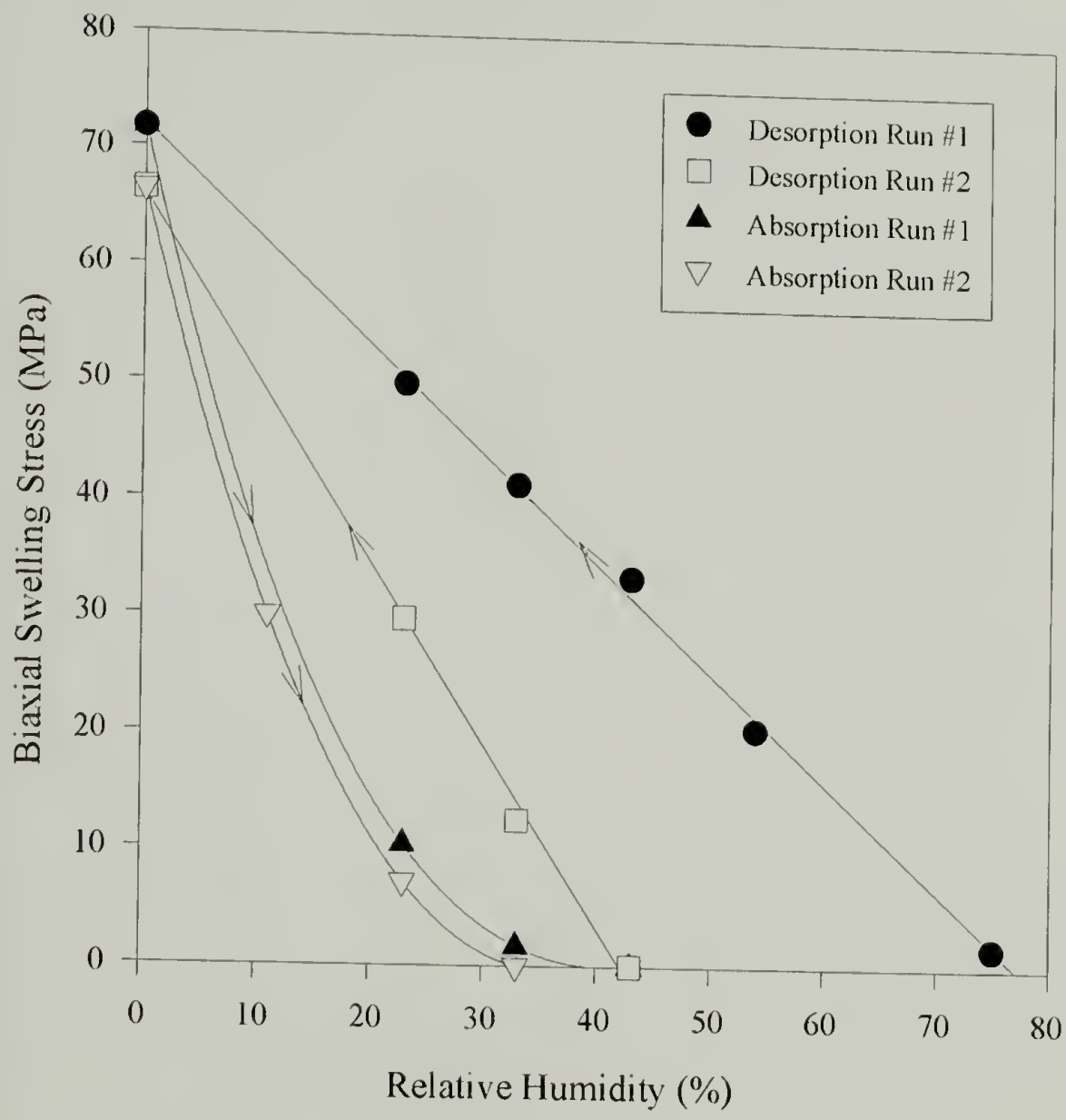

Figure 5.12 Typical biaxial swelling stress vs. relative humidity behavior for alkaline processed bone gelatin membranes. Biaxial swelling stress was measured using holographic interferometry. This particular curve was plotted from a gelatin sample with 0% crystallinity and 1.58% crosslinking agent present.

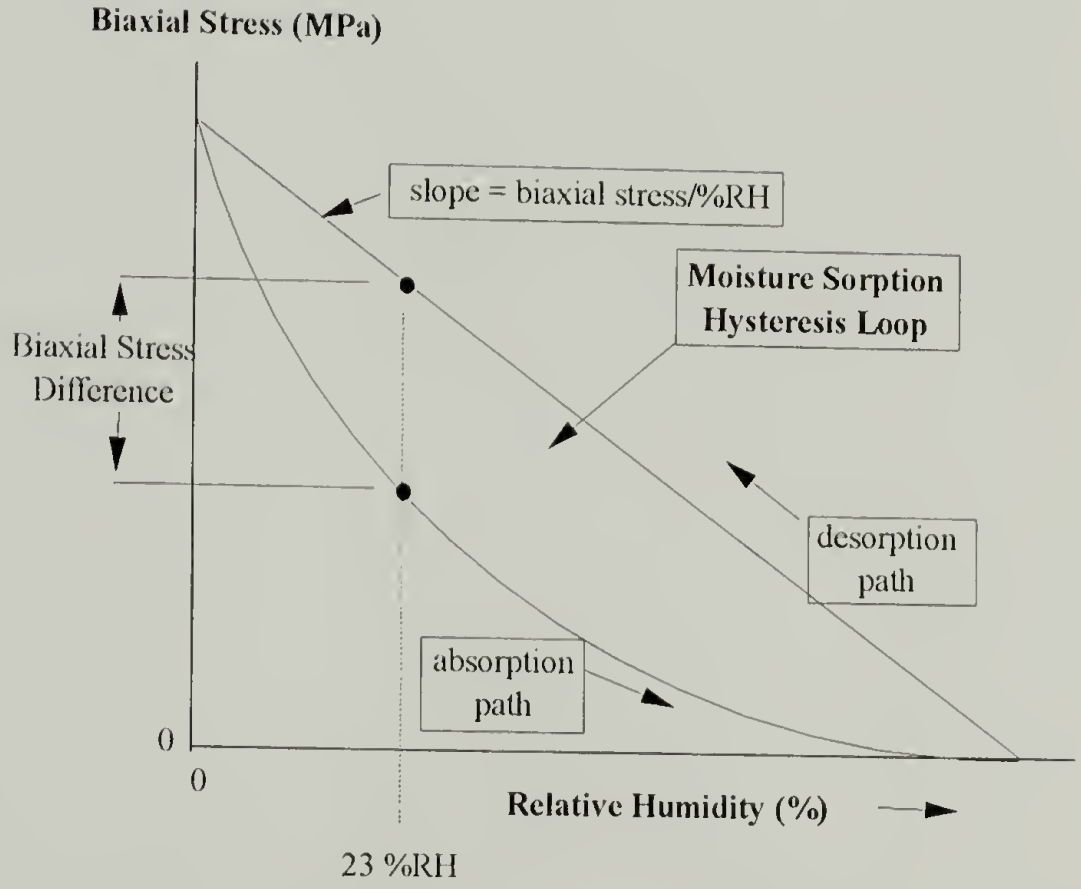

Figure 5.13 Illustration of terms adopted to describe the results of the biaxial stress experiments as a function of percent crystallinity and amount of crosslinking agent (hardener).

Recall in figure 5.4, the gelatin membrane was fabricated from a cellulose acetate substrate which is quite hydrophilic. The gelatin membrane prepared for the crystallinity and crosslinking investigation was removed from a PET substrate which is primarily hydrophobic. The zero stress state in a gelatin/cellulose acetate bilayer occurred at 54%RH. The zero stress state for gelatin/PET was observed at 75%RH. Besides the hydrophobicity of the substrate materials, the viscoelastic nature of the substrates plays an important role [12,13]. The gelatin/cellulose acetate was stored on a 5" diameter roll. The tension of the roll imposes a constant stress on the bilayer system. Under this constant stress, the substrate material tends to creep over time. For the bilayer to be flat, the stress at the interface between the gelatin and substrate must be zero. In other words, the sum of the opposing forces equals zero. If the substrate has a permanent set (known as core-set) as a result of creep, the opposing force of the gelatin must be greater than the force required if the substrate had no permanent set.

Additionally, the stress as a function of relative humidity is proportional to the stiffness and humidity swelling coefficient. The ratio of uniaxial stress to relative humidity for PET is less than that of the cellulose acetate (0.11 MPa/%RH and 0.16 MPa/%RH, respectively). These values were the product of the modulus and humidity expansion coefficients. As a result, the RH required to obtain the same stress in PET as in cellulose acetate is 1.45 times that of cellulose acetate. For example, at 54%RH, cellulose acetate exhibits a stress of 8.64 MPa. For the equivalent stress in PET, the RH must be 78%. This value coincides with earlier results.

A comparison of the desorption characteristics for gelatin at various crystallinities and amounts of crosslinking agent is presented in Figures 5.14 through 5.18. The "slope" indicated in each of theses figures is the ratio of the biaxial swelling stress to the relative humidity. The slope values were extracted from the biaxial swelling stress vs. relative humidity desorption data similar to that represented in figure 5.12.

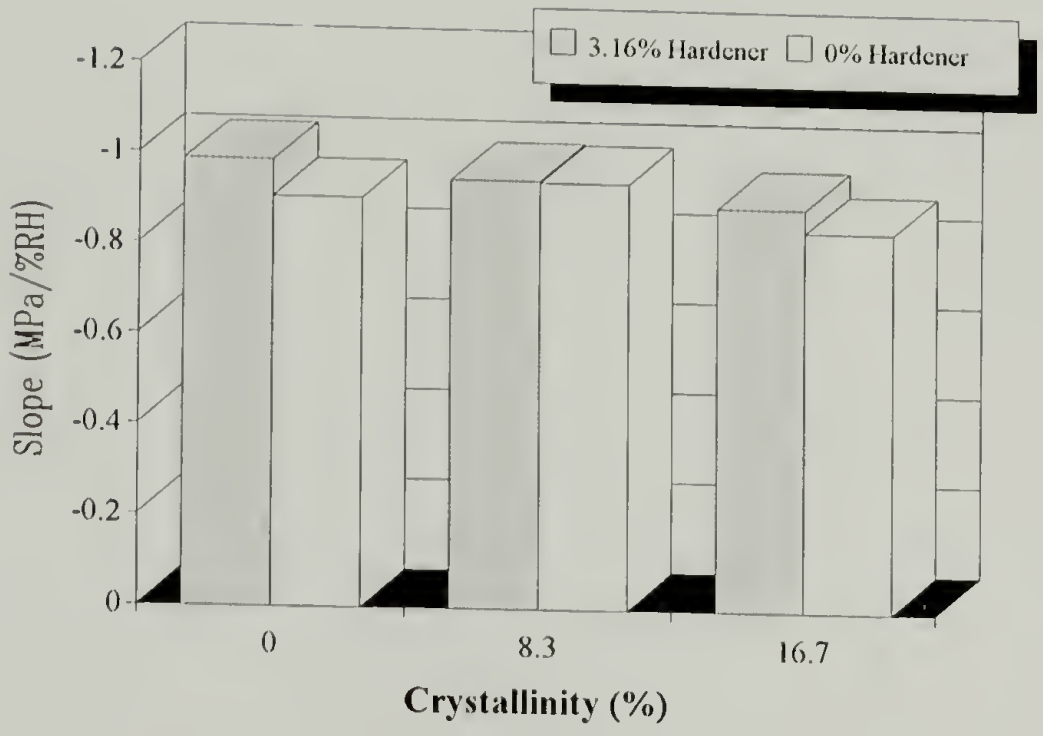

Figure 5.14 Comparison of the first desorption path for gelatin with 0% and 3.16% hardener and varying percent crystallinity. There is a slight dependence of the stress/%RH ratio on the crystallinity with 3.16% hardener present.

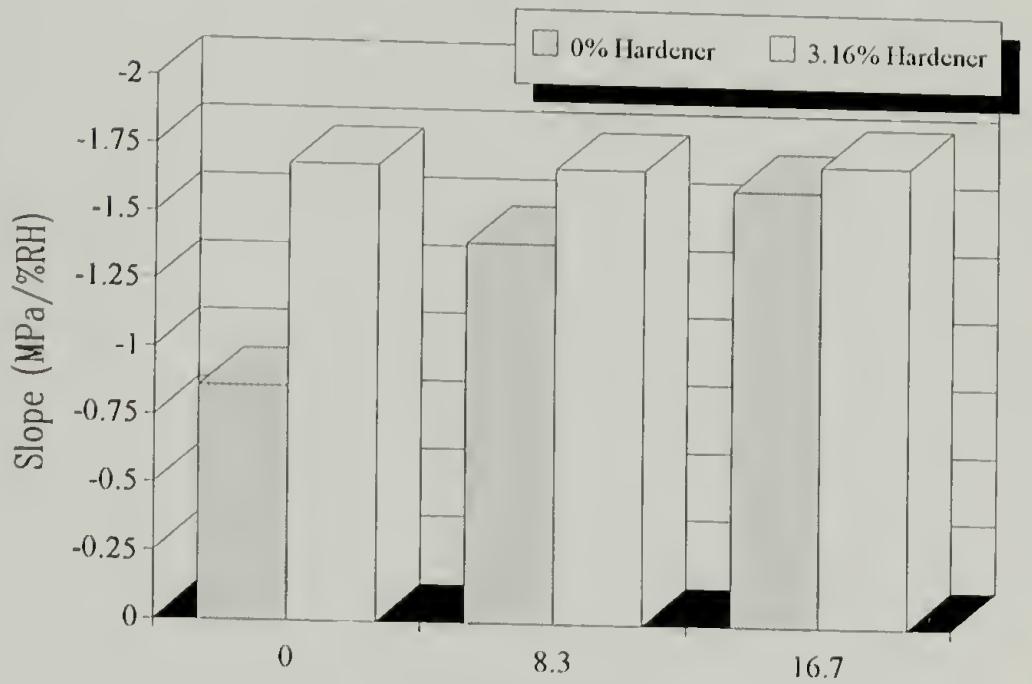

Figure 5.15 Comparison of the second desorption path for gelatin with 0% and 3.16% hardener and varying percent crystallinity. There is a dependence of the stress/%RH ratio on the % crystallinity with 0% hardener present. This same ratio is independent of crystallinity when 3.16% hardener was added.

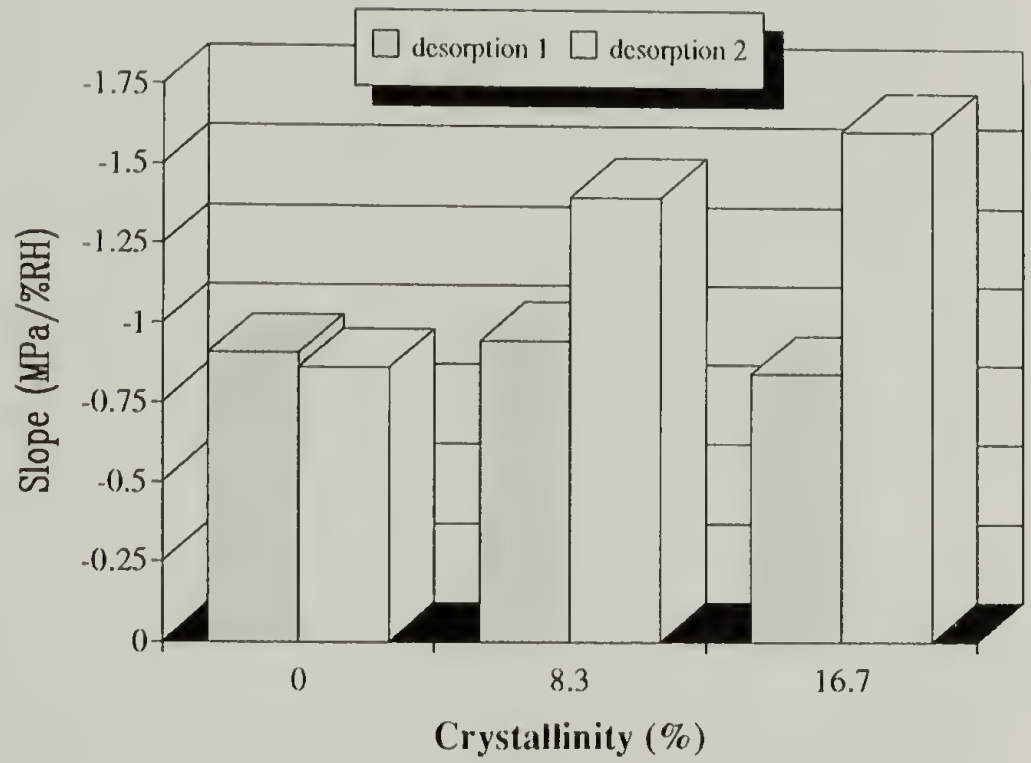

Figure 5.16 Comparison of the first and second desorption paths for gelatin with 0% hardener and varying percent crystallinity. There was no dependence on the crystallinity during the first desorption. The second desorption cycle shows a trend towards increasing biaxial stress/%RH with increasing crystallinity.

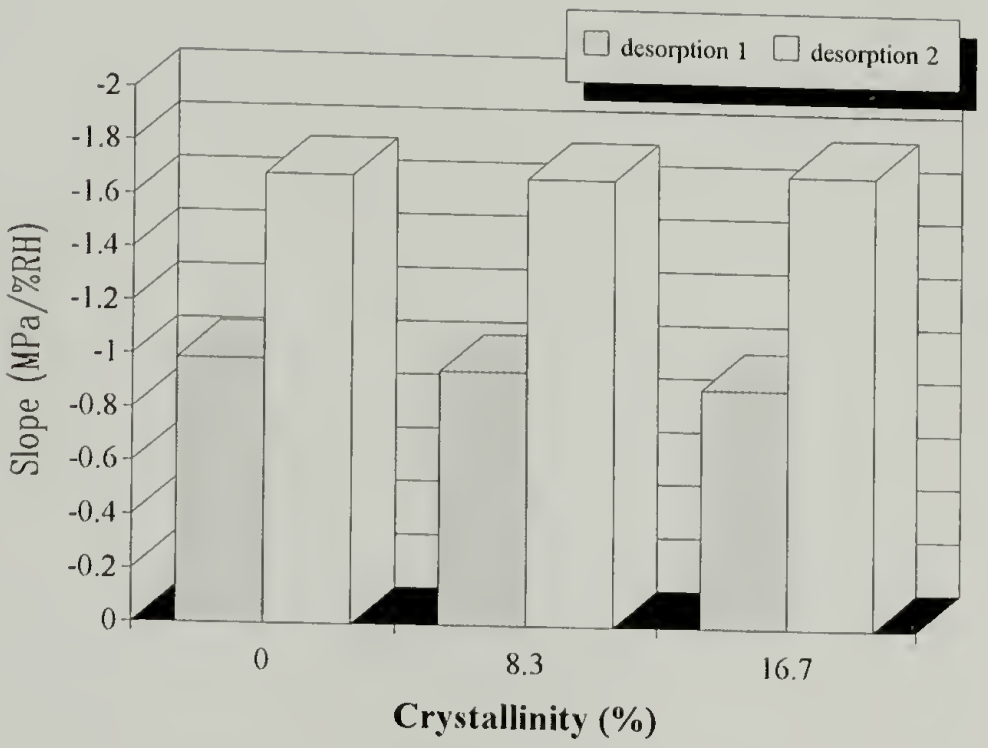

Figure 5.17 Comparison of the first and second desorption paths for gelatin with 3.16% hardener and varying percent crystallinity. With hardener present, the biaxial stress/%RH was independent of the percent crystallinity.

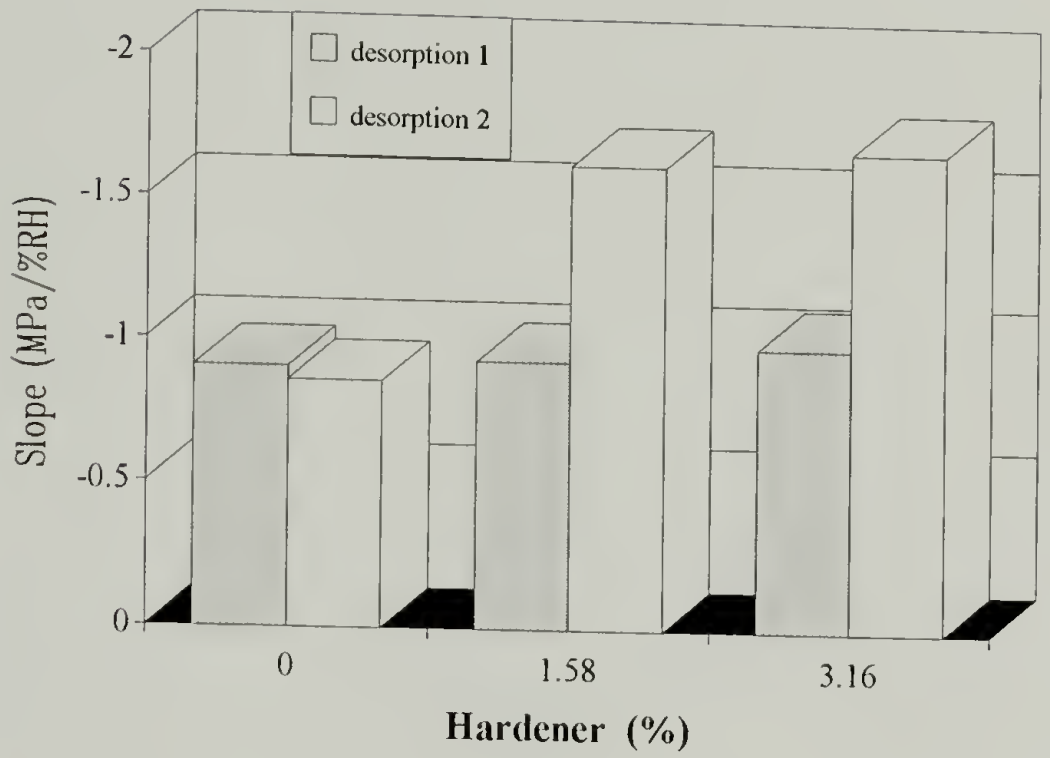

Figure 5.18 Comparison of the first and second desorption runs on the biaxial stress/%RH in gelatin with 0% crystallinity as a function of % hardener present. A completely amorphous gelatin shows a slight increase in the biaxial stress/%RH relationship with increasing amounts of hardener. The higher hardener amounts increase the biaxial stress/%RH relationship in the gelatin.

In general, there is a significant difference between the biaxial stress/%RH ratio for each desorption run. Recall that the biaxial stress/%RH proportional to the product of the stiffness and humidity expansion coefficient. This is represented by the linear elastic relationship in equation 5.3:

$$\frac{\partial \sigma}{\partial RH} = -\frac{E\beta}{(1 - \nu)} \qquad (5.3)$$

where,

$\frac{\partial \sigma}{\partial RH}$ = biaxial stress/%RH ratio or the slope of the biaxial stress vs. RH curve

E = modulus

β = humidity expansion coefficient (also represented by HEC)

ν = Poisson's ratio

For example, applying this equation to compare the two (2) desorption runs of an amorphous gelatin containing 1.58% hardener yields:

		<u>For a 30%RH decrease,</u>
Desorption Run #1:	Slope = -0.933 MPa/%RH	biaxial stress = 28.0 MPa
Desorption Run #2:	Slope = -1.625 MPa/%RH	biaxial stress = 48.8 MPa

Therefore either the modulus, humidity expansion coefficient have increased during the second desorption run or that Poisson's ratio has decreased for the same run. The dependence of the modulus, humidity expansion coefficient and Poisson's ratio on the sorption cycle was outside the scope of this investigation.

Figures 5.14 through 5.18 indicate that the biaxial stress/%RH is greater for the second desorption run. With 0% hardener in the gelatin, increasing the % crystallinity

increases the stress/%RH ratio. Analogously for gelatin with 3.16% hardener added, the stress/%RH ratio was independent of the % crystallinity for the second desorption run. The first sorption run showed a slight decrease in stress/%RH ratio with an increase in % crystallinity for gelatin samples containing 3.16% hardener.

For a completely amorphous gelatin, an increase in the hardener amount increases the stress/%RH ratio. Although this trend is small, it is apparent for each desorption run.

Table 5.4 summarizes the biaxial stress/%RH dependence on the crystallinity and hardener in the gelatin.

Analysis of the absorption paths was more complicated due to the 3rd order polynomial nature of the biaxial stress vs. RH curves. The first derivative of these curves is equivalent to the biaxial stress/%RH ratio. To simplify the analysis, the moisture sorption hysteresis loop was investigated. The biaxial stress at 23%RH for the absorption path was subtracted from the biaxial stress at 23%RH for the desorption path of the same sorption cycle. The difference indicates the stress hysteresis as a function of sorption cycle, % crystallinity and % crosslinking agent (hardener) in the gelatin membrane. It was postulated earlier in this text, that crosslinking and crystallinity would affect the magnitude of the moisture sorption hysteresis loop. Therefore, comparisons were made with each gelatin sample. The results are plotted in figures 5.19 through 5.23 and summarized in table 5.5.

Table 5.4 A summary of the data from figures 5.14 through 5.18 for gelatin. The slope indicated in this table is the ratio of the biaxial stress to relative humidity.

Properties		Desorption #1	Desorption #2
Crystallinity (%)	**Hardener (%)**	**Slope (MPa/%RH)**	**Slope (MPa/%RH)**
0.0	0.00	-0.907	-0.861
0.0	1.58	-0.933	-1.625
0.0	3.16	-0.988	-1.683
0.0	0.00	-0.907	-0.861
8.3	0.00	-0.948	-1.402
16.7	0.00	-0.845	-1.612
0.0	3.16	-0.988	-1.683
8.3	3.16	-0.951	-1.680
16.7	3.16	-0.898	-1.708

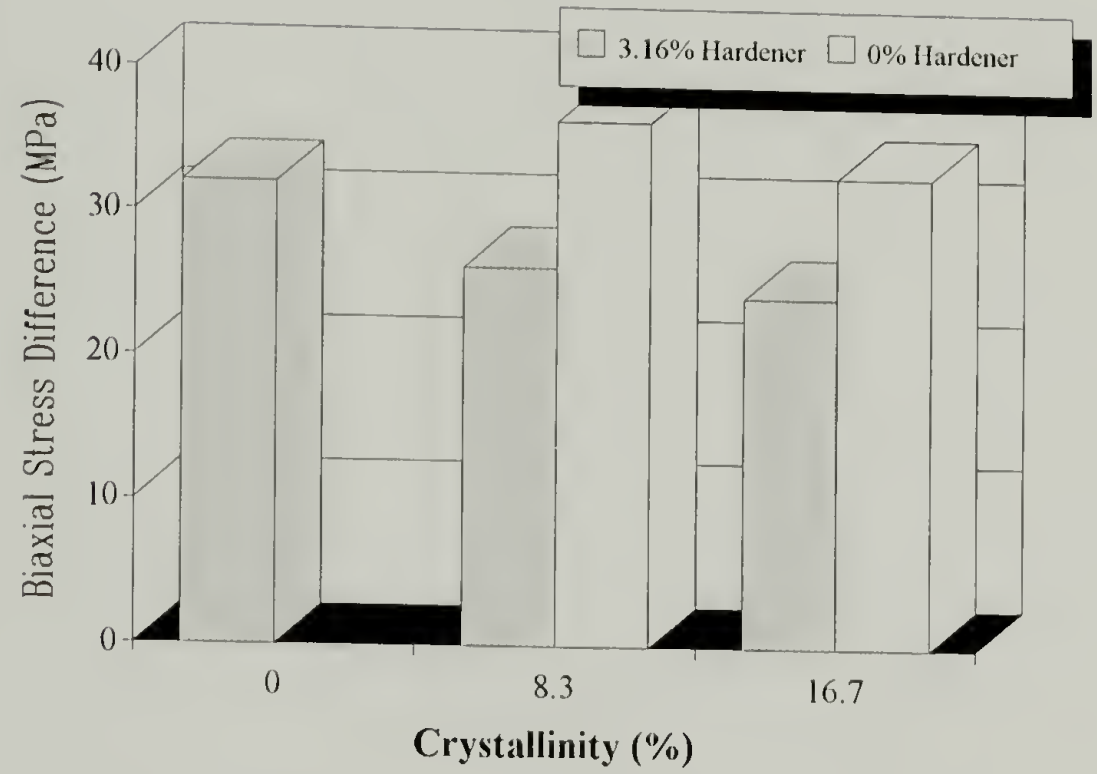

Figure 5.19 Comparison of the first sorption cycle stress hysteresis loop at 23%RH for gelatin with various crystallinities and % hardener present. Stress difference was not obtained for an amorphous sample of gelatin with 0% hardener.

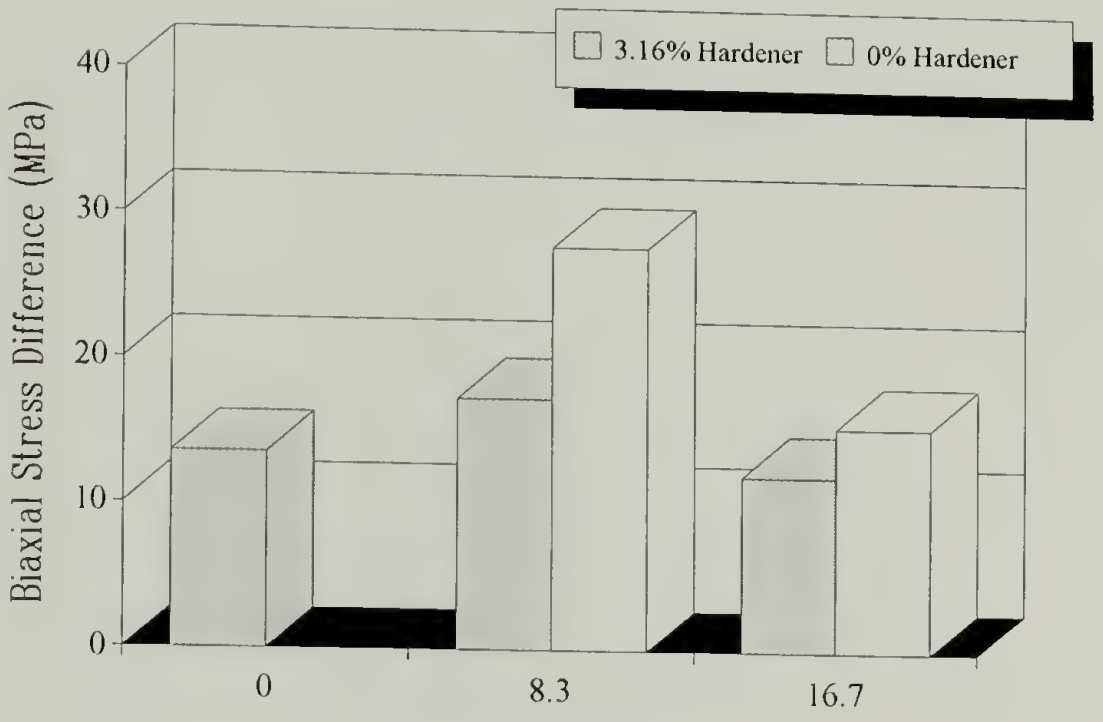

Figure 5.20 Comparison of the second sorption cycle stress hysteresis loop at 23%RH for gelatin with various crystallinities and % hardener. Stress difference was not obtained for an amorphous sample of gelatin with 0% hardener.

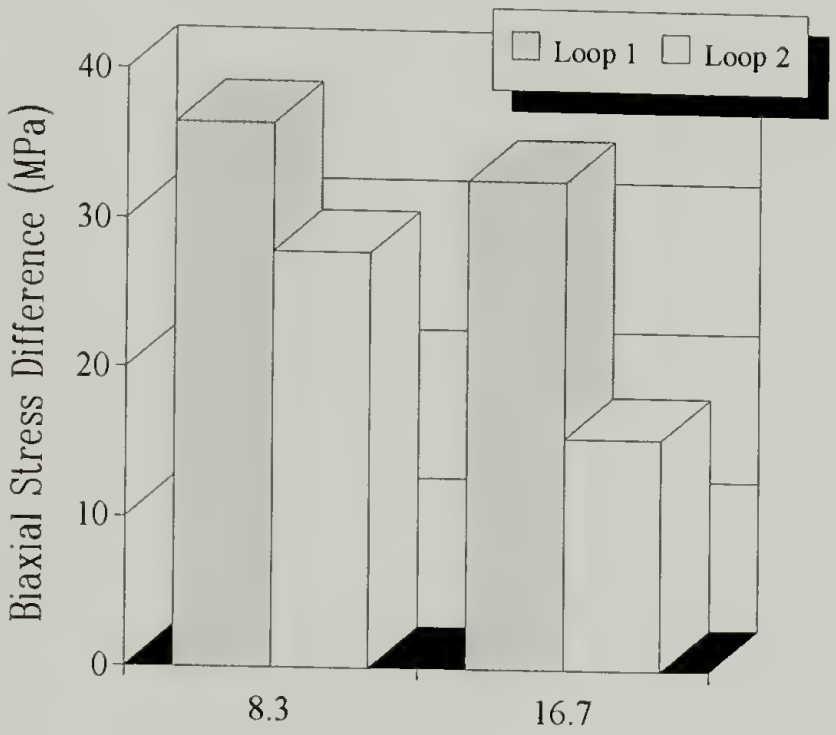

Figure 5.21 Comparison of the first and second moisture hysteresis loops at 23%RH for gelatin with 0% hardener content. The biaxial stress difference decreases with increasing crystallinity and increased sorption cycles.

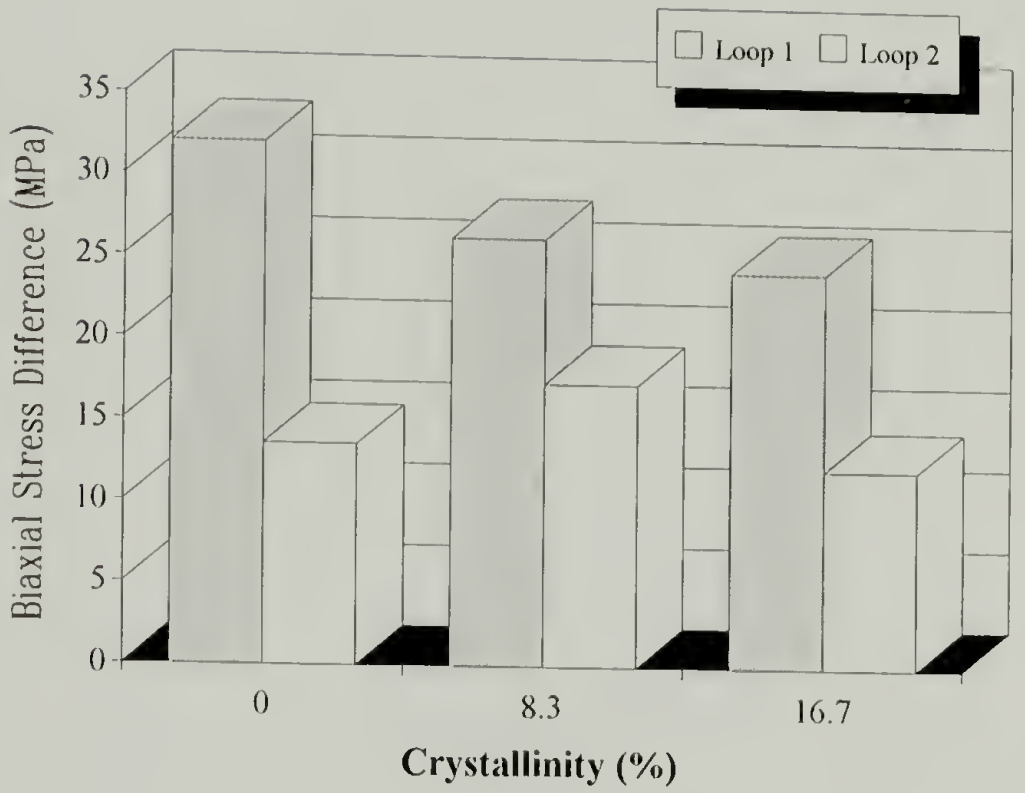

Figure 5.22 Comparison of the first and second moisture hysteresis loops at 23%RH for gelatin with 3.16% hardener content. The biaxial stress difference decreases with increasing crystallinity during the first sorption cycle.

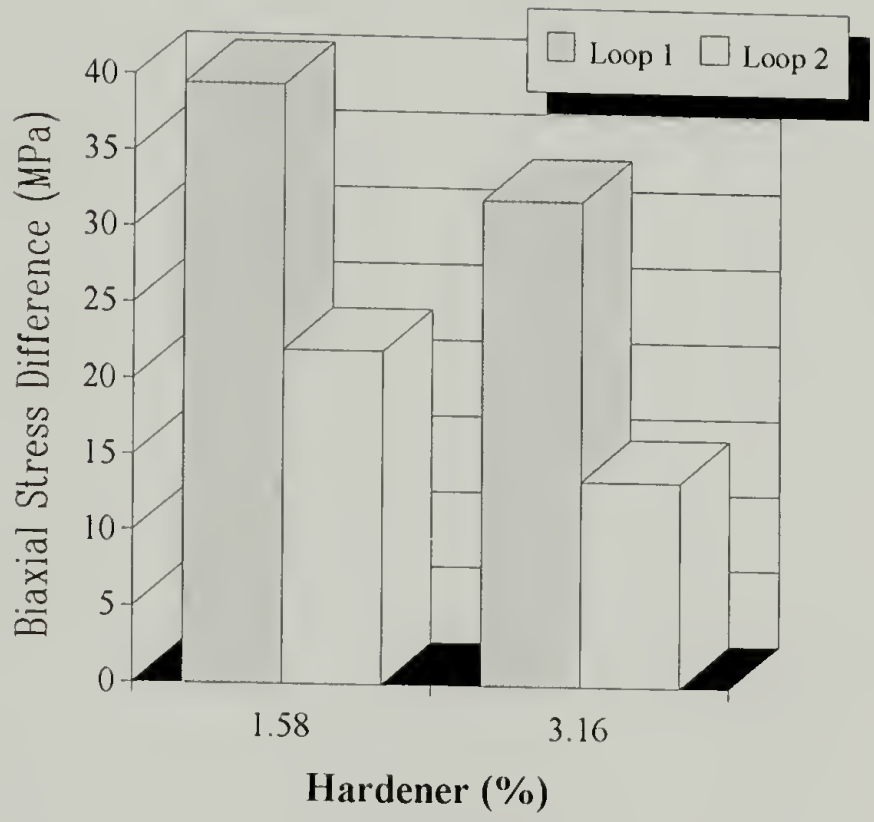

Figure 5.23 Comparison of the first and second moisture hysteresis loops at 23%RH for amorphous gelatin. The biaxial stress difference decreases with increasing hardener content.

Table 5.5 Comparison of the biaxial stress difference at 23%RH for gelatin as a function of crystallinity and hardener.

Properties		Hysteresis Loop 1	Hysteresis Loop 2
Crystallinity (%)	**Hardener (%)**	**Biaxial Stress Difference (MPa)**	**Biaxial Stress Difference (MPa)**
0.0	1.58	39.52	22.00
0.0	3.16	32.06	13.57
8.3	0.0	36.46	27.89
16.7	0.0	32.79	15.60
0.0	3.16	32.06	13.57
8.3	3.16	26.21	17.39
16.7	3.16	24.34	12.20

As observed thus far, at specific hardener contents, the magnitude of the moisture sorption hysteresis loop narrows. This implies that an increase in crystallinity reduces the amount of "bound" water (or hydrogen bonding of the water to the gelatin hydrophilic groups). Since the "bound" water dictates the hysteresis in polymers, by reducing or hindering the hydrogen bonding, the magnitude of the hysteresis loop decreases.

In addition, the sorption cycle contributes to the magnitude of the hysteresis. Sorption cycle 1 has a higher magnitude of hysteresis than sorption cycle 2. After the gelatin sample is subjected to 0%RH, the second sorption curve exhibits lower stress. This may be attributed to the stress relaxation or the increase in the cis-conformations of the poly(L-proline) and glycyl residues in the gelatin as described in earlier arguments.

In general, an increase in the crystallinity in the gelatin reduced the magnitude of the moisture sorption hysteresis loop as compared at 23%RH. The magnitude of the hysteresis loop was dependent upon the sorption cycle. After the first sorption cycle, the hysteresis loop narrowed.

Conclusions

Holographic interferometry was applied successfully in the determination of dependence of relative humidity, % crystallinity and amount of crosslinking agent on the biaxial stress in a gelatin coating. Helium was used as a transport gas for the relative humidity to the holographic interferometry chamber. Results indicate that the use of this low molecular weight gas does not alter the apparent stress values, therefore no correction to the stress results was required.

Gelatin exhibited a moisture sorption hysteresis. Desorption occurred linearly but the absorption of relative humidity was non-linear and was fitted with a 3rd order polynomial. After 24 hours at 0%RH, the biaxial stress in gelatin relaxed by 4 MPa. This phenomenon coincides with earlier investigations. The stress relaxation was believed to result from the cis-conformations of proline and glycydl residues in the gelatin. The conformations inhibit hydrogen bonding between water and the oxygen in the proline carbonyl group. The amount of the cis-conformation was also believed to contribute to the moisture sorption hysteresis.

Poly(vinyl alcohol) showed moisture sorption hysteresis characteristics. It was postulated that the coating fabrication conditions could be tailored to control the hysteresis in this material. For PVOH dried at 54%RH and 20°C. above 54%RH, no hysteresis exists. Below 54%RH, hysteresis was evident.

No hysteresis was observed for DGEBA epoxy. It is believed that the "bound" water is a primary contributor to hysteresis behavior in polymers. Since epoxy is a

crosslinked network and little hydrogen bonding occurs with water, hysteresis is essentially non-existent.

The moisture sorption hysteresis loop in gelatin was diminished by the addition of hardener (crosslinking agent) or through increased crystallinity. The biaxial stress in the gelatin membrane is dependent upon the sorption path. The biaxial stress decreased after the first sorption cycle.

References

1. D.Y. Perera and D. Vanden Eynde, "Moisture and Temperature Induced Stresses (Hygrothermal Stresses) in Organic Coatings," Journal of Coatings Technology, **59**(748), 55 (1987).

2. H.M. Tong and K.L. Saenger, "Bending Beam Characterization of Thin Polymer Films," New Characterization Techniques for Thin Polymer Films, eds., H.M. Tong and L.T. Nguyen, (New York: John Wiley and Sons, Inc., 1990).

3. J.K. Vrtis and R.J. Farris, "Hysteresis of Biaxial Swelling Stresses in Humidity Sensitive Polymer Coatings," Proceedings of the American Chemical Society: Division of Polymeric Materials: Science and Engineering, **69**, 440 (1993).

4. T.Z. Fu, C.J. Durning, and H.M. Tong, "Simple Model for Swelling-Induced Stresses in a Supported Polymer Thin Film," Journal of Applied Polymer Science, **43**, 709 (1991).

5. J.M. Calhoun, "The Physical Properties and Dimensional Behavior of Motion Picture Film," Journal of the Society of Motion Picture Engineering, **43**, 222 (1944).

6. J.Q. Umberger, "The Fundamental Nature of Curl and Shrinkage in Photographic Films," Photographic Science and Engineering, **1**(2), 69 (1957).

7. J.M. Calhoun and D.A. Leister, "Effect of Gelatin Layers on the Dimensional Stability of Photographic Film," Photographic Science and Engineering, **3**(1), 8 (1959).

8. R.B. Pipes, J.R. Vinson and T.W. Chou, "On the Hygrothermal Response of Laminated Composite Systems," Journal of Composite Materials, **10**, 129 (1976).

9. B.S. Berry and W.C. Pritchet, "Bending-Cantilever Method for the Study of Moisture Swelling in Polymers," IBM Journal of Research and Development, **28**(6), 662 (1984).

10. J. Jou, R. Huang, P. Huang and W. Shen, "Structure Effect on Water Diffusion and Hygroscopic Stress in Polyimide Films," Journal of Applied Polymer Science, **43**, 857 (1991).

11. A. Morinaka and Y. Asano, "Residual Stress and Thermal Expansion Coefficients of Plasma Polymerized Films," Journal of Applied Polymer Science, **27**, 2139 (1982).

12. J.H. Jou and L.J. Chen, "Simultaneous Determination of the Biaxial Relaxation Modulus and Thermal Expansion Coefficient of Rigid Rod Polyimide Films Using a Bending-Beam Technique," Macromolecules, **25**, 179 (1992).

13. Z.C. Feng and H.D. Lui, "Generalized Formula for Curvature Radius and Layer Stresses Caused by Thermal Strain in Semiconductor Multilayer Structures," Journal of Applied Physics, **54**(1), 83 (1983).

14. J.H. Jou, L. Hsu and L.S. Chang, "An Analysis of Thermal Stresses in a Multilayer Thin Film Printhead," Thin Solid Films, **201**, 253 (1991).

15. M. Oosterbroek, R.J. Lammers, L.G.J. van der Van and D.Y. Perera, "Crack Formation and Stress Development in an Organic Coating," Journal of Coatings Technology, **63**(797), 55 (1991).

16. M. Shimbo, M. Ochi and K. Arai, "Effect of Solvent and Solvent Concentration on the Internal Stress of Epoxide Resin Coatings," Journal of Coatings Technology, **57**(728), 93 (1985).

17. Maden, M.A. The Determination of Stresses and Material Properties of Polyimide Coatings and Films Using Real Time Holographic Interferometry, Ph.D. diss., University of Massachusetts, Amherst, MA (1992).

18. "Standard Practice for Preparation of Uniform Free Films of Organic Coating," ASTM Designation: D4708, American Society for Testing and Materials, Philadelphia, PA (1988).

19. M. Yaseen and H.E. Ashton, "Effect of Free Film Preparation Method on Physical Properties of Organic Coatings," Journal of Coatings Technology, **49**(629), 50 (1977).

20. M. Yaseen and K.V.S.N. Raju, "A Critical Analysis of Various Methods for Preparation of Free Films of Organic Coatings," Progress in Organic Coatings, **10**, 125 (1982).

21. M.A. Maden, K. Tong and R.J. Farris, "Measurement of Stresses in Thin Films Using Holographic Interferometry: Dependence on Atmospheric Conditions," Materials Research Society Symposium, **188**, 29 (1990).

22. C.S. Jou and R.J. Farris, "Moisture Transport in Bi-layer Cantilever Beam by Holographic Interferometry," (submitted to Acta Polymerica, 1993).

23. S.T. Sackinger, The Determination of Swelling Stresses in Polyimide Films, Ph.D. diss., University of Massachusetts, Amherst, MA (1990).

24. E.K. Colton and E.J. Wiegand, "Moisture in Photographic Film and its Measurement," Photographic Science and Engineering, **2**, 170 (1958).

25. K.S. Rao and B. Das, "Varietal Differences in Gelatin, Egg Albumin, and Casein in Relation to Sorption - Desorption Hysteresis with Water," Journal of Physical Chemistry, **72**(4), 1223 (1968).

26. P.York, "Analysis of Moisture Sorption Hysteresis in Hard Gelatin Capsules, Maize Starch, and Maize Starch: Drug Powder Mixtures," Journal of Pharmacy and Pharmacology, **33**, 269 (1981).

27. K. Boki and S. Ohno, "Moisture Sorption Hysteresis in Kudzu Starch and Sweet Potato Starch," Journal of Food Science, **56**(1), 125 (1991).

28. "Physical Properties of Kodak Aerial Films," Properties of Kodak Materials for Aerial Photographic Systems, Vol. II, (Rochester, NY: Eastman Kodak Co., 1972).

29. H. Hermel, R. Wetzel, E. Buder, C. Roth, H. Hebrich, and H. Legutke, " Moisture, Triple - Helical Content and Brittleness of Gelatin Layers," Journal of Photographic Science, **39**, 16 (1991).

30. I.W. Kellaway, C. Marriott and J.A.J. Robinson, "The Mechanical Properties of Gelatin Films: I. The Influence of Water Content and Preparative Conditions," Canadian Journal of Pharmaceutical Sciences, **13**(4), 83 (1978).

31. T.O. Norris and J. McGraw, "Gelatin Coatings and Tensile Strength of Gelatin Films," Journal of Applied Polymer Science, **8**, 2139 (1964).

32. E. Bradbury and C. Martin, "Mechanical Properties and Structure of Sol-type and Gel-type Gelatine Films," Nature, **168**, 837 (1951).

33. D.W. Jopling, "The Swelling of Gelatin Films. The Effects of Drying Temperature and of Conditioning the Layers in Atmospheres of High Relative Humidity," Journal of Applied Chemistry, **6**, 79 (1956).

34. J.R. Katz, J.C. Derksen and W.F. Bon, "Zur Polymorphie Hochmolekularer Substanzen. I. Ueber Amorphie und Kristallinische Gelatine und Ueber Das Wesen Des Gelatinier - Ungsprozesses Bei Der Gelatine," Trav. chim. Pays - Bas, **50**, 725 (1931).

35. T.H. James and G.C. Higgins, Fundamentals of Photographic Theory, (New York: Morgan and Morgan, Inc., 1960).

36. G. Xu and E. Ruckenstein, "Emulsion Pathway for Gelatin Cross-Linking," Journal of Applied Polymer Science, **47**, 1343 (1993).

37. N. Yamamoto and Y. Oishi, "Photographic Gelatin Hardening Composition," United States Patent, 3,325,287 (1967).

38. D.M. Burness and B.D. Wilson, "Gelatin Compositions Containing a Bisisomaleimide Hardener," United States Patent, 3,232,763 (1966).

39. J.C.W. Chien, "Solid-State Characterization of the Structure and Property of Collagen," Journal of Macromolecular Science - Reviews in Macromolecular Chemistry, **C12**(1), 1 (1975).

40. P.I. Rose, "Gelatin", Encyclopedia of Polymer Science and Engineering, eds., H. Marks and N. Bikales, Vol. 7, (New York: Wiley Interscience, 1986).

41. B. Alberts, D. Bray, J. Lewis, M. Raff, K. Roberts and J. Watson, Molecular Biology of the Cell, (New York: Garland Publishing, Inc., 1983).

42. J.F. Hamilton, G.C. Higgins and J.E. Starr, eds., The Theory of the Photographic Process, 4th ed., (Rochester, NY: Eastman Kodak Co., 1977).

43. R. Wetzel, E. Buder, H. Hermel and A. Hüttner, "Conformations of Different Gelatins in Solutions and in Films.: An Analysis of Circular Dichroism (CD) Measurements," Colloid and Polymer Science, **265**, 1036 (1987).

44. S. Tanoka and H.A. Scherage, "Theory of the Cooperative Transition Between Two Conformations of Poly(L-proline): II. Molecular Theory in the Absence of Solvent," Macromolecules, **8**(4), 504 (1975).

45. A. Wollmer, W. Straβberger and U. Glatter, "Perspectives in the Circular Dichroic Analysis of Protein Main-Chain Conformation," Modern Methods in Protein Chemistry - Review Articles, (New York: Walter de Gruyter and Co., 1983).

46. F.L. Marten, "Vinyl Alcohol Polymers," Encyclopedia of Polymer Science and Engineering, eds., H. Marks and N. Bikales, Vol. 17, (New York: Wiley Inter-Science, 1986).

CHAPTER 6

MASS TRANSPORT PROPERTIES

Introduction

"Diffusion is the process by which matter is transported from one part of the system to another as a result of random molecular motions" [1]. The rate of diffusion per unit area is proportional to a diffusion gradient by a specific material coefficient known as the diffusion coefficient, D_m. For a plane case (eg., a film of material), the diffusion occurs only in one direction which is normal to the plane. Mathematically, the relationship for a one dimensional diffusion is introduced in equation (6.1).

$$\frac{\partial c}{\partial t} = D_m \frac{\partial^2 c}{\partial z^2} \qquad (6.1)$$

where,

t = time

z = space coordinate in the direction of the film thickness

c = concentration of the penetrant

D_m = diffusion coefficient

Equation (6.1) is Fick's Law which assumes the diffusion coefficient is concentration independent [2]. Details regarding the derivation of solutions for Fick's equation are available elsewhere [1]. Applying the following boundary and initial conditions for one dimensional Fickian diffusion through a film of thickness, h, to equation (6.1):

I.C. $c = c_i = 0$ $\quad -h/2 < z < h/2$

B.C. $c = c_{eq}$ $\quad z = h/2$

where,

c_i, c_{eq} = initial and equilibrium concentration, respectively

h = film thickness

z = spacial coordinate through the thickness

yields the solution in equation (6.2) [3]:

$$\frac{M_t}{M_\infty} = 1 - \frac{8}{\pi^2} \sum_{n=0}^{\infty} \frac{1}{(2n+1)^2} \exp\left\{\frac{-D_m(2n+1)^2 \pi^2 t}{h^2}\right\} \qquad (6.2)$$

where, $\frac{M_t}{M\infty} = \frac{c - c_i}{c_{eq} - c_i}$

This is pictorially represented in Figure 6.1.

The effective transport properties of a film sample can be calculated knowing the sample geometry and the mass uptake (weight ratio) as a function of time. The diffusion coefficient is determined from the plot of mass uptake, M_t/M_∞ vs. time$^{1/2}$. For a concentration independent diffusion coefficient and a material to exhibit Fickian diffusion behavior, two criteria must be met. First, the desorption and absorption curves must be linear up to $M_t/M_\infty < 0.6$ for small times. Secondly, the absorption and desorption curves should be identical when superimposed [1].

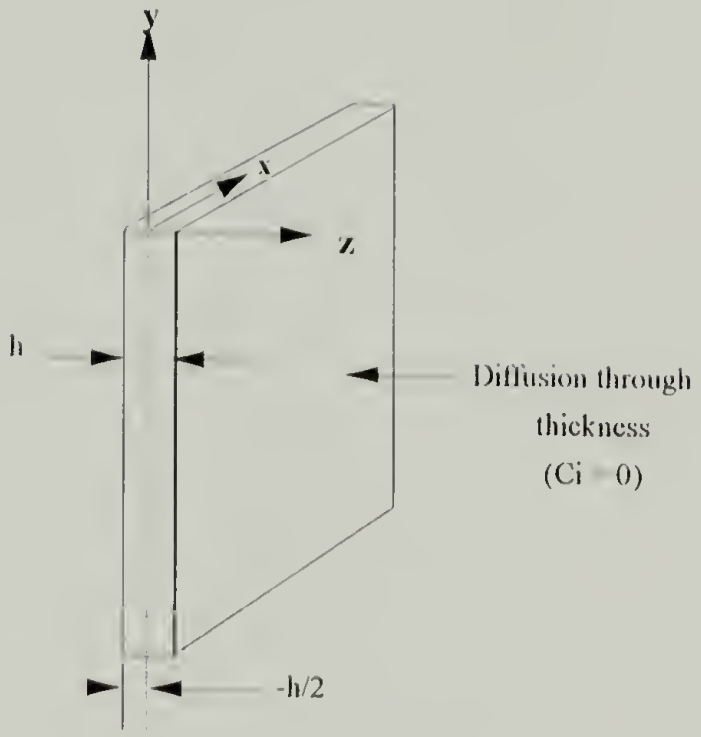

Figure 6.1 Schematic of initial and boundary conditions for mass diffusion through a film

There are four methods used to estimate the effective diffusion coefficient, D_{eff} for a material exhibiting Fickian behavior: the half-time method, the initial slope method, the moment method and the limiting slope method.

Using the half-time method to calculate the D_{eff} for a plane film of thickness, h, is presented in equation (6.3) [3]:

$$D_{eff} = \frac{0.0492 h^2}{t_{1/2}} \qquad (6.3)$$

where, $t_{1/2}$ is defined as time where $M_t/M_\infty = 0.5$.

The initial slope method uses the initial slope of the M_t/M_∞ vs. $t^{1/2}$ [1]. The initial slope is proportional to the square root of the effective diffusion coefficient, D_{eff}, through equation (6.4):

$$D_{eff} = \pi\left[\frac{(\text{slope})h}{4}\right]^2 \qquad (6.4)$$

The moment method uses the entire sorption curve instead of a single point (half-time method) or a numerical derivative (initial slope or limiting slope method). The entire curve is integrated and the D_{eff} is calculated for a plane sheet (ie., a film) from equation (6.5) [4]:

$$D_{eff} = \frac{h^2}{12\left[\int_0^\infty \left(1 - \frac{M_t}{M_\infty}\right)dt\right]} \qquad (6.5)$$

The limiting slope method was introduced by Beren [4]. For long times, $t > t_{1/2}$, a plot of log $(1-M_t/M_\infty)$ vs. time is linear. The D_{eff} of a film of thickness, h, is proportional to the slope of the line by the relation in equation (6.6):

$$D_{eff} = -(\text{slope})\left[\frac{4h}{\pi}\right]^2 \qquad (6.6)$$

This method relies on the later stages of the experiment when the initial conditions are not well defined.

Besides the assumptions that the sample obey Fick's law and that the diffusion coefficient is concentration independent, a few additional assumptions must be satisfied for equations (6.3 through 6.6) to be valid. (1) The initial concentration of the penetrant (in this investigation, the penetrant is moisture) in the film sample must be uniform and equal to zero. (2) Equilibrium is obtained instantly at the interface of the sample and the atmosphere. (3) A step change in the penetrant concentration at the interface begins at t = 0. (4) There are no diffusion limitations in the gas (vapor) phase.

The mass diffusion coefficient is determined using one of several techniques. The most common are gravimetric techniques [1]. Other techniques have been designed which are simpler than the conventional gravimetric methods [6,7]. In these techniques, the property measured as a function of time at specific relative humidities is correlated to the mass uptake. The mathematical relationship was developed elsewhere [8] and is outlined by Jou [7]. For example, the swelling strain or swelling stress can be monitored as a function of time. These properties are then related to mass uptake through application of linear elasticity theory.

Recall the stress - strain relationship for a one dimensional, homogeneous, linear elastic, isotropic material subjected to isothermal conditions:

$$E\left[\varepsilon_{xx} - \beta' \Delta c(x, y, z, t)\right] = \sigma_{xx} \tag{6.7}$$

where,

E = tensile modulus

ε_{xx} = strain

β' = swelling coefficient

c = concentration

σ_{xx} = stress

Establishing a relationship [7] for the average property through the volume by:

$$\overline{\Gamma} = \frac{1}{V}\int \Gamma(x, y, z, t)dV \tag{6.8}$$

where,

Γ = ε_{xx}, σ_{xx}, or Δc

V = volume of the sample

The average mass uptake per unit volume is expressed by equation (6.9):

$$\Delta\bar{c}(t) = \frac{1}{V}\int \Delta c(x, y, z, t)dV \tag{6.9}$$

The total amount of moisture absorbed by the film is written as:

$$M_t(t) = \int \Delta c(x, y, z, t)dV = V\Delta\bar{c}(t) \tag{6.10}$$

Equation (6.7) is integrated through the volume to yield equation (6.11):

$$\bar{\sigma}_{xx}(t) = E\left[\varepsilon_{xx} - \beta' \Delta\bar{c}(t)\right] \tag{6.11}$$

For a constrained sample, $\varepsilon_{xx} = 0$, therefore equation (6.11) reduces to:

$$\Delta\bar{\sigma}_{xx}(t) = -E\beta' \Delta\bar{c}(t) \tag{6.12}$$

where, $\Delta\bar{\sigma}_{xx}(t) = \bar{\sigma}_{xx}(t) - \bar{\sigma}_{xx}(0)$.

Analogously for a material under constant stress, $\sigma_{xx} = 0$, equation (6.11) yields:

$$\Delta\bar{\varepsilon}_{xx}(t) = \beta' \Delta\bar{c}(t) \tag{6.13}$$

where, $\Delta\bar{\varepsilon}_{xx}(t) = \bar{\varepsilon}_{xx}(t) - \bar{\varepsilon}_{xx}(0)$.

Applying the general relationship of equation (6.8) and normalizing the stress and strain of equations (6.12) and (6.13), the transient swelling stress and strains can be expressed as:

$$\frac{\Delta\bar{c}(t)}{\Delta\bar{c}(\infty)} = \frac{\Delta\bar{\sigma}(t)}{\Delta\bar{\sigma}(\infty)} = \frac{\Delta\bar{\varepsilon}(t)}{\Delta\bar{\varepsilon}(\infty)} = \frac{M(t)}{M(\infty)} \tag{6.14}$$

Through the relationship of equation (6.14), the change in stress or strain with time can be correlated to the mass uptake with time relationship. Therefore, experiments designed to measure stress or strain as a function of time can be used to determine D_{eff}.

This relationship was the premise for applying holographic interferometry to the determination of the mass diffusion coefficients of the materials used in this research.

Experimental

Holographic interferometry has recently been used to determine the mass diffusion coefficients of polymers [7]. This technique used a one dimensional beam sample of a polymer coated on a substrate. A hologram was made of the beam sample prior to moisture diffusion. The beam was then subjected to a specific humidity and the number of interference fringes as a function of time were counted. From these measurements, the mass diffusion coefficient was determined.

In this work, holographic interferometry is applied to a two dimensional membrane sample. The stress is measured as function of time at various relative humidities. A plot of the normalized stress vs. time$^{1/2}$ correlates well with analogous mass uptake experiments. This technique will be detailed later in the text. A comparison of this technique to the holographic interferometry beam bending technique [7], swelling strain technique [6] and a gravimetric technique is presented.

Three materials were used in these experiments: alkaline processed bone gelatin, cellulose acetate and polyimide (PMDA-ODA). The thickness of the gelatin, cellulose acetate and polyimide averaged 20 μm,128 μm, and 25.6μm, respectively. Uniaxial samples with dimensions 5 mm wide and 100 mm long were used for the Cahn 2000 microbalance. Swelling strain samples were uniaxial averaging 5 mm wide and 100 mm in length. Membranes of gelatin, cellulose acetate and polyimide were fabricated by the procedure described in chapter 5 and were used for the holographic interferometry investigation.

Gravimetric Method

The most common method for determining the mass diffusion coefficient is by a gravimetric technique. A Cahn 2000 microbalance was employed to determine the mass

uptake and the mass diffusion coefficient of a material [9]. A uniaxial sample was hung from the microbalance and the mass uptake as a function of time at various humidities was recorded. Figure 6.2 depicts the microbalance set-up. A 5 mg weight was hung from the bottom of the sample to avoid interaction with the chamber walls. The sample was initially dried at 0%RH for 24 hours. Relative humidity was introduced and the weight increase as a function of time monitored until equilibrium was reached. The sample was once again exposed to 0%RH and the weight loss monitored.

The % weight gain (loss) was recorded as a function of time and a normalized mass uptake, M_t/M_∞, vs. time$^{1/2}$ plotted. The initial slope and half-time methods were employed to calculate the effective mass diffusion coefficient, D_{eff}.

Humidity Swelling Strain Method

The swelling strain method designed by Sackinger [6] and used by Jou [7] for humidity studies was adopted to provide an additional method for determining the mass diffusion coefficient. A set-up of the apparatus is represented in figure (6.3). The experimental procedure was described in chapter 4.

In general, the experiment was performed by securing the 5 x 100 mm uniaxial sample of a known thickness between the clamps. After the 130 g counterweight was hung in place, relative humidity was introduced to the sample chamber. Relative humidity was generated using binary aqueous saturated salt solutions which was described in chapter 3. The length change due to moisture was monitored using a Linear Variable Differential Transformer, LVDT. The swelling strain was then calculated as the length change due to humidity exposure divided by the initial length of the sample.

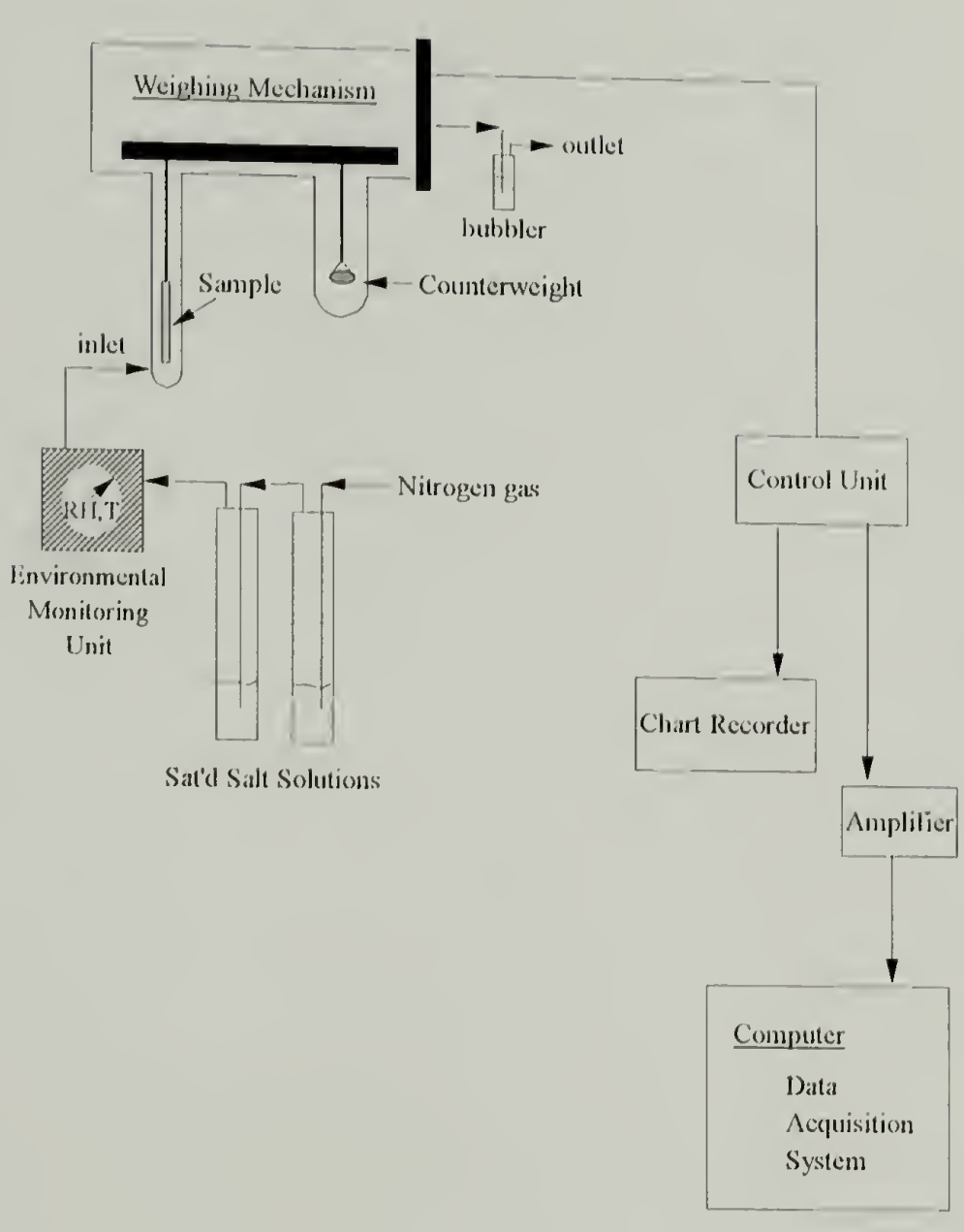

Figure 6.2 Schematic of Cahn 2000 microbalance used to determine mass uptake as a function of time at various relative humidities.

The humidity swelling strain as a function of time was monitored. The normalized humidity swelling strain vs. time$^{1/2}$ was plotted. The mass diffusion coefficient was calculated by employing the initial slope and half-time methods described earlier.

Holographic Interferometry Method

An experimental set-up equivalent to that described in chapter 5 was used to determine the biaxial stress as a function of time at various humidities. The frequency of the 2,1 mode was monitored as a function of time. Initially the membrane was brought to its zero stress state and then dried at 0%RH. From the zero stress state to 0%RH, the stress and time were monitored After equilibrium was reached, the membrane was then subjected to a higher relative humidity and again, the stress and time were monitored. A normalized stress vs. time$^{1/2}$ was plotted as well as the stress as a function of time.

Results and Discussion

Mass Diffusion Coefficient via Gravimetric Method

Two materials were run using the Cahn 2000 microbalance: gelatin and cellulose acetate. As mentioned earlier, a 5 mg weight was hung from each unixial sample to avoid contact with the chamber walls as a result of the gas flow introduced at the bottom of the sample (see Figure 6.2 for the Cahn 2000 microbalance schematic). A chart recorder and a computer data acquisition program (LabTech Notebook) were used to monitor the mass uptake with time. The mass uptake was then normalized and plotted against time$^{1/2}$.

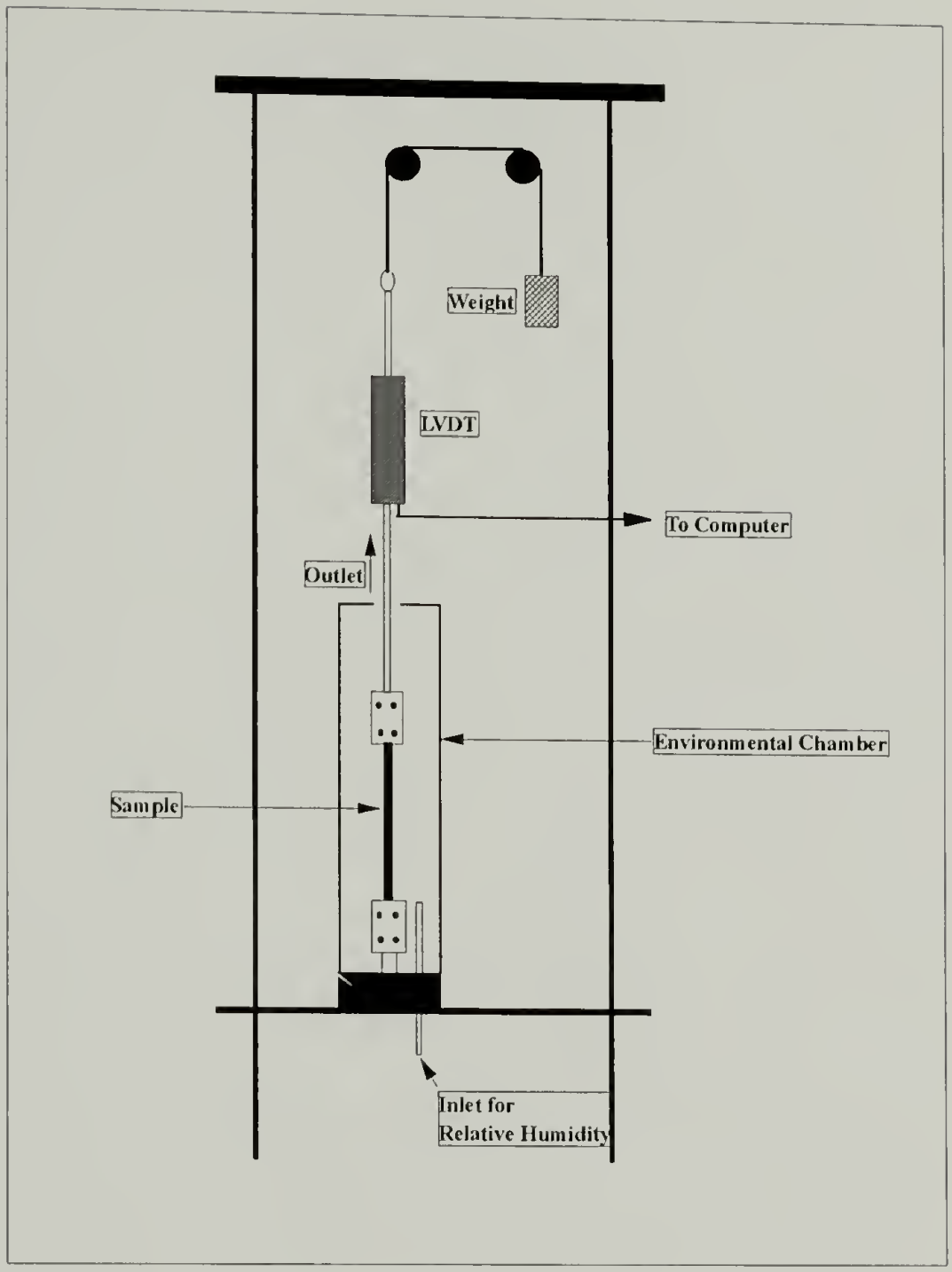

Figure 6.3 Apparatus for measuring the in-plane humidity swelling strains in the x-y plane.

If Fickian diffusion is observed, the initial slope is related to the mass diffusion coefficient using equation (6.1). Figure 6.4 and 6.5 depict the mass uptake characteristics at various relative humidities for gelatin and cellulose acetate, respectively.

Alkaline processed bone gelatin (#SC5-5S-5020-01) is the material represented in figures 6.4. At 23%RH, the gelatin absorbed 6.0% of its weight in moisture. At 54%RH and 75%RH, the gelatin absorbed 13.4 and 22.2%, respectively. These values correlate well with literature results [10]. As seen in figure 6.5, cellulose acetate at 54%RH and 100%RH absorbed 1.9% and 5.1% moisture, respectively. Figure 6.6 provides a comparison of the % mass uptake of gelatin and cellulose acetate at 54%RH. These results are compiled in table 6.1. The normalized mass uptake vs. $time^{1/2}$ relationships for gelatin and cellulose acetate are presented in figures 6.7 and 6.8, respectively.

The absorption of moisture by gelatin was very different than its desorption. Up to $M(t)/M(\infty) < 0.6$, the curves were identical. Beyond $M(t)/M(\infty) = 0.6$, the diffusion appeared to increase with concentration as indicated by the higher absorption curve although it does necessary imply the diffusion is "Pseudo-Fickian" [4]. In a Pseudo-Fickian diffusion, the absorption and desorption curves would not intersect except at the origin. Thus, the anomaly between the absorption and desorption curves at $M(t)/M(\infty) = 0.6$ was inherent of the moisture sorption hysteresis exhibited by this material.

This anomaly was not observed for cellulose acetate. It is apparent from figure 6.8 that cellulose acetate exhibits Fickian diffusion.

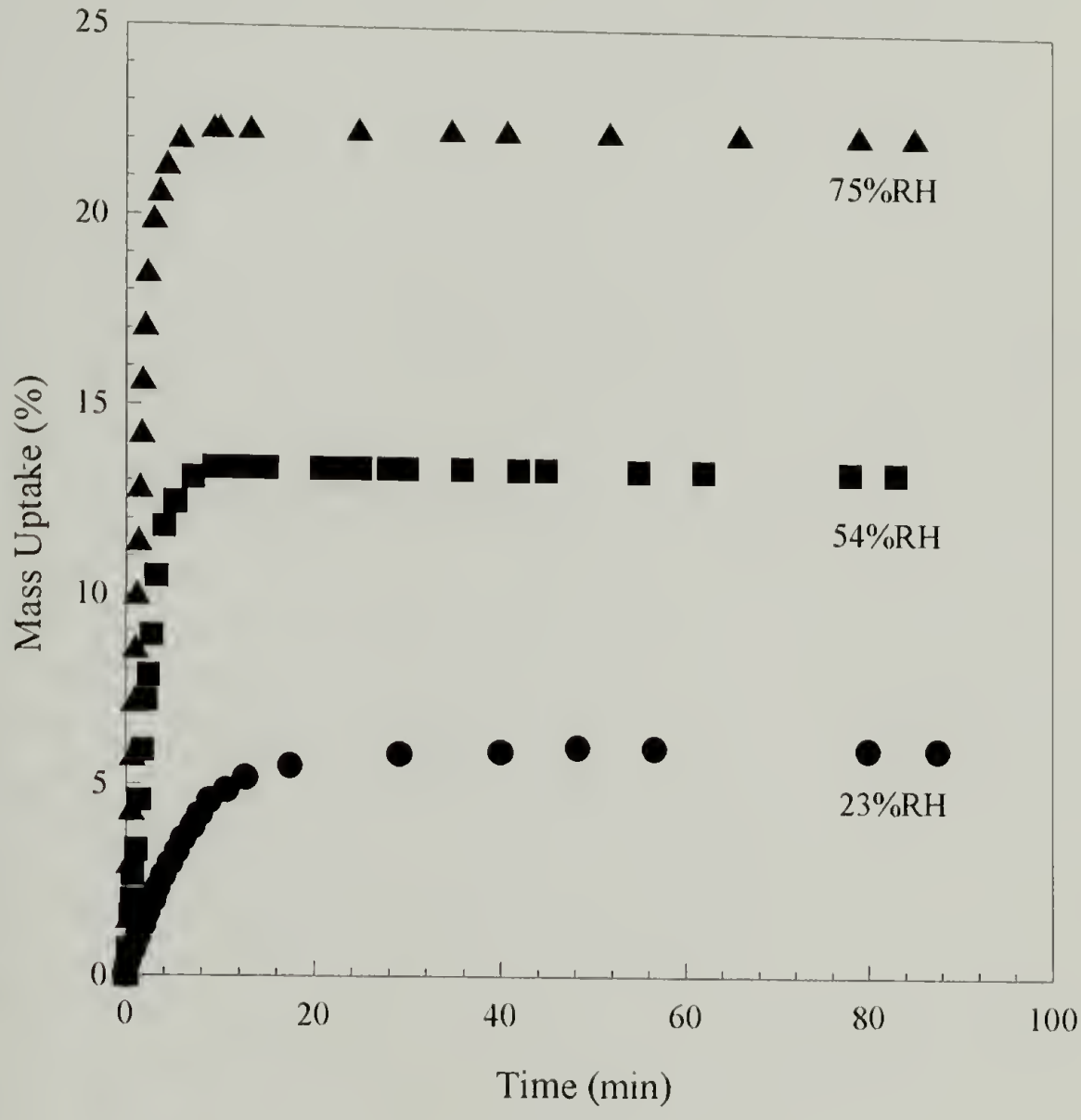

Figure 6.4 Mass uptake (%) as a function of time during absorption of 23%RH, 54%RH, and 75%RH from 0%RH for gelatin via gravimetric technique.

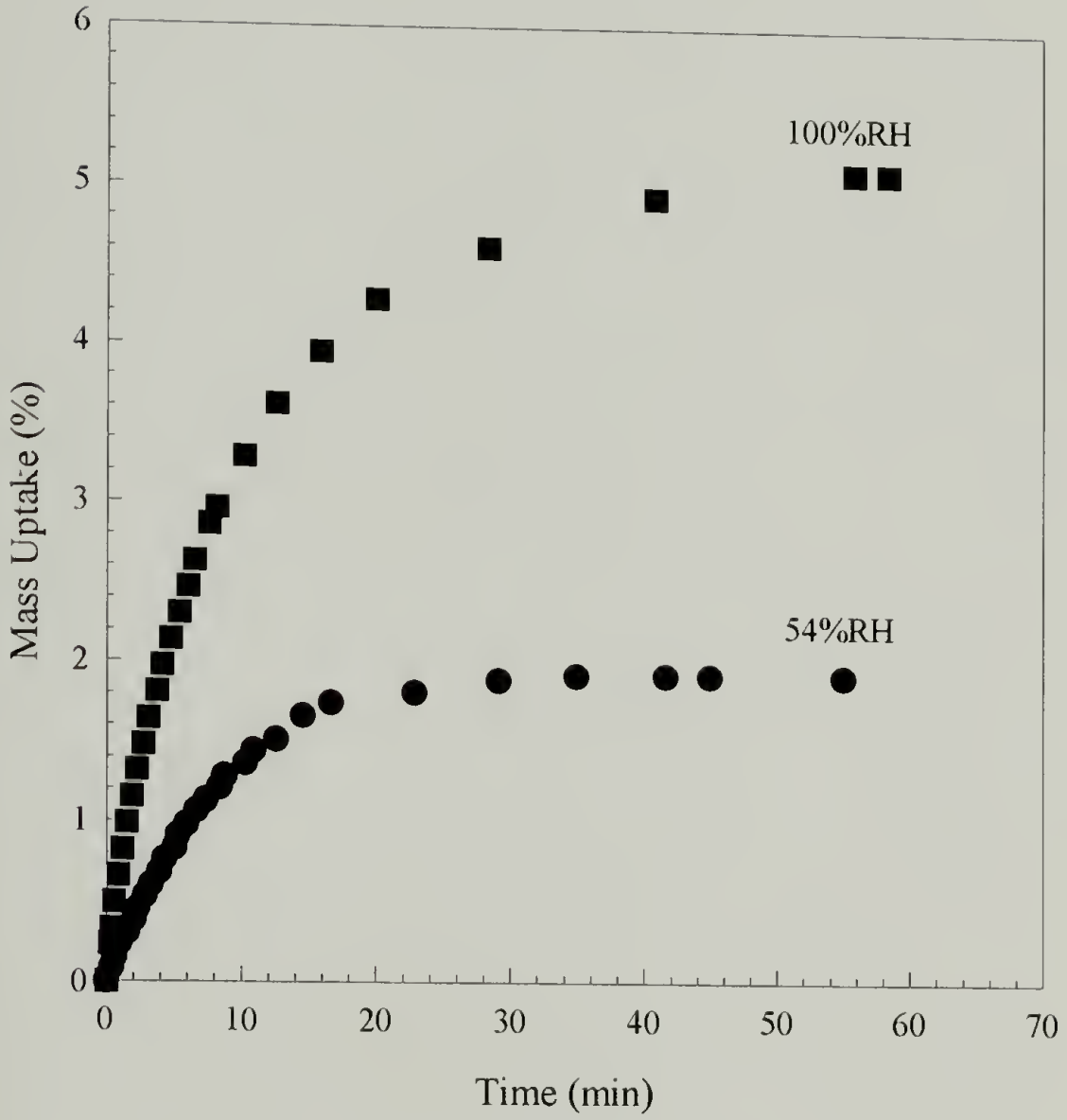

Figure 6.5 Mass uptake (%) as a function of time during absorption of 54%RH and 100%RH from 0%RH for cellulose acetate employing the gravimetric technique.

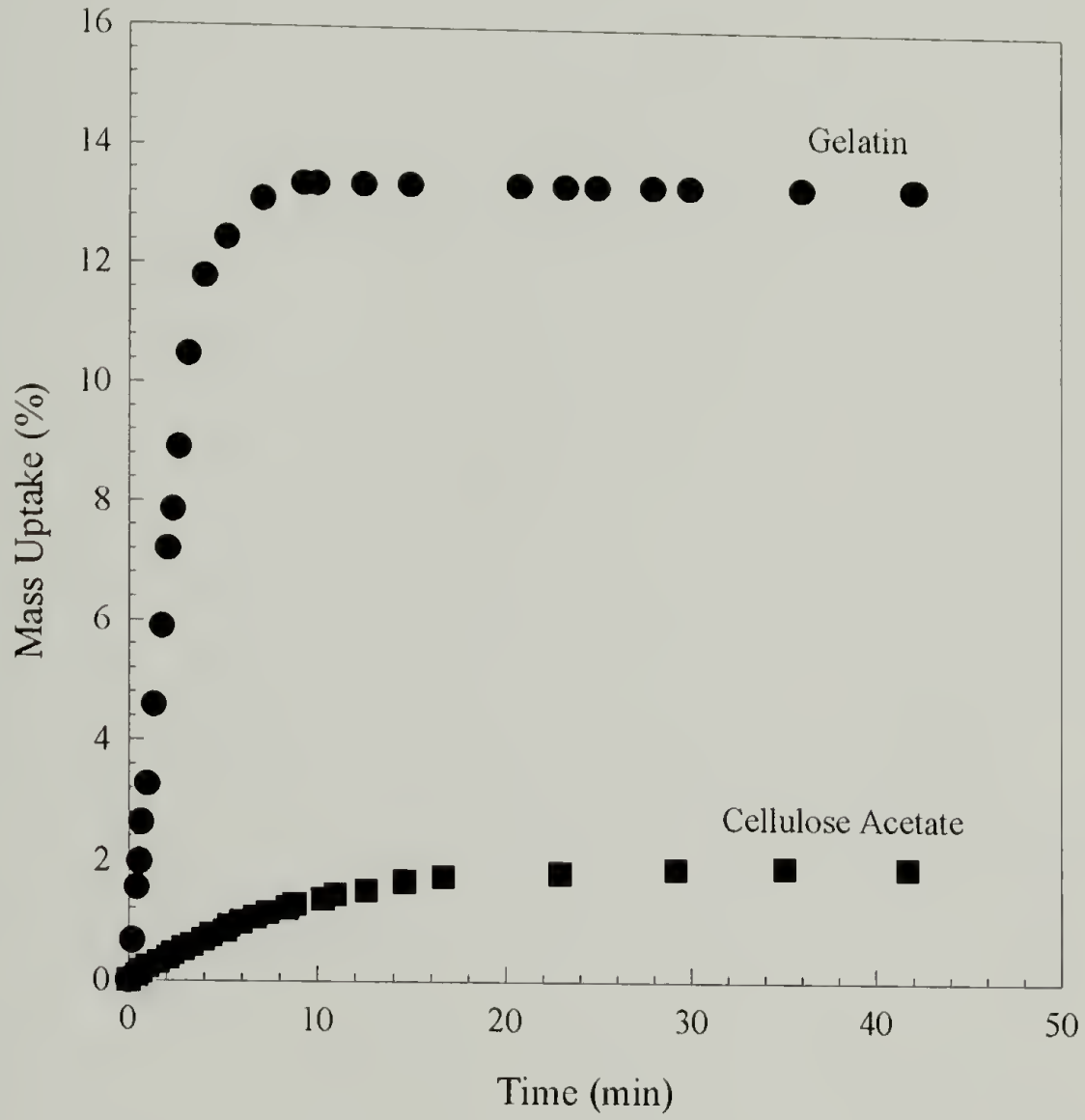

Figure 6.6 Comparison of the mass uptake of alkaline processed bone gelatin and cellulose acetate at 54%RH as a function of time.

Table 6.1 Comparison of the mass uptake values of gelatin and cellulose acetate at various relative humidities.

Gelatin		
Relative Humidity (%)	**Mass Uptake (%) Measured**	**Mass Uptake (%) Literature***
23	6.0	8.5
54	13.4	13.5
75	22.2	20.0
Cellulose Acetate		
54	1.9	
100	5.1	

* Values were extracted from graph presented in the literature and therefore are average values.

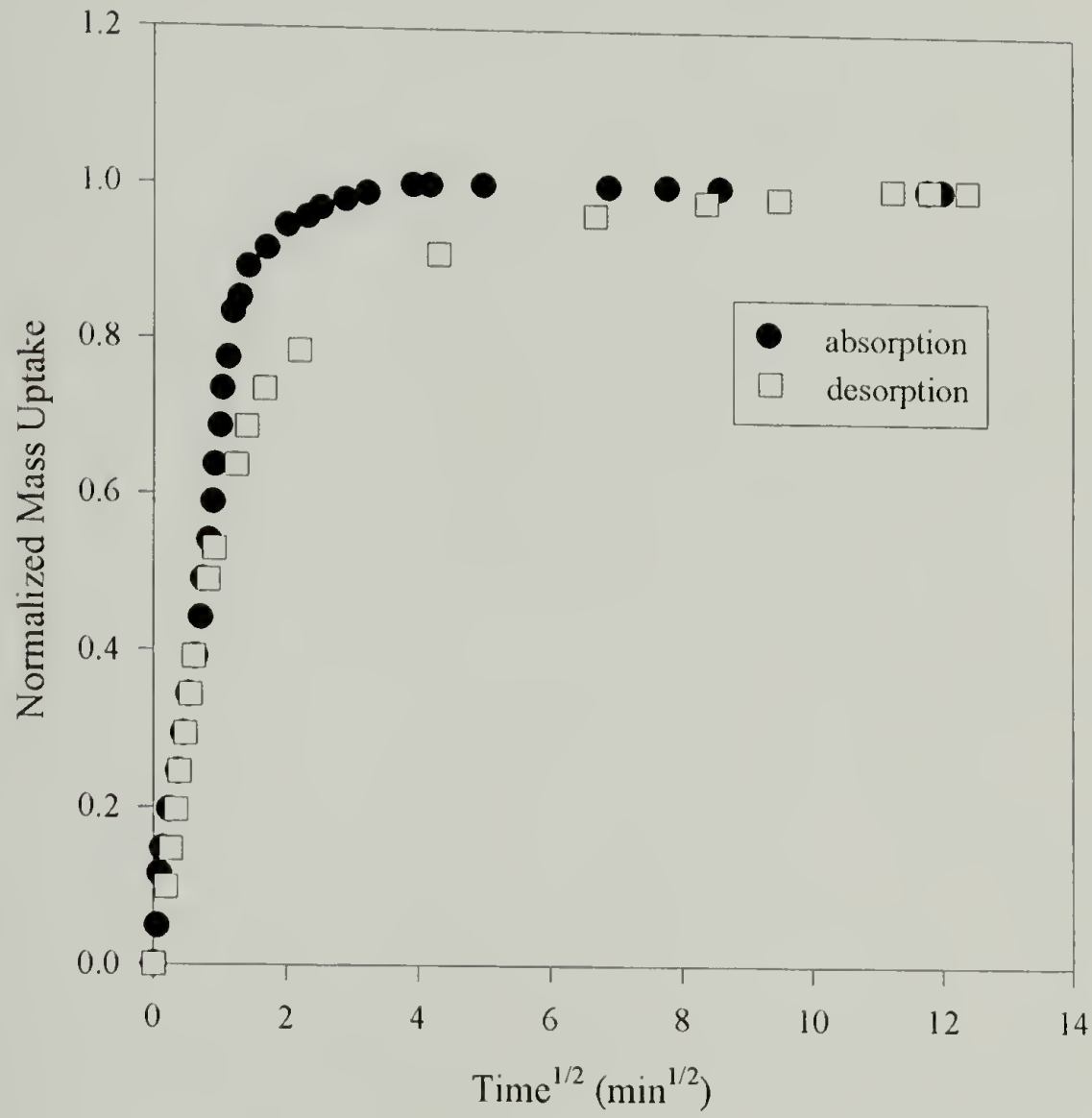

Figure 6.7 Normalized mass uptake vs. time$^{1/2}$ for gelatin using the gravimetric technique.

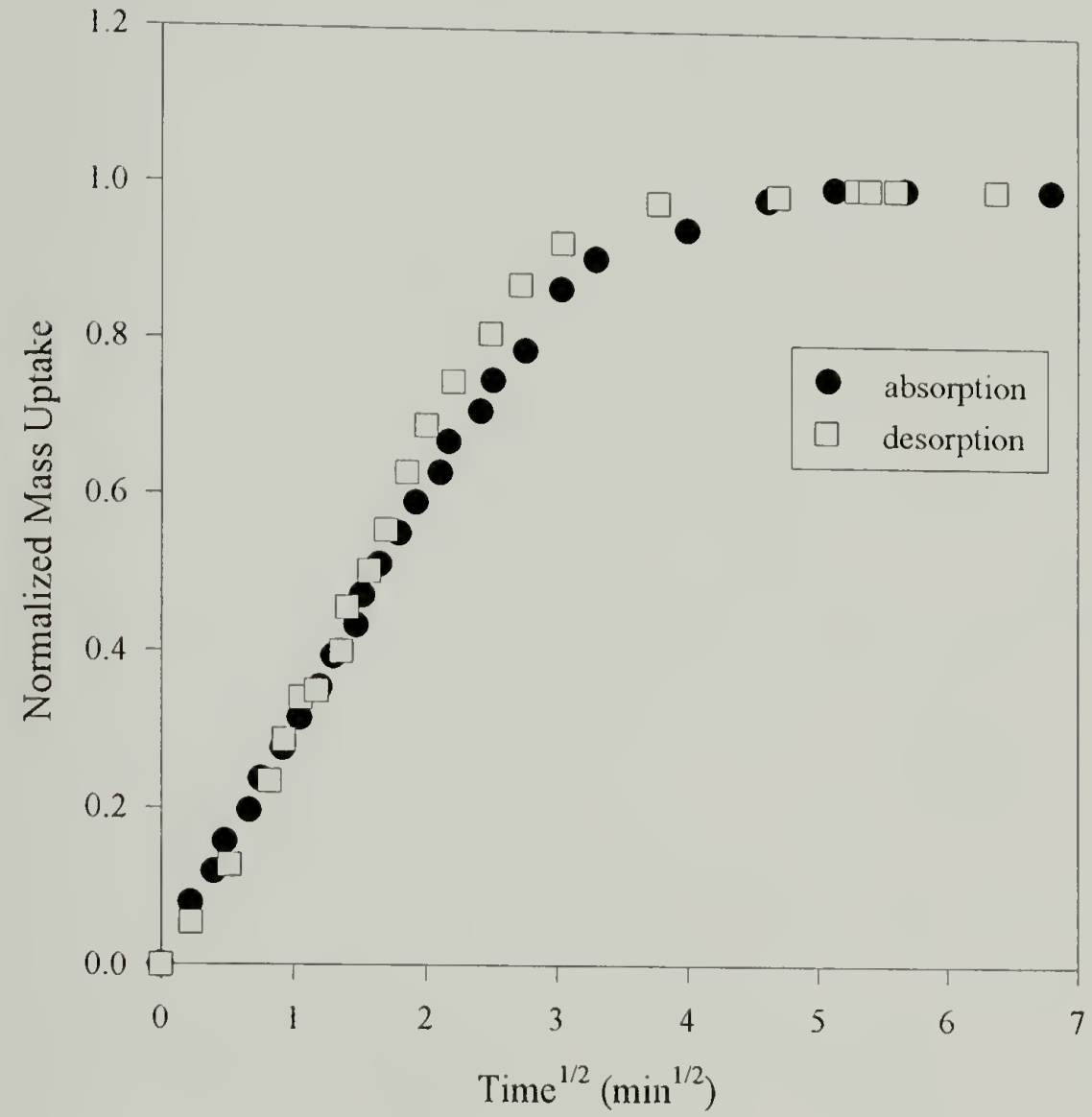

Figure 6.8 Normalized mass uptake vs. time$^{1/2}$ for cellulose acetate using the gravimetric technique.

The effective mass diffusion coefficients, D_{eff}, for the gelatin and cellulose acetate are presented in Table 6.2. The diffusion coefficients were calculated using the initial slope and half-time methods.

Table 6.2 The mass diffusion coefficients, D_{eff}, for alkaline processed bone gelatin (i.d. #SC5-5S-5020-01) and cellulose acetate films using gravimetric technique.

Gravimetric Technique		**Diffusion Coefficient, D_{eff}, (cm^2/s)**	
Material	**Analysis Method**	**Absorption**	**Desorption**
Gelatin	Initial Slope	4.61 E-09	5.51 E-09
	Half-Time	4.62 E-09	5.53 E-09
Cellulose Acetate	Initial Slope	5.00 E-08	4.86 E-08
	Half-Time	5.02 E-08	4.87 E-08

From Table 6.2, it became apparent that the diffusion coefficient for gelatin is less than that of cellulose acetate by approximately an order of magnitude. It was earlier postulated that the gelatin should have a greater mass diffusion coefficient than cellulose acetate due to its quick response to humidity variations.

To better understand this phenomenon, recall that the diffusion coefficient is a measure of the movement of a penetrant through a film or sheet. Its units of measure are cm^2/s. Therefore the diffusion coefficient does not express the amount of penetrant entering the film but instead indicates the rate at which it enters through the thickness.

Referencing figure 6.6, it was apparent that the amount of moisture absorbed by gelatin in the first five (5) minutes is ~ 13 times greater than the amount absorbed by

cellulose acetate in the same time interval. As discussed in prior chapters, it is the amount of moisture that affects the material properties of gelatin and cellulose acetate. Therefore, the humidity swelling coefficient combined with the diffusion coefficient are required to understand the transient dimensional instability behavior of the bilayer system.

Mass Diffusion Coefficient via Humidity Swelling Strain Method

The humidity swelling strain as a function of time was monitored for a sorption cycle of 0%RH to 54%RH to 0%RH. In this study, only gelatin was investigated. The results of this investigation are depicted in figure 6.9.

The design of this experiment requires a constant load be applied to the sample. A 130g counterweight was used in this case. This is equivalent to a 35g load on the sample. As indicated in chapter 4, the counterweight causes the gelatin to creep at higher humidities. This is the reason for the "Pseudo-Fickian" behavior of this material. As a matter of comparison, the diffusion coefficients were calculated as 1.28 E-08 cm^2/s and 3.5 E-09 cm^2/s for absorption and desorption, respectively. These values were determined using the initial slope method. This analysis is erroneous since the initial slope method is only valid for Fickian diffusion and a diffusion coefficient that is independent of concentration.

Mass Diffusion Coefficient via Holographic Interferometry

As discussed in chapter 5, the transient swelling stress as a function of time was monitored to ensure equilibrium stress was reached. It was the behavior of the transient

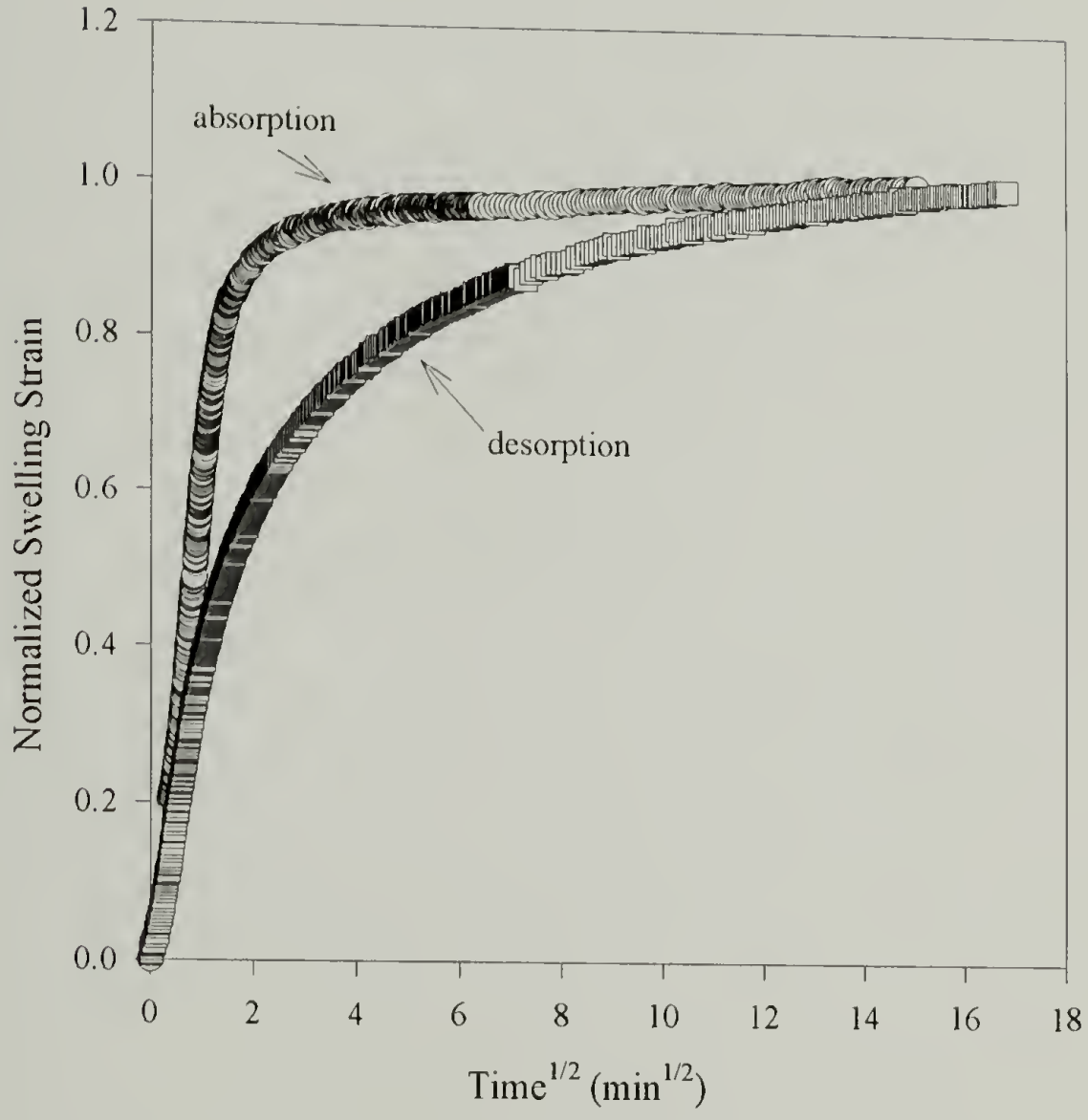

Figure 6.9 Normalized swelling strain vs time$^{1/2}$ for gelatin (#8247-2-3) for sorption cycle 0%RH to 54%RH to 0%RH. A 130 g counterweight (used as the constant load) was hung from the sample.

swelling stress that led to the pursuit of holographic interferometry for determining the diffusion coefficient using a two (2) dimensional membrane sample.

Gelatin, cellulose acetate and polyimide (PMDA-ODA) were investigated. The gelatin membrane was fabricated from a bilayer gelatin on a substrate as described in chapter 5. The cellulose acetate and polyimide samples were made from films.

A steel washer was adhered to cellulose acetate using a diglycyl ether bisphenol A type epoxy. The assembly was placed in a 135°C oven for 2 hours. At 135°C, the cellulose acetate was above its glass transition temperature and the manufacturing stress stored in the material was released. Upon cooling, the stresses were reintroduced and stored in tension in the membrane.

A similar procedure was applied to make the polyimide membrane sample. The polyimide membrane was used as a control. Polyimide has been widely studied and its mass diffusion coefficient is well documented [11,12,13]. Therefore, the holographic technique applied to diffusion using membrane geometries can be validated using the polyimide sample and comparing the results to the literature value.

Each material was subject to a specific sorption cycle. The gelatin and cellulose acetate membranes were initially dried at 0%RH using dry compressed helium gas as the transport medium. Each was exposed to 54%RH for a defined period of time and then again subjected to 0%RH. Plots of stress vs. time for gelatin and cellulose acetate are depicted in Figures 6.10 and 6.11, respectively.

Cellulose acetate is a biaxially oriented material. Normally to resolve the stresses in a biaxially oriented material, a square membrane is used and the stresses along the two principal directions are determined [14]. The determination of the diffusion coefficient requires the normalization of the swelling stresses. Therefore, by monitoring only the frequency change of a single mode (in this case, the 2,1 resonant frequency mode) as a function of time, the average swelling stress was used determine the mass diffusion coefficient.

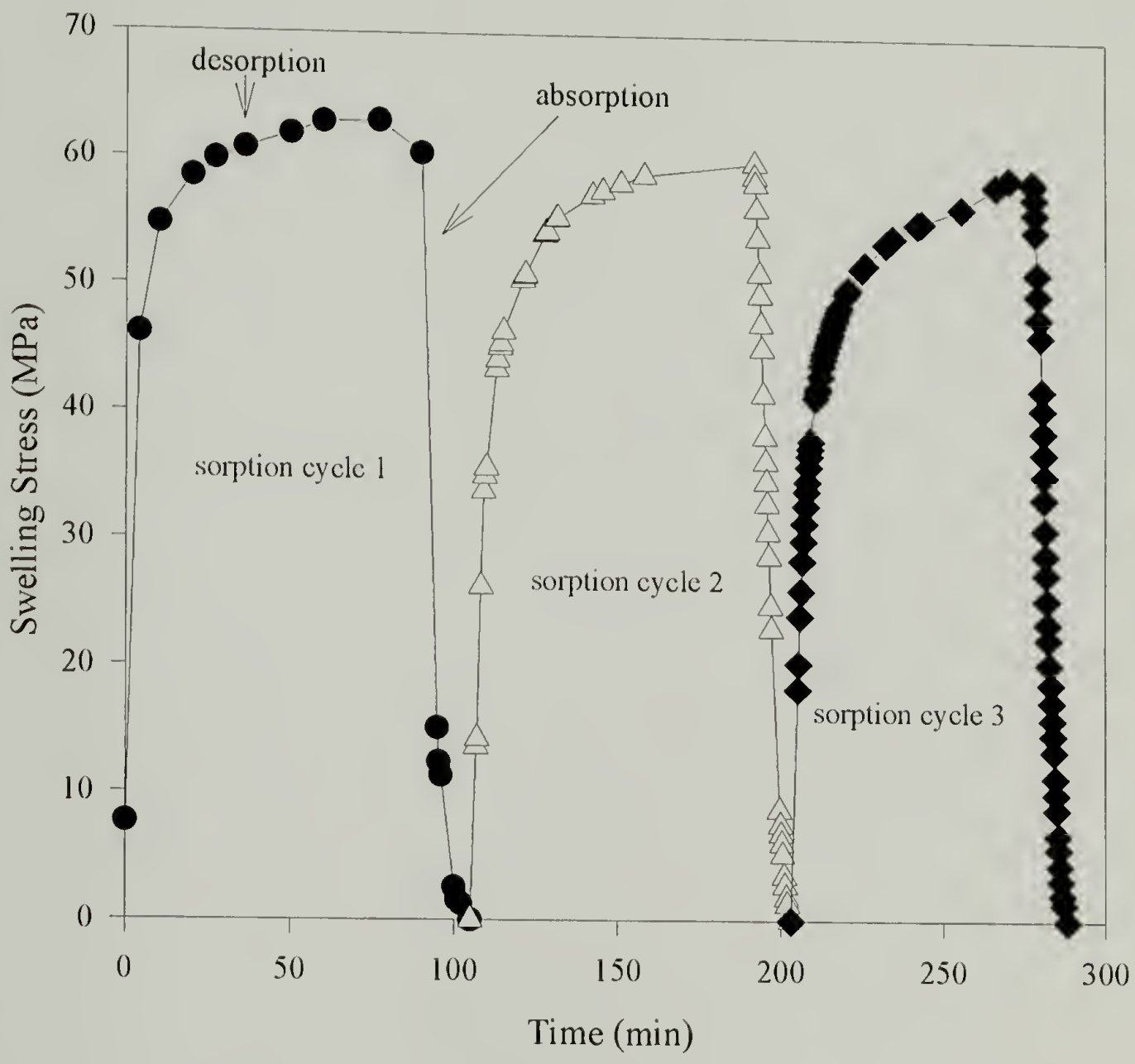

Figure 6.10 Three sorption cycles of 0%RH to 54%RH to 0%RH for gelatin as determined from holographic interferometry.

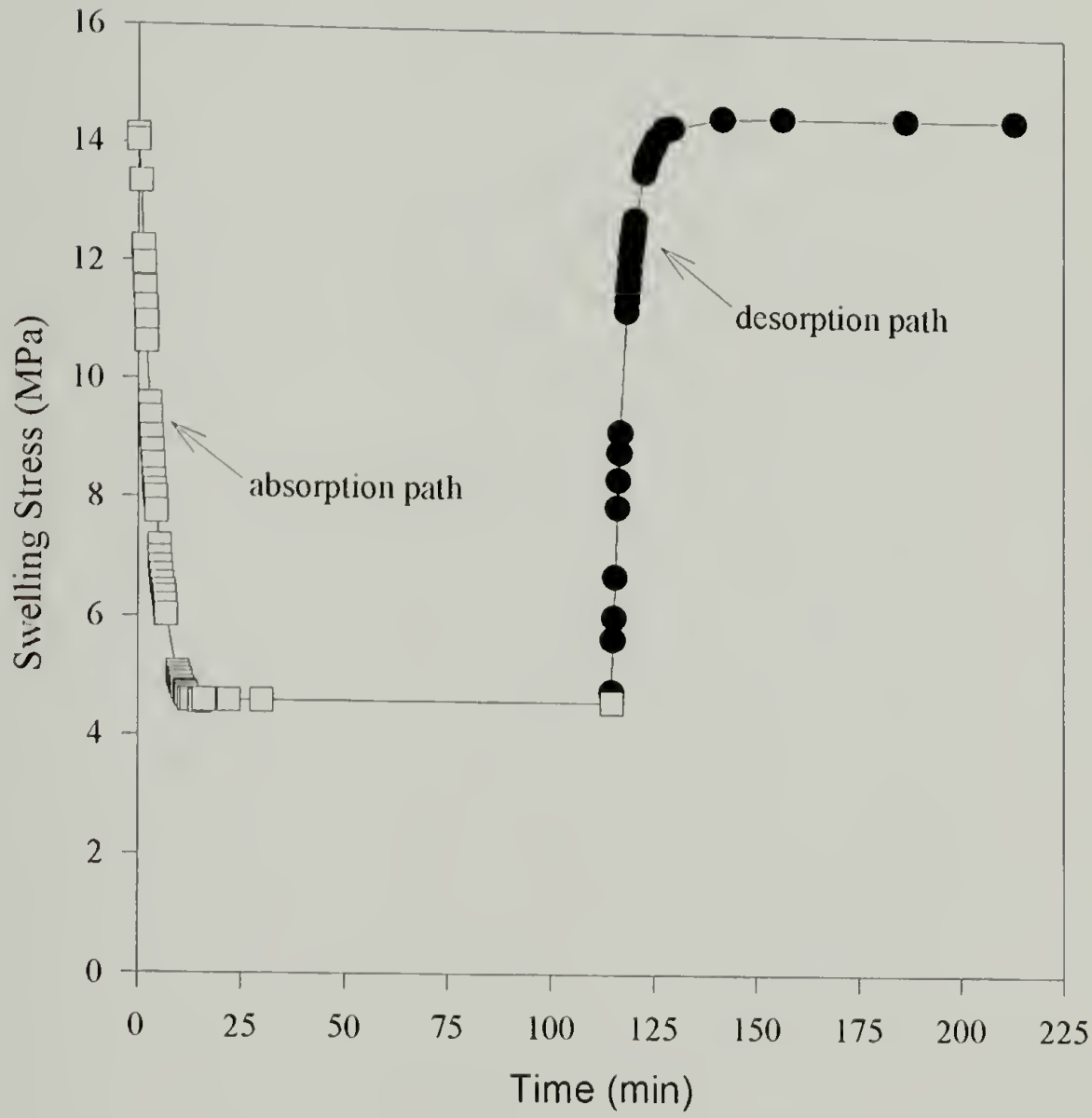

Figure 6.11 Sorption characteristics for cellulose acetate subjected to 0%RH to 54%RH to 0%RH as determined by holographic interferometry.

The mass diffusion coefficients for gelatin (#SC5-5S-5020-01) and cellulose acetate were calculated from the data presented in figure 6.12 and 6.13, respectively. The plots of normalized swelling stress vs. time$^{1/2}$ for both gelatin and cellulose acetate indicated that the diffusion was Fickian. Therefore the mass diffusion coefficients were determined using both the initial slope and half-time methods. Table 6.3 provides a summary of these results.

Table 6.3 Mass diffusion coefficients of gelatin (#SC5-5S-5020-01) and cellulose acetate determined using holographic interferometry.

Holographic Interferometry Technique		**Diffusion Coefficient, D_{eff}, (cm^2/s)**	
Material	**Analysis Method**	**Absorption**	**Desorption**
Gelatin	Initial Slope	2.17 E-09	2.11 E-09
	Half-Time	2.18 E-09	2.09 E-09
Cellulose Acetate	Initial Slope	5.02 E-08	4.87 E-08
	Half-Time	5.00 E-08	4.88 E-08

As the results in table 6.3 confirm, the diffusion is Fickian. Two (2) lots of gelatin were investigated. Both were 16.7% crystalline as determined by the melt enthalpies values provided by Eastman Kodak Co. The first lot of gelatin (#SC5-5S-5020-01) was provided on a cellulose acetate substrate and stored in roll form at room conditions which fluctuated. The second lot of gelatin (#8247-2-3) was received on a PET substrate in flat sheet form. This lot was stored in a controlled low temperature environment (a freezer) to slow the aging process.

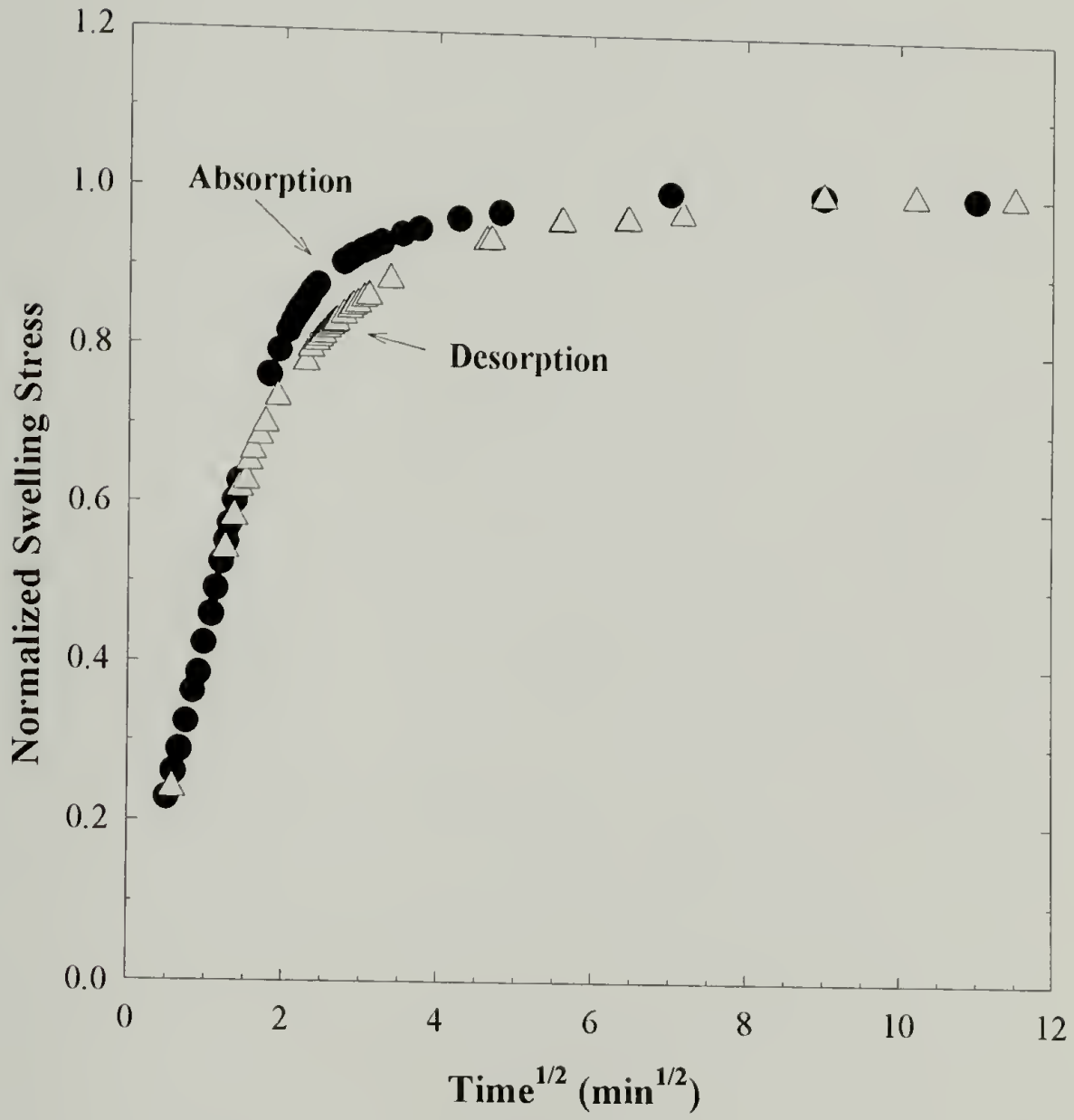

Figure 6.12 Normalized biaxial swelling stress vs. time$^{1/2}$ for gelatin (#SC5-5S-5020-01) as measured using holographic interferometry method.

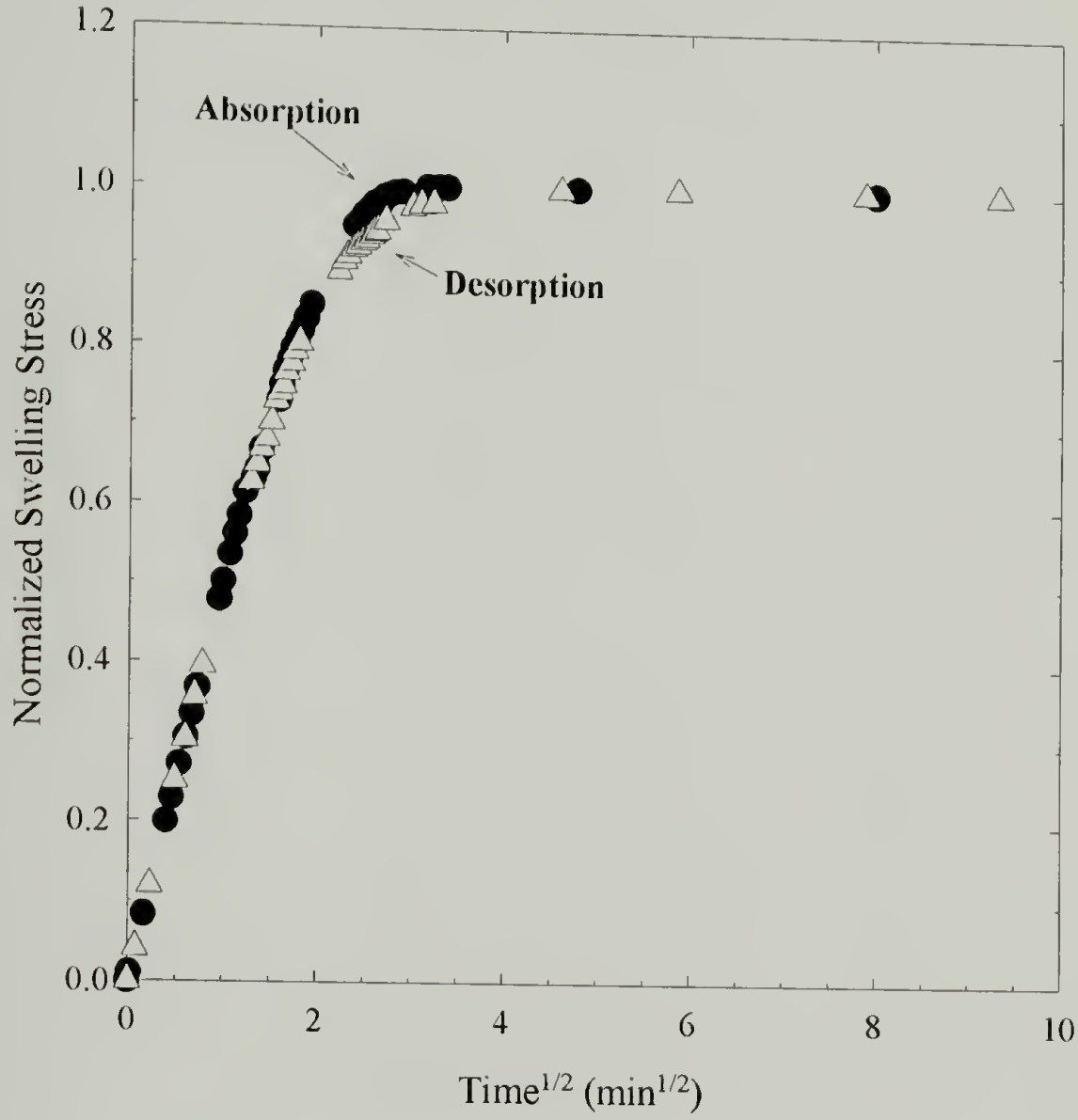

Figure 6.13 Normalized biaxial swelling stress vs. time$^{1/2}$ for cellulose acetate determined by holographic interferometry

Lot 1 gelatin (received on a cellulose acetate substrate) was studied eight (8) months after its receipt. Lot 2 gelatin (provided on a PET substrate) was studied six (6) weeks after receipt. Because of storage conditions and its application on different substrates, it was postulated that the two lots of gelatin might exhibit different diffusion coefficients. Figure 6.14 represents the normalized swelling stress vs. time$^{1/2}$ results for gelatin (#8247-2-3).

Table 6.4 provides a comparison of the mass diffusion coefficients for the two lots of gelatin, #SC5-5S-5020-01 and #8247-2-3, respectively.

Table 6.4 Comparison of mass diffusion coefficients for two lots of gelatin, #SC5-5S-5020-01 and #8247-2-3. Both lots were 16.7% crystalline.

Gelatin Lot No.	**Method**	**Diffusion Coefficient, D_{eff}, (cm^2/s)**	
		Absorption	**Desorption**
SC5-5S-5020-01	Initial Slope	2.17 E -09	2.11 E -09
	Half-Time	2.18 E -09	2.09 E -09
8247-2-3	Initial Slope	2.62 E -08	2.65 E -08
	Half-Time	2.61 E -08	2.64 E -08

There was a small difference in the diffusion coefficients between the two lots of gelatin. The #SC5-5S-5020-01 gelatin was older and stored in an uncontrolled environment (room conditions) and therefore its diffusion coefficient should be lower than the #8247-2-3 gelatin. The difference was small but apparent.

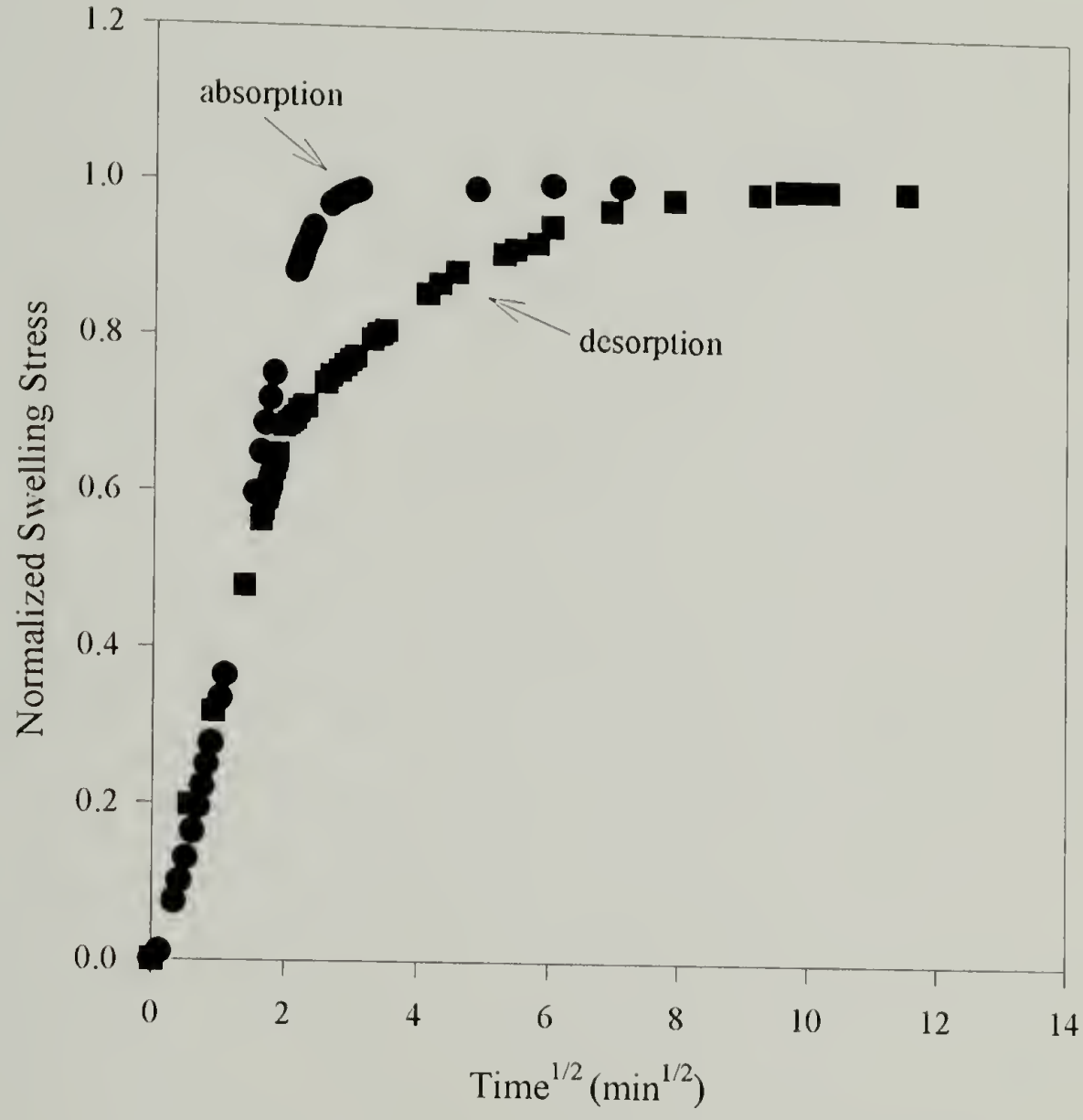

Figure 6.14 Normalized swelling stress vs. time$^{1/2}$ for gelatin (#8247-2-3) using the holographic interferometry technique.

Comparison of the figures 6.12 and 6.14 presents a difference in the absorption behavior of the two gelatins at a normalized swelling stress > 0.6. The absorption and desorption curves of Lot 1 gelatin (#SC5-5S-5020-01) are very similar and are almost identical when superimposed. This is not characteristic of the transport behavior of Lot 2 gelatin (#8247-2-3). Lot 2 gelatin has a higher rate of absorption over longer times than Lot 1 gelatin. The physical aging of the Lot 2 gelatin was hindered by the controlled storage conditions and therefore was not subjected to the environmental fluctations experienced by Lot 1 gelatin.

Gelatin performs many functions in photographic film. One of the requirements of gelatin is that it must swell to facilitate chemical processing [15]. It was shown earlier in chapter 5, that the sorption cycle changes the sorption properties of gelatin. Since Lot 1 gelatin was exposed to environmental fluctuations, the sorption characteristics were altered.

The validity of the holographic interferometry method to determine the mass diffusion coefficient was investigated using a polyimide (PMDA-ODA) membrane. The polyimide was exposed to similar sorption cycles and the 2,1 resonant frequency mode was monitored as a function of time. Figure 6.15 depicts the normalized swelling stress vs. time$^{1/2}$ characteristics.

The effective mass diffusion coefficient of PMDA-ODA polyimide was calculated by the initial slope and half-time methods. The polyimide exhibited Fickian diffusion. The calculated diffusion coefficient for polymide using this holographic interferometry method was 2.08 E-09 cm^2/s (absorption, initial slope method). This result agrees with the reported literature value of 2.00 E-09 cm^2/s [7].

The polyimide diffusion coefficient results from the holographic interferometry correlated well with the published value. Therefore, holographic interferometry using the membrane geometry was a valid method for determining the mass diffusion coefficient. The holographic interferometry and gravimetric results are compared in Table 6.5.

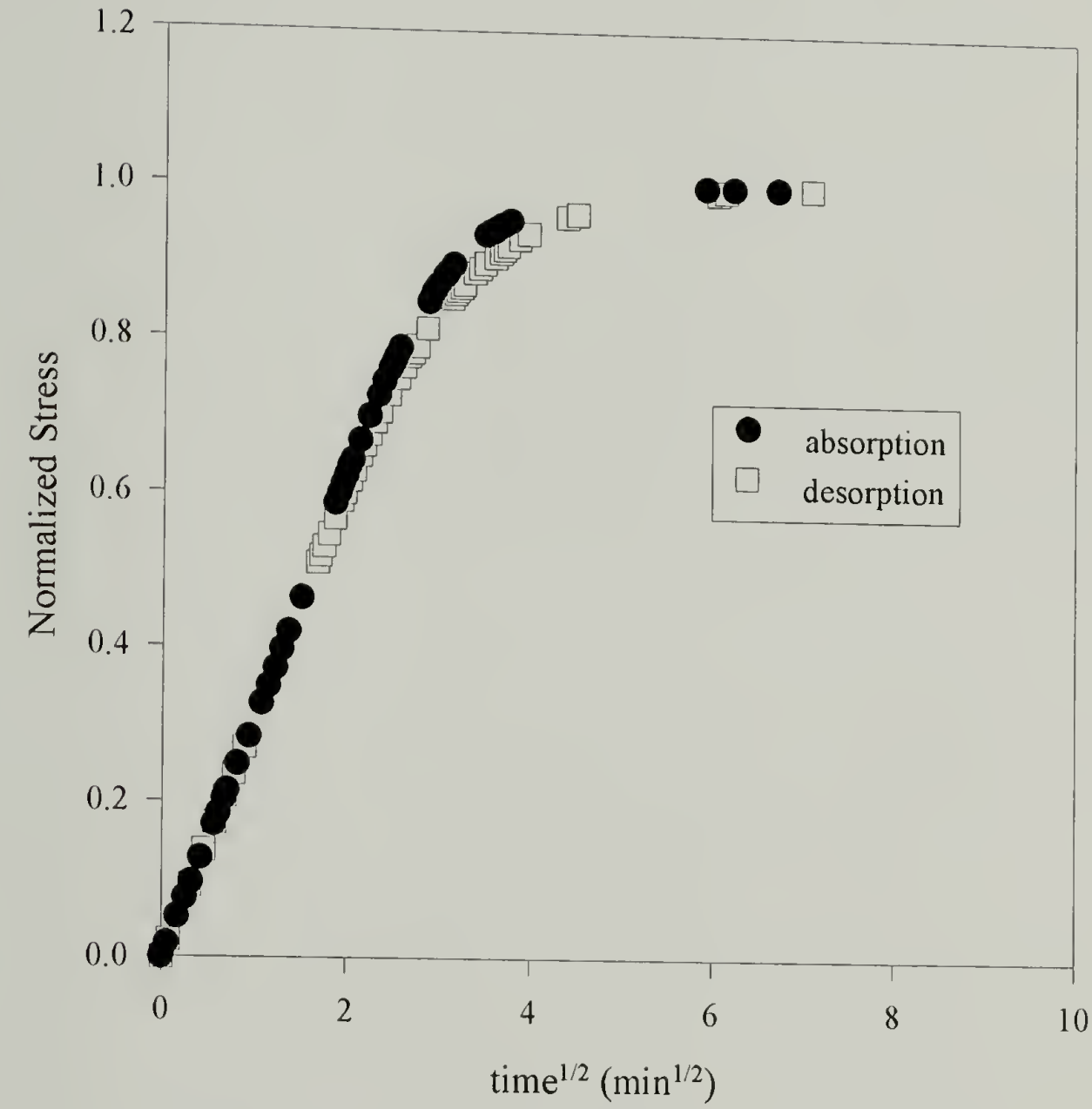

Figure 6.15 Normalized swelling stress vs. time$^{1/2}$ for polyimide (PMDA-ODA) using holographic interferometry.

Table 6.5- Comparison of the mass diffusion coefficients for gelatin, cellulose acetate and polyimide using holographic interferometry and gravimetric techniques.

			Diffusion Coefficient, D_{eff} (cm^2/s)	
Material	**Technique**	**Analysis Method**	**Absorption**	**Desorption**
Gelatin #SC5-5S-5020-01	Gravimetric	Initial Slope	4.61 E-09	5.51 E-09
	Gravimetric	Half-Time	4.62 E-09	5.53 E-09
	Holographic	Initial Slope	2.17 E-09	2.11 E-09
	Holographic	Half-Time	2.18 E-09	2.09 E-09
Gelatin #8247-2-3	Holographic	Initial Slope	2.61 E-09	2.64 E-09
	Holographic	Half-Time	2.62 E-09	2.65 E-09
Cellulose Acetate	Gravimetric	Initial Slope	5.00 E-08	4.86 E-08
	Gravimetric	Half-Time	5.02 E-08	4.87 E-08
	Holographic	Initial Slope	5.02 E-08	4.87 E-08
	Holographic	Half-Time	5.00 E-08	4.88 E-08
Polyimide PMDA-ODA	Holographic	Initial Slope	2.08 E-09	1.98 E-09
	Holographic	Half-Time	2.04 E-09	1.97 E-09

Overall, the mass diffusion coefficients were the same whether holographic interferometry or the gravimetric method was used. There was a discrepancy in the

diffusion coefficients for gelatin between the two methods. Several possible explanations can be argued. First, the volume of the Cahn 2000 chamber was greater than the holographic chamber. It is possible that the sample in the gravimetric chamber was not completely dry for the same drying interval as the holographic interferometry chamber. This could lead to inflated diffusion coefficient results. Secondly, recall that a small weight was hung from the bottom of the gravimetric sample. This was necessay due to the adverse affect of the sample clinging to the walls of the chamber as a result of the moisture/compressed gas flowrate. Although the weight was small, gelatin creeps at higher humidities and this phenomenon could contribute to erroneous diffusion coefficient results.

The biaxial swelling stress as a function of percentage mass uptake of moisture was also investigated. Figure 6.16 and 6.17 illustrate the characteristic curves for gelatin and cellulose acetate respectively. The swelling stress vs. mass uptake curve was fit with a 3rd order polynomial:

$$\sigma = -0.035c^3 + 0.736c^2 - 8.64c + 67.45 \qquad (6.15)$$

where, c is the % mass uptake and σ is the biaxial swelling stress (MPa) for gelatin.

The cellulose acetate showed a different swelling stress vs. mass uptake behavior. Initially the curve is linear. This inferred that the mass uptake is directly proportional to the measured stress. An equilibrium plateau was observed at which point the stress drops only slightly with increasing amounts of moisture. This data was fit by a 2nd order polynomial:

$$\sigma = 3.21c^2 - 11.43c + 14.67 \qquad (6.16)$$

where, c is the % mass uptake and σ is the biaxial swelling stress for cellulose acetate.

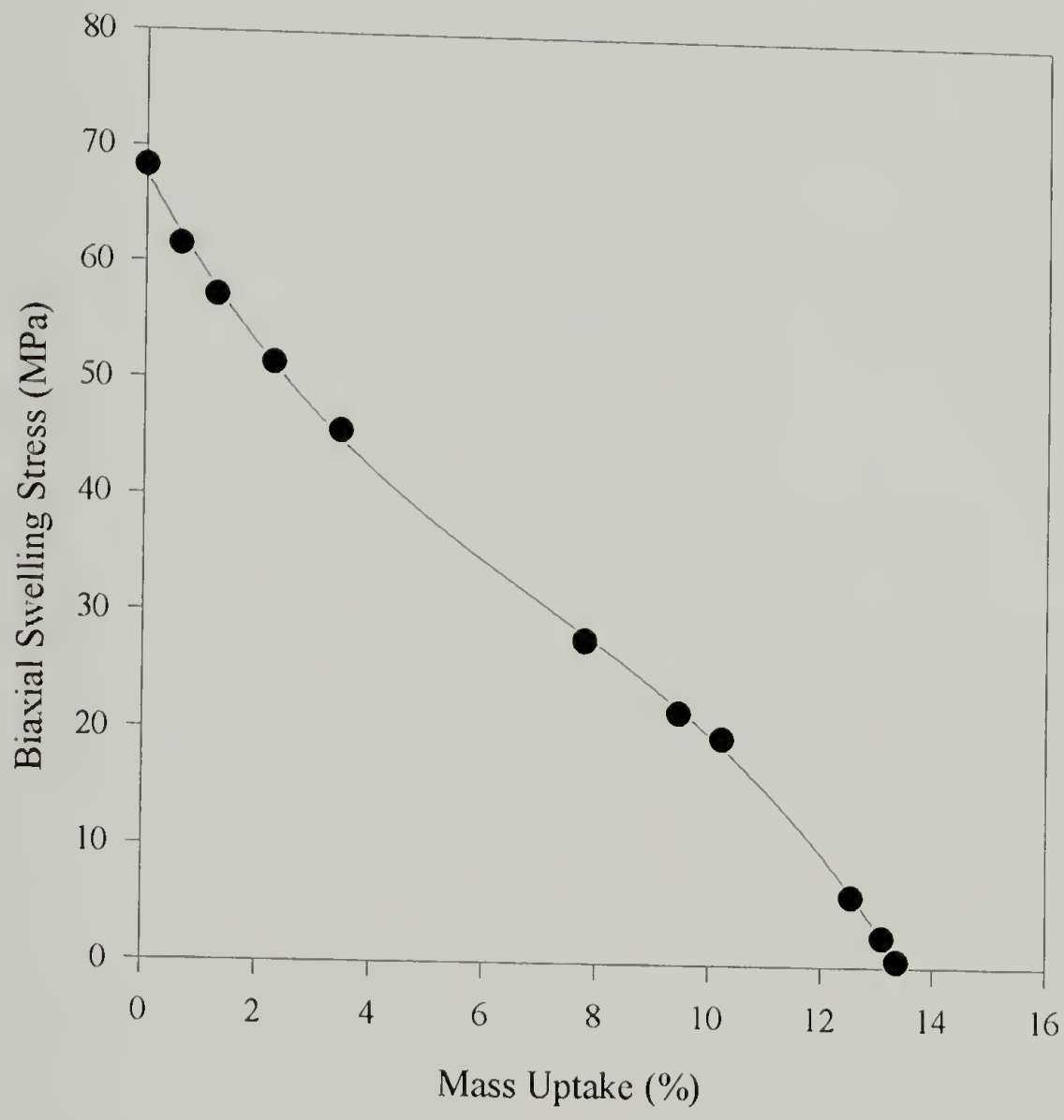

Figure 6.16 Biaxial swelling stress as a function of mass uptake for gelatin during absorption from 0%RH to 54%RH

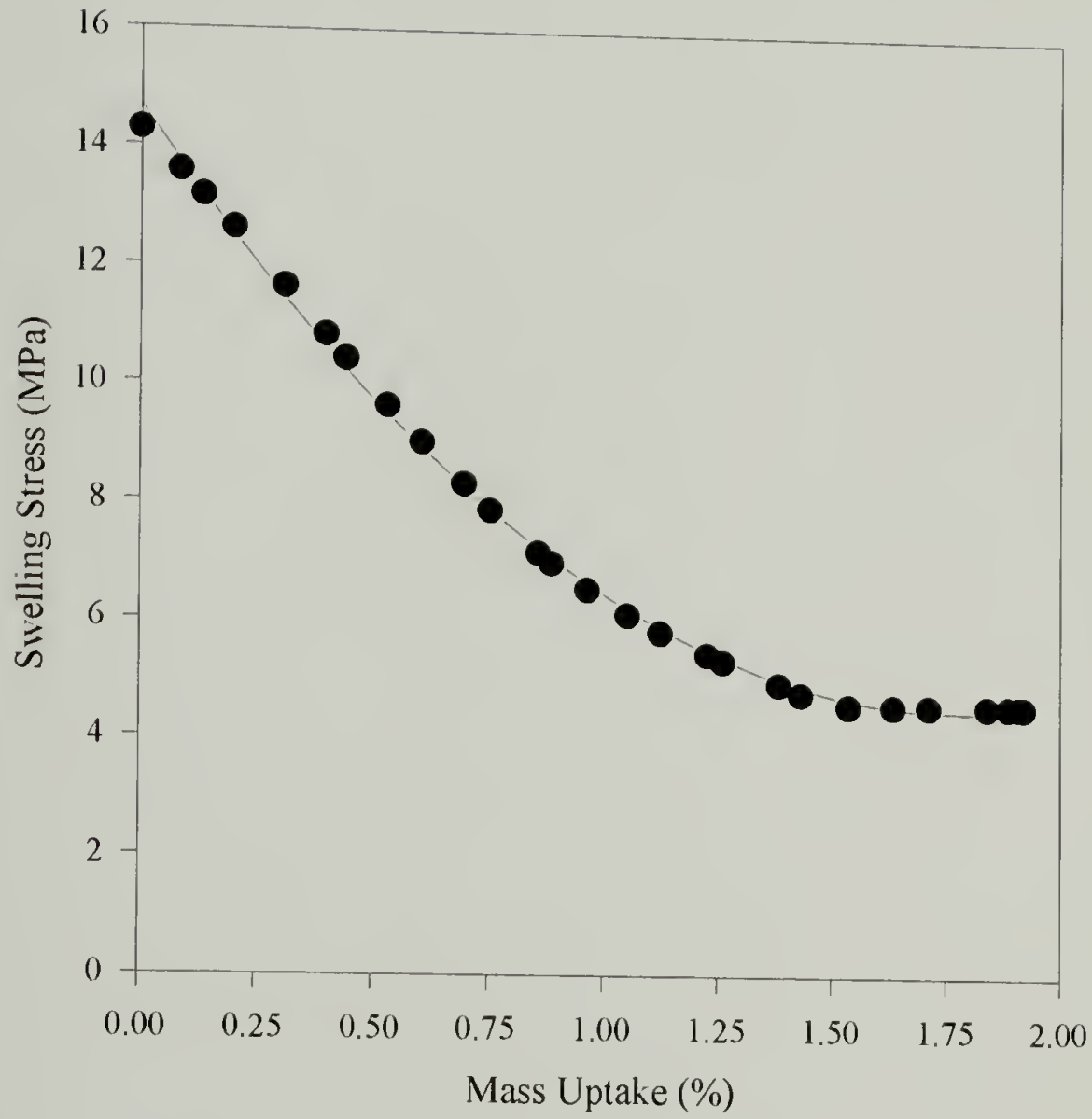

Figure 6.17 Swelling stress vs. % mass uptake for cellulose acetate during absorption from 0%RH to 54%RH.

Conclusions

Alkaline processed bone gelatin, cellulose acetate and polyimide exhibit Fickian moisture diffusion. Comparison of the diffusion coefficients for two lots of gelatin indicated a slight difference which was the result of storage conditions and physical aging. Lot 2 gelatin, #8247-2-3, (the newer lot) showed a higher diffusion coefficient. This lot seemed to have a greater propensity to absorb a larger amount of moisture for the same time interval as compared to the older lot of gelatin, #SC5-5S-5020-01

A new technique for determining the mass diffusion coefficient was introduced. Its validity was experimentally verified using PMDA-ODA polyimide with a known diffusion coefficient. This technique employed holographic interferometry and used a circular membrane sample geometry to study the mass transport properties of coating and films.

The gelatin and cellulose acetate diffusion coefficients varied by an order of magnitude with cellulose acetate exhibiting a higher diffusion coefficient. The diffusion coefficients determined by holographic interferometry for gelatin and cellulose acetate were 2.11 E-09 cm^2/s and 5.00 E-09 cm^2/s, respectively. This variation was intuitively thought to be incorrect due to the quick response of gelatin coated bilayer systems to humidity changes. Observations by the naked eye indicated that gelatin reacted very quickly to moisture changes. The reason for the quick response to moisture changes by gelatin was due to the amount of moisture the gelatin picked up in the same interval compared to that of cellulose acetate or polyimide. This response is not solely related to the rate at which the moisture penetrated through the film thickness. This phenomenon was illustrated in a comparison of the percentage of moisture taken up by gelatin with that of cellulose acetate over the same time interval.

The biaxial swelling stress as a function of the mass uptake of gelatin showed a 3rd order response. The stress dropped quickly with the introduction of moisture. The same behavior was not observed for cellulose acetate. The cellulose acetate exhibited a 2nd

order reponse to the biaxial swelling stress as a function of moisture uptake. Initially , the stress is linearly proportional to the mass uptake. At 1.25% mass uptake, the stress begins to plateau indicating that the material is nearing saturation and the stress decreased minimally with addition moisture.

References

1. J. Crank, The Mathematics of Diffusion, (Oxford, England: Clarendon Press, 1956).

2. C.D. Shirrell, "Diffusion of Water Vapor in Graphite/Epoxy Composites," Advanced Composite Materials - Environmental Effects, ASTM STP 658, ed. J.R. Vinson, (Philadelphia, PA: American Society for Testing and Materials, 1978).

3. J. Crank and G.S. Park, "An Evaluation of the Diffusion Coefficient for Chloroform in Polystyrene from Simple Absorption Experiments," Transactions of the Faraday Society, **45**, 240 (1949).

4. R.M. Felder and G.S. Huvard, Methods of Experimental Physics, (New York: Academic Press, 1980).

5. A.Y. Malkin, A.A. Askadsky, V.V. Kovriga and A.E. Chalykh, Experimental Methods of Polymer Physics, (Englewood Cliffs, NJ: Prentice-Hall, Inc., 1983).

6. S.T. Sackinger, The Determination of Swelling Stresses in Polyimide Films, Ph.D. diss., University of Massachusetts, Amherst, MA, (1990).

7. C.S. Jou, Stresses Associated with Transport in Polymer Films, Ph.D. diss., University of Masschusetts, Amherst, MA, (1993).

8. G.C. Sih, J.G. Michopoulos and S.C. Chou, eds., Hygrothermoelasticity, (Boston, Martinus Nijhoff Publishers, 1986).

9. Cahn Instruments, Inc., Cerritos, CA 90701

10. J.M. Calhoun and D.A. Leister, "Effect of Gelatin Layers on the Dimensional Stability of Photographic Film," Photographic Science and Engineering, **3**(1), 8 (1959).

11. D.K. Yang, W.J. Koros, H.B. Hopfenberg and V.T. Stannett, "Sorption and Transport Studies of Water in Kapton Polyimide," Journal of Applied Polymer Science, **30**, 1035 (1985).

12. H. Pranjoto and D.D. Denton, "Gravimetric Measurements of Steady-State Moisture Uptake in Spin-Coated Polyimide Films," Journal of Applied Polymer Science, **42**, 75 (1991).

13. C.S. Jou and R.J. Farris, "Moisture Transport in Bilayer Cantilever Beam by Holographic Interferometry," (submitted to Acta Polymerica, 1993).

14. J.K. Vrtis and R.J. Farris, "Experimental Stress Analysis Methods and Some Thin Film Applications," (accepted to Materials Research Society Symposium Proceedings, 1994).

15. J.F. Hamilton, G.C. Higgins and J.E. Starr, eds., The Theory of the Photographic Process, (Rochester, NY: Eastman Kodak Co., 1977).

CHAPTER 7

CONCLUSIONS AND FUTURE WORK

This dissertation has focussed on the stresses and mass transport properties in polymer films and coatings. Hygroscopic effects on the dimensional stability in a bilayer system were investigated and a theoretical model representing the bending of a two dimensional bilayer polymer system as a function of relative humidity was proposed. The model is applied and verified in this chapter for the gelatin/cellulose acetate bilayer studied throughout this work.

Application of the Two Dimensional Bending Model

The dimensional instability of the gelatin/cellulose acetate bilayer was discussed in the previous chapters. The curvature dependence on relative humdity is presented in figure 7.1 where "a" and "b" are defined as the curvature along the x and y axes, respectively. From observations, it was noted that the bilayer tends to curl towards the gelatin along the x axis into a cylindrical geometry at relative humidities less that 54%RH for this specific case. There was no curvature in the y-direction, $b = 0$, at low relative humidities. Above 54%RH, the bilayer curled towards the cellulose acetate into a cylindrical geometry but inverted its axis of curvature to the y-direction. At higher humidities, the curvature along x was zero, $a = 0$. At 54%RH, the bilayer was relatively flat, therefore, a and b are both zero.

The two dimensional bending model developed in chapter 2 was based on the Classical Lamination Theory with a nonlinear mathematical modification. The Theorem of Minimum Potential Energy was applied to the case of pure bending.

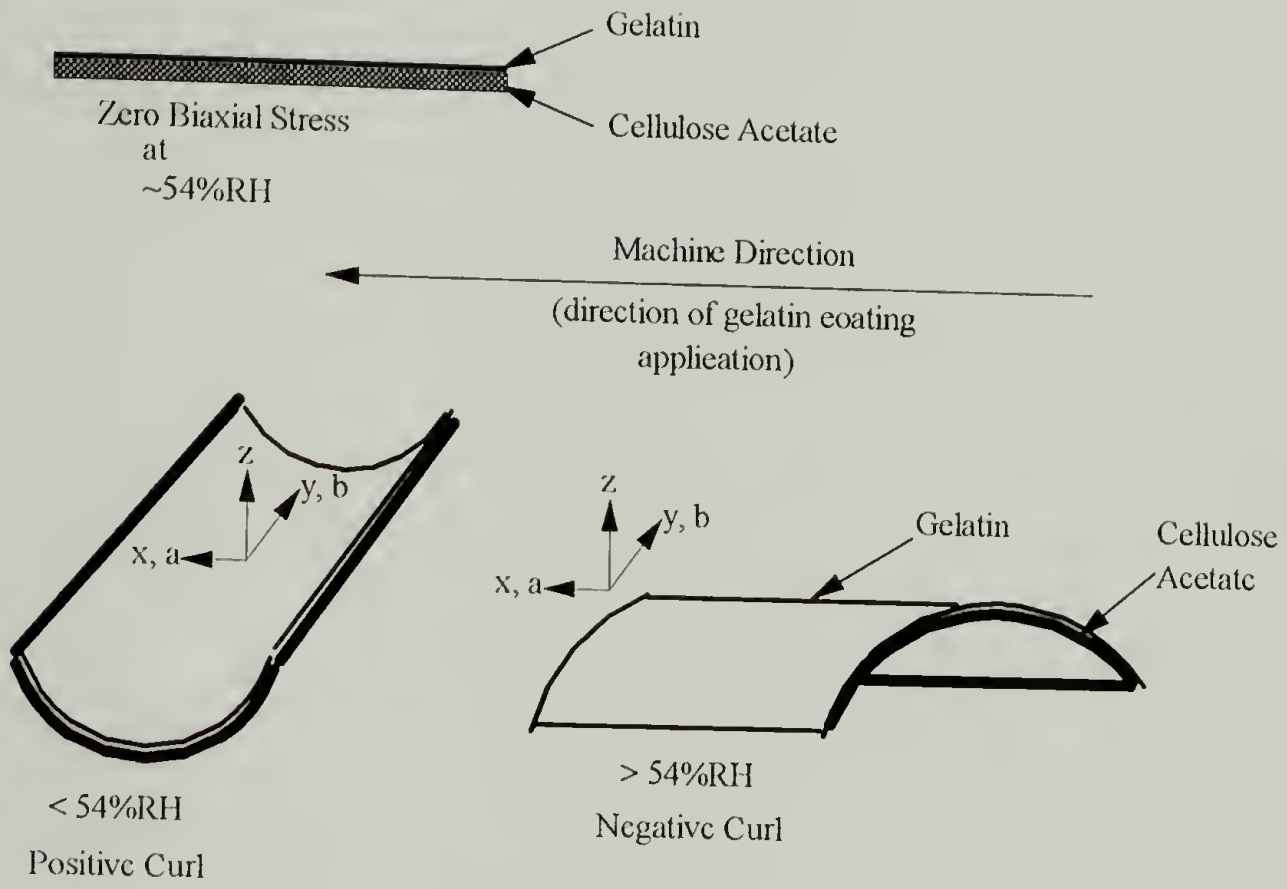

Figure 7.1 Curvature characteristics of the gelatin/cellulose acetate bilayer as a function of relative humidity

The observed shapes were therefore associated with the minimum energy in the bilayer system. The governing equation (2.26) for the total potential energy in the system is reiterated here as equation (7.1):

$$W = \sum_{k=1}^{2} \int_{h_{k-1}}^{h_k} \int_{-L_y/2}^{L_y/2} \int_{-L_x/2}^{L_x/2} \omega\left(a, b, c, d, \overline{Q}_{ij}, \beta_x^b, \beta_y^b, \Delta RH, x, y, z\right) dx dy dz \qquad (7.1)$$

Chapter 2 elaborates on the details of the model derivation. In general, the first variation of equation (7.1) yields the function:

$$\delta W = f_1(a,b,c,d)\delta a + f_2(a,b,c,d)\delta b + f_3(a,b,c,d)\delta c + f_4(a,b,c,d)\delta d \qquad (7.2)$$

From equation (7.2), f_1, f_2, f_3 and f_4 were determined as:

$$\begin{aligned} f_1 = 0 = {} & \frac{N_x^{II} L_y^2 b}{48} + M_x^{II} + \frac{N_y^{II} L_x^2 b}{48} - J_1 bc + J_2 ab^2 + J_3 bc + J_4 ab^2 \\ & + J_5 bd + J_6 bd + J_7 ab^2 - B_{11} c + 2J_8 ab + J_9 b^2 - B_{12} d + 2J_{10} ab \\ & + D_{12} b + J_{11} b^2 + D_{11} a \end{aligned} \qquad (7.3)$$

$$\begin{aligned} f_2 = 0 = {} & \frac{N_x^{II} L_y^2 a}{48} + M_y^{II} + \frac{N_y^{II} L_x^2 a}{48} - J_1 ac + J_2 a^2 b + J_3 ac + J_4 a^2 b \\ & + J_5 ad + J_6 ad + J_7 ab^2 + J_8 a^2 + D_{12} c + 2J_9 ab + J_{10} a^2 + B_{12} a \\ & - B_{22} d + 2J_{11} ab + D_{22} b \end{aligned} \qquad (7.4)$$

$$f_3 = 0 = -N_x^{II} + A_{11} c - J_1 ab + A_{12} d + J_3 ab - B_{11} a + B_{12} b \qquad (7.5)$$

$$f_4 = 0 = -N_y^{II} + A_{12} c - J_5 ab + A_{22} d + J_6 ab - B_{12} a + B_{22} b \qquad (7.6)$$

where,

$$J_1 = \frac{A_{11}L_y^2}{48} \qquad J_2 = \frac{A_{11}L_y^4}{1280} \qquad J_3 = \frac{A_{12}L_x^2}{48}$$

$$J_4 = \frac{A_{12}L_x^2L_y^2}{1152} \qquad J_5 = \frac{A_{12}L_y^2}{48} \qquad J_6 = \frac{A_{22}L_x^2}{48}$$

$$J_7 = \frac{A_{22}L_x^4}{1280} \qquad J_8 = \frac{B_{11}L_y^2}{48} \qquad J_9 = \frac{B_{12}L_y^2}{48}$$

$$J_{10} = \frac{B_{12}L_x^2}{48} \qquad J_{11} = \frac{B_{22}L_x^2}{48}$$

By arranging equations (7.5) and (7.6) in terms of c and d and incorporating these equations into equations (7.3) and (7.4), c and d can be written in terms of a and b. The solutions to these equations are determined numerically.

The numerical solution is dependent upon the moduli and the humidity expansion coefficients for each layer. In chapters 3 and 4, these properties are characterized for a bilayer system consisting of a gelatin coating on a cellulose acetate substrate. The mechanical and humidity expansion properties are summarized in Table 7.1. The Poisson's ratios for cellulose acetate were chosen to make the reduced stiffness matrix symmetrical thus simplifying the analysis. The curvature is defined as the inverse of the radius and has units of length^{-1}. The curvatures, a and b, (m^{-1}), were calculated by applying the following assumptions:

(1. ΔRH is defined as $RH_f - RH_0$, where $RH_0 = 54\%$ and RH_f is the equilibrium relative humidity

(2. When the bilayer is flat (at 54%RH), $\Delta RH = 0$ and a, $b = 0$.

(3. At relative humidities < 54%RH, $b = 0$.

(4. At relative humidities > 54%RH, $a = 0$.

These assumptions are valid since they coincide by the geometries observed at the various relative humidities. The assumptions are specific to the bilayer of gelatin and cellulose acetate.

Table 7.1 Summary of the moduli and humidity expansion coefficients for gelatin and cellulose acetate.

Material	Modulus, E, GPa	Poisson's Ratio	Shear Modulus, G, GPa	Humidity Expansion Coefficient, β, mm/mm/%RH
Gelatin				
33%RH	3.51	0.37	2.79	4.00 E-04
54%RH	2.75	0.37	2.18	4.00 E-04
75%RH	1.75	0.37	1.39	4.00 E-04
Cellulose Acetate				
parallel to coating direction	3.72	0.33	0.94	4.45 E-05
perpendicular to coating direction	4.05	0.36	0.94	6.53 E-05

Note: Poisson's ratios for cellulose acetate are estimated values.

By rearranging equations (7.5) and (7.6) in terms of c and d and incorporating these equations into equations (7.3) and (7.4), c and d can be written in terms of a and b. The solutions to these equations were determined numerically.

Two sample geometries were investigated: a 101.6 mm square sample and a 35 mm by 175 mm rectangular sample. Each consisted of a 19 μm thick gelatin coating on a 127 μm thick cellulose acetate substrate. The curvature for each geometry was predicted at various relative humidities under isothermal conditions. Applying assumptions (1 through 4) and solving for a and b leads to three possible solutions for each scenario. Table 7.2 lists the possible curvatures for each sample geometry.

By deduction, several of the solutions can be eliminated. For the 101.6 mm square geometry, the lowest radius possible without overlapping is 1.62×10^{-3} m. The equivalent curvature is 61.8 m^{-1}. For a solution to be valid, the radius must be greater than the absolute value of 1.62×10^{-3} m or the curvature should be less than absolute value of 61.8 m^{-1}.

Using this logic and recalling the curvature observations, only the root, a = 46.25 m^{-1}, is valid for 33%RH and b = 0. Similarly at 75%RH and a = 0, the only possible root to the solution is -25.97 m^{-1}. At 54%RH, both a and b are zero. This solution coincides with earlier observations.

For the rectangular sample, the smallest possible radius without overlapping along the y axis (parallel the width of 35 mm or the "b" radius of curvature) is the absolute value of 5.56×10^{-3} m. Analogously for the "a" radius of curvature (in the x direction or along the 175 mm length), the smallest possible radius without overlapping is the absolute value of 2.79×10^{-2} m. Therefore, in order for the solution to be valid, the "a" curvature must be less than the absolute values of 35.8 m^{-1} when "b" = 0 or the "b" must be less than the absolute value of 180 m^{-1} when "a" = 0.

Table 7.2 Possible curvatures for a bilayer of gelatin and cellulose acetate.

Relative Humidity (%)	curvature, a, (m^{-1})	curvature, b, (m^{-1})
SQUARE GEOMETRY: 101.6 mm by 101.6 mm		
33	46.25	0
33	0	0
33	-1.04 E+04	0
54	0	0
75	0	-25.97
75	0	0.449
75	0	0.551
RECTANGULAR GEOMETRY: 35 mm by 175 mm		
33	3.80	0
33	0	~0
33	0	3329
54	0	0
75	-3.37	0
75	0	-14.79
75	0	-0.15

Observations of the bending phenomena in the rectangular sample showed no inversion from the x-axis to the y-axis contrary to the observations recorded for the square sample. At 54%RH, the rectangular sample was flat. Below 54%RH, the sample curled towards the gelatin along the x-axis. Thus the model must predict a positive curvature value for "a" and a value of zero for "b". Above 54%RH, the sample curved towards the cellulose acetate along the -x-axis. The model should therefore predict a negative curvature for "a" and a value of zero for "b".

According to the model, at 33%RH, the gelatin/cellulose acetate bilayer exhibits a positive "a" curvature (along the x axis) and a "b" curvature of zero. This coincides with the predicted curvature of 3.80 m^{-1} as indicated in Table 7.2 and agrees with the requirement that the curvature must be less than 35.8 m^{-1}. The model also predicts the rectangular sample is flat at 54%RH. Again, this is confirmed by observations.

At 75%RH, the model predicts that the rectangular sample can have 3 possible solutions. Each is valid since they conform to the minimum radius requirement discussed earlier. Therefore, the correct solution must be validated by observations and must satisfy the mathematical requirement that the second variation of δ^2W must be positive definite. Since, the rectangular sample showed no inversion from the x axis to the y axis as was observed in the square sample geometry, the only possible solution indicated in Table 7.2 is a negative "a" curvature of -3.37 m^{-1} and no "b" curvature.

Recall that the cylindrical geometric shapes observed are associated with the minimum potential energy in the system. At the minimum potential energy, the shapes are considered to be equilibrium stable. To verify the solutions, the second variation of δ^2W must be positive definite. Therefore the determinant of δ^2W must be > 0. The determinant of δ^2W is written as:

$$\begin{vmatrix} \frac{\partial f_1}{\partial a} & \frac{\partial f_1}{\partial b} & \frac{\partial f_1}{\partial c} & \frac{\partial f_1}{\partial d} \\ \frac{\partial f_2}{\partial a} & \frac{\partial f_2}{\partial b} & \frac{\partial f_2}{\partial c} & \frac{\partial f_2}{\partial d} \\ \frac{\partial f_3}{\partial a} & \frac{\partial f_3}{\partial b} & \frac{\partial f_3}{\partial c} & \frac{\partial f_3}{\partial d} \\ \frac{\partial f_4}{\partial a} & \frac{\partial f_4}{\partial b} & \frac{\partial f_4}{\partial c} & \frac{\partial f_4}{\partial d} \end{vmatrix} \qquad (7.7)$$

The determinant for each relative humidity was positive and therefore the solutions for a and b equate to stable equilibrium geometries at the minimum potential energy in the system. Therefore, the two dimensional bending model is valid for the gelatin/cellulose acetate bilayer.

Figures 7.2 and 7.3 represent the curvatures in the gelatin/cellulose acetate bilayer as a function of relative humidity for the square and rectangular geometry samples, respectively. The two dimensional bending model effectively predicts the dependence of relative humidity on the dimensional instability in the gelatin/cellulose acetate bilayer.

From the model, it was shown that the bending phenomena are dependent upon the mechanical property dependence on relative humidity as well as the sample geometries. From observation and model predictions, it was apparent the sample geometry dictates the inversion phenomena from the x to y axis. The square geometry shows the x to y inversion phenomenon. A rectangular geometry with a length to width ratio of 5:1 indicates no x to y inversion but instead predicts a positive to negative curvature along the length of the sample with increasing relative humidity (eg. +x to -x with increasing RH). This was confirmed by observations. Further work is required to determine if there exists a minimum length to width ratio which predicts an x to y inversion. Although this model only predicts the dimensional instability as a function of relative humidity, temperature effects on the dimensional stability can be added. This model can be expanded to other multilayer systems which exhibit similar dimensional instabilities.

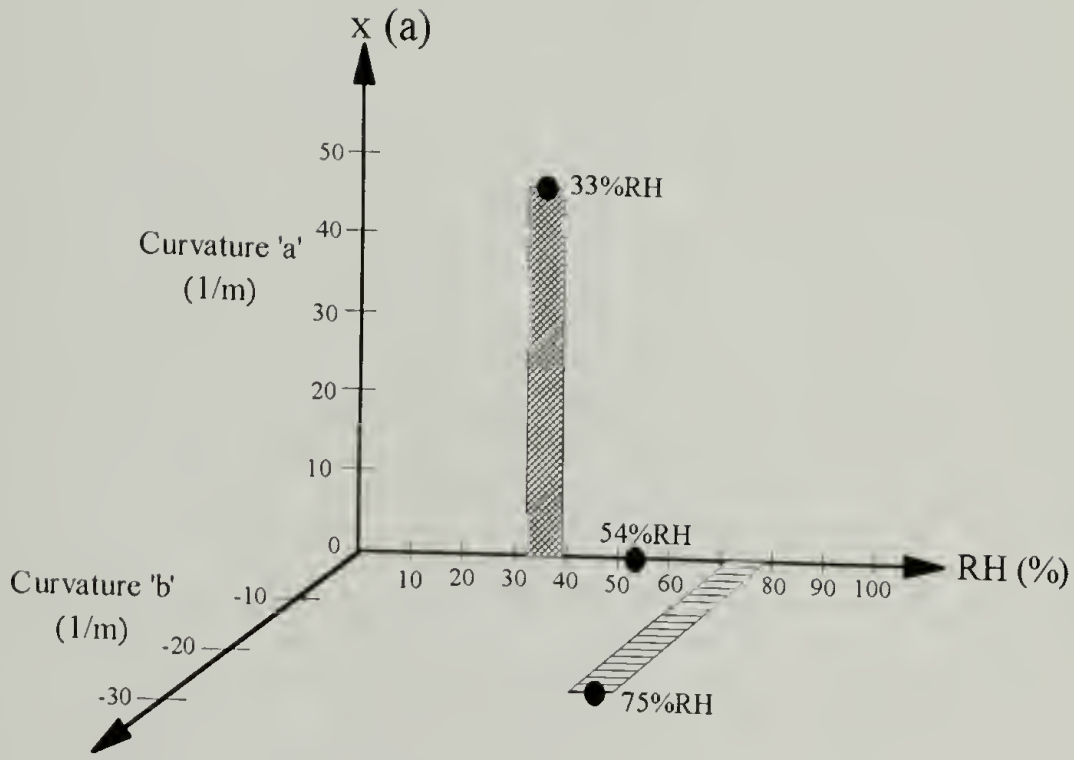

Figure 7.2 Curvature of gelatin/cellulose acetate bilayer as a function of relative humidity predicted by the two dimensional bending model. Predicted values are for a 101.6 mm square geometry sample.

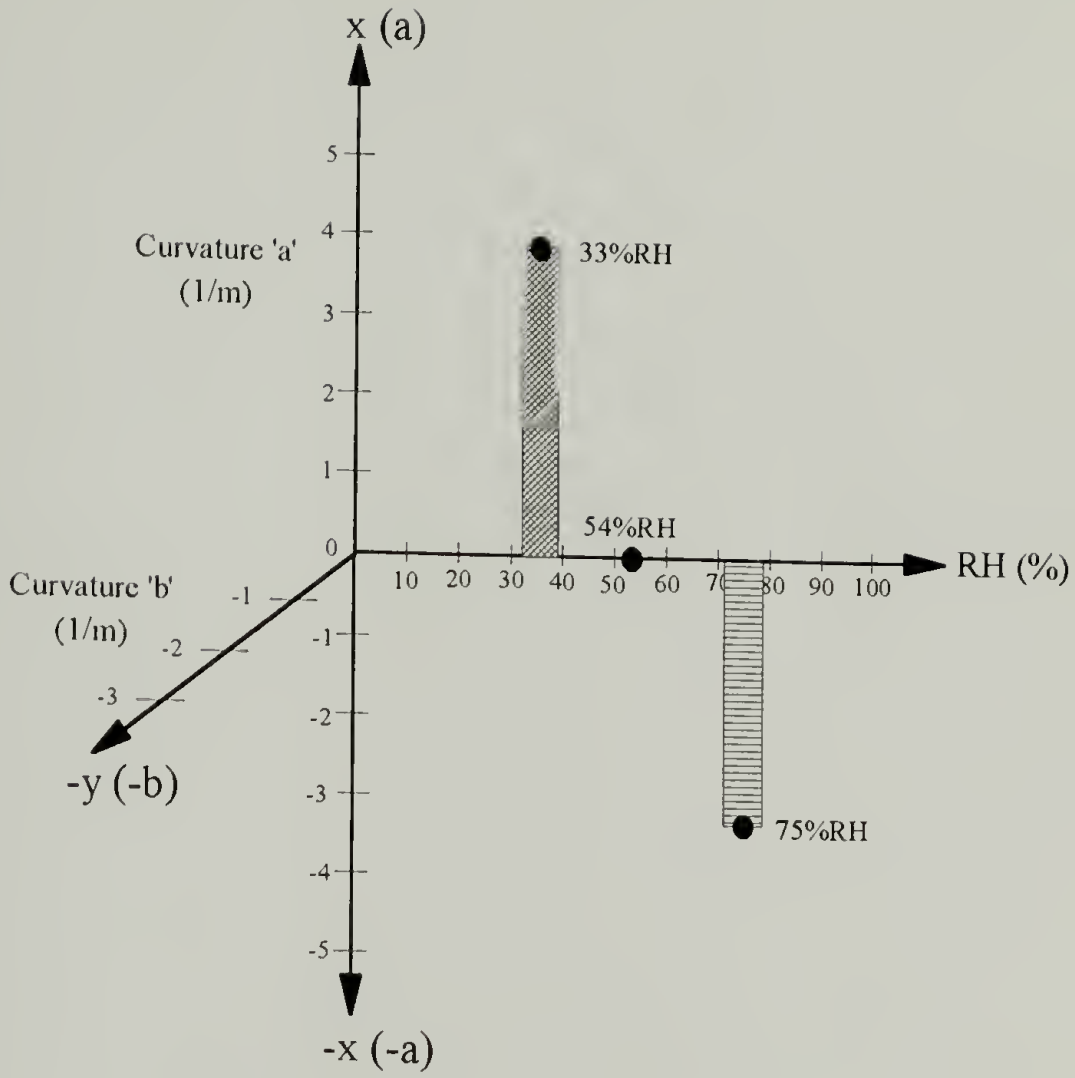

Figure 7.3 Curvature of gelatin/cellulose acetate bilayer as a function of relative humidity predicted by the two dimensional bending model. Predicted values are for a 35 mm x 175 mm rectangular geometry sample.

Conclusions

Observations have shown that the dimensional instability of a gelatin/cellulose acetate bilayer was dependent upon relative humidity. These observations initiated the direction pursued in this dissertation.

In general, when a gelatin/cellulose acetate bilayer was exposed to a relative humidity lower than 54%, the bilayer curled. The bilayer bent towards the gelatin along the x axis into a cylindrical shape. At these low relative humidities, the gelatin was in tension and the cellulose acetate was in compression. At 54%RH, no curvature was observed which meant that there was no stress in the bilayer at that humidity. As the relative humidity exceeded 54%RH, the bilayer exhibited a curvature inversion. The cylindrical geometry observed at the higher humidities was along the y axis, 90° to the lower relative humidity shapes. In addition, the gelatin was now in compression and the cellulose acetate was in tension.

These observations prompted the development of a two dimensional bending model which relates the curvature of a bilayer to the relative humidity. In addition, the observed bending phenomena led to the investigation of the biaxial stress in the gelatin coating as a function of relative humidity.

The two dimensional bending model was based on a nonlinear solution to Classical Lamination Theory. A similar two dimensional bending model had been derived for an unsymmetrical composite laminate in which the curvature as a function of temperature and sample dimensions effects were predicted. This model assumed that the modulus was independent of temperature. The two dimensional bending model developed in this dissertation accounts for the dependence of the dimensional instability and the moduli on the relative humidity.

The two dimensional bending model predicts the observed cylindrical shapes and the curvature inversion as a function of relative humidity. In general, the model predicted

that the bending phenomena are dependent upon the mechanical property dependence on relative humidity as well as the sample geometries. From observation and model predictions, it was apparent the sample geometry dictates the inversion phenomena from the x to y axis. The square geometry shows an x to y inversion phenomenon. A rectangular geometry with a length to width ratio of 5:1 indicates no x to y inversion but instead predicts a positive to negative curvature along the length of the sample with increasing relative humidity (eg. +x to -x with increasing RH). This was confirmed by observations. Further work is required to determine if there exists a minimum length to width ratio which predicts an x to y inversion. Although this model only predicts the dimensional instability as a function of relative humidity, temperature effects on the dimensional stability can be added. This model can be expanded to other multilayer systems which exhibit similar dimensional instabilities.

To solve the two dimensional model, the mechanical and swelling properties of the materials were required. Several materials were investigated: alkaline processed bone gelatin, cellulose acetate, poly(ethylene terephthalate), epoxy, poly(vinyl alcohol), PMDA-ODA polyimide and nickel. It was determined that the mechanical properties of gelatin are highly dependent upon relative humidity. As the relative humidity increased, the moduli and strength of the gelatin decreased and the elongation at break increased. The strength of the cellulose acetate was the only mechanical property which showed a dependence on relative humidity. The other materials listed were used to study the effect of relative humidity on the biaxial swelling stress in coatings and films.

The in-plane humidity expansion coefficient for gelatin and cellulose acetate was investigated using a constant load apparatus. The swelling strain (expansion or contraction) was measured as a function of relative humidity. From this study, it was determined that the gelatin coating was isotropic in the plane of the coating which explains the single humidity expansion coefficient of gelatin, 4.00 E-04 RH^{-1}. The cellulose acetate

was biaxial oriented in the plane of the film and exhibited two humidity expansion coefficients, 4.45 E-05 and 6.53 E-05 RH^{-1}. The humidity swelling strain vs. relative humidity was plotted and the slope of the line (between 23%RH and 75%RH) was determined as the humidity expansion coefficient. The interval between 23%RH and 75%RH was chosen to maintain consistency with industrial analysis.

Gelatin has a tendency to creep at high relative humidity. The effect of the magnitude of the constant load was investigated. Three loads were applied. It was apparent from the results, that the humidity expansion coefficient for gelatin was influenced by the specific applied load. A plot of the apparent humidity expansion coefficient as a function of the load shows a linear relationship. The actual humidity expansion coefficient was determined as the ordinate intercept of the apparent humidity expansion coefficient vs. load curve.

There is a significant difference between the absorption humidity expansion coefficient and the desorption humidity expansion coefficient, 4.00 E-04 and 1.67 E-04 RH^{-1}, respectively. This difference may be the result of the creep experienced by the gelatin or the moisture sorption hysteresis which is inherent of gelatin.

The out-of-plane humidity expansion coefficient was determined using an optical interference technique known as laser interferometry. Gelatin film was investigated. It was apparent that the out-of-plane humidity expansion coefficient was not the same as the in-plane. This out-of-plane anisotropy is commonly seen in gelatin. Literature results indicate the swelling anisotropic relationship between the out-of plane and in-plane humidity expansion coefficients should be greater than 1 for gelatin. The swelling anisotropy in this investigation was 1.23.

The biaxial stress in the coating contributes to the dimensional instability of the bilayer system. Holographic interferometry was employed to determine the biaxial swelling stress as a function of relative humidity. In the past, the sample used in holographic interferometry was investigated in a vacuum atmosphere due to air pressure

loading effects. Since relative humidity was required in this study, an investigation was conducted to minimize the effect relative humidity would have on the apparent values.

A nickel membrane was used to determine the effect of relative humidity on the biaxial stress values. If a large effect existed, a correction to the apparent values would be required. The relative humidity was generated by employing binary aqueous saturated salts which have specific relative humidities at room temperature. A compressed gas was bubbled through the salt solution to transport the humidity to the holographic chamber. To minimize the pressure effect, helium gas was chosen due to its low molecular weight.

The nickel membrane was subjected to the various humidities which were transported by the helium gas to the holographic chamber. It was determined that the use of helium minimized the depression of the actual values. The results of this test were compared with those found for the nickel membrane in a vacuum atmorsphere. It was apparent by comparison, that no correction to the data was required and therefore, helium was the best choice as the transport medium.

Moisture sorption hysteresis is the phenomenon in which different paths exist for absorption and desorption of moisture from the same material. Dimensional hysteresis often results. Alkaline processed bone gelatin coating exhibits a biaxial stress hysteresis as determined by holographic interferometry. The stress hysteresis in gelatin coincides with the dimensional hysteresis of the gelatin/cellulose acetate bilayer system. At 54%RH, the bilayer was flat. This is equivalent to zero stress in the coating. As the humidity was lowered, the bilayer curled to a smaller and smaller radius. This was seen as increased biaxial stress in the coating. As the humidity was increased, the bilayer quickly increased its cylindrical radius. This was viewed as a large decrease in biaxial stress. Comparison of the stresses at the same relative humidity, but along the different sorption paths, indicated that the stress during desorption was always greater than during absorption.

The moisture sorption hysteresis in gelatin is believed to be related to the amount of cis- and trans-conformations of proline present. Circular dichroism studies discussed in

the literature suggest that the cis-conformation of proline (which is present in gelatin and collagen) inhibits the hydrogen bonding of the water molecule to the oxygen in proline's carbonyl group.

The dependence of the biaxial swelling stress in poly(vinyl alcohol) and epoxy as a function of relative humidity was also investigated. The poly(vinyl alcohol) was blade coated on a PET substrate and dried at 54%RH, 20°C. Holographic interferometry results revealed a moisture sorption hysteresis at relative humidities less than 54%RH. Above 54%RH, the hysteresis was non-existent. Therefore, the hysteresis of the PVOH coating may be controlled by altering the drying conditions. The Epon 828/V40 epoxy showed no moisture sorption hysteresis. This may be due to the lack of hydrogen bonding of the water molecule to the epoxy matrix. It is believed that the amount of "bound" or hydrogen bonded water to the material strongly contributes to the hysteresis.

Alkaline processed bone gelatin was provided with various crystallinities and amounts of crosslinking agent (hardener) present. The effect of the crystallinity and amount of hardener on the magnitude of the hysteresis loop at 23%RH was investigated. The hysteresis loop was defined as the difference between the stress during desorption and the stress during absorption. The magnitude of the biaxial stress difference in the hysteresis loop at 23%RH was greatest for amorphous gelatin with no hardener for the first sorption cycle. With 16.7% crystallinity and 3.16% hardener present, the biaxial stress difference in the hysteresis loop was the lowest. Therefore, the amount of crystallinity and hardener affect the magnitude of the moisture sorption hysteresis in alkaline processed bone gelatin. With no hardener present, an increase in crystallinity decreases the biaxial stress difference at 23%RH. This may be due to an increase in the cis-conformation of the proline in the gelatin chain which inhibits the amount of "bound" water. For an amorphous gelatin, the increase in hardener content decreases the biaxial stress difference. The biaxial stress difference is also dependent upon the sorption cycle. The first cycle exhibits higher biaxial stress differences than the second cycle.

The biaxial swelling stress discussed above was monitored as a function of time to ensure equilibrium was achieved. During the course of that study, it was realized that the biaxial swelling stress vs. time behavior was characteristic of mass transport behavior. This discovery led to the study of the mass transport properties using holographic interferometry. Holographic interferometry combined with beam bending theory had been adopted by earlier researchers to study mass transport. The mathematics relating the swelling stress to mass uptake was described earlier.

In this work, holographic interferometry using a circular membrane was adopted. No beam bending assumptions were required, only the density of the membrane was necessary. The resonant frequency of the 2,1 mode as a function of time at various relative humidities was monitored as a function of time until equilibrium was reached. A plot of the normalized biaxial swelling stress vs. $time^{1/2}$ was analogous to the normalized mass uptake vs. $time^{1/2}$ curve determined via a gravimetric technique. The initial slope and half-time methods were introduced to calculate the mass diffusion coefficient. The mass diffusion coefficient for alkaline processed bone gelatin with 16.7% crystallinity and 0% hardener present was 2.17 E-09 cm^2/s. Similarly, the mass diffusion coefficient for cellulose acetate was calculated as 5.00 E-08 cm^2/s. It was initially believed that the mass diffusion coefficient of gelatin would be greater than the cellulose acetate. Through further study, it was apparent that the amount of moisture absorbed by gelatin was 13 times greater than that absorbed by cellulose acetate over the same time interval. Since the mass diffusion coefficient represents the time at which the moisture passes through the thickess of the material, it does not quantify the amount of moisture that is transported over that same distance.

A study regarding the physical aging effect on the mass diffusion coefficient was performed using two different lots of gelatin. Each gelatin was 16.7% crystalline and contained no crosslinking agent. The first lot of gelatin was 8 months old prior to use and had been stored at room conditions which fluctuate from day to day. The second lot of

gelatin was stored in a controlled low temperature environment (in a freezer) and was used 6 weeks after receipt. The diffusion coefficient was determined using holographic interferometry. A slight dependence on physical aging was noted. The diffusion coefficient of lot 1 was less than lot 2. Lot 1 and 2 had mass diffusion coefficient values of 2.17 E-09 cm^2/s and 2.62 E-09 cm^2/s, respectively. In the photographic industry, physical aging affects the swelling characteristics of the gelatin/substrate systems. Physical aging may affect the amount of moisture absorbed by the gelatin (although this was not studied). In this investigation, physical aging indicated only a slight affect on the diffusion characteristics of the gelatin.

The validity of the holographic interferometry technique was tested using PMDA-ODA polyimide since this material has a well known mass diffusion coefficient. The mass diffusion coefficient determined by holographic interferometry was calculated as 2.08 E-09 cm^2/s. This agreed well with the reported literature value of 2.00 E-09 cm^2/s.

Future Work

There are several areas which time did not allow to investigate in this research. Some of the ideas described below were suggested by the Eastman Kodak Co. They are included in this future work section so they will not be lost in the archives of lab notebooks and research files.

Gelatin is a fascinating material. In this research, it was obvious the attention focussed on the effects of relative humidity on the dimensional instability, biaxial stress and mass transport of gelatin and the gelatin/substrate bilayer. Eastman Kodak suggested the following topics be considered for future research.

(1. Understand and quantify the in-plane Poisson's ratio of cellulose acetate and Estar®, PET, and their stress relaxation behavior under plane strain conditions.

(2. Since photographic films contain silver halide particles, investigating the effect of the filler particle on the stress in the bilayer. Determine if there is a size and shape dependency on the mechanical and dimensional stability of the bilayer.

(3. Learn more about the out-of-plane properties for the gelatin (filled and unfilled) and for the bilayer.

(4. Investigate how drying conditions effect the stress in the film.

In addition to these suggestions, the effect of temperature and hygrothermal conditions on the biaxial stress in gelatin and its substrates should be considered. The holographic interferometry would work ideally for this investigation.

Expansion of the two dimensional bending model to other bilayer systems is highly recommended. The PET film provided by Kodak is biaxially oriented. The principal axes do not align with the gelatin coating direction. Also, the humidity expansion coefficient is less than cellulose acetate which is probably the reason the gelatin/PET bilayer lies flat at 75%RH vs. 54%RH for gelatin coated on cellulose acetate. As a result, the bending characteristics will be different. With a PET substrate, the "inversion" from gelatin in tension to gelatin in compression at cylindrical shapes 90° from each would occur at a humidity greater that 75%. The dependence of the sample dimensions on the two dimensional bending model also warrants some investigation.

Lastly, further investigation into the control of the moisture sorption hysteresis in poly(vinyl alcohol) as a function of drying conditions would make for a great study. If the hysteresis can be controlled, this may lead to a better understanding of the moisture sorption hysteresis mechanism.

BIBLIOGRAPHY

Adelstein, P.Z., "Physical Properties of Photographic Materials," SPSE Handbook of Photographic Science and Engineering, ed., W. Thomas, (New York: Wiley Interscience, 1973).

"Airvol® Polyvinyl Alcohol," (Pittsburgh, PA: Air Products and Chemicals, Inc., 1990).

Alberts, B., Bray, D., Lewis, J., Raff, M, Roberts, K. and Watson, J., Molecular Biology of the Cell, (New York: Garland Publishing, Inc., 1983).

Aleck, B.J., "Thermal Stresses in a Rectangular Plate Clamped Along an Edge," Journal of Applied Mechanics, **16**, 118 (1949).

Bauer, C.L., personal communication, (1991).

Bauer, C.L., Farris, R.J. and Vratsanos, M.S., "Determination of the Stresses and Properties of Polymer Coatings," Journal of Coatings Technology, **60**(760), 51 (1988).

Bauer, C.L. and Farris, R.J., "Determination of Poisson's Ratio for Polyimide Films," Polymer Engineering and Science, **29**(16), 1107 (1989).

Berry, B.S. and Pritchet, W.C., "Bending-Cantilever Method for the Study of Moisture Swelling in Polymers," IBM Journal of Research and Development, **28**(6), 662 (1984).

Boki, K. and Ohno, B., "Moisture Sorption Hysteresis in Kudzu Starch and Sweet Potato Starch," Journal of Food Science, **56**(1), 125 (1991).

Bradbury, E. and Martin, C., "Mechanical Properties and Structure of Sol-Type and Gel-Type Gelatine Films," Nature, **168**, 837 (1951).

Brewer, B.J., "Cellulose Esters, Organic," Encyclopedia of Polymer Science and Engineering, eds. H. Marks and N. Bikales, Vol. 3, (New York: Wiley Interscience, 1986).

Burness, B.M. and Wilson, B.D., "Bis(Beta-Acyloxyethyl) Ketones as Gelatin Hardeners," U.S. Patent No.: 3,360,372, December 26, 1967.

Burness, B.M. and Wilson, B.D., "Gelatin Compositions Containing a Bisisomaleimide Hardener," United States Patent, 3,232,763 (1966).

Cahn Instruments, Inc., Cerritos, CA 90701

Calhoun, J.M., "The Physical Properties and Dimensional Stability of Safety Aerographics Film," Photogrammetric Engineering, **13**, 163 (1947).

Calhoun, J.M., "The Physical Properties and Dimensional Behavior of Motion Picture Film," Journal of the Society of Motion Picture Engineering, **43**, 227 (1944).

Calhoun, J.M. and Leister, D.A., "Effect of Layers on the Dimensional Instability of Photographic Film," Photographic Science and Engineering, **3**(1), 8 (1959).

Calhoun, J.M., Adelstein, P.Z. and Parker, J.T., "Physical Properties of Estar Polyester Base Aerial Films for Topographic Mapping," Photogrammetric Engineering, **27**, 461 (1961).

Campbell, D., and White, J.R., Polymer Characterization: Physical Techniques, (New York: Chapman and Hall Publishing Co., 1989).

Campbell, D.S., "Mechanical Properties of Thin Films," Handbook of Thin Film Technology, eds. L.I. Maissel and R. Glang, (New York: McGraw Hill Book Co., 1988).

Centa, J.M., "Effect of Base and Emulsion Thickness on Dimensional Stability of Graphic Arts Films," Proceeding of the Annual Technical Meeting: Technical Associates of Graphic Arts, **8**, 75 (1956).

Chien, J.C.W., "Solid-State Characterization of the Structure and Property of Collagen," Journal of Macromolecular Science - Reviews in Macromolecular Chemistry, **C12**(1), 1 (1975).

Chipalkatti, M.H., Stresses and Deformation Coupled Moisture Transport in Polymers, Ph.D. diss., University of Massachusetts, Amherst, MA, (1988).

Colton, E.K. and Wiegand, E.J., "Moisture in Photographic Film and its Measurement," Photographic Science and Engineering, **2**, 170 (1958).

Conforti, R.M. and Barbari, T.A., "A Thermodynamic Analysis of Gas Sorption-Desorption Hysteresis in Glassy Polymers," Macromolecules, **26**, 5209 (1993).

Corcoran, E.M., "Determining Stresses in Organic Coatings Using Plate Beam Deflection," Journal of Paint Technology, **41**(538), 635 (1969).

Crank, J., The Mathematics of Diffusion, (Oxford, England: Clarendon Press, 1956).

Crank, J. and Park, G.S., "An Evaluation of the Diffusion Coefficient for Chloroform in Polystyrene from Simple Absorption Experiments," Transactions of the Faraday Society, **45**, 240 (1949).

Croll, S.G., "The Origin of Residual Internal Stress in Solvent-Cast Thermoplastic Coatings," Journal of Applied Polymer Science, **23**(3), 847 (1979).

Davis, J.M. and Bächinger, H.P., "Hysteresis in the Triple Helix-Coil Transition of Type III Collagen," Journal of Biological Chemistry, **268**(34), 25965 (1993).

Easwar, N., Ofcarcik, C., Vrtis, J.K. and Farris, R.J., "Optical Interferometric Method for the Measurement of the Out of Plane Thickness Changes of Weakly Absorbing Thin Solid Films," (in process).

"Effects of Relative Humidity and Elevated Temperatures on Composite Structures," Proceedings of the AFOSR Workshop, Newark, DE, March (1976).

Eliassaf, J. and Eirich, F.R., "Creep Studies on Gelatin at 100% Relative Humidity," Journal of Applied Polymer Science, **IV**(11), 200 (1960).

Felder, R.M. and Huvard, G.S., Methods of Experimental Physics, (New York: Academic Press, 1980).

Feng, Z.C. and Lui, H.D., "Generalized Formula for Curvature Radius and Layer Stresses Caused by Thermal Strain in Semiconductor Multilayer Structures," Journal of Applied Physics, **54**(1), 83 (1983).

Flaggs, D.L., Elastic Stability of Generally Laminated Composite Plates Including Hygrothermal Effects, M.MMAE. thesis, University of Delaware, Newark, DE, (1977).

Flory, P.J. and Garrett, R.R., "Phase Transitions in Collagen and Gelatin Systems," Journal of American Chemical Society, **80**, 4836 (1958).

Fu, T.Z., Durning, C.J. and Tong, H.M., "Simple Model for Swelling-Induced Stresses in Supported Polymer Thin Films," Journal of Applied Polymer Science, **43**, 709 (1991).

Goldberg, J.L., O'Toole, K.M. and Roper, H., Journal of Testing and Evaluation, **3**(4), 263 (1975).

Greener, J., personal communication, June, 1994.

Greenspan, L., "Humidity Fixed Points of Binary Saturated Aqueous Solutions," Journal of Research of the National Bureau of Standards: *A. Physics and Chemistry*, **81A**(1), 89 (1977).

Gregg, S.J., The Surface Chemistry of Solids, 2nd ed., (London: Chapman and Hall, Ltd., 1961).

Hamilton, J.F., Higgins, J.C. and Starr, J.E., eds., The Theory of the Photographic Process, 4th ed., (Rochester, NY: Eastman Kodak Co., 1977).

Hermel, H., Wetzel, R., Buder, E., Roth, C., Herbrich, H. and Legutke, H., "Moisture, Triple Helical Content and Brittlenes of Gelatin Layers," Journal of Photographic Science, **39**, 16 (1991).

Hoeve, C.A.J. and Lue, P.C., "The Structure of Water Absorbed in Collagen. I. The Dielectric Properties." Biopolymers, **13**, 1661 (1974).

Hyer, H.W., "Calculations of the Room-Temperature Shapes of Unsymmetrical Laminates," Journal of Composite Materials, **15**, 296 (1981).

Hyer, H.W., "The Room-Temperature Shapes of Four-Layer Unsymmetric Cross-Ply Laminates," Journal of Composite Materials, **16**, 318 (1982).

James, T.H. and Higgins, G.C., Fundamentals of Photographic Theory, (New York: Morgan and Morgan, 1960).

Jennings, R.M., An Investigation of the Effects of Curing Conditions on the Residual Stress and Dimensional Instability of Polyimide Films, Ph.D. diss., University of Massachusetts, Amherst, MA, (1993).

Jones, R.M., Mechanics of Composite Materials, (New York: McGraw-Hill Book Co. 1975).

Jopling, D.W., "The Swelling of Gelatin Films. The Effects of Drying Temperature and of Conditioning the Layers in Atmospheres of High Relative Humidity," Journal of Applied Chemistry, **6**, 79 (1956).

Jou, J., Huang, R., Huang, P. and Shen, W., "Structure Effect on Water Diffusion and Hygroscopic Stress in Polyimide Films," Journal of Applied Polymer Science, **43**, 857 (1991).

Jou, J.H. and Chen, L.J., "Simultaneous Determination of the Biaxial Relaxation Modulus and Thermal Expansion Coefficient of Rigid Rod Polyimide Films Using a Bending-Beam Technique," Macromolecules, **25**, 179 (1992).

Jou, J.H., Hsu, L. and Chang, L.S., "An Analysis of Thermal Stresses in a Multilayer Thin Film Printhead," Thin Solid Films, **201**, 253 (1991).

Jou, C.S., Stresses Associated with Transport in Polymeric Films, Ph.D. diss., University of Massachusetts, Amherst, MA, (1993).

Jou, C.S. and Farris, R.J., "Moisture Transport in a Bilayer Cantilever Beam by Holographic Interferometry," (submitted to Acta Polymerica, 1993).

Kämpf, G., Characterization of Plastics by Physical Methods, (New York: Hanser Publishers, 1986).

Katz, J.R., Derksen, J.C. and Bon, W.F., "Zur Polymorphie Hochmolekularer Substanzen. I. Ueber Amorphie und Kristallinische Gelatine und Ueber Das Wesen Des Gelatinier - Ungsprozesses Bei Der Gelatine," Trav. chim. Pays - Bas, **50**, 725 (1931).

Kellaway, I.W., Marriott, C. and Robinson, J.A.J., "The Mechanical Properties of Gelatin Films: I. The Influence of Water Content and Preparative Conditions," Canadian Journal of Pharmaceutical Sciences, **13**(4), 83 (1978).

Koedam, M., "Determination of Small Dimensions by Diffraction of a Laser Beam," Philips Technical Review, **27**(7), 208 (1966).

Kroschwitz,J.I., ed., Polymers: Polymer Characterization and Analysis, (New York: John Wiley and Sons, 1990).

Liu, H., Zhang, L., and Seaton, N.A., "Analysis of Sorption Hysteresis in Mesoporous Solids Using a Pore Network Model," Journal of Colloid and Interface Science, **156**, 285 (1993).

Maden, M.A., The Determination of Stresses and Material Properties of Polyimide Coatings and Films Using Real Time Holographic Interferometry, Ph.D. diss., University of Massachusetts, Amherst, MA, (1992).

Maden, M.A., Tong, K. and Farris, R.J., "Measurement of Stresses in Thin Films Using Holographic Interferometry: Dependence on Atmospheric Conditions," Materials Research Society Symposium, **188**, 29 (1990).

Malkin, A.Y., Askadsky, A.A., Kovriga, V.V. and Chalykh, A.E., Experimental Methods of Polymer Physics, (Englewood Cliffs, NJ: Prentice Hall, Inc., 1983).

Mallick, P.K., Fiber-Reinforced Composites: Materials, Manufacturing and Design, (New York: Marcel Dekker, Inc., 1988).

Manzione, L.T., Plastic Packaging of Microelectronic Devices, (New York: Van Nostrand Publishing Co., 1990).

Marshall, A.S. and Petrie, S.E.B., "Thermal Transitions in Gelatin and Aqueous Gelatin Solutions," Journal of Photographic Science, **28**, 128 (1980).

Marten, F.L.,"Vinyl Alcohol Polymers," Encyclopedia of Polymer Science and Engineering, eds. H. Marks and N. Bikales, Vol. 17, (New York: Wiley Interscience, 1986)

Mattli, M.L. and Rüegg, M., "Thermodynamic Functions of Biopolymer Hydration: I. Their Determination by Vapor Pressure Studies Discussed in an Analysis of the Primary Hydration Process," Biopolymers, **21**, 403 (1982).

Morinaka, A. and Asano, Y., "Residual Stress and Thermal Expansion Coefficients of Plasma Polymerized Films," Journal of Applied Polymer Science, **27**, 2139 (1982).

Nguyen, L.T., "Surface Sensors for Moisture and Stress Studies," New Characterization Techniques for Thin Polymer Films, eds., H.M. Tong and L.T. Nguyen, (New York: John Wiley and Sons, 1990).

Ni, B., personal communication, 1992.

Ni, B., personal communication, 1993.

Norris, T.O. and McGraw, J., "Gelatin Coatings and Tensile Strength of Gelatin Films," Journal of Applied Polymer Science, **8**, 2139 (1964).

Noyan, I.C. and Cohen, J.B., Residual Stress: Measurement by Diffraction and Interpretation, (New York: Springer-Verlag, 1987).

O'Brien, F.E.M., "Control of Humidity by Saturated Salt Solutions," Journal of Scientific Instrumentation, **25**, 73 (1948).

Ohyama, T., Endoh, K., Mikami, A. and Mori, Y.H., "Optical Interferometry for Measuring Instantaneous Thickness of Transparent Solid and Liquid Films," Review Scientific.Instrumentation, **59**(9), 2018 (1988).

Ohyama, T. and Mori, Y.H., "Optical Method for Measuring Uniform Thickness of the order of 10 μm - 1 mm of Transparent Solid and Liquid Films," Review of Scientific Instrumentation, **58**(10), 1860 (1987).

Oosterbroek, M., Lammers, R.J., van der Van, L.G.J. and Perera, D.Y., "Crack Formation and Stress Development in an Organic Coating," Journal of Coatings Technology, **63**(797), 55 (1991).

Perera, D.Y. and Vanden Eynde, D., "Moisture and Temperature Induced Stresses (Hygrothermal Stresses) in Organic Coatings," **59**(748), 55 (1987).

Perry, A.J., Ineichen, B. and Eliasson, B.,"Fiber Diameter Measurement by Laser Diffraction," Journal of Materials Science, **9**, 1376 (1974).

"Physical Properties of Kodak Aerial Films," Properties of Kodak Materials For Aerial Photographic Systems, Vol. II, (Rochester, NY: Eastman Kodak Co., 1972).

"Physical and Chemical Behavior of Kodak Aerial Films," Properties of Kodak Materials for Aerial Photographic Systems, Vol. III, (New York: Eastman Kodak Co., 1972).

Pipes, R.B., Vinson, J.R. and Chou, T.W., "On the Hygrothermal Response of Laminated Composite Systems," Journal of Composite Materials, **10**, 130 (1976).

Plepys, A.R., A Study of Residual Stress Formation in Three Dimensionally Constrained Epoxy Resins, Ph.D. diss., University of Massachusetts, Amherst, MA, (1992).

Pouradier, J., "II: Properties of Gelatin in Relation to Its Use in the Preparation of Photographic Emulsions," The Theory of the Photographic Process, 4th ed., eds., J.F. Hamilton, G.C. Higgins and J.E. Starr, (Rochester, NY: Eastman Kodak Co., 1977).

Pranjoto, H., and Denton, D.D., "Gravimetric Measurements of Steady-State Moisture Uptake in Spin-Coated Polyimide Films," Journal of Applied Polymer Science, **42**, 75 (1991).

Rabek, J.F., Experimental Methods in Polymer Chemistry, (New York: John Wiley and Sons, 1980).

Ramachandran, G.N. and Chandrasekharan, R., "Interchain Hydrogen Bonds via Bound Water Molecules in the Collagen Triple Helix," Biopolymers, **6**, 1649 (1968).

Rao, K.S. and Das, B., "Varietal Differences in Gelatin, Egg Albumin, and Casein in Relation to Sorption - Desorption Hysteresis with Water," Journal of Physical Chemistry, **72**(4), 1223 (1968).

Rose, P.I., "Gelatin: I. General Properties," The Theory of the Photographic Process, 4th ed., eds., J.F. Hamilton, G.C. Higgins and J.E. Starr, (Rochester, NY: Eastman Kodak Co., 1977).

Rose, P.I., "Gelatin," Encyclopedia of Polymer Science and Engineering, eds. H. Marks and N. Bikales, Vol. 3, (New York: Wiley Interscience, 1986).

Sackinger, S., The Determination of Swelling Stresses in Polyimide Films, Ph.D. diss., University of Massachusetts, Amherst, MA, (1990).

Saenger, K.L. and Tong, H.M., "Laser Interferometry: A Measurement Tool for Thin Film Polymer Properties and Processing Characteristics," New Characterization Techniques in Thin Polymer Films, eds., H.M. Tong and L.T. Nguyen, (New York: John Wiley and Sons, Inc., 1990).

Sato, K., "The Internal Stress in Coating Films," Progress in Organic Coatings, **8**, 143 (1980).

Shen, G. and Springer, G.S., "Moisture Absorption and Desorption of Composite Materials," Journal of Composite Materials, **10**, 2 (1976).

Shimbo, M., Ochi, M. and Arai, K., "Effect of Solvent and Solvent Concentration on the Internal Stress of Epoxide Resin Coatings," Journal of Coatings Technology, **57**(728), 93 (1985).

Shirrell, C.D., "Diffusion of Water Vapor in Graphite/Epoxy Composites," Advanced Composite Materials - Environmental Effects, ASTM STP 658, ed. J.R. Vinson, (Philadelphia, PA: American Society for Testing and Materials, 1978).

Sih, G.C., Michopoulos, J.G., and Chou, S.C., eds., Hygrothermoelasticity, (Boston, Martinus Nijhoff Publishers, 1986).

Simitses, G.J., An Introduction to the Elastic Stability of Structure, (Englewood, NJ: Prentice-Hall, Inc., 1976).

Singer, P., "Film Stress and How to Measure It," Semiconductor International, (October 1992), pp 54.

Sloan, J.G. and Vinson, J.R., "Behavior of Rectangular Composite Material Plates Under Lateral and Hygrothermal Loads," Proceedings of the American Society of Engineers Winter Meeting, (New York: American Society of Mechanical Engineers, 1978).

Smith, S.E., "The Sorption of Water Vapor by High Polymers," Journal of the American Chemical Society, **69**, 646 (1947).

"Standard Test Methods for Tensile Properties of Thin Plastic Sheeting," ASTM Designation: D882, American Society for Testing and Materials, Philadelphia, PA (1988).

"Standard Test Methods for Tensile Stength and Young's Modulus for High Modulus Single Filament Materials," ASTM Designation: D3379, American Society for Testing and Materials, Philadelphia, PA (1988).

"Standard Practice for Preparation of Uniform Free Films of Organic Coating," ASTM Designation: D4708, American Society for Testing and Materials, Philadelphia, PA (1988).

Subramanian, R., Pottiger, M.T., Morris, J.T. and Curilla, J.P., "Effect of Moisture on the Physical Properties of Polyimide Films," Materials Research Society Symposium Proceedings, Vol. 227, (1991).

Tanoka, S. and Scherage, H.A., "Theory of the Cooperative Transition Between Two Conformations of Poly(L-proline): II. Molecular Theory in the Absence of Solvent," Macromolecules, **8**(4), 504 (1975).

Taylor, J.F., An Experimental Evaluation of the State of Stress and Mechanical Performance of a Polyacrylate Photoresist Coating, Ph.D. diss., University of Massachusetts, Amherst, MA, (1993).

Technical Bulletin No.: SC: 235-91.828, (Houston, TX: Shell Chemical Co., 1991).

Timoshenko, S. and Woinowsky-Krieger, S., Theory of Plates and Shells, 2nd ed., (New York: McGraw-Hill Book Co., 1959).

Tong, H.M. and Saenger, K.L., "Bending-Beam Study of Water Sorption by Thin Poly(methyl Methacrylate) Films," Journal of Applied Polymer Science, **38**, 937 (1989).

Tsai, S.W. and Hahn, H.T., Introduction to Composite Materials, (Westport, CT: Technomic Publishing Co., 1980).

Turek, D.E., "On the Tensile Testing of High Modulus Polymers and the Compliance Correction," Polymer Engineering and Science, **33**(6), 328 (1993).

Umberger, J.Q., "The Fundamental Nature of Curl and Shrinkage in Photographic Films," Photographic Science and Engineering, **1**(2), 69 (1957).

Vinson, J.R., Structural Mechanics: The Behavior of Plates and Shells, (New York: John Wiley & Sons, Inc., 1974).

Vinson, J.R. and Sierakowski, R.L., The Behavior of Structures Composed of Composite Materials, (Boston, MA: Kluwer Academic Publishers, 1993).

Vrtis, J.K. and Farris, R.J., "Experimental Stress Analysis Methods and Some Thin Film Applications," (accepted to Materials Research Society Symposium Proceedings, 1994).

Vrtis, J.K. and Farris, R.J., "Hysteresis of Biaxial Swelling Stresses in Humidity Sensitive Polymer Coatings," Proceedings of the American Chemical Society: Division of Polymeric Materials: Science and Engineering, **69**, 440 (1993).

Wake, W.C., Developments in Adhesives, (London: Applied Science Publishers, Ltd., 1977).

Ward, A.G. and Courts, A., The Science and Technology of Gelatin, (New York: Academic Press, Inc., 1977).

Weast, R.C., Handbook of Chemistry and Physics, 60th ed., (Boca Raton, FL: CRC Press, Inc., 1979).

Weibs, T.P., Hong, S., Bravman, J.C. and Nix, W.D., "Mechanical Defection of Cantilever Microbeams: A New Technique for Testing the Mechanical Properties of Thin Films," Journal of Materials Reseach, **3**(5), 931 (1988).

Wetzel, R., Buder, E., Hermel, H. and Hüttner, A., "Conformations of Different Gelatins in Solutions and in Films: An Analysis of Circular Dichroism (CD) Measurements," Colloid and Polymer Science, **265**, 1036 (1987).

Whitney, J.M. and Ashton, J.E., "Effect of Environment on the Elastic Response of Layered Composite Plastics," AIAA Journal, **9**, 9 (1971).

Witnauer, J.P. and Fee, J.G., "Effects of Diluents on Fusion Temperature of the Crystalline Regions in Plain and Tanned Cowhide," Journal of Polymer Science, **26**, 141 (1957).

Wollmer, A., Straβberger, W. and Glatter, U., "Perspectives in the Circular Dichroic Analysis of Protein Main-Chain Conformation," Modern Methods in Protein Chemistry - Review Articles, (New York: Walter de Gruyter and Co., 1983).

Xu, G. and Ruckenstein, E., "Emulsion Pathway for Gelatin Crosslinking," Journal of Applied Polymer Science, **47**, 1343 (1993).

Yamamoto, N. and Oishi, Y., "Photographic Gelatin Hardening Composition," U.S. Patent No.: 3,325,287, June 13, 1967.

Yang, D.K., Koros, W.J., Hopfenberg, H.B. and Stannett, V.T., "Sorption and Transport Studies of Water in Kapton Polyimide," Journal of Applied Polymer Science, **30**, 1035 (1985).

Yaseen, M. and Ashton, H.E., "Effect of Free Film Preparation Method on Physical Properties of Organic Coatings," Journal of Coatings Technology, **49**(629), 50 (1977).

Yaseen, M. and Raju, K.V.S.N., "A Critical Analysis of Various Methods for Preparation of Free Films of Organic Coatings," Progress in Organic Coatings, **10**, 125 (1982).

York, P., "Analysis of Moisture Sorption Hysteresis in Hard Gelatin Capsules, Maize Starch, and Maize Starch: Drug Powder Mixtures," Journal of Pharmaceutical and Pharmacology, **33**, 269 (1981).